A University of Sussex PhD thesis

Available online via Sussex Research Online:

http://sro.sussex.ac.uk/

This thesis is protected by copyright which belongs to the author.

This thesis cannot be reproduced or quoted extensively from without first obtaining permission in writing from the Author

The content must not be changed in any way or sold commercially in any format or medium without the formal permission of the Author

When referring to this work, full bibliographic details including the author, title, awarding institution and date of the thesis must be given

Please visit Sussex Research Online for more information and further details

University of Sussex

DOCTORAL THESIS

Quantum Theory of the Penning Trap

an exploration of the low temperature regime

Author:

Frances CRIMIN

Supervisor:

Prof. Barry M. GARRAWAY

Second supervisor:

Dr. José VERDÚ-GALIANA

A thesis submitted in fulfilment of the requirements
for the degree of Doctor of Philosophy
in the
School of Mathematical and Physical Sciences

UNIVERSITY OF SUSSEX

February 2018

Declaration of Authorship

I, Frances CRIMIN, declare that this thesis titled, 'Quantum Mechanics of the Penning Trap - *an exploration of the low temperature regime*' and the work presented in it are my own. I confirm that:

- This work was done wholly or mainly while in candidature for a research degree at this University.
- Where any part of this thesis has previously been submitted for a degree or any other qualification at this University or any other institution, this has been clearly stated.
- Where I have consulted the published work of others, this is always clearly attributed.
- Where I have quoted the work of others, the source is always given. With the exception of such quotations, this thesis is entirely my own work.
- I have acknowledged all main sources of help.
- Where this thesis is based on work done by myself jointly with others, I have made clear exactly what was done by others and what I have contributed myself.

_____

Signature

_____

Date

Abstract

UNIVERSITY OF SUSSEX

Atomic Molecular and Optical Physics

School of Mathematical and Physical Sciences

Doctor of Philosophy

Quantum Theory of the Penning Trap

an exploration of the low temperature regime

by Frances CRIMIN

The objective of this thesis is to develop the quantum theory of the motional degrees of freedom of a charged particle in a Penning trap. The theory is treated within the formalism of quantum optics, and explores the use of dressed-atom methods by exploiting the three-fold $SU(N)$ algebraic structure of the problem. The quantum form of the experimental techniques of sideband coupling and driving to the ultra-elliptical regime are examined in this context, and resulting future applications considered. Interpretation of the quantum dynamics of the separate x and y motions of an electron is discussed, motivated by the desire to modify the trapping potential without changing the basic experimental configuration. A detailed discussion of operator methods which exploit the algebraic structure of the problem is given. This results in a clearer understanding of the physical manifestations of a range of unitary transformations upon a general three-dimensional system, and a novel interpretation of the mapping between canonical angular momentum components of isotropic and anisotropic trapping systems. The results highly promote future use of these methods in Penning trap theory, detailing a robust formulation of unitary operations which can be used to prepare the quantum state of a charged particle. The majority of the results can be applied to any Penning trap, but the theory is based throughout upon the "Geonium Chip" trap at Sussex; the scalability and planar design of this trap promotes it as natural candidate in experimental quantum optics and Gaussian quantum information studies. The work in this thesis aims to provide framework for such future applications.

Acknowledgements

I would firstly like to thank Prof. Barry Garraway and Dr. José Verdú-Galiana for their guidance throughout this PhD. I have greatly enjoyed working with them both. I also owe a great deal of thanks to the other members of the Geonium Chip group, whose friendship has been invaluable. I would additionally like to acknowledge EPSRC as the main source of funding.

Above all, I thank my family, for all their love and support.

Contents

List of Figures

Abbreviations

- CPW Coplanar-waveguide
- MW Microwave
- 2D Two-dimensional
- RF Radio-frequency
- RWA Rotating wave approximation
- TLS Two-level system
- CSCO Complete set of commuting observables
- 3D Three-dimensional
- LZ Landau-Zener
- LZS Landau-Zener-Stückelberg

Chapter 1

Introduction

"To test reality we must see it on the tightrope.
When the verities become acrobats, we can judge them."
Oscar Wilde [1]

1.1 Introduction

Scientific progress is driven by an ability to test the theories of nature we construct, along with an insatiable curiosity and a considerable amount of perseverance. In modern physics, the refinement of our theories is then largely contingent upon the accuracy of experimental results. In this cycle of theoretical and experimental investigation, the Penning trap plays a vital role.

The device resulted from the advancement of a technique discovered by Penning in 1936 [2], of increasing the confinement time of an electron by use of electric and magnetic fields. Responsible for this "*development of the ion trap technique*", Hans Georg Dehmelt and Wolfgang Paul shared the Nobel prize in 1989 [3], with Dehmelt's group achieving single electron trapping in 1973 [4]. The Penning trap has since become an indispensable tool in high precision mass spectrometry [5, 6], in anti-matter experiments [7, 8, 9], and in providing increasingly precise measurements of the g-factor of the electron [10] and proton [11, 12] against which fundamental theory can be tested. The framework for these, and the ever expanding applications of the device [13], has been laid down by extensive and successful study of Penning trap theory [14, 15, 16, 17, 18, 19].

The goal of achieving quantum information processing by confinement of single electrons in Penning traps [20, 21, 22, 23, 24] motivated the enterprise of *planar* traps [25], in an effort to optimise both the scalability of the system, and addressability of the trapped

particles [26]. The Geonium Chip [27] at Sussex forms such a trap, furthermore designed to form a compact, mobile device. It is with the Geonium Chip in mind that the work of this thesis was conducted, in an effort to expand upon its future applications.

In pursuit of this, an extensive quantum theory of both the ideal circular and elliptical Penning trap has been developed, providing a mapping from one to the other in an elegant way. Inspired by Kretzschmar's use of the Bloch Vector model in studying coupled oscillator modes in the Penning trap [28], his method has been greatly developed and used to investigate a number of theoretical challenges, and to reinterpret some of the basic quantum theory of the Penning trap in an illuminating way. The result is a concise and logical formalism for studying the quantum theory of the Penning trap, which takes advantage of inherent algebraic structure of the quantum Hamiltonian. From this, novel applications result, and the low temperature regime of the trap can be explored.

1.1.1 Motivation and research topics

The lines of inquiry of this thesis roughly fall into four categories, although they are not strictly divided up as such between the chapters.

The first challenge encountered upon developing the theory was the question of whether or not the system, i.e. an electron in a combination of static electric and magnetic fields, has an interpretable potential energy landscape which can be plotted along the three axes in space. This is motivated by a desire to couple these individual motions in a quantum calculation, and so access the associated degrees of freedom experimentally. In Chapter 4 this is first treated classically, and then compared to quantum mechanical results. The most intuitive solution to the problem is quickly found to be inconsistent in quantum form, and the investigation of both the cause and solution to this produce an extensive analysis.

In consequence, the quantum theory of angular momentum in the Penning trap is thoroughly examined. Rather than comprising of three independent harmonic oscillators, the Hamiltonian can be treated as three, two-dimensional harmonic oscillator *systems*, each with its own set of mutually commuting angular momentum algebra. This reveals a total of twelve angular momentum-like operators in the Hilbert space of the problem. This thesis aims to address the question of how they all relate to each other, and how rotation around them affects the spatial coordinates of the system. Development of this framework is crucial in ensuring the robustness of some of the later proposed experimental techniques. This forms the second major topic of the thesis, chiefly discussed in Chapter 5.

The third topic again follows naturally, by studying the behaviour of these angular momentum operators upon a change of the trapping frequency along a particular axis. This is of consequence in the Penning trap, and of particular significance to the Geonium Chip, since the trap is driven to the ultra-elliptical regime [29] by effectively changing the frequencies of the oscillator modes which comprise its Hamiltonian. Thus both the quantum elliptical and ultra-elliptical Penning traps are investigated in Chapter 8.

The other principal research topic in this thesis results from the quantum mechanical treatment of sideband coupling in the Penning trap. First calculated in Chapter 2, it is again addressed in different bases and under different conditions throughout Chapters 7, 8, and 9. The formation of an avoided crossing in the adiabatic energy levels of the coupled quantum system arguably motivates much of the work in this thesis. The observation of the phenomenon leads to at least two potential applications in the Penning trap, which are discussed in Chapters 9 and 10. The adopted dressed-atom formalism enabling these methods could have huge applications in Penning trap experiments.

1.1.2 Basic confinement and types of Penning trap

The term "Geonium" was first used by Dehmelt in reference to the trapping of a single electron, since "ultimately the electron is bound to the earth via the trap structure and the magnet" [30]. In a Penning trap, this binding is provided by two static fields: an electric quadrupole which, in its simplest form, produces the potential $\phi \propto z^2 - (x^2 + y^2)/2$, and a homogeneous magnetic field pointing along the z axis. The former provides a potential minimum and hence confinement along the z axis, and in consequence of the Laplace equation $\nabla^2\phi = 0$, a potential *maximum* in the xy plane. This is illustrated in Figure 1.1.

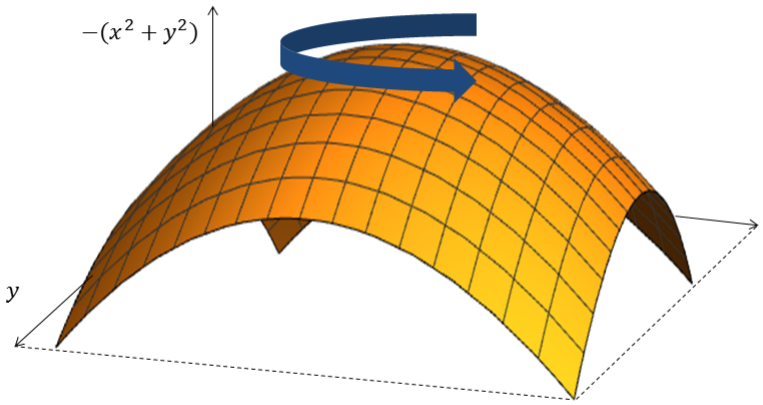

Figure 1.1: A quadrupole potential of the form $\phi \propto z^2 - (x^2+y^2)/2$ produces a two-dimensional inverted oscillator in the xy plane of the Penning trap, atop which the motion of an electron is unbounded. Successful trapping therefore requires radial confinement by an additional magnetic field.

An electron in the presence of a magnetic field $|\vec{B}|\hat{e}_z$ will precess around this field in the perpendicular plane, and providing the Larmor frequency is large enough [14], this counteracts the potential hill of the electric field. The crossing of the fields must also act to alter the motion of the electron from a sum of that induced by the two fields separately. This is considered in more detail in 1.2.1.

The quadrupole electric field can itself be provided in a number of ways, leading to hyperbolic [5] and cylindrical traps [31] in addition to planar traps [25, 32, 33, 34]. As the name suggests, hyperbolic traps use three electrodes which form a hyperbolic shape, with the resultant equipotential surfaces following that of the electrodes. However, they are difficult to manufacture [27], and so cylindrical traps, with the electrodes constructed in tube shapes, were proposed as a result [31]. These traps additionally allowed for easier access to the trapped particle, but *harmonic* trapping requires the addition of two extra electrodes, the so-called correction electrodes, to counteract any anharmonicities created by the cylindrical shape.

In 1.5 the generation of the required trapping fields are considered in the specific case of the Geonium Chip, a planar trap [27]. However, in the following section, the basic classical and quantum theory is discussed for a general trap with cylindrical symmetry.

1.2 The ideal Penning trap with axial rotational symmetry

1.2.1 Classical theory

The Lagrangian and conjugate momenta

For a charged particle in an electromagnetic field, the action of a free particle, and that describing the interaction of the particle with the field, must be considered separately [35]. The properties of an electromagnetic field are characterised by its *four-potential* A_i, comprising three spatial components A_x, A_y and A_z which form the vector potential $\vec{A}$, and one temporal component $A_0 = \phi$, the scalar potential. For a particle with charge q and mass m, the total action is written [36]:

$$\begin{aligned} S &= \int_a^b \left(-mc\,ds - q\,A_i dx^i\right) \\ &= \int_a^b \left(-mc\,ds + q\,\vec{A}\cdot d\vec{r} - q\phi\,dt\right). \end{aligned} \tag{1.1}$$

Changing to an integration over t and taking the non-relativistic limit $v \ll c$ leads to

$$S = \int_{t_1}^{t_2} \left(\frac{1}{2}mv^2 + q\,\vec{A}\cdot\vec{v} - q\phi\right) dt, \tag{1.2}$$

with the resulting Lagrangian of a charged particle in an electromagnetic field given by:

$$\boxed{\mathcal{L} = \frac{1}{2}m\vec{v}^2 - q\phi + q\vec{v}\cdot\vec{A}}. \tag{1.3}$$

The form of this can be verified by employing the Euler-Lagrange equations [37], $\frac{d}{dt}\frac{\partial\mathcal{L}}{\partial\dot{x}_1} - \frac{\partial\mathcal{L}}{\partial x_i} = 0$, which produce the equations of motion, $m\dot{\vec{v}} = q\vec{E} + q\vec{v}\times\vec{B}$. The Lagrange function (1.3) is clearly not of the conventional form $\mathcal{L} = \mathcal{T} - \mathcal{U}$, due to the interaction term $\vec{v}\cdot\vec{A}$; should this be called kinetic energy $\mathcal{T}$, since it depends on the velocity of the particle, or potential $\mathcal{U}$, since it is due to the externally produced field [35]? In fact, this part of the interaction term of the particle and the field *cannot be ascribed to either kinetic or potential energy.* In Chapters 4 and 6, the question of whether this is possible following transformation to an alternate reference frame for both a classical and quantum system is discussed in detail.

From the Lagrangian (1.3) the form of the conjugate momenta follows [37]

$$p_i = \frac{\delta\mathcal{L}}{\delta v_i} = mv_i + qA_i. \tag{1.4}$$

The subsequent Hamiltonian is then given by:

$$\begin{aligned} \mathcal{H} &= \vec{v}\cdot\vec{p} - \mathcal{L} \\ &= \frac{1}{2}m\vec{v}^2 + q\phi, \end{aligned} \tag{1.5}$$

where

$$\vec{v} = \frac{1}{m}\left(\vec{p} - q\vec{A}\right). \tag{1.6}$$

The form of this velocity, or equivalently the conjugate momentum in (1.4), is a direct consequence of the field-particle interaction term in the Lagrangian (1.3). It is highly significant in the Penning trap; the non-zero Poisson brackets of the components [37]

$$\{v_x, v_y\} = \frac{1}{m}\left(\frac{\partial v_y}{\partial A_y}\frac{\partial A_y}{\partial x} - \frac{\partial v_x}{\partial A_x}\frac{\partial A_x}{\partial y}\right) \neq 0, \tag{1.7}$$

hints at the consequence of these expressions for $\vec{v}$.

Classical Hamiltonian of the Penning trap

As discussed in 1.1, confinement in a Penning trap is provided by a static, homogeneous magnetic field $\vec{B}$ and a static electric field $\vec{E}$ derived from a potential ϕ whose ideal form for a cylindrically symmetric, or circular trap, is that of the quadrupole. Throughout this thesis, trapping is considered either in this ideal configuration, or in the ideal elliptical trap which is detailed in 1.5. The distinction will be made where appropriate.

The following fields provide the basic trapping mechanism:

$$\vec{B} = |\vec{B}|\hat{e}_z, \tag{1.8}$$

$$\vec{E} = -\vec{\nabla}\phi, \tag{1.9}$$

where

$$\phi = U_0\left(z^2 - \frac{x^2 + y^2}{2}\right). \tag{1.10}$$

The units of U_0 are Vm^{-2} and the sign of this field curvature will be seen to depend upon the charge of the trapped particle in (1.14). The Coulomb gauge $\vec{\nabla}\cdot\vec{A} = 0$ [38] leads to the convenient form [14] of the magnetic potential $\vec{A} = \frac{1}{2}\vec{B}\times\vec{r}$, which admits the components

$$A_x = -\frac{1}{2}By, \quad A_y = \frac{1}{2}Bx, \quad A_z = 0. \tag{1.11}$$

Expanding out Hamiltonian (1.5):

$$\begin{aligned}\mathcal{H} = \frac{1}{2m}\big(&p_x^2 + p_y^2 + p_z^2 - 2q(p_xA_x + p_yA_y + p_zA_z)\\ &+q^2(A_x^2 + A_y^2 + A_z^2)\big) + q\phi,\end{aligned} \tag{1.12}$$

and inserting (1.10, 1.11):

$$\mathcal{H} = \frac{1}{2m}\left(p_x^2 + p_y^2 + p_z^2 - qB\left(xp_y - yp_x\right) + \left(\frac{qB}{2}\right)^2\left(x^2+y^2\right)\right) + \frac{1}{2}m\omega_z^2\left(z^2 - \frac{x^2+y^2}{2}\right). \tag{1.13}$$

The frequencies

$$\omega_c = \frac{|q||\vec{B}|}{m}, \quad \omega_1 = \sqrt{\omega_c^2 - 2\omega_z^2}, \quad \omega_z = \sqrt{\frac{2qU_0}{m}}, \tag{1.14}$$

are defined, and at this point the charge

$$q = -e \tag{1.15}$$

is inserted for electron trapping, so that the classical Hamiltonian in the laboratory frame is written:

$$\boxed{\mathcal{H} = \frac{1}{2m}\left(p_x^2 + p_y^2 + p_z^2\right) + \frac{\omega_c}{2}\left(xp_y - yp_x\right) + \frac{1}{8}m\omega_1^2\left(x^2+y^2\right) + \frac{1}{2}m\omega_z^2 z^2}. \tag{1.16}$$

Equations of motion

The equations of motion of an electron in the fields defined in (1.8) and (1.9) are obtained from $\vec{F} = -e\vec{E} - e(\vec{v}\times\vec{B})$:

$$\ddot{z} = \frac{2eU_0}{m}z, \tag{1.17}$$

$$\begin{pmatrix}\ddot{x}\\ \ddot{y}\end{pmatrix} = -\frac{e\,U_0}{m}\begin{pmatrix}1 & 0\\ 0 & 1\end{pmatrix}\begin{pmatrix}x\\ y\end{pmatrix} - \frac{e|\vec{B}|}{m}\begin{pmatrix}0 & 1\\ -1 & 0\end{pmatrix}\begin{pmatrix}\dot{x}\\ \dot{y}\end{pmatrix}. \tag{1.18}$$

The radial motions are decoupled by rotation of the vector $\vec{r}$ by a unitary matrix $\underline{U}$, where

$$\underline{U} = \frac{1}{\sqrt{2}}\begin{pmatrix}1 & -i\\ -i & 1\end{pmatrix}, \tag{1.19}$$

so that (1.18) becomes

$$\underline{U}\begin{pmatrix}\ddot{x}\\ \ddot{y}\end{pmatrix} = -\frac{e\,U_0}{m}\underline{U}\begin{pmatrix}1 & 0\\ 0 & 1\end{pmatrix}\underline{U}^\dagger\cdot\underline{U}\begin{pmatrix}x\\ y\end{pmatrix} - \frac{e|\vec{B}|}{m}\underline{U}\begin{pmatrix}0 & 1\\ -1 & 0\end{pmatrix}\underline{U}^\dagger\cdot\underline{U}\begin{pmatrix}\dot{x}\\ \dot{y}\end{pmatrix}. \tag{1.20}$$

The new coordinates r_+ and r_- then admit the equations of motion

$$\begin{pmatrix}\ddot{r}_+\\ \ddot{r}_-\end{pmatrix} = -\frac{eU_0}{m}\begin{pmatrix}r_+\\ r_-\end{pmatrix} - \frac{e|\vec{B}|}{m}i\begin{pmatrix}1 & 0\\ 0 & -1\end{pmatrix}\begin{pmatrix}\dot{r}_+\\ \dot{r}_-\end{pmatrix}; \tag{1.21}$$

$$r_+ = \frac{1}{\sqrt{2}}(x - iy) \quad r_- = \frac{1}{\sqrt{2}}(y - ix). \tag{1.22}$$

The original coordinates are given by

$$\begin{pmatrix} x \\ y \end{pmatrix} = \underline{U}^{\dagger} \begin{pmatrix} r_{+} \\ r- \end{pmatrix}, \tag{1.23}$$

and the decoupled solutions are found:

$$\begin{aligned} x(t) &= A_{+}\sin(\omega_{+}t + \varphi_{+}) + A_{-}\sin(\omega_{-}t + \varphi_{-}), \\ y(t) &= A_{+}\cos(\omega_{+}t + \varphi_{+}) + A_{-}\cos(\omega_{-}t + \varphi_{-}), \end{aligned} \tag{1.24}$$

along with the straightforward axial motion

$$z(t) = A_z \cos(\omega_z t). \tag{1.25}$$

The amplitudes of the motion are given by [39]

$$A_{+} = \sqrt{\frac{2E_{+}}{m(\omega_{+}^2 - \frac{\omega_z^2}{2})}}, \quad A_{-} = \sqrt{\frac{2E_{-}}{m(\omega_{-}^2 - \frac{\omega_z^2}{2})}}, \quad A_z = \sqrt{\frac{2E_z}{m\omega_z^2}}, \tag{1.26}$$

The energies E_{+}, E_{-} and E_z of the modes are controlled via the cryogenic cooling of the system [14]:

$$E_{+} = k_B T_{+}, \quad E_{-} = k_B T_{-}, \quad E_z = k_B T_z, \tag{1.27}$$

and the cyclotron $(+)$ and magnetron $(-)$ mode frequencies are defined

$$\boxed{\omega_{+} = \frac{1}{2}(\omega_c + \omega_1) \quad \omega_{-} = \frac{1}{2}(\omega_c - \omega_1)}, \tag{1.28}$$

where ω_c, ω_1, and ω_z are given in (1.14). For an electron in a strong magnetic field ($|\vec{B}| \gtrsim 0.5\,\mathrm{T}$), the general hierarchy of the trapping frequencies is [14]

$$\boxed{\omega_{+} \gg \omega_z \gg \omega_{-}}, \tag{1.29}$$

with

$$\omega_{+} \sim \mathrm{GHz}, \quad \omega_z \sim \mathrm{MHz}, \quad \omega_{-} \sim \mathrm{kHz}. \tag{1.30}$$

This is the regime of the Geonium Chip trap [27], and as such will be assumed throughout this thesis unless otherwise stated.

For traps held at liquid helium temperatures, coupling of the detection circuit to the motional modes results in [14]:

$$T_{+} = 4.2\,\mathrm{K}, \quad T_z = 4.2\,\mathrm{K}, \quad T_{-} = -T_z \left(\frac{\omega_{-}}{\omega_z}\right). \tag{1.31}$$

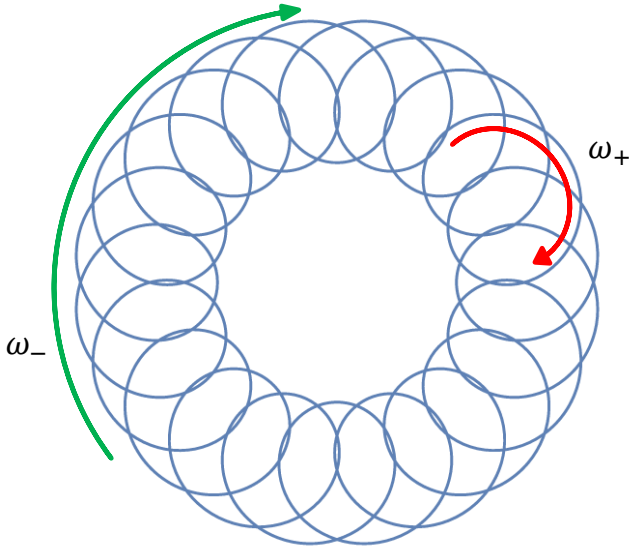

Figure 1.2: From (1.24), the radial motion of a charged particle in the circular Penning trap traces out an epicyclic curve. The cyclotron motion with amplitude A_+ and frequency ω_+ is superposed onto a slow magnetron drift orbit with amplitude A_- and frequency ω_-. The relative size of the orbits are not drawn to scale: from (1.33), $A_-/A_+ \approx 3 \times 10^3$.

From (1.26), the requirement $A_+ \in \Re$ imposes the following trapping condition [14] upon the relative sizes of ω_+ and ω_z:

$$\boxed{\omega_+ > \frac{\omega_z}{\sqrt{2}}}. \tag{1.32}$$

From (1.29) and (1.31), $\omega_- < \omega_z$, and $E_- < 0$ respectively, which guarantees $A_- \in \Re$. The curious nature of this negative thermal energy is further discussed in 1.4.1, but for now it is straightforward to verify that a lower temperature T_z results in a larger (less negative) energy E_-, and from (1.26), a smaller amplitude A_-. In this way, the magnetron motion can be bounded.

From (1.24), the motion of the electron in the radial plane is therefore given by an epicyclic orbit, comprising a fast rotation of frequency ω_+ superposed upon a slow magnetron drift at ω_-, as shown in Figure 1.2. From (1.25), the axial motion is simply given by harmonic oscillation at frequency ω_z. For an electron in a trap with typical values of $B = 0.5\,\mathrm{T}$ and $V_r = -1\mathrm{V}$:

$$A_+ \approx 0.1\mu\mathrm{m}, \quad A_- \approx 3\mathrm{mm}, \quad A_z \approx 90\mu\mathrm{m}, \tag{1.33}$$

so that the orbits in Figure 1.2 are not to scale. A discussion of how this radial orbit varies with the axial confinement is given in 3.3.

The average quantum number of the modes can be found from the simple energy equality $\hbar\omega_+\overline{n}_+ = k_B T_+$. At $T = 4.2\,\mathrm{K}$, and for sufficiently strong $\vec{B}$ fields, a quantum

mechanical description of the cyclotron motion is therefore required for an electron in the trap [14]. For further cooling of the system down to mK, this is also true for the axial and magnetron motions, as shall be discussed further in 1.4.

1.3 Existing quantum theory

1.3.1 Hamiltonian

To quantize Hamiltonian (1.16), the standard procedure is to first decouple the motions by defining the canonically conjugate variables [15]:

$$\begin{aligned}
q_+ &= \frac{1}{\sqrt{2}}\left(\sqrt{\frac{m\omega_1}{2}}x + \sqrt{\frac{2}{m\omega_1}}p_y\right), \\
q_- &= \frac{1}{\sqrt{2}}\left(\sqrt{\frac{m\omega_1}{2}}x - \sqrt{\frac{2}{m\omega_1}}p_y\right), \\
p_+ &= \frac{1}{\sqrt{2}}\left(-\sqrt{\frac{m\omega_1}{2}}y + \sqrt{\frac{2}{m\omega_1}}p_x\right), \\
p_- &= \frac{1}{\sqrt{2}}\left(\sqrt{\frac{m\omega_1}{2}}y + \sqrt{\frac{2}{m\omega_1}}p_x\right), \\
q_z &= \sqrt{m\omega_z}z, \\
p'_z &= \frac{1}{\sqrt{m\omega_z}}p_z \equiv p_z.
\end{aligned} \tag{1.34}$$

Quantization is then achieved by interpreting the classical canonical variables as Hilbert space operators with equal time commutation relations [28]:

$$[\hat{q}_j(t), \hat{p}_k(t)] = i\hbar\delta_{j,k}, \quad [\hat{q}_j(t), \hat{q}_k(t)] = [\hat{p}_j(t), \hat{p}_k(t)] = 0. \tag{1.35}$$

Thus Hamiltonian (1.16) is written:

$$\hat{\mathcal{H}} = \frac{1}{2}\omega_+\left(\hat{q}_+^2 + \hat{p}_+^2\right) - \frac{1}{2}\omega_-\left(\hat{q}_-^2 + \hat{p}_-^2\right) + \frac{1}{2}\omega_z\left(\hat{q}_z^2 + \hat{p}_z^2\right). \tag{1.36}$$

Creation and annihilation operators are now constructed from the above canonically conjugate pairs [28]:

$$\begin{aligned}
\hat{a}_+ &= \frac{1}{\sqrt{2\hbar}}(\hat{q}_+ + i\hat{p}_+) = \frac{1}{2\sqrt{\hbar}}\left(\sqrt{\frac{m\omega_1}{2}}(\hat{x} - i\hat{y}) + \sqrt{\frac{2}{m\omega_1}}(\hat{p}_y + i\hat{p}_x)\right), \\
\hat{a}_+^\dagger &= \frac{1}{\sqrt{2\hbar}}(\hat{q}_+ - i\hat{p}_+) = \frac{1}{2\sqrt{\hbar}}\left(\sqrt{\frac{m\omega_1}{2}}(\hat{x} + i\hat{y}) + \sqrt{\frac{2}{m\omega_1}}(\hat{p}_y - i\hat{p}_x)\right), \\
\hat{a}_- &= \frac{1}{\sqrt{2\hbar}}(\hat{q}_- + i\hat{p}_-) = \frac{1}{2\sqrt{\hbar}}\left(\sqrt{\frac{m\omega_1}{2}}(\hat{x} + i\hat{y}) - \sqrt{\frac{2}{m\omega_1}}(\hat{p}_y - i\hat{p}_x)\right), \\
\hat{a}_-^\dagger &= \frac{1}{\sqrt{2\hbar}}(\hat{q}_- - i\hat{p}_-) = \frac{1}{2\sqrt{\hbar}}\left(\sqrt{\frac{m\omega_1}{2}}(\hat{x} - i\hat{y}) - \sqrt{\frac{2}{m\omega_1}}(\hat{p}_y + i\hat{p}_x)\right), \\
\hat{a}_z &= \frac{1}{\sqrt{2\hbar}}(\hat{q}_z + i\hat{p}_z) = \frac{1}{\sqrt{2\hbar}}\left(\sqrt{m\omega_z}\hat{z} + i\frac{1}{\sqrt{m\omega_z}}\hat{p}_z\right), \\
\hat{a}_z^\dagger &= \frac{1}{\sqrt{2\hbar}}(\hat{q}_z - i\hat{p}_z) = \frac{1}{\sqrt{2\hbar}}\left(\sqrt{m\omega_z}\hat{z} - i\frac{1}{\sqrt{m\omega_z}}\hat{p}_z\right),
\end{aligned} \tag{1.37}$$

so that the Hamiltonian can be written as a sum of uncoupled quantum harmonic oscillators:

$$\boxed{\hat{\mathcal{H}} = \hbar\omega_+\left(\hat{a}_+^\dagger\hat{a}_+ + \frac{1}{2}\right) - \hbar\omega_-\left(\hat{a}_-^\dagger\hat{a}_- + \frac{1}{2}\right) + \hbar\omega_z\left(\hat{a}_z^\dagger\hat{a}_z + \frac{1}{2}\right)}, \tag{1.38}$$

with the mode frequencies defined in (1.80) and (1.28). The negative sign in front of the magnetron motion is worth emphasising. It is a direct result of the particle-field interaction term in the Lagrangian (1.3). It is also important to note the mixing of $\hat{x}$ and $\hat{y}$, $\hat{p}_x$ and $\hat{p}_y$ operators for future discussion.

By inverting the operator definitions in (1.37), the operators $\hat{x}(t)$, $\hat{y}(t)$ and $\hat{z}(t)$ can be expressed [28]:

$$\begin{aligned}
\hat{x}(t) &= \sqrt{\frac{\hbar}{2m\omega_1}}\left(\hat{a}_+^\dagger(t) + \hat{a}_+(t) + \hat{a}_-^\dagger(t) + \hat{a}_-(t)\right), \\
\hat{y}(t) &= -i\sqrt{\frac{\hbar}{2m\omega_1}}\left(\hat{a}_+^\dagger(t) - \hat{a}_+(t) - \hat{a}_-^\dagger(t) + \hat{a}_-(t)\right), \\
\hat{z}(t) &= \sqrt{\frac{\hbar}{2m\omega_z}}\left(\hat{a}_z^\dagger(t) + \hat{a}_z(t)\right).
\end{aligned} \tag{1.39}$$

The time dependence of the creation and annihilation operators follows from the Heisenberg equations of motion $i\hbar\partial_t\hat{A} = \left[\hat{A}, \hat{H}\right]$ [40]:

$$\begin{aligned}
\hat{a}_+(t) &= \hat{a}_+e^{-i\omega_+t}; \qquad \hat{a}_+^\dagger(t) = \hat{a}_+^\dagger e^{i\omega_+t}, \\
\hat{a}_-(t) &= \hat{a}_-e^{i\omega_-t}; \qquad \hat{a}_-^\dagger(t) = \hat{a}_-^\dagger e^{-i\omega_-t}, \\
\hat{a}_z(t) &= \hat{a}_ze^{-i\omega_zt}; \qquad \hat{a}_z^\dagger(t) = \hat{a}_z^\dagger e^{i\omega_zt},
\end{aligned} \tag{1.40}$$

where $\hat{a} \equiv \hat{a}(0)$, $\hat{a}^\dagger \equiv \hat{a}^\dagger(0)$. In this way, the electron trajectories can be calculated from the expectation values of (1.39).

1.3.2 States and expectation values

The quantum Hamiltonian (1.38) admits Fock state solutions [41]

$$|n_+, n_-, n_z\rangle = \frac{1}{\sqrt{n_+!\, n_-!\, n_z!}} \cdot (\hat{a}_+^\dagger)^{n_+} (\hat{a}_-^\dagger)^{n_-} \hat{a}_z^\dagger)^{n_z} |0_+ 0_- 0_z\rangle, \tag{1.41}$$

in addition to time dependent three mode quasi-classical coherent states [28]:

$$\begin{aligned} |\alpha_+(t)\alpha_-(t)\alpha_z(t)\rangle &= |\alpha_+ e^{-i\omega_+ t} \alpha_- e^{i\omega_- t} \alpha_z e^{-i\omega_z t}\rangle \\ &= \hat{D}(\alpha_+(t))\hat{D}(\alpha_-(t))\hat{D}(\alpha_z(t))|0_+0_-0_z\rangle. \end{aligned} \tag{1.42}$$

Here, $\hat{D}(\alpha(t))$ is a general one dimensional time dependent displacement operator which acts on the vacuum state as follows [41]

$$\begin{aligned} \hat{D}(\alpha(t))|0\rangle &= \exp\left[\alpha(t)\hat{a}^\dagger - \alpha^*(t)\hat{a}\right]|0\rangle \\ &= e^{-|\alpha|^2} \sum_{n=0}^{\infty} \frac{(\alpha(t))^n}{\sqrt{n!}} |n\rangle. \end{aligned} \tag{1.43}$$

From (1.39), expectation values of the semi-classical trajectories can be calculated in these coherent states. For example, defining the complex amplitudes $\alpha_+ = |\alpha_+| \exp(-i(\phi_+))$ and $\alpha_- = |\alpha_-| \exp(i(\phi_-))$ leads to:

$$\begin{aligned} \langle \hat{x}(t)\rangle &= \sqrt{\frac{\hbar}{2m\omega_1}} \left(\alpha_+^*(t) + \alpha_+(t) + \alpha_-^*(t) + \alpha_-(t)\right), \\ &= \sqrt{\frac{\hbar}{2m\omega_1}} \left(2|\alpha_+| \cos(\omega_+ t + \phi_+) + 2|\alpha_-| \cos(\omega_- t + \phi_-)\right). \end{aligned} \tag{1.44}$$

An arbitrary phase shift $\phi_+ \to \phi_+ - \pi/2$, $\phi_- \to \phi_- - \pi/2$ reveals

$$\langle \hat{x}(t)\rangle = \sqrt{\frac{2\hbar}{m\omega_1}} \left(|\alpha_+| \sin(\omega_+ t + \phi_+) + |\alpha_-| \sin(\omega_- t + \phi_-)\right), \tag{1.45}$$

which corresponds exactly to the classical solution in (1.24) upon assigning

$$A_+ = \sqrt{\frac{2\hbar}{m\omega_1}} |\alpha_+|, \quad A_- = \sqrt{\frac{2\hbar}{m\omega_1}} |\alpha_-|. \tag{1.46}$$

1.3.3 Spin and the electron g-factor

A particle with magnetic moment $\vec{\mu}$ in a magnetic field $\vec{B}$ must contribute the spin-field interaction Hamiltonian [40]

$$\hat{\mathcal{H}}_s = -\vec{\mu} \cdot \vec{B}. \tag{1.47}$$

For an electron in the Penning trap, this results in [14]

$$\hat{\mathcal{H}}_s = \frac{g}{2} \hbar \omega_c \frac{1}{2} \sigma_z, \tag{1.48}$$

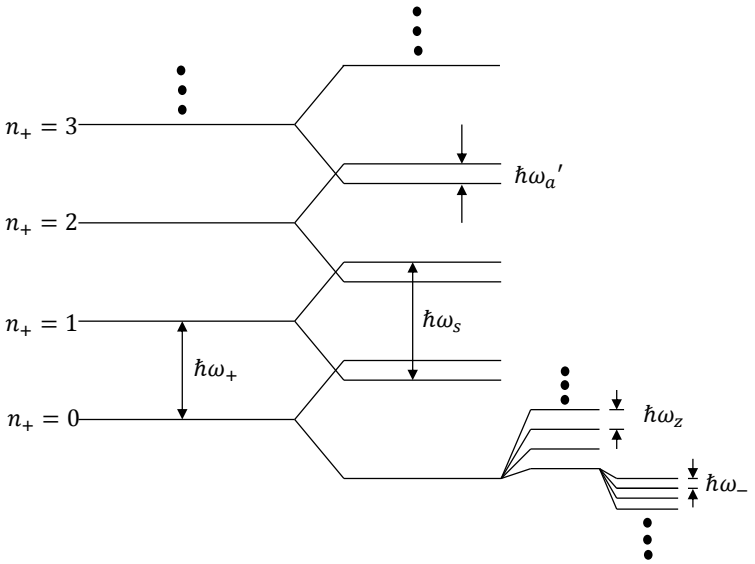

Figure 1.3: Splitting of the energy levels in the Penning trap. From left to right, each cyclotron level is split by the $\pm\frac{1}{2}$ spin values of the electron. Each of these levels is then split by the axial confinement, and finally by the negative energy of the magnetron motion [14].

where σ_z is the usual z, or third component Pauli matrix [41]

$$\sigma_z = \begin{pmatrix} 1 & 0 \\ 0 & -1 \end{pmatrix}. \tag{1.49}$$

Penning trap literature [14] commonly defines

$$\omega_s = \frac{g}{2}\omega_c, \tag{1.50}$$

so that

$$\hat{\mathcal{H}}_s = \hbar\omega_s \frac{1}{2}\sigma_z. \tag{1.51}$$

In this way the g-factor of a spin-$\frac{1}{2}$ particle can be expressed as the dimensionless ratio of two frequencies of the Penning trap:

$$\frac{g}{2} = \frac{\omega_s}{\omega_c}. \tag{1.52}$$

In terms of the directly measurable frequencies, the *anomaly* is given by

$$a = \frac{g}{2} - 1 = \frac{\omega_a^{'} - \omega_-}{\omega_+ + \omega_-}, \tag{1.53}$$

where

$$\omega_a^{'} = \omega_s - \omega_+. \tag{1.54}$$

Furthermore, the powerful Brown-Gabrielse invariance theorem of the trap [42]

$$\omega_+^2 + \omega_z^2 + \omega_-^2 = \omega_c^2 \tag{1.55}$$

ensures that trap misalignments of the $\vec{B}$ field and imperfections of the trap electrodes do not affect the precision with which a can be determined [14].

The energy levels of the motional modes plus those of the spin degree of freedom are depicted in Figure 1.3, where the relative splitting between the levels for each mode is not drawn to scale. For the remainder of this thesis however, the spin contribution to the Hamiltonian will be neglected as it remains unchanged throughout all the calculations.

1.4 The temperature of the Penning trap

The above discussion has focused on well known Penning trap theory, and has laid out the framework for classical and quantum calculation. The work in this thesis aims to explore extended theoretical possibilities of the Penning trap in an exclusively quantum regime, so this section will define such a regime, and discuss the thermal state of the Penning trap as governed by finite temperature.

1.4.1 Thermal states

Since the temperature of the trap is held at T_+, T_- and T_z for the three modes, the probability of excitation of states with respective energy $\hbar\omega_+(n_+ + 1/2)$, $-\hbar\omega_-(n_- + 1/2)$ and $\hbar\omega_z(n_z + 1/2)$ must be those predicted by statistical mechanics.

General thermal states

In thermal equilibrium, the state of a system with Hamiltonian $\hat{H}$ is represented by the density matrix operator [41]

$$\hat{\rho} = \frac{\exp(-\beta\hat{H})}{Tr[\exp(-\beta\hat{H})]}, \tag{1.56}$$

where $\beta = (k_B T)^{-1}$. For a general harmonic oscillator Hamiltonian with quantum number n and frequency ω, this becomes

$$\hat{\rho} = \frac{\exp(-\beta\hbar\omega\left(\hat{n} + \frac{1}{2}\right))}{Tr[\exp(-\beta\hbar\omega\left(\hat{n} + \frac{1}{2}\right))]}. \tag{1.57}$$

The normalisation factor of (1.57) is the partition function $\mathcal{Z}$, evaluated to [43]

$$\begin{aligned}\mathcal{Z} &= Tr\left[\exp\left(-\beta\hbar\omega\left(\hat{n} + \frac{1}{2}\right)\right)\right] \\ &= \frac{\exp(-\beta\hbar\omega/2)}{1 - \exp(-\beta\hbar\omega)}.\end{aligned} \tag{1.58}$$

The probability of occupying energy level n is given by the diagonal matrix elements of $\hat{\rho}$ [43]:

$$\begin{aligned}P(n) = \langle n|\hat{\rho}|n\rangle &= \frac{1}{\mathcal{Z}}\langle n|\exp\left(-\beta\hbar\omega\left(\hat{n} + \frac{1}{2}\right)\right)|n\rangle \\ &= \exp(-\beta\hbar\omega n)(1 - \exp(-\beta\hbar\omega)),\end{aligned} \tag{1.59}$$

and the off-diagonal terms are zero:

$$\begin{aligned}\rho_{nm} = \langle n|\hat{\rho}|m\rangle &= \frac{1}{\mathcal{Z}}\langle n|\exp\left(-\beta\hbar\omega\left(\hat{n} + \frac{1}{2}\right)\right)|m\rangle \\ &= \rho_{nn}\delta_{nm}.\end{aligned} \tag{1.60}$$

The mean occupation number is given by [41]

$$\begin{aligned}\overline{n} = \langle\hat{n}\rangle &= Tr\left[\hat{\rho}\hat{n}\right] \\ &= \frac{1}{\exp(\beta\hbar\omega) - 1}.\end{aligned} \tag{1.61}$$

The thermal states of the three oscillator modes of the Penning trap are governed in this way by the external temperatures T_+, T_- and T_z. The resulting classical energies given in (1.27) follow from the well known result from statistical mechanics [43]

$$\langle E \rangle = -\frac{\partial}{\partial \beta} \ln \mathcal{Z} \tag{1.62}$$

for the separate partition function $\mathcal{Z}$, and β of each mode.

The magnetron motion

Due to its negative energy contribution in Hamiltonian (1.38), care must be taken when treating the thermal state behaviour of the magnetron motion. The long radiative decay time of this motion [14] ensures that it is never in thermal equilibrium with the blackbody radiation of the trap, so it must in fact be cooled separately to achieve the limiting expression of T_- in (1.31) [14]. The mechanism of this cooling [44] is discussed more fully in Chapter 2.

Labelling the magnetron contribution in the Hamiltonian (1.38)

$$\hat{\mathcal{H}}_- = -\hbar\omega_- \left(\hat{n}_- + \frac{1}{2}\right), \tag{1.63}$$

this is compared to the average thermal energy of this motion

$$\langle E_- \rangle = k_B T_- = -k_B T_z \left(\frac{\omega_-}{\omega_z}\right). \tag{1.64}$$

The effective β for this mode is therefore

$$\beta_- = \frac{1}{k_B T_-} = -\frac{1}{k_B T_z}\frac{\omega_z}{\omega_-}. \tag{1.65}$$

Now, both β_- and $\hat{\mathcal{H}}_-$ contribute negative terms in a density operator of the system in thermal equilibrium in (1.56), so that the overall sign of $\hat{\rho}_-$, the density operator of the thermal state of the magnetron motion, will remain unchanged from that of a standard harmonic oscillator:

$$\hat{\rho}_- = \frac{\exp(-|\beta_-|\hbar\omega_-\left(\hat{n}_- + \frac{1}{2}\right))}{Tr[\exp(-|\beta_-|\hbar\omega_-\left(\hat{n}_- + \frac{1}{2}\right))]}. \tag{1.66}$$

In this way, the results in (1.59) and (1.61) follow analogously for the magnetron mode, with $\beta_- \to |\beta_-|$.

The combined thermal state of the Penning trap

Treating the three mode of the electron as independent and distinct, the density matrix of the Penning trap is given by [43]

$$\hat{\rho}_{\pm,z} = \hat{\rho}_+ \bigotimes \hat{\rho}_- \bigotimes \hat{\rho}_z. \tag{1.67}$$

Identifying $T_+ = T_z \equiv T$ from (1.31), the values of β for each mode become similarly linked:

$$\begin{aligned} \beta_+ = \beta_z &= \frac{1}{k_B T} \equiv \beta, \\ \implies \beta_- &= -\frac{1}{k_B T}\frac{\omega_z}{\omega_-} = -\beta\frac{\omega_z}{\omega_-}. \end{aligned} \tag{1.68}$$

The density matrix operators in (1.67) are then given explicitly by

$$\begin{aligned} \hat{\rho}_+ &= \frac{\exp(-\beta\hbar\omega_+\left(\hat{n}_+ + \frac{1}{2}\right))}{Tr[\exp(-\beta\hbar\omega_+\left(\hat{n}_+ + \frac{1}{2}\right))]}, \\ \hat{\rho}_- &= \frac{\exp(-\beta\hbar\omega_z\left(\hat{n}_- + \frac{1}{2}\right))}{Tr[\exp(-\beta\hbar\omega_z\left(\hat{n}_- + \frac{1}{2}\right))]}, \\ \hat{\rho}_z &= \frac{\exp(-\beta\hbar\omega_z\left(\hat{n}_z + \frac{1}{2}\right))}{Tr[\exp(-\beta\hbar\omega_z\left(\hat{n}_z + \frac{1}{2}\right))]}, \end{aligned} \tag{1.69}$$

noting the dependence $\hat{\rho}_- \equiv \hat{\rho}_-(\omega_z)$. In fact, (1.58) shows that the partition functions of the axial and magnetron modes are identical, as are the mean occupation numbers of these modes:

$$\overline{n}_z = \frac{1}{\exp(\beta\hbar\omega_z) - 1} = \overline{n}_-. \tag{1.70}$$

This is the result of the mode coupling used to cool the magnetron motion [44]. The total probability of occupation of the state $|n_+ n_- n_z\rangle$ is given by the product of the independent probabilities of each mode:

$$\begin{aligned} P(n_+ n_- n_z) &= P(n_+) \cdot P(n_-) \cdot P(n_z) \\ &= \exp\left(-\beta\hbar(\omega_+ n_+ + \omega_z(n_- + n_z))\right) \cdot (1 - \exp(-\beta\hbar\omega_+)) \cdot (1 - \exp(-\beta\hbar\omega_z))^2 . \end{aligned} \tag{1.71}$$

1.4.2 The average quantum number

From (1.61), the average quantum number of each of the motions is determined by the trap temperature and the appropriate mode frequency. Since all three frequencies are dependent on $1/m$, for a given temperature T the mean quantum number of an electron in the trap is significantly lower than for other charged particles, making its quantum regime more accessible [14].

Unless otherwise stated, a ring voltage $V_r = -1\,\mathrm{V}$ and magnetic field $|\vec{B}| = 0.5\,\mathrm{T}$ will be assumed throughout this thesis. At liquid helium temperature $T = 4.2\,\mathrm{K}$, this results in the following average quantum numbers for an electron:

$$\begin{aligned} &T = 4.2\ \mathrm{K}: \\ &\implies \overline{n}_+ = 5.8, \quad \overline{n}_z = \overline{n}_- = 4372. \end{aligned} \tag{1.72}$$

There are two ways in which the quantum numbers of the axial and magnetron motion can be lowered. The first is by direct cooling of the trap to mK temperatures by use of a dilution refrigerator [45]:

$$\begin{aligned} &T = 80\,\mathrm{mK}: \\ &\implies \overline{n}_+ = 0.0002, \quad \overline{n}_z = \overline{n}_- = 82.7. \end{aligned} \tag{1.73}$$

The second method requires coupling of the axial and cyclotron motions which reduces $\overline{n}_z$ until $\overline{n}_z = \overline{n}_+$. This will be discussed extensively in Chapter 2. Cooling to the ground state of ions in a Penning trap has been successfully achieved by this method [46]. Further lowering of the axial quantum number is also possible by increasing the trap depth, i.e. by increasing the ring voltage.

For the purposes of this thesis, the *low temperature regime*, and one requiring quantum treatment, will refer to temperatures resulting in an average quantum number $\overline{n} \lesssim 100$ of the modes being discussed. Calculations involving classical mechanics will be included for comparison only, and unless otherwise stated, this low temperature regime should be assumed. The thermal distribution of the system should be included when considering the physical implementations of any theory in this thesis. Other quantum states, specifically Fock states and coherent states, are investigated for theoretical purposes, in the assumption that the electron could be prepared in these states. Their analysis also serves to lay the foundation for future study of interesting quantum optical states of the Penning trap: thermal coherent states [47], squeezed thermal states [48], and indeed squeezed coherent thermal states [49].

1.5 The Geonium Chip and the elliptical Penning trap

The Geonium trap is in the final stages of construction within the *Geonium group* at Sussex, its purpose being to achieve the precision measurements of existing Penning traps in a more compact device with a planar magnetic field source [27]. Taking advantage of the scalability of design this offers, future generations of the trap could be adapted to explore new possibilities in the field of quantum computation. This section will introduce some of the novel features of the Geonium Chip, laying down the framework for discussion of the low temperature regime of the trap in Chapter 8.

1.5.1 Genesis of the trap

The Geonium Chip is a progression of the coplanar-waveguide (CPW) Penning trap [39] proposed at Sussex. In addition to the magnetic field source being parallel to the surface of the trap, the Geonium Chip also aims to implement both the magnetic field source and the trap electrodes into a single chip [50, 51], offering huge advantages in scalability over other planar Penning traps [25, 32, 33, 34].

As shown in Figures 1.4 and 1.5, the CPW trap is based upon a projection of a standard five electrode cylindrical Penning trap onto a plane, shielded by two outer ground planes. The flattened electrodes form part of a CPW transmission line [39], enabling the possibility of integrating the trapped electron into quantum circuits for quantum electrodynamic (QED) purposes [52, 53].

The Geonium Chip expands the capabilities [29] of the CPW trap by adding two side electrodes to the design shown in Figure 1.4. The trap is then boxed within a closed metallic cavity, the dimensions of which are chosen so that the spontaneous emission of the cyclotron motion is strongly inhibited through the Purcell effect [52].

For electron trapping, a magnetic field of $|\vec{B}| = 0.5\,\mathrm{T}$, resulting in a cyclotron frequency of $\omega_z = 2\pi \cdot 13.99\,\mathrm{GHz}$, allows coupling of the electron cyclotron mode frequency by microwave (MW) photons to other quantum systems [29]. The cavity enclosing the chip suppresses the emission and absorption of these photons, but coupling can be achieved through the near-field of the CPW transmission line [39, 54].

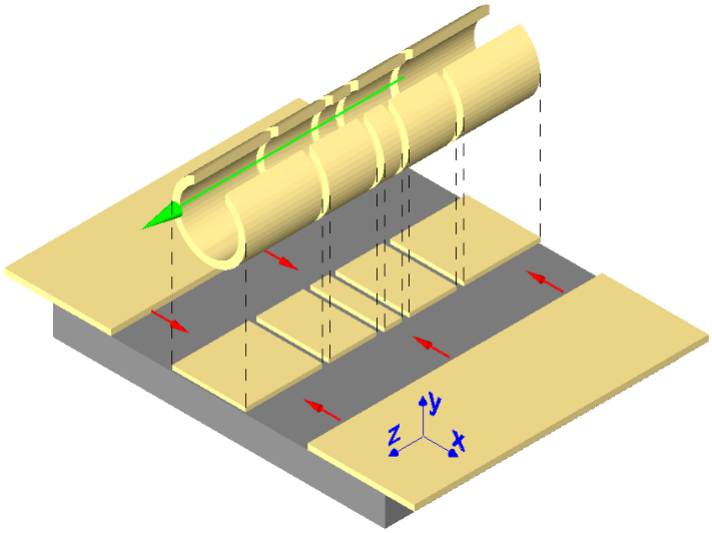

Figure 1.4: The projection of a cylindrical Penning trap onto a plane, with the magnetic field parallel to the z axis. This diagram is taken directly from [39].

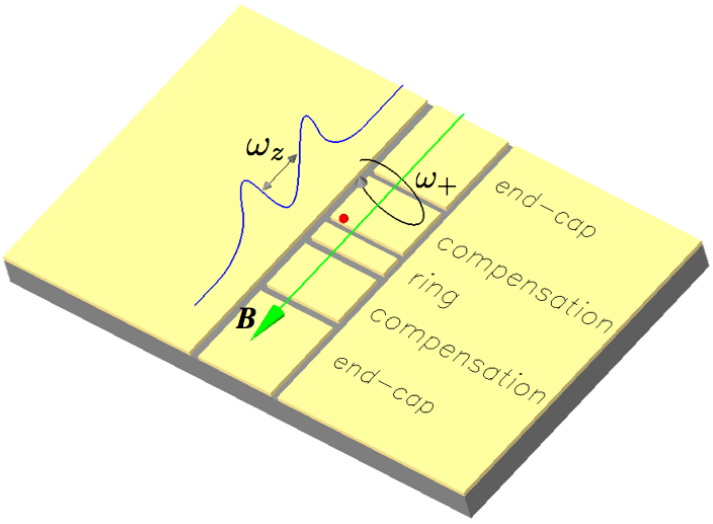

Figure 1.5: The cyclotron and axial motions sketched above the dielectric substrate with the standard five electrodes patterned onto its surface. This diagram is taken directly from [39].

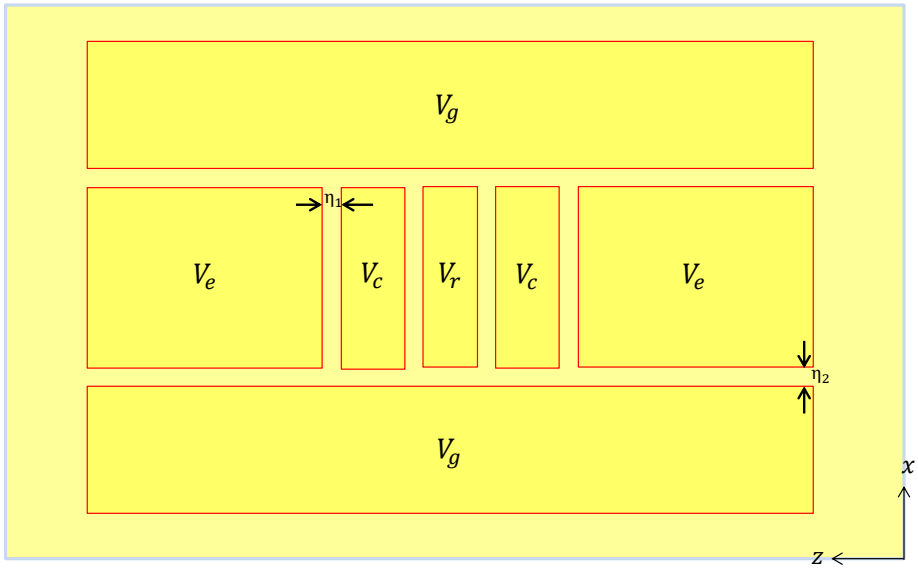

Figure 1.6: Electrode structure of the Geonium Chip, with V_r, V_c, V_e, V_g indicating the ring, correction, endcap, and side-electrode voltage respectively. The ratios of these voltages given in (1.83) define the equilibrium position y_0, and V_r determines the overall trapping potential [29].

1.5.2 Classical theory of the ideal elliptical trap

The electrode structure of the Geonium Chip is shown Figure 1.6, where the insulating gaps η_1 and η_2 can be seen. These must be taken into account when engineering the total trapping potential, which is calculated from the Green's function for the Laplace equation which fulfils Dirichlet's boundary conditions in a box. Details of this calculation is given in [29], and the resulting potential of the Geonium Chip for $V_g = 0$ is shown in Figure 1.7. For the purposes of this thesis, it is sufficient to consider the resulting series expansion of

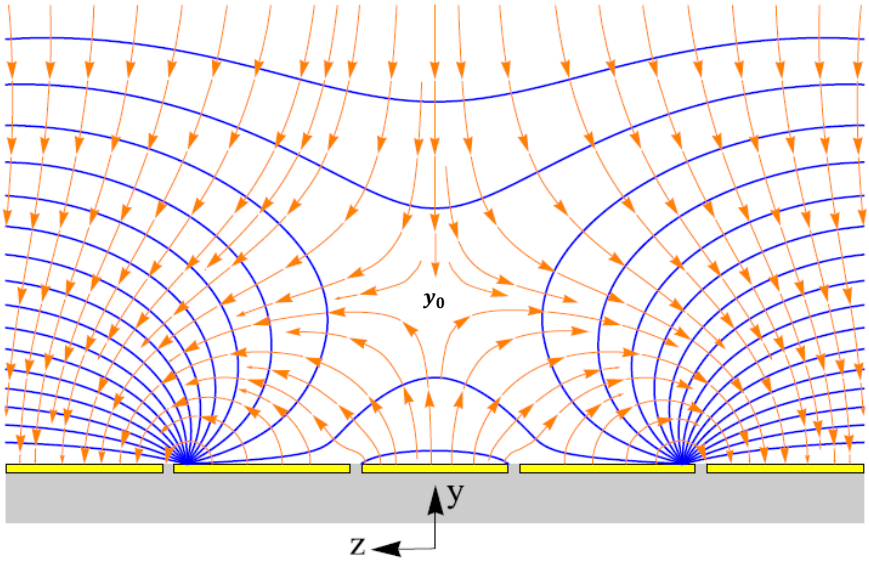

Figure 1.7: The electric field produced by the Geonium Chip with $V_g = 0$ is indicated by the red lines, with the blue lines showing the resulting equipotentials. The quadrupole form of the field is clearly visible at the equilibrium position y_0. The figure is taken from [54].

the electrostatic potential around the equilibrium position of the trap $(0, y_0, 0)$ [39]:

$$\begin{aligned}\Phi(x,y,z) = \Phi(0,y,0) &+ \underbrace{C_{002}z^2 + C_{200}x^2 + C_{020}(y-y_0)^2}_{\phi_\epsilon(x,y,z)} \\ &+ \underbrace{C_{012}z^2(y-y_0) + C_{210}x^2(y-y_0) + C_{030}(y-y_0)^3}_{odd\ anharmonicities} \\ &+ \underbrace{C_{202}z^2x^2 + C_{022}z^2(y-y_0)^2 + C_{220}x^2(y-y_0)^2 + C_{004}z^4 + C_{400}x^4 + C_{040}(y-y_0)^4}_{even\ anharmonicities} \\ &+ ..., \end{aligned} \tag{1.74}$$

where

$$C_{ijk} = V_r\, c_{ijk} \tag{1.75}$$

and

$$c_{ijk} = \frac{1}{i!j!k!} \cdot \frac{\partial^{i+j+k}\Phi(x,y,z)}{\partial x^i \partial y^j \partial z^k}|_{(0,y_0,0)}. \tag{1.76}$$

The vanishing of all C_{ijk} with odd i and/ or k is implied by the symmetry of Φ along the x and z axes, while the remaining contributions must be carefully optimised to remove the anharmonicities and produce an ideal trapping configuration [39]. In this way, these

coefficients are largely responsible for the proficiency of the trap. Constraints imposed by the Laplace equation $\nabla^2\Phi = 0$ lead to [39]

$$C_{200} + C_{020} + C_{002} = 0, \tag{1.77}$$

and indistinguishability of the x and y coordinates for *radially symmetric* traps results in $C_{200} = C_{020}$, so that (1.77) becomes $C_{200} = -2C_{020}$. This results in the potential of an ideal circular trap, where U_0 in (1.10) is given by C_{002}. However, in the Geonium Chip x and y are distinguishable, so that the curvatures C_{200} and C_{020} are non-identical, and the general form of the quadrupole potential including terms only up to the second order is given by [39]

$$\phi_\epsilon(x, y, z) = C_{002} \cdot \left(z^2 - \frac{x^2 + (y - y_0)^2}{2} \right) + \frac{1}{2} C_{002}\epsilon \cdot \left(x^2 - (y - y_0)^2 \right), \tag{1.78}$$

where the *ellipticity parameter* ϵ is defined as

$$\epsilon = \frac{C_{200} - C_{020}}{C_{002}}, \tag{1.79}$$

and $-1 < \epsilon < 1$. If $|\epsilon|$ becomes greater than 1, the magnetron orbit becomes unbounded and the electron is lost from the trap [15]. In this approximation, (1.78) represents the total potential supplied by the Geonium Chip, the *ideal elliptical potential* of a Penning trap [15]. Comparing this to (1.10), the axial frequency in the Geonium Chip is identified as

$$\omega_z = \sqrt{\frac{2V_r\, c_{002}\, q}{m}}, \tag{1.80}$$

so that the Hamiltonian of the Geonium Chip, and the ideal elliptical Penning trap, can be written in terms of the radially symmetric Hamiltonian (1.16):

$$\begin{aligned} \mathcal{H}_\epsilon &= \mathcal{H} + \frac{1}{4}\epsilon m\omega_z^2(x^2 - y^2) \\ &= \frac{1}{2m}(p_x^2 + p_y^2 + p_z^2) + \frac{\omega_c}{2}(xp_y - yp_x) \\ &\quad + \frac{1}{8}m\omega_c^2(x^2 + y^2) - \frac{1}{8}m\omega_z^2\left(x^2(1 - \epsilon) + y^2(1 + \epsilon)\right) + \frac{1}{2}m\omega_z^2 z^2. \end{aligned} \tag{1.81}$$

The trapping height y_0 has been absorbed into the y coordinate:

$$(y - y_0) \longrightarrow y. \tag{1.82}$$

Throughout this thesis, the coordinate y will *always* refer to $y - y_0$, so that for example, $\{x, 0\}$ refers to $\{x, y_0\}$.

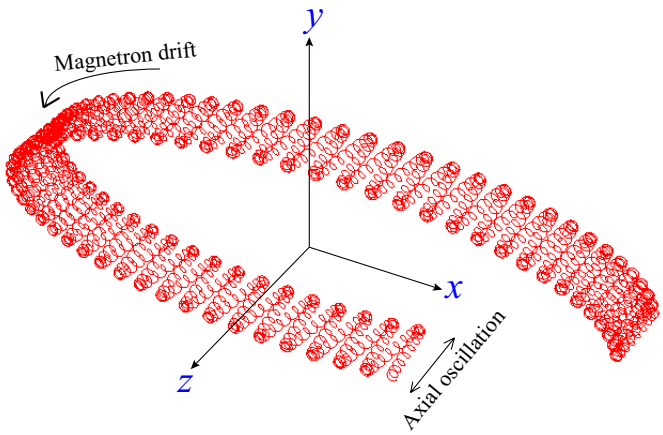

Figure 1.8: The motion of an electron in the ideal elliptical trap with the potential given in (1.78). The figure is taken from [29].

The following ratios are critical in the Penning trap, and determine this trapping height y_0:

$$\begin{aligned} \text{Tuning ratio}: \quad T_c &= \frac{V_c}{V_r}, \\ \text{Endcap} - \text{to} - \text{ring ratio}: \quad T_e &= \frac{V_e}{V_r}, \\ \text{Side electrode} - \text{to} - \text{ring ratio}: \quad T_g &= \frac{V_g}{V_r}. \end{aligned} \tag{1.83}$$

Crucially, T_c allows the linear fluctuations of the axial frequency ω_z to be eliminated, whereas T_g enables variation of ellipticity in the trap [29]. This will be discussed further in 1.6 and again throughout Chapter 8.

1.5.3 Frequencies and equations of motion

In [15], Kretzschmar rigorously discusses the ideal elliptical trap, and shows by various canonical transformation that the classical Hamiltonian (1.81) can be solved analytically. This section will only quote the results, but a full, quantum calculation is given in Chapter 8. The z dimension is unaffected by the ellipticity, so the axial motion remains unchanged from that in the circular Penning trap in (1.25).

$\mathcal{H}_\epsilon$ can be written as the sum of three harmonic oscillators with radial frequencies modified from the circular case [15]:

$$\begin{aligned} \tilde{\omega}_+ &= \sqrt{\frac{1}{2}\left(\omega_c^2 - \omega_z^2\right) + \frac{1}{2}\sqrt{\omega_c^2\omega_1^2 + \epsilon^2\omega_z^4}}, \\ \tilde{\omega}_- &= \sqrt{\frac{1}{2}\left(\omega_c^2 - \omega_z^2\right) - \frac{1}{2}\sqrt{\omega_c^2\omega_1^2 + \epsilon^2\omega_z^4}}. \end{aligned} \tag{1.84}$$

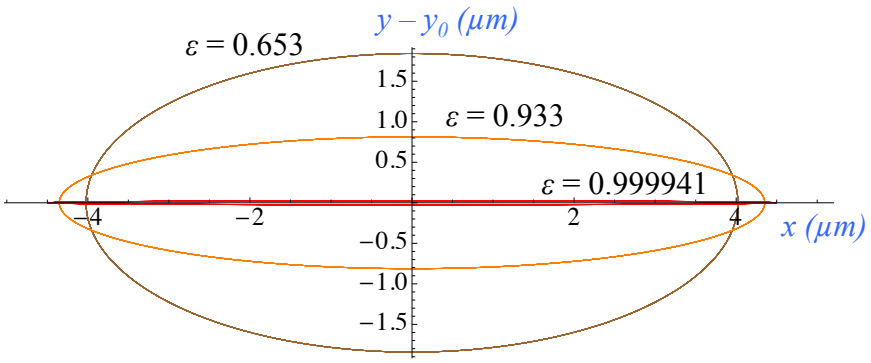

Figure 1.9: The magnetron orbit of an electron calculated from (1.85) for different values of T_g. The values are 0.522, 0.653, 1.653 for the three values of ϵ in ascending order. The plot has been taken from [29], and the axial energy is $E_z = 4.2\,k_B$.

The equations of motion of an electron in the ideal elliptical trap are given by [15]:

$$\begin{aligned} x(t) &= \xi_+ \cdot \tilde{A}_+ \cos(\tilde{\omega}_+ t) + \xi_- \cdot \tilde{A}_- \cos(\tilde{\omega}_- t), \\ y(t) &= -\eta_+ \cdot \tilde{A}_+ \sin(\tilde{\omega}_+ t) - \eta_- \cdot \tilde{A}_- \sin(\tilde{\omega}_- t), \end{aligned} \tag{1.85}$$

where

$$\begin{aligned} \xi_\pm &= \sqrt{\frac{\omega_c^2 + \epsilon\omega_z^2 \pm \sqrt{\omega_c^2\omega_1^2 + \epsilon^2\omega_z^4}}{2\tilde{\omega}_\pm/\omega_1 \sqrt{\omega_c^2\omega_1^2 + \epsilon^2\omega_z^4}}}, \\ \eta_\pm &= \sqrt{\frac{\omega_c^2 - \epsilon\omega_z^2 \pm \sqrt{\omega_c^2\omega_1^2 + \epsilon^2\omega_z^4}}{2\tilde{\omega}_\pm/\omega_1 \sqrt{\omega_c^2\omega_1^2 + \epsilon^2\omega_z^4}}}, \end{aligned} \tag{1.86}$$

and the amplitudes are similarly modified:

$$\tilde{A}_+ = \sqrt{\frac{2E_+}{m(\tilde{\omega}_+^2 - \frac{\omega_z^2}{2})}}, \quad \tilde{A}_- = \sqrt{\frac{2E_-}{m(\tilde{\omega}_-^2 - \frac{\omega_z^2}{2})}}. \tag{1.87}$$

A plot of the motion of a trapped electron in the ideal elliptical Penning trap is shown in Figure 1.8. Cylindrical symmetry can be described in a straightforward way as a special case of the above equations, occurring when $\epsilon = 0$ and $|\xi_\pm| = |\eta_\pm| = 1$ [15].

1.6 The tunable dimensionality of the Geonium Chip

1.6.1 The ground planes V_g

As introduced in 1.5, the standard five electrodes of a Penning trap are additionally flanked by side electrodes in the Geonium Chip, held at voltages V_g. Without making use of them ($V_g = 0$), the basic tuning ratios in (1.83) are $T_e > T_c \simeq 1$, but this section examines the scope of the trap when the ground planes are held at finite voltage.

A voltage V_g must affect the coefficients C_{ijk} in the series expansion of the potential shown in (1.74), which modifies the ellipticity parameter through (1.79). In this way, the

ellipticity of the Geonium trap can be modified. This in turn alters the mode frequencies and orbits of the electron (8.28, 1.85). The cyclotron frequency, typically being of MHz value, along with the coefficients ξ_+ and η_+, are largely unaffected by the ellipticity: $|\xi_+| \simeq |\eta_+| \simeq 1$ [15]. In contrast, the magnetron motion, through the frequency $\tilde{\omega}_-$ and coefficients ξ_-, η_-, is significantly modified by non-zero voltage V_g. Figure 1.9 shows a plot of the magnetron orbit of an electron for three different values of the ratio T_g [29]. As ϵ increases, the motion becomes a narrow ellipse along the x axis, so that in the limit $\epsilon \to 1$, the magnetron orbit is confined to the x axis. The cyclotron orbit is a fast oscillation superposed on top of the magnetron motion with a typical orbit size $\tilde{A}_+ \sim 0.1\,\mu$m for $B = 0.5\,$T. Including the axial oscillation, the motion of the electron therefore becomes quasi two-dimensional (2D) as $\epsilon \to 1$. This is known as the "ultra-elliptical regime" of the Penning trap [29].

1.6.2 The ultra-elliptical regime

As shown in Figure 1.9, the semi-major axis of the ellipse becomes increasingly large with ϵ. In order that the electron does not orbit outside the harmonic trapping region [29], magnetron-sideband cooling must be applied [14]. It was discussed in 1.4.1 how this technique reduces the average quantum number of the magnetron motion $\overline{n}_-$ until it equals that of the axial mode, which accordingly reduces the size of the amplitude A_-.

The series expansion of the potential in (1.74) is around the equilibrium position $(0, y_0, 0)$, so that y_0 itself is determined by $\partial_y \Phi = 0$. The C_{ijk} coefficients in this expansion change with T_g, and in turn new anharmonicities of order 3 and 4 are generated with each new voltage of the ground plane [29]. These generate a linear dependence of the mode frequencies with the energies [54, 39]. In order to compensate for this, the tuning ratio T_c must be adapted to a new optimal value T_c^{opt} for each new T_g, and hence each new y_0, so that the linear dependence of ω_z is eliminated; the precise determination of all the trap frequencies *rely* on this value being well defined [14].

In summary, increasing the ellipticity through V_g changes y_0, and in turn the anharmonic coefficients in $\Phi(x, y, z)$ (1.78). These must then be eliminated by modifying T_c to some value T_c^{opt}. In the upper plot of Figure 1.10, the variation of ellipticity for an increasing value of T_g for three fixed values of T_e is shown [29]. The resulting optimal tuning ratios T_c^{opt} for each of these with increasing T_g is shown in the lower part of the figure [29]. The frequencies ω_z and ω_- must be well defined in order that magnetron cooling can be applied at every stage of the ramping process [29], meaning that experimental

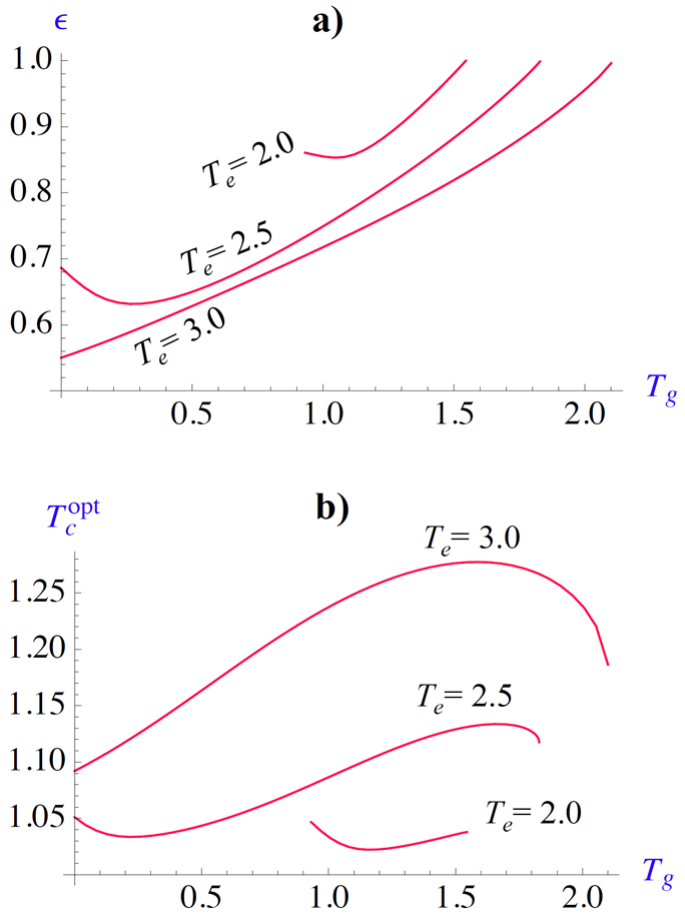

Figure 1.10: a) Ellipticity ϵ with icreasing T_g for three values of $T_e = V_e/V_r$. b) Optimal tuning ratio T_g^{opt} with increasing T_g for each of these fixed T_e values. Driving of the Geonium trap to the ultra-elliptical regime must follow one of these lines, to eliminate the frequency shifts of ω_z. This enables cooling of the magnetron motion, so that the electron remains in the harmonic trapping region. The graph has been taken directly from [29].

adiabaticity requires one of the lines in Figure 1.10 b) to be followed.

In Chapter 8, the quantum theory of driving to the ultra-elliptical regime will be examined, and a scheme proposed for using the process to produce potentially robust squeezed states.

Chapter 2

Sideband Coupling

2.1 Background theory

Coupling of the motional modes of an electron in a Penning trap is a well established technique for the resonant conversion of these modes to enable easier detection of the oscillator frequencies [28].

This method was first employed as a means of cooling the magnetron degree of freedom [55], whose motion is unstable, and must subsequently be minimised so as to prevent the electron from striking the ring electrode and being lost from the trap. "Motional Sideband Cooling" [44] has since become an invaluable technique in Penning trap experiments, enabling further control and detection of the particle's motion. It has prompted subsequent theoretical and experimental investigation into the coupling of, for example, the axial and cyclotron motional modes [56], and more recently, the effect of using octupolar radio-frequency (RF) fields to couple the radial modes of an ion [28] .

Although a purely classical process, the general mechanism can be readily described in terms of thermodynamics and quantum mechanical language [14]. For coupling of the axial and cyclotron modes, it is sufficient to consider the ladder of states of shown in Fig. 2.1 [14]. If an electron in the (n_+, n_z) level receives a quantum of energy $\hbar(\omega_+ - \omega_z)$, the resulting transition is to the state $(n_+ - 1, n_z + 1)$, or to the state $(n_+ + 1, n_z - 1)$. The transition probabilities are determined by the relative sizes of n_+ and n_z [14], so that if the two modes are held at the same temperature, then $\omega_+ \gg \omega_z$ demands that $n_z \gg n_+$. The axial motion is therefore reduced until $\overline{n}_+ = \overline{n}_z$, at such a time when the photon will be exchanged back and forth between the oscillator states [14].

In the seminal work by Cornell et al. on mode coupling in a Penning trap [56], the cyclotron and axial modes of a single N_2^+ ion in a Penning trap are coupled by an RF field.

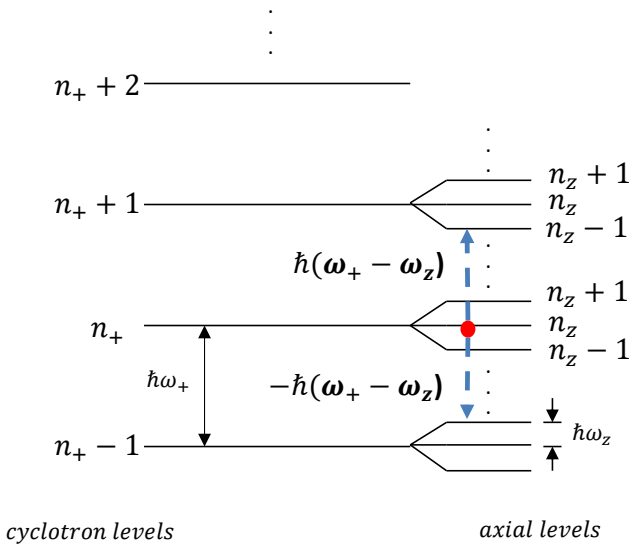

Figure 2.1: Coupling of the cyclotron and axial energy levels in the Penning trap by an incoming photon with frequency matching the splitting between the levels. If n_+ is greater (less) than n_z, the cyclotron quantum number will decrease (increase) and the axial one increase (decrease) until they are equal [14].

It is shown how the resulting energy of the coupled system can be treated in the dressed-atom formalism [57], with an avoided crossing structure emerging from the calculation. This chapter discusses the quantum analogue of the coupling in the circular Penning trap, where again ideas are borrowed from the dressed-atom approach [57]. Extension to the elliptical trap is discussed in Chapter 8.

2.2 The coupling field

As outlined above, cyclotron-axial coupling requires an electric field of the same frequency as the frequency difference between the two sets of ladder states. Following [56], this frequency will be denoted ω_p and a classical quadrupole field of the form

$$E_p(t) = Re\left(\epsilon_p e^{i\omega_p t}\right)(x\hat{e}_z + z\hat{e}_x) \tag{2.1}$$

is applied in the lab. Such a field (with $\epsilon_p \in \Re$) has an associated potential of the form

$$V_p(t) = -\epsilon_p \cos(\omega_p t)(xz). \tag{2.2}$$

This is now quantized and re-expressed in terms of the time dependent creation and annihilation operators for the three oscillator modes using the expansion of $\hat{x}$ and $\hat{z}$ in

(1.39):

$$\begin{aligned}\hat{V}_p(t) &= -\epsilon_p \cos(\omega_p t)\,\hat{x}\,\hat{z} \\ &= -\frac{\hbar}{2m}\frac{1}{\sqrt{\omega_1\omega_z}}\epsilon_p \cos(\omega_p t)\times \\ &\quad\times\Big\{\hat{a}_+\hat{a}_z + \hat{a}_+^\dagger\hat{a}_z + \hat{a}_z^\dagger\hat{a}_+ + \hat{a}_+^\dagger\hat{a}_z^\dagger \\ &\quad+\hat{a}_-\hat{a}_z + \hat{a}_-^\dagger\hat{a}_z + \hat{a}_z^\dagger\hat{a}_- + \hat{a}_-^\dagger\hat{a}_z^\dagger\Big\}. \end{aligned} \tag{2.3}$$

The total Hamiltonian of the electron in this potential is given by

$$\hat{\mathcal{H}}_p = \hat{\mathcal{H}} + q\hat{V}_p(t). \tag{2.4}$$

Following the prescription for time dependent unitary transformation of a general quantum Hamiltonian [41]

$$\hat{U}(t)H\hat{U}^\dagger(t) + i\hbar\dot{\hat{U}}(t)\hat{U}^\dagger(t), \tag{2.5}$$

in a frame of reference defined by the unitary operator

$$\hat{U}_p(t) = \exp\left\{-i\frac{\omega_p}{2}\left(\hat{n}_z - \hat{n}_+\right)t\right\}, \tag{2.6}$$

the coupled Hamiltonian (2.4) becomes

$$\begin{aligned}\hat{\mathcal{H}}_{pt} =& \hbar\omega_+\left(\hat{n}_+ + \frac{1}{2}\right) + \hbar\omega_z\left(\hat{n}_z + \frac{1}{2}\right) - \hbar\omega_-\left(\hat{a}_-^\dagger\hat{a}_- + \frac{1}{2}\right) + \hbar\frac{\omega_p}{2}(\hat{n}_z - \hat{n}_+) \\ &+ e\frac{\hbar}{2m}\frac{1}{\sqrt{\omega_1\omega_z}}\epsilon_p\cos(\omega_p t)\Big\{\hat{a}_+\hat{a}_z + \hat{a}_+^\dagger\hat{a}_z e^{i\omega_p t} + \hat{a}_z^\dagger\hat{a}_+ e^{-i\omega_p t} + \hat{a}_+^\dagger\hat{a}_z^\dagger \\ &+\hat{a}_-\hat{a}_z e^{i\frac{\omega_p}{2}t} + \hat{a}_-^\dagger\hat{a}_z e^{i\frac{\omega_p}{2}t} + \hat{a}_z^\dagger\hat{a}_- e^{-i\frac{\omega_p}{2}t} + \hat{a}_-^\dagger\hat{a}_z^\dagger e^{-i\frac{\omega_p}{2}t}\Big\}. \end{aligned} \tag{2.7}$$

The cosine function is expanded into exponential form, so that in this frame, the explicit time dependence of the additional potential energy $q\hat{V}_p$ is given by:

$$\begin{aligned}\hat{U}_p(t)\,q\hat{V}_p(t)\,\hat{U}_p^\dagger(t) = e\frac{\hbar}{4m}\frac{1}{\sqrt{\omega_1\omega_z}}\epsilon_p \\ \times\Big\{\hat{a}_+\hat{a}_z[e^{i\omega_p t} + e^{-i\omega_p t}] + \hat{a}_+^\dagger\hat{a}_z[e^{2i\omega_p t} + \underbrace{e^0}_{RWA}] \\ +\hat{a}_z^\dagger\hat{a}_+[\underbrace{e^0}_{RWA} + e^{-2i\omega_p t}] + \hat{a}_+^\dagger\hat{a}_z^\dagger[e^{i\omega_p t} + e^{-i\omega_p t}] \\ +\hat{a}_-\hat{a}_z[e^{i\frac{3}{2}\omega_p t} + e^{-i\frac{\omega_p}{2}t}] + \hat{a}_-^\dagger\hat{a}_z[e^{i\frac{3}{2}\omega_p t} + e^{-i\frac{\omega_p}{2}t}] \\ +\hat{a}_z^\dagger\hat{a}_-[e^{i\frac{\omega_p}{2}t} + e^{-i\frac{3}{2}\omega_p t}] + \hat{a}_-^\dagger\hat{a}_z^\dagger[e^{i\frac{\omega_p}{2}t} + e^{-i\frac{3}{2}\omega_p t}]\Big\}. \end{aligned} \tag{2.8}$$

Defining the coupling frequency

$$\omega_p = \omega_+ - \omega_z + \delta, \tag{2.9}$$

where

$$\delta \sim 0, \tag{2.10}$$

leads to only two terms in (2.8) which are not oscillating at GHz or MHz frequencies, allowing for variation in the realtive strengths of ω_+ and ω_z. By a second-level rotating wave approximation (RWA), or secular approximation [58], only the terms marked "RWA" in (2.8) remain. Following this, the total Hamiltonian (2.7) in this rotating frame becomes

$$\hat{\mathcal{H}}_{pt} = \hbar\frac{\omega_0}{2}\left(\hat{n}_+ + \frac{1}{2}\right) + \hbar\frac{\omega_0}{2}\left(\hat{n}_z + \frac{1}{2}\right) + \hbar\frac{\delta}{2}\left(\hat{n}_z - \hat{n}_+\right) - \hbar\omega_-\left(\hat{a}_-^\dagger\hat{a}_- + \frac{1}{2}\right) + \hbar\xi(\hat{a}_+^\dagger\hat{a}_z + \hat{a}_z^\dagger\hat{a}_+), \tag{2.11}$$

where the renormalised coupling strength ξ has been defined

$$\xi \equiv \frac{e}{4m}\frac{1}{\sqrt{\omega_1\omega_z}}\epsilon_p, \tag{2.12}$$

and

$$\omega_0 = \omega_+ + \omega_z. \tag{2.13}$$

Hamiltonian $\hat{\mathcal{H}}_{pt}$ must now be made diagonal in order to interpret the effects of the field (2.1) upon the motional modes of the system.

2.3 Dressing the energy levels

2.3.1 Interpretation I: the dressed frame

$\hat{\mathcal{H}}_{pt}$ can be written in diagonal form by application of

$$\hat{U}_\theta = \exp\left\{\frac{\theta}{2}(\hat{a}_z^\dagger\hat{a}_+ - \hat{a}_+^\dagger\hat{a}_z)\right\}, \tag{2.14}$$

where the rotation angle θ is given by

$$\theta = \arctan\left[\frac{2\xi}{\delta}\right]. \tag{2.15}$$

This produces:

$$\begin{aligned}\hat{\mathbb{H}} &= \hat{U}_\theta\hat{\mathcal{H}}_{pt}\hat{U}_\theta^\dagger \\ &= \hbar\begin{pmatrix}\hat{a}_z^\dagger & \hat{a}_+^\dagger & \hat{a}_-^\dagger\end{pmatrix}\begin{pmatrix}\left(\frac{\omega_0+\Delta}{2}\right) & 0 & 0\\ 0 & \left(\frac{\omega_0-\Delta}{2}\right) & 0\\ 0 & 0 & -\omega_-\end{pmatrix}\begin{pmatrix}\hat{a}_z\\ \hat{a}_+\\ \hat{a}_-\end{pmatrix} + \hbar\frac{(\omega_1+\omega_z)}{2},\end{aligned} \tag{2.16}$$

where

$$\Delta = \sqrt{4\xi^2 + \delta^2}. \tag{2.17}$$

The Hamiltonian has been rotated to a new frame of reference in the same local basis. The rotation is defined by (2.14), and the frame of reference will be called the *dressed frame*.

Statistical properties of the coupled modes I

In this dressed frame, it is straightforward to determine the average occupation numbers $\overline{n}_+$ and $\overline{n}_z$ as a result of the coupling. Labelling

$$\begin{aligned} \varepsilon_+ &= \frac{\omega_0 - \Delta}{2}, \\ \varepsilon_z &= \frac{\omega_0 + \Delta}{2}, \end{aligned} \tag{2.18}$$

the thermal density matrices of the two modes become

$$\begin{aligned} \hat{\rho}_{\varepsilon_+} &= \frac{\exp(-\beta\hbar\varepsilon_+ \left(\hat{n}_+ + \frac{1}{2}\right))}{Tr[\exp(-\beta\hbar\varepsilon_+ \left(\hat{n}_+ + \frac{1}{2}\right))]}, \\ \hat{\rho}_{\varepsilon_z} &= \frac{\exp(-\beta\hbar\varepsilon_z \left(\hat{n}_z + \frac{1}{2}\right))}{Tr[\exp(-\beta\hbar\varepsilon_z \left(\hat{n}_z + \frac{1}{2}\right))]}. \end{aligned} \tag{2.19}$$

In both cases, β is unchanged from the value given in the uncoupled case in (1.68), since it assumed that the physical temperature at which the trap is held remains unchanged. From this, the average occupation numbers of the modes in this dressed frame are given by

$$\begin{aligned} \overline{n}_{\varepsilon_+} &= Tr\left[\hat{\rho}_{\varepsilon_+}\, \hat{n}_+\right] = \frac{1}{\exp(\beta\hbar\varepsilon_+) - 1}, \\ \overline{n}_{\varepsilon_z} &= Tr\left[\hat{\rho}_{\varepsilon_z}\, \hat{n}_z\right] = \frac{1}{\exp(\beta\hbar\varepsilon_z) - 1}. \end{aligned} \tag{2.20}$$

The thermal states of the coupled system in the lab are therefore governed by the density matrices $\hat{U}_\theta^\dagger \hat{U}_p^\dagger(t)\, \hat{\rho}_{\varepsilon_+}\, \hat{U}_p(t)\hat{U}_\theta$ and $\hat{U}_\theta^\dagger \hat{U}_p^\dagger(t)\, \hat{\rho}_{\varepsilon_z}\, \hat{U}_p(t)\hat{U}_\theta$ for the respective modes, with $\hat{U}_p(t)$ and $\hat{U}_\theta$ given in (2.6) and (2.14). These can be used to determine the statistical properties of the coupled trap in the lab frame. As an example, $\overline{n}_+$ is now calculated explicitly.

The operator $\hat{U}_\theta$ involves the mixing of the operators of the axial and cyclotron modes, so that the transformed density matrix

$$\hat{\rho}_{+z} = \hat{U}_\theta^\dagger \hat{U}_p^\dagger(t)\, \hat{\rho}_{\varepsilon_+}\, \hat{U}_p(t)\hat{U}_\theta \tag{2.21}$$

is necessarily a function of the operators of both modes. These operators belong to different Hilbert spaces, and so the reduced density matrix $\hat{\rho}^+$ [41] must be used to determine $\langle \hat{n}_+ \rangle$.

This is given by

$$\begin{aligned}\hat{\rho}^{+} &= Tr_z\left[\hat{\rho}_{+z}\right] \\ &= Tr_z\left[\hat{U}_\theta^\dagger \hat{U}_p^\dagger(t)\,\hat{\rho}_{\varepsilon_+}\,\hat{U}_p(t)\hat{U}_\theta\right] \\ &= Tr_z\left[\hat{U}_p^\dagger(t)\,\hat{\rho}_{\varepsilon_+}\,\hat{U}_p(t)\hat{U}_\theta\hat{U}_\theta^\dagger\right] \\ &= Tr_z\left[\hat{\rho}_{\varepsilon_+}\,\hat{U}_p(t)\hat{U}_p^\dagger(t)\right] \\ &= Tr_z\left[\hat{\rho}_{\varepsilon_+}\right] \\ &= \hat{\rho}_{\varepsilon_+},\end{aligned} \tag{2.22}$$

where the calculation is trivialised by the cyclic properties of the trace [59].

The average occupation number of the cyclotron mode in the coupled system in the lab frame is therefore given by

$$\overline{n}_+ = Tr\left[\hat{\rho}^+\hat{n}_+\right] = Tr\left[\hat{\rho}_{\varepsilon_+}\hat{n}_+\right] = \overline{n}_{\varepsilon_+}. \tag{2.23}$$

Likewise, the average occupation number of the axial mode in the lab frame is equivalent to the average occupation number of this mode in the dressed frame, (2.20). This of course follows from the preservation of expectation values upon unitary transformation of both the state and operator [59].

2.3.2 Interpretation II: dressed states

In the way $\hat{U}_\theta$ has been applied to $\hat{\mathcal{H}}_{pt}$ above, the whole Hamiltonian has been transformed to an alternate reference frame from the laboratory. Where this frame of reference is, if indeed the rotation is purely spatial, motivates some of the discussion in Chapter 5.

For a calculation more analogous to the classical one in [56], instead of *transforming* the Hamiltonian (2.11), consider that there exists a basis within the original frame with respect to which this Hamiltonian can be written in diagonal form. The eigenstates of this basis are *the original states dressed by the coupling field* [60]. In the present case of coupling the axial and cyclotron modes of the Penning trap, the Hamiltonian $\hat{\mathcal{H}}_{pt}$ *rewritten* in terms of operators of this dressed basis is given by

$$\boxed{\hat{\mathcal{H}}_{pt} = \hbar\varepsilon_\alpha\left(\hat{n}_\alpha + \frac{1}{2}\right) + \hbar\varepsilon_\beta\left(\hat{n}_\beta + \frac{1}{2}\right) - \hbar\omega_-\left(\hat{a}_-^\dagger\hat{a}_- + \frac{1}{2}\right)}, \tag{2.24}$$

where

$$\begin{aligned}\varepsilon_\alpha = \varepsilon_z &= \frac{\omega_0 + \Delta}{2}, \\ \varepsilon_\beta = \varepsilon_+ &= \frac{\omega_0 - \Delta}{2}.\end{aligned} \tag{2.25}$$

The creation and annihilation operators of these new modes are defined

$$\begin{aligned}\hat{a}_\alpha^\dagger &= \cos\frac{\theta}{2}\hat{a}_z^\dagger + \sin\frac{\theta}{2}\hat{a}_x^\dagger; \quad \hat{a}_\alpha = \cos\frac{\theta}{2}\hat{a}_z + \sin\frac{\theta}{2}\hat{a}_x, \\ \hat{a}_\beta^\dagger &= \cos\frac{\theta}{2}\hat{a}_x^\dagger - \sin\frac{\theta}{2}\hat{a}_z^\dagger; \quad \hat{a}_\beta = \cos\frac{\theta}{2}\hat{a}_x - \sin\frac{\theta}{2}\hat{a}_z,\end{aligned} \tag{2.26}$$

and θ and Δ are given in (2.15) and (2.17) respectively.

There is only a subtle difference between the two interpretations, of the dressed frame in 2.3.1 and the dressed states of this section, both of which solve Hamiltonian (2.11). They are of course mathematically equivalent, but it will prove important to retain the distinction that has been made throughout the remainder of this thesis. From now on, the approach of *rotating* a general Hamiltonian, $\hat{U}_\theta H \hat{U}_\theta^\dagger$, will be always referred to as transforming or rotating to another frame of reference. The method of diagonalising by *rewriting* a general Hamiltonian H will be referred to as "rotating" the states only, with the new states being the dressed states of a coupled system.

Statistical properties of the coupled modes II

Analogously to 2.3.1, the diagonal Hamiltonian in (2.24) directly reveals the statistical properties of the dressed modes at finite temperature. In fact, it is straightforward to show that $\overline{n}_\alpha = \overline{n}_z$ and $\overline{n}_\beta = \overline{n}_+$ as given in (2.23) and (2.20). For future reference, the density operators of the dressed modes α and β are given explicitly by

$$\begin{aligned}\hat{\rho}_\alpha &= \frac{\exp(-\beta\hbar\varepsilon_\alpha\left(\hat{n}_\alpha + \frac{1}{2}\right))}{Tr[\exp(-\beta\hbar\varepsilon_\alpha\left(\hat{n}_\alpha + \frac{1}{2}\right))]}, \\ \hat{\rho}_\beta &= \frac{\exp(-\beta\hbar\varepsilon_\beta\left(\hat{n}_\beta + \frac{1}{2}\right))}{Tr[\exp(-\beta\hbar\varepsilon_\beta\left(\hat{n}_\beta + \frac{1}{2}\right))]},\end{aligned} \tag{2.27}$$

from which other characteristics of the dressed system follow naturally:

$$\begin{aligned}P(n_\alpha) &= \exp(-\beta\hbar\varepsilon_\alpha n_\alpha)(1 - \exp(-\beta\hbar\varepsilon_\alpha)), \\ P(n_\beta) &= \exp(-\beta\hbar\varepsilon_\beta n_\beta)(1 - \exp(-\beta\hbar\varepsilon_\beta)).\end{aligned} \tag{2.28}$$

These statistical results are significant for the calculation in Chapter 9, where time dependent driving between the energy levels of these dressed modes is considered.

2.3.3 Introduction of Schwinger boson operators

Throughout this thesis, the formation of problems in terms of sets of operators with angular momentum-like algebra will be exploited. The method is introduced below, for the

present purpose of studying the nature of the dressed modes in 2.3.2.

Motivated by Kretzschmar's study of the "interconversion of motional modes" by analysis of the rotation of the Bloch vector [28], the following operators are formed:

$$\begin{aligned}
\hat{T}_0 &= \frac{\hbar}{2}\left(\hat{a}_z^\dagger \hat{a}_z + \hat{a}_+^\dagger \hat{a}_+\right), \\
\hat{T}_1 &= \frac{\hbar}{2}\left(\hat{a}_z^\dagger \hat{a}_+ + \hat{a}_+^\dagger \hat{a}_z\right), \\
\hat{T}_2 &= -\frac{i\hbar}{2}\left(\hat{a}_z^\dagger \hat{a}_+ - \hat{a}_+^\dagger \hat{a}_z\right), \\
\hat{T}_3 &= \frac{\hbar}{2}\left(\hat{a}_z^\dagger \hat{a}_z - \hat{a}_+^\dagger \hat{a}_+\right),
\end{aligned} \tag{2.29}$$

where [61]

$$\left[\hat{T}_i, \hat{T}_j\right] = i\hbar\varepsilon_{ijk}\hat{T}_k, \quad \left[\hat{T}_0, \hat{T}_i\right] = 0; \quad i = 1, 2, 3. \tag{2.30}$$

The circular components are given by [61]

$$\begin{aligned}
\hat{T}_+ &= \hat{T}_1 + i\hat{T}_2 = \hbar\, \hat{a}_z^\dagger \hat{a}_+, \\
\hat{T}_- &= \hat{T}_1 - i\hat{T}_2 = \hbar\, \hat{a}_+^\dagger \hat{a}_z,
\end{aligned} \tag{2.31}$$

with the resulting commutation relations

$$\left[\hat{T}_3, \hat{T}_\pm\right] = \pm\hat{T}_\pm, \quad \left[\hat{T}_+, \hat{T}_-\right] = 2\hat{T}_3. \tag{2.32}$$

These are completely equivalent to (2.30). The $SU(2)$ Lie algebra of these Schwinger Boson operators can of course be obtained from any 2D harmonic oscillator system [61], and indeed several sets of operators analogous to $\underline{T} = \{\hat{T}_0, \hat{T}_1, \hat{T}_2, \hat{T}_3\}$ are formed in later sections. A discussion of the interconnection of these sets, and their use in the Penning trap, is given in Chapter 5.

2.3.4 Avoided crossings

The coupled Hamiltonian (2.11) is now rewritten in terms of these Schwinger boson operators of the set $\underline{T}$, defined in (2.29). Before dressing:

$$\hat{\mathcal{H}}_{pt} = \omega_0\hat{T}_0 + \delta\hat{T}_3 + 2\xi\hat{T}_1 + \frac{\hbar\omega_0}{2} - \hbar\omega_-\left(\hat{a}_-^\dagger \hat{a}_- + \frac{1}{2}\right). \tag{2.33}$$

Focusing on the axial and cyclotron levels only, the magnetron Hamiltonian in (1.63) is taken away to define:

$$\begin{aligned}
\hat{\mathcal{H}}_d &= \hat{\mathcal{H}}_{pt} - \hat{\mathcal{H}}_- \\
&= \omega_0\hat{T}_0 + \delta\hat{T}_3 + 2\xi\hat{T}_1 + \frac{\hbar\omega_0}{2}.
\end{aligned} \tag{2.34}$$

where ω_0 is given in (2.13).

The quantum numbers

$$N = n_z + n_+, \quad l = n_z - n_+ \tag{2.35}$$

are defined so that:

$$\begin{aligned} \hat{T}_0|n_+, n_z\rangle &= \frac{\hbar}{2} N|n_+, n_z\rangle, \\ \hat{T}_3|n_+, n_z\rangle &= \frac{\hbar}{2} l|n_+, n_z\rangle, \end{aligned} \tag{2.36}$$

where $N = 0, 1, 2, 3, ...,$ and $l = -N, -N+2, ..., N-2, N$.[1] The expectation value of $\hat{\mathcal{H}}_d$ in the Fock state $|n_+, n_z\rangle$ follows:

$$\langle \hat{\mathcal{H}}_d \rangle = \frac{\hbar\omega_0}{2}(N+1) + \frac{\hbar\delta}{2} l. \tag{2.37}$$

Similarly, the magnetron Hamiltonian (1.63) is subtracted from the *dressed* Hamiltonian (2.24), and it is rewritten:

$$\hat{\mathcal{H}}_d = \frac{\hbar}{2}(\varepsilon_\alpha + \varepsilon_\beta)(\hat{n}_\alpha + \hat{n}_\beta) + \frac{\hbar}{2}(\varepsilon_\alpha - \varepsilon_\beta)(\hat{n}_\alpha - \hat{n}_\beta) + \frac{\hbar\omega_0}{2}. \tag{2.38}$$

It is clear that the $\hat{n}_\alpha$ and $\hat{n}_\beta$ operators must form a set of Schwinger boson operators $\underline{T}^{\alpha\beta}$ completely analogous to $\underline{T}$ in (2.29). In terms of this $\underline{T}^{\alpha\beta}$ set of the dressed modes, Hamiltonian (2.38) is written:

$$\hat{\mathcal{H}}_d = \omega_0 \hat{T}_0^{\alpha\beta} + \Delta \hat{T}_3^{\alpha\beta} + \frac{\hbar\omega_0}{2}, \tag{2.39}$$

where Δ is given in (2.11). The expectation value of the dressed Hamiltonian (2.39) in the states $|n_\alpha, n_\beta\rangle$ is clearly

$$\langle \hat{\mathcal{H}}_d \rangle = \frac{\hbar\omega_0}{2}(N_{\alpha\beta} + 1) + \frac{\hbar}{2}\Delta\, l_{\alpha\beta}, \tag{2.40}$$

where $N_{\alpha\beta} = n_\alpha + n_\beta$, $l_{\alpha\beta} = n_\alpha - n_\beta$.

Comparing the expectation values in (7.15) and (2.40), it is straightforward to see the effects of this "dressing": the degeneracy of the l levels at the point $\delta = 0$ is lifted by the non-zero value of $\Delta = \sqrt{4\xi^2 + \delta^2}$. This is shown pictorially in Figure 2.2, where the expectation values of the bare and dressed Hamiltonians has been plotted as a function of δ for the first few total quantum numbers N. The plot shows how an *avoided crossing*

[1] The allowed values of l are clearly different from that of standard eigenvalues of a third component angular momentum operator [40], as they are in steps of two rather than one. This is a simple consequence of the fact that $\hat{T}_0$ and $\hat{T}_3$ both contain two *independently varying* number operators.

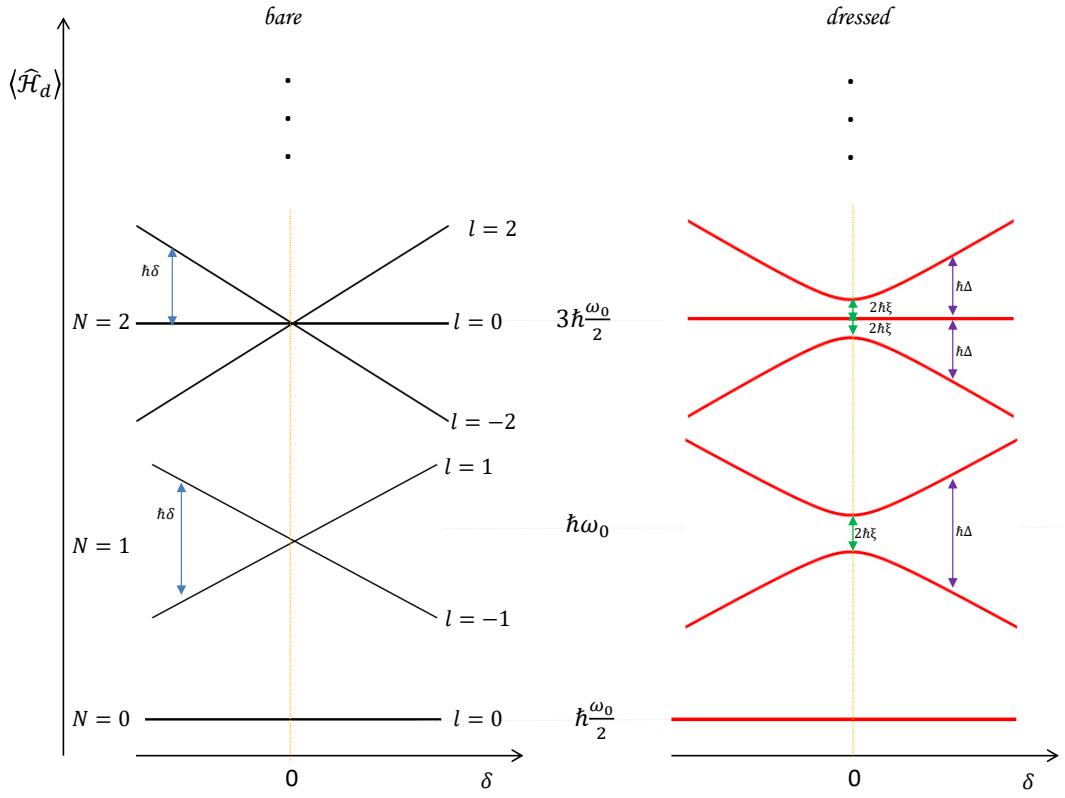

Figure 2.2: Left: The expectation values of the coupled Hamiltonian in the Fock states $|n_+, n_z\rangle$, as given in (7.15). These are the so-called "bare" states of the system. Right: Expectation values of the coupled Hamiltonian in the "dressed" states $|n_\alpha, n_\beta\rangle$, given in (2.40). The effects of the dressing is the formation of an avoided crossing between the $l = n_z - n_+$ sub-levels of the system at the point $\delta = 0$. The size of the splitting is dependent on the electric coupling field strength in (2.1), where the renormalised strength ξ is defined in (2.12). The bare and dressed levels of the modes for the different values of N are not drawn to scale.

occurs at the point $\delta = 0$ due to the dressing of the modes [57]. The size of the splitting is given by $2\hbar\xi$, and accordingly varies with the strength of the applied field in (2.1).

In comparing the results of the above quantum calculation to the classical one in [56], it is clear that the dressed-atom formalism [57] is directly applicable to the combined quantum modes of the axial and cyclotron motions, with the distinction that the latter is clearly not a two-level system (TLS). In the present case of the coupled Penning trap, there are N avoided crossings formed at the point $\delta = 0$ for *each* N when the system is dressed. Consequently there are a total of $\sum_{N=0}^{K} N$ avoided crossings formed between the l sub-levels in the entire spectrum. The upper limit K of this sum must depend upon the temperature of the trap.

The description of mode coupling as taking place between the separate ladders of cyclotron and axial energy levels is convenient [14]. However, in order to discuss the quantum avoided crossing, the more appropriate description is that the coupling takes place between the *combined* levels of this 2D spectrum, l.

2.3.5 Analysis of statistical results

The statistical results of 2.3.1 and 2.3.2 are now compared alongside those of the uncoupled system.

In terms of the bare basis in the lab frame, the values of $\overline{n}_+$ and $\overline{n}_z$ are modified from those of the uncoupled system, as discussed in 1.4.1, by the frequency shifts $\omega_+ \to \varepsilon_+$ and $\omega_z \to \varepsilon_z$ (2.18). Since in general $\omega_+ \gg \omega_z$, it is clear that the mean occupation of the cyclotron mode is little changed by this shift, whereas that of the axial motion must be greatly reduced, assuming the value β is the same for both modes. This is in general agreement with the discussion at the beginning of this chapter on the basic mechanism of mode coupling, illustrated in Figure 2.1.

From (2.26), it appears that $\hat{a}_\alpha \to \hat{a}_z$ and $\hat{a}_\beta \to \hat{a}_+$ as the coupling is removed ($\theta \to 0$). The eigenvalues of the modes ϵ_α and ϵ_β also appear to reduce to ω_z and ω_+ respectively (2.25). However, such association between the modes of the two bases $\{z, +\}$ and $\{\alpha, \beta\}$ themselves is much more subtle; once the coupling has been established, the dressed energy levels on the right hand side of Figure 2.2 do not collapse into those of the bare basis on the left when the coupling field is then removed, $\xi \to 0$. This is manifest in the fact that the *reduced* density matrix must be used when calculating the statistical properties of the coupled axial and cyclotron modes in the lab frame, as in (2.23). Once the coupling has been established, information about one of these modes must necessarily assume complete

ignorance of the other; restricting attention to observables associated with only one of the coupled modes leads to a loss of information on the correlation between them [41]. When the coupling field is switched off, let us assume that the α mode does "become" the axial mode, and that the cyclotron mode is similarly recovered from the α mode. In this way, information about both modes is available, which in turn reveals information about both modes of the coupled system. This is in contradiction to the necessary use of the reduced identity matrix $\hat{\rho}^{+}$, and hence cannot be true.

2.4 Manipulation of adiabatic potentials in atom traps

Dressed adiabatic potentials are of course more commonly discussed in the context of trapped atoms [57]. In this section, combinations of static and time dependent *magnetic* fields used to dress atoms with RF radiation are considered. Carefully constructed spatial variation in these fields can lead to control over the trapping potential of the atoms [60], enabling a huge variety of traps to be constructed. In particular, the method has been used to create an adiabatic double well potential, leading to matter-wave interferometry in atom chips [62]. Such interference experiments enables the study of matter at a fundamental, quantum level [63, 64, 65], and lead to high-precision sensing of gravitational fields [62]. Additionally, they allow for the engineering and control of quantum states, an important feature in the pursuit of quantum information processing [66].

As discussed in 1.5, the planar formation of electrodes in the Geonium Chip offers the possibility of an integrated CPW transmission line. For the purposes of mode coupling in the trap, the coupling potential in (2.2) is communicated to the electron via this waveguide, with the chip designed to be transparent to microwave fields [27]. It was proposed [67] that the possible customisation of fields thus generated could be used to spatially vary the amplitude and/ or detuning of the coupling field along the x and z axes of the trap. This is turn could generate control over the adiabatic potential of the electron in a similar way to the dressed-atom traps [60]. To investigate this further, a brief introduction to the theory of the generation of a double well through RF dressing in atom traps is given below.

2.4.1 RF dressing in atom traps

An atom with magnetic dipole moment $\vec{\mu} = -g_F \mu_B \vec{F}/\hbar$ in a magnetic field $\vec{B}$ interacts with the field via the magnetic dipole moment $\vec{\mu} \cdot \vec{B}$ [68]. In this case g_F is the Landé g-factor and μ_B the Bohr magneton [40]. In a magnetic trap with an additional RF

interacting field, this coupling results in the Hamiltonian [60]

$$H_Z(\vec{r},t) = -\frac{\mu_B\, g_F}{\hbar}\vec{F}\cdot(\vec{B}_0(\vec{r}) + \vec{B}_{RF}(\vec{r},t)). \tag{2.41}$$

The magnetic field $\vec{B}_0(\vec{r})$ is responsible for the basic trapping of the atoms and induces splitting between the m_F Zeeman levels [40]. This stationary field is constructed by a pair of coils with opposing currents to produce a potential minimum at the centre of the trap [60]:

$$\begin{aligned}\vec{B}_0(\vec{r}) &= b'\left(x\hat{i} + y\hat{j} - 2zk\right)\\ \implies U_0(\vec{r}) &= m_F\, g_F\, \mu_B |\vec{B}_0(\vec{r})|\\ &= m_F\, g_F\, \mu_B\, b'\sqrt{x^2+y^2+4z^2}.\end{aligned} \tag{2.42}$$

The uncoupled potentials of the $F = 1$ sub-levels are therefore given by parabolic functions along the x axis, as shown in a) of Figure 2.3. The purpose of the RF field is to induce transition between these levels. Suppose that the static component defines the local quantisation direction along the z axis, $\vec{B}_0(\vec{r}) = |\vec{B}_0(\vec{r})|\hat{F}_z$. The RF radiation is then chosen to be linearly polarised and assumed to be a cosine function [60]. The RWA is applied, to the effect of neglecting the counting-rotating terms [69], and (2.41) becomes [60]

$$H_Z(\vec{r},t) = -\frac{\mu_B\, g_F}{\hbar}\left(|\vec{B}_0(\vec{r})|\hat{F}_z + \frac{1}{2}|\vec{B}_{RF}(\vec{r})|\left[\hat{F}_+\exp(\mp i\omega_{RF}\, t) + \hat{F}_-\exp(\pm i\omega_{RF}\, t)\right]\right). \tag{2.43}$$

The components $\hat{F}_\pm$ are the angular momentum raising and lowering operators $\hat{F}_\pm = \hat{F}_x \pm i\hat{F}_y$ [68]. Moving to the interaction picture by changing to a frame rotating at ω_{RF} in the same local basis [60] leads to the time independent Hamiltonian

$$H_Z(\vec{r}) = \pm\left(-\delta(\vec{r})\hat{F}_z + \Omega_0(\vec{r})\hat{F}_x\right). \tag{2.44}$$

The RF Rabi frequency and detuning are given by $\Omega_0(r) = \frac{\mu_B\, g_F}{2\hbar}|\vec{B}_{RF}(\vec{r})|$ and $\delta(r) = \omega_{RF} - \omega_L(r)$ accordingly, and the Larmor frequency has its usual definition, $\omega_L(r) = \frac{\mu_B|g_F|}{\hbar}|\vec{B}_0(\vec{r})|$ [60]. The $\pm$ and $\mp$ signs throughout depend upon the sign of g_F.

RF dressing The dressed states of $H_Z(\vec{r})$ are found by defining a new quantization axis z' which enables (2.44) to be written in diagonal form:

$$H_Z(\vec{r}) \to \Omega(\vec{r})\hat{F}_{z'}, \tag{2.45}$$

where the generalised Rabi frequency is given by [60]:

$$\Omega(\vec{r}) = \sqrt{\delta^2(\vec{r}) + \Omega_0^2(\vec{r})}. \tag{2.46}$$

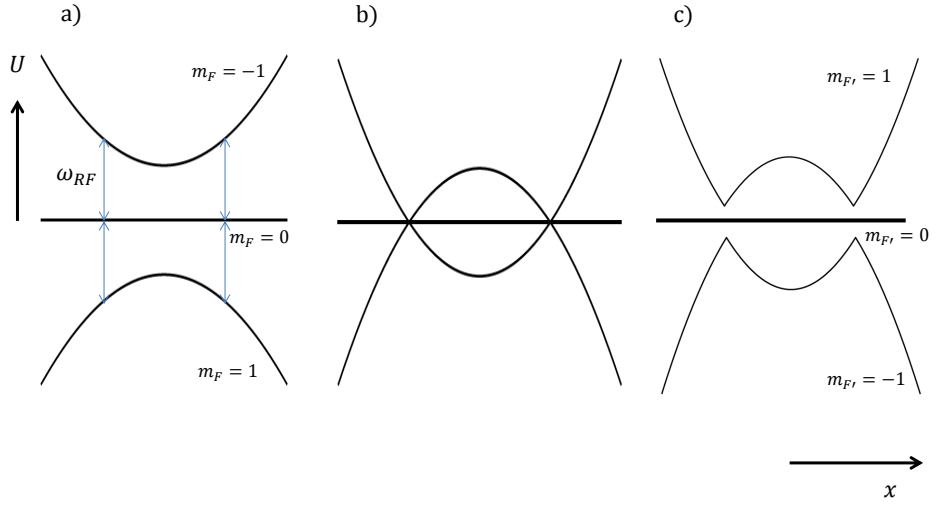

Figure 2.3: RF dressing of the $m_{F'} = 0, \pm 1$ levels in a magnetic atom trap. a) The potential energy of the trap before the RF field is applied is given in (2.42), where the Larmor frequency $\omega_L(\vec{r})$ varies in space with the trapping field $B_0(\vec{r})$. When the RF field is added, at the point where ω_L matches the frequency ω_{RF}, the m_F levels are coupled. b) The diabatic energy levels cross as a result of this coupling. c) The adiabatic potentials as given in (2.47) are drawn, showing the avoided crossings, the mechanism by which a double well potential is formed in the trap [70].

The dressed potentials are therefore [60]

$$\begin{aligned} U(\vec{r}) &= \hbar\, m_{F'} \Omega(\vec{r}) \\ &= \hbar\, m_{F'} \sqrt{\delta^2(\vec{r}) + \Omega_0^2(\vec{r})} \\ &= \hbar\, m_{F'} \sqrt{(\omega_{RF} - \omega_L(\vec{r}))^2 + \left(\frac{\mu_B\, g_F}{2\hbar} |\vec{B}_{RF}(\vec{r})|\right)^2}, \end{aligned} \tag{2.47}$$

where $m_{F'}$ is a label for the states in the adiabatic basis, with $2F + 1$ values that range from $-F$ to F.

The RF dressing can be viewed as a rotation of (2.44) around the local y axis through an angle defined by $\cos\theta(\vec{r}) = -\delta(\vec{r})/\Omega(\vec{r})$ [60].

Creation of a double well potential The spatial dependence of $\omega_L(\vec{r})$ with the confining potential (2.42) means the frequency ω_{RF} of the applied field is resonant only at two points in space. In terms of the adiabatic basis: the potential energy of the dressed levels, as given in (2.47), lifts the degeneracy of the coupled diabatic energy levels at the points where $\delta(\vec{r}) = 0$, leading to avoided crossings and the creation of a double well along

the x axis [60].

Both the detuning $\delta(\vec{r})$ and Rabi frequency $\Omega_0(\vec{r})$ can change in space, but for the dressed potentials in (2.47) to be valid, their relative change must be small compared to the generalised Rabi frequency [60], $|\Omega_0'\delta| \ll \Omega^3$, $|\Omega_0\delta'| \ll \Omega^3$. It should be noted that the Hamiltonian does not contain a kinetic term; the validity of this approximation is discussed in [60].

2.5 Comparison of RF dressing in atom traps and mode coupling in Penning traps

The calculations above, of mode coupling in Penning traps in 2.2 and 2.3, and RF dressing in atom traps in 2.4, have an obvious semblance, as well as some clear differences.

After both calculations are transformed to their respective interaction pictures, the remaining Hamiltonians (2.34) and (2.44) both contain first and third-component angular momentum operators. Re-writing these together explicitly:

$$\hat{\mathcal{H}}_d = \omega_0\hat{T}_0 + \delta\hat{T}_3 + 2\xi\hat{T}_1 + \frac{\hbar\omega_0}{2}, \qquad H_Z = \pm\left(-\delta(\vec{r})\hat{F}_z + \Omega_0(\vec{r})\hat{F}_x\right). \tag{2.48}$$

Following transformation by $\hat{T}_2$ and $\hat{F}_y$ respectively, the dressed Hamiltonians (2.39) and (2.45) are written in terms of third angular momentum components of dressed mode operators[2]:

$$\hat{\mathcal{H}}_d \longrightarrow \omega_0\hat{T}_0^{\alpha\beta} + \Delta\hat{T}_3^{\alpha\beta} + \frac{\hbar\omega_0}{2}, \qquad H_Z \longrightarrow \Omega(\vec{r})\hat{F}_{z'}. \tag{2.49}$$

In the case of the dressed atoms, the term $\Omega(\vec{r})\hat{F}_{z'}$ is interpreted directly as potential energy of each m_F' level of the dressed system. In the Penning trap, the equivalent "Rabi frequency", Δ, is instead attached to some sub-levels $l_{\alpha\beta}$ of the dressed modes of the coupling. If the detuning and field strength were made variable in space as proposed [67], so that $\Delta \to \Delta(r)$, the effects upon the potential energy of the electron in the trap are not obvious. This idea will be re-addressed in Chapter 10.

In fact, the potential energy of the electron in the Penning trap is not directly interpretable even before the coupling field is applied. This is due to the presence of the magnetic field and its associated magnetic vector potential, which leads to the $\vec{v}\cdot\vec{A}$ term and ultimately the $xp_y - yp_x$ term in the Hamiltonian (1.16). This leads to some of the

[2]The dressed Penning trap Hamiltonian furthermore contains a $\hat{T}_0$ and ground state energy term, but this represents only an energy shift.

considerations of Chapters 3, 4 and 6, through which an interpretation of the potential in the quantum regime of the trap is sought.

This calculations in this chapter expose a number of parallels between the dressed-atom formalism [57] and the joint oscillator modes of the Penning trap in general. This is further examined throughout the remainder of this thesis.

Chapter 3

Comparison of Three Systems

This chapter is devoted to studying three distinct systems: the 2D harmonic oscillator, the "Landau system", comprising a single charged particle in a homogeneous magnetic field, and the Penning trap. After laying out the framework for the first two, their connection to the Penning trap is discussed.

3.1 The two-dimensional harmonic oscillator

3.1.1 Classical

The Hamiltonian of a particle of mass m confined by a potential $V(x,y) = \frac{1}{2}m(\frac{\omega_c}{2})^2(x^2 + y^2)$ is written:

$$H = \frac{1}{2m}\left(p_x^2 + p_y^2\right) + \frac{1}{2}m\left(\frac{\omega_c}{2}\right)^2\left(x^2 + y^2\right). \tag{3.1}$$

The equations of motion are integrated to yield [71]

$$\begin{aligned} x(t) &= x_m \cos\left(\frac{\omega_c}{2}t - \varphi_x\right), \quad p_x(t) = -m\frac{\omega_c}{2}x_m \sin\left(\frac{\omega_c}{2}t - \varphi_x\right), \\ y(t) &= y_m \cos\left(\frac{\omega_c}{2}t - \varphi_y\right), \quad p_y(t) = -m\frac{\omega_c}{2}y_m \sin\left(\frac{\omega_c}{2}t - \varphi_y\right), \end{aligned} \tag{3.2}$$

where the constants x_m, φ_x, y_m and φ_y depend on initial conditions, and x_m and y_m are assumed positive. The particle orbit as shown in Figure 3.1 depends upon the relative phase and amplitudes of the x and y motions. For example, if $\varphi_y - \varphi_x = 0$, the motion follows a diagonal line BD through the origin of the plane [71]. The condition $\varphi_y - \varphi_x = \pm\pi/2$ induces anticlockwise motion about this point, whereas the motion is always clockwise for $-\pi < \varphi_y - \varphi_x < 0$ [71]. This is all summarized by the component of the orbital angular momentum $L_z = xp_y - yp_x$ which is written, according to the above

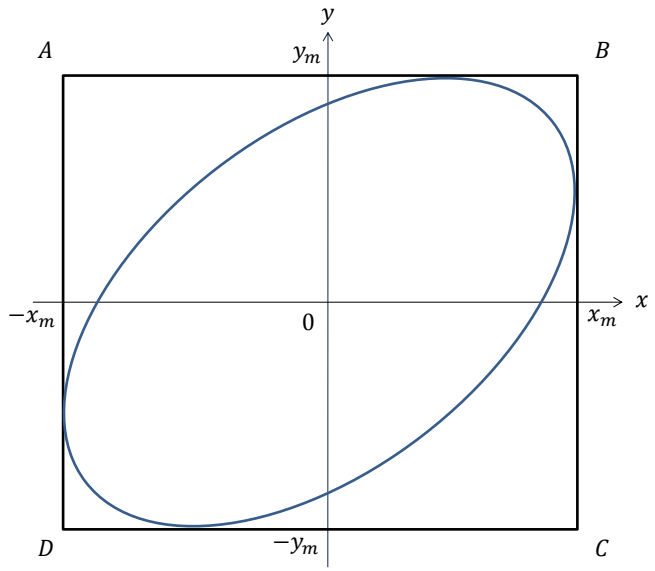

Figure 3.1: Classical trajectory of an particle in the xy plane, with motion governed by Hamiltonian (3.1). The motion in this 2D harmonic potential depends upon the initial conditions x_m, y_m, φ_x and φ_y in the equations of motion (3.2). The figure is copied closely from [71].

expressions for $x(t)$ and $y(t)$ [71]:

$$L_z = m\frac{\omega_c}{2}x_m y_m \sin(\varphi_y - \varphi_x). \tag{3.3}$$

This value is clearly maximal for $\varphi_y - \varphi_x = \pm\pi/2$, and describes circular motion for the additional condition $x_m = y_m$ [71].

3.1.2 Quantum mechanical

Imposing the canonical commutation relations $[\hat{x}_i, \hat{p}_j] = \delta_{ij} i\hbar$ enables construction of the operators:

$$\begin{aligned}
\hat{a}_x &= \frac{1}{\sqrt{2\hbar}}\left(\sqrt{\frac{m\omega_c}{2}}\hat{x} + i\sqrt{\frac{2}{m\omega_c}}\hat{p}_x\right), \quad \hat{a}_x^\dagger = \frac{1}{\sqrt{2\hbar}}\left(\sqrt{\frac{m\omega_c}{2}}\hat{x} - i\sqrt{\frac{2}{m\omega_c}}\hat{p}_x\right), \\
\hat{a}_y &= \frac{1}{\sqrt{2\hbar}}\left(\sqrt{\frac{m\omega_c}{2}}\hat{y} + i\sqrt{\frac{2}{m\omega_c}}\hat{p}_y\right), \quad \hat{a}_y^\dagger = \frac{1}{\sqrt{2\hbar}}\left(\sqrt{\frac{m\omega_c}{2}}\hat{y} - i\sqrt{\frac{2}{m\omega_c}}\hat{p}_y\right),
\end{aligned} \tag{3.4}$$

where $[\hat{a}_x, \hat{a}_x^\dagger] = [\hat{a}_y, \hat{a}_y^\dagger] = 1$, with all other commutators going to zero. The quantum Hamiltonian in the xy plane is given by

$$\hat{H}_{xy} = \hbar\frac{\omega_c}{2}\left(\hat{a}_x^\dagger\hat{a}_x + \frac{1}{2}\right) + \hbar\frac{\omega_c}{2}\left(\hat{a}_y^\dagger\hat{a}_y + \frac{1}{2}\right). \tag{3.5}$$

The basis of eigenstates of $\hat{H}_{xy}$ is composed of vectors of the form [71]

$$|\phi_{n_x,n_y}\rangle = |\phi_{n_x}\rangle \bigotimes |\phi_{n_y}\rangle, \tag{3.6}$$

and the energy is given by

$$E_{xy} = \hbar\frac{\omega_c}{2}\left(n_x + \frac{1}{2}\right) + \hbar\frac{\omega_c}{2}\left(n_y + \frac{1}{2}\right). \tag{3.7}$$

The eigenvalues of $|\phi_{n_x,n_y}\rangle$ in the state space ε_{xy} associated with the variables x and y are clearly degenerate: for an energy $E_{xy} = \hbar(\omega_c/2)(n+1)$, where $n = n_x + n_y$, there corresponds the various orthogonal eigenvectors [71]:

$$|\phi_{n_x=n,n_y=0}\rangle,\ |\phi_{n_x=n-1,n_y=1}\rangle, ..., |\phi_{n_x=0,n_y=n}\rangle. \tag{3.8}$$

The eigenvalue E_{xy} is therefore $(n+1)$-fold degenerate in ε_{xy}, so that $\hat{H}_{xy}$ alone does not constitute a complete set of commuting observables (CSCO) [71]. Taking better advantage of the symmetry of the system, consider first that the component of the angular momentum $\hat{L}_z$ can be expressed in terms of the creation and annihilation operators in (3.4):

$$\hat{L}_z = -i\hbar\left(\hat{a}_x^\dagger\hat{a}_y - \hat{a}_y^\dagger\hat{a}_x\right). \tag{3.9}$$

It is straightforward to show $\left[\hat{H}_{xy}, \hat{L}_z\right] = 0$, which promotes a basis of eigenvectors common to both $\hat{H}_{xy}$ and $\hat{L}_z$. This is found by introducing the operators of left and right "circular quanta" [71]:

$$\begin{aligned}
\hat{a} &= \frac{1}{\sqrt{2}}(\hat{a}_x - i\hat{a}_y) = \frac{1}{2\sqrt{\hbar}}\left(\sqrt{\frac{m\omega_c}{2}}(\hat{x} - i\hat{y}) + \sqrt{\frac{2}{m\omega_c}}(\hat{p}_y + i\hat{p}_x)\right),\\
\hat{a}^\dagger &= \frac{1}{\sqrt{2}}(\hat{a}_x^\dagger + i\hat{a}_y^\dagger) = \frac{1}{2\sqrt{\hbar}}\left(\sqrt{\frac{m\omega_c}{2}}(\hat{x} + i\hat{y}) + \sqrt{\frac{2}{m\omega_c}}(\hat{p}_y - i\hat{p}_x)\right),\\
\hat{b} &= \frac{1}{\sqrt{2}}(\hat{a}_x + i\hat{a}_y) = \frac{1}{2\sqrt{\hbar}}\left(\sqrt{\frac{m\omega_c}{2}}(\hat{x} + i\hat{y}) - \sqrt{\frac{2}{m\omega_c}}(\hat{p}_y - i\hat{p}_x)\right),\\
\hat{b}^\dagger &= \frac{1}{\sqrt{2}}(\hat{a}_x^\dagger - i\hat{a}_y^\dagger) = \frac{1}{2\sqrt{\hbar}}\left(\sqrt{\frac{m\omega_c}{2}}(\hat{x} - i\hat{y}) - \sqrt{\frac{2}{m\omega_c}}(\hat{p}_y + i\hat{p}_x)\right).
\end{aligned} \tag{3.10}$$

Hamiltonian (3.5) is rewritten

$$\hat{H}_{xy} = \hbar\frac{\omega_c}{2}\left(\hat{a}^\dagger\hat{a} + \hat{b}^\dagger\hat{b} + 1\right) = \hbar\frac{\omega_c}{2}\left(\hat{a}^\dagger\hat{a} + \frac{1}{2}\right) + \hbar\frac{\omega_c}{2}\left(\hat{b}^\dagger\hat{b} + \frac{1}{2}\right), \tag{3.11}$$

and the angular momentum in (3.9) is now given by

$$\hat{L}_z = \hbar\left(\hat{a}^\dagger\hat{a} - \hat{b}^\dagger\hat{b}\right). \tag{3.12}$$

Since $[\hat{a},\, \hat{a}^\dagger] = [\hat{b},\, \hat{b}^\dagger] = 1$, $[\hat{a},\, \hat{b}] = [\hat{a},\, \hat{b}^\dagger] = [\hat{a}^\dagger,\, \hat{b}] = [\hat{a}^\dagger\, \hat{b}^\dagger] = 0$, it is possible to construct states of the independent harmonic oscillators [71]

$$|\chi_{n_a,n_b}\rangle = \frac{1}{\sqrt{(n_a)!\,(n_b)!}}(\hat{a}^\dagger)^{n_a}(\hat{b}^\dagger)^{n_b}|\phi_{0,0}\rangle. \tag{3.13}$$

These are eigenstates of both $\hat{H}_{xy}$ and $\hat{L}_z$, with eigenvalues $\hbar(\omega_c/2)(n_a + n_b + 1) \equiv \hbar(\omega_c/2)(n + 1)$ and $\hbar\omega_c(n_a - n_b) = \hbar(\omega_c/2)m$ respectively. The quantum numbers n and m therefore form a CSCO in ε_{xy}; to a pair of values n and m, there corresponds a *single* state vector $|\chi_{n_a,n_b}\rangle$ as given in (3.13), where $a = (n+m)/2$, $b = (n-m)/2$ [71].

It is clear that the action of the operator $\hat{a}^\dagger$ on $|\chi_{n_a,n_b}\rangle$ is to add a quanta of energy and increase the angular momentum of the system, whereas $\hat{b}^\dagger$ must similarly add energy, but reduce the angular momentum by inducing an anticlockwise rotation [71].

3.2 The Landau system

3.2.1 Classical

A charged particle of mass m in the field $\vec{B} = |\vec{B}|\hat{e}_z$ has following Hamiltonian in the radial plane [40]:

$$\begin{aligned} H_L &= \frac{1}{2m}(\vec{p} - q\vec{A}(\vec{r}))^2 \\ &= \frac{1}{2m}\left(p_x^2 + p_y^2\right) + \frac{\omega_c}{2}\left(x\,p_y - y\,p_x\right) + \frac{1}{2}m\left(\frac{\omega_c}{2}\right)^2\left(x^2 + y^2\right), \end{aligned} \tag{3.14}$$

where the gauge conditions from 1.2.1 have been used, and $\omega_c = |q||\vec{B}|/m$.

3.2.2 Quantum mechanical

The sole difference between H_L and H_{xy} is is the additional angular momentum term $xp_y - yp_x$. From (3.12), the quantum form of this term is known. Adding it to $\hat{H}_{xy}$ in (3.11), the quantum Hamiltonian of the Landau system is given by:

$$\begin{aligned} \hat{H}_L &= \hat{H}_{xy} + \hat{L}_z \\ &= \hbar\frac{\omega_c}{2}\left(\hat{a}^\dagger\hat{a} + \frac{1}{2}\right) + \hbar\frac{\omega_c}{2}\left(\hat{b}^\dagger\hat{b} + \frac{1}{2}\right) + \hbar\frac{\omega_c}{2}\left(\hat{a}^\dagger\hat{a} - \hat{b}^\dagger\hat{b}\right) \\ &= \omega_c\left(\hat{a}^\dagger\hat{a} + \frac{1}{2}\right). \end{aligned} \tag{3.15}$$

Through the matching frequency contributions of the angular momentum and harmonic oscillator terms, the Hamiltonian can be written in terms of a single mode of circular quanta. The operators $\hat{H}_L$ and $\hat{L}_z$ again form a CSCO for the Landau system, but the "collapse" of the Hamiltonian into a single mode in (3.15) makes transparent the infinite degeneracy of the Landau levels [40]; states with a different value of $m = n_a - n_b$ but the same $n = n_a + n_b$ have the same energy; the angular momentum term does not contribute to the energy of the system [71].

3.3 The spectrum of the Penning trap

The cyclotron and magnetron mode operators of the circular Penning trap in (1.37) are compared to those of the harmonic oscillator and Landau systems in (3.10). It is clear that the only difference in the sets $\{\hat{a}_+^\dagger, \hat{a}_+, \hat{a}_-^\dagger, \hat{a}_-\}$ and $\{\hat{a}^\dagger, \hat{a}, \hat{b}^\dagger, \hat{b}\}$ is the frequency term, with ω_1 in the former, and ω_c in the latter. Moreover, since $\omega_1 \longrightarrow \omega_c$ as $\omega_z \longrightarrow 0$ (1.14) as the axial trapping is removed, it is clear that the radial Hamiltonian of the Penning trap (1.38) is reduced to that of the Landau system (3.15).

The Hamiltonians of the Penning trap ($\hat{\mathcal{H}}$) and Landau systems ($\hat{H}_L$) can be most readily compared by plotting the energy spectrum of $\hat{\mathcal{H}}$ as a function of ω_z.

The expectation values of the *radial* part of the $\hat{\mathcal{H}}$ with respect to Fock states $|n_+, n_-\rangle$ is first defined:

$$\langle \hat{\mathcal{H}}_r \rangle_\pm = \hbar\omega_+ \left(n_+ + \frac{1}{2}\right) - \hbar\omega_- \left(n_- + \frac{1}{2}\right). \tag{3.16}$$

Rearranging this reveals

$$\begin{aligned} \langle \hat{\mathcal{H}}_r \rangle_\pm &= \hbar\frac{(\omega_+ - \omega_-)}{2}(n_+ + n_- + 1) + \hbar\frac{(\omega_+ + \omega_-)}{2}(n_+ - n_-) \\ &= \hbar\frac{\omega_1}{2}\left(n_+ + \frac{1}{2}\right) + \hbar\frac{\omega_1}{2}\left(n_- + \frac{1}{2}\right) + \hbar\frac{\omega_c}{2}(n_+ - n_-). \end{aligned} \tag{3.17}$$

The parameter ν is defined [72]:

$$\nu = \frac{\omega_c - \omega_1}{2\omega_1}, \tag{3.18}$$

so that $\langle \hat{\mathcal{H}}_r \rangle_\pm$ can be written as a renormalized function of ν:

$$\mathcal{E}(\nu) = \frac{\langle \hat{\mathcal{H}}_r \rangle_\pm}{\hbar\omega_1/2} = n_+ + n_- + (2\nu + 1)(n_+ - n_-) + 1. \tag{3.19}$$

Figure 3.2 shows a plot of $\mathcal{E}(\nu)$ for the first ten total quantum numbers $(n_+ + n_-)$ of the Penning trap. Bhaduri et *al* provide a thorough analysis of this spectrum in [72], and they were indeed the first to recognise the generation of the Farey fan pattern [73] for this "cranked oscillator" system.

At $\nu = 0$, $\omega_c = \omega_1$, which corresponds to setting $\omega_z = 0$. At this point, there is no axial trapping and the electron is "confined" by the magnetic field only; this is exactly the Landau system described by Hamiltonian (3.15). To the right of this point, these levels are smeared out by the axial trapping in the Penning trap. This corresponds to the region $\omega_c > \omega_1$, and so a real Penning trap exists in this first quadrant. For typical trapping parameters $|\vec{B}| = 0.5\,\mathrm{T}$ and $V_r = -1\,\mathrm{V}$, $\nu \approx 1 \times 10^{-6}$. The point $\nu = -0.5$ corresponds to $\omega_c = 0$ and the spectrum reduces to that of a 2D harmonic oscillator with frequency $\omega_1/2$. Thus it is clear how the (radial spectra) of the three systems are linked.

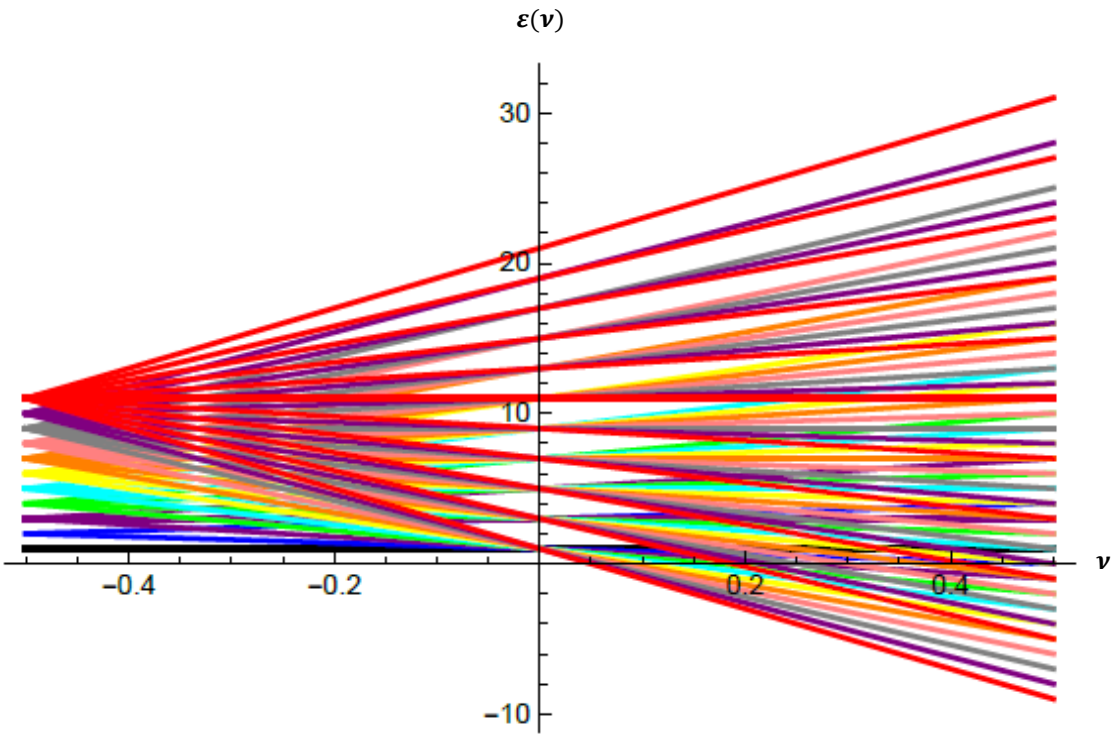

Figure 3.2: The expectation value spectrum of the radial motion in the Penning trap as a function of ν (3.18, 3.19) for the first ten total quantum numbers $n_+ + n_-$. The Landau levels form at $\nu = 0$, where $\omega_z = 0$, and are smeared out by the real trapping frequency along the z axis. The plot is symmetric about the point $\nu = -1/2$, corresponding to $\omega_c = 0$, where the spectrum reduces to that of a simple 2D harmonic oscillator with frequency $\omega_1/2$.

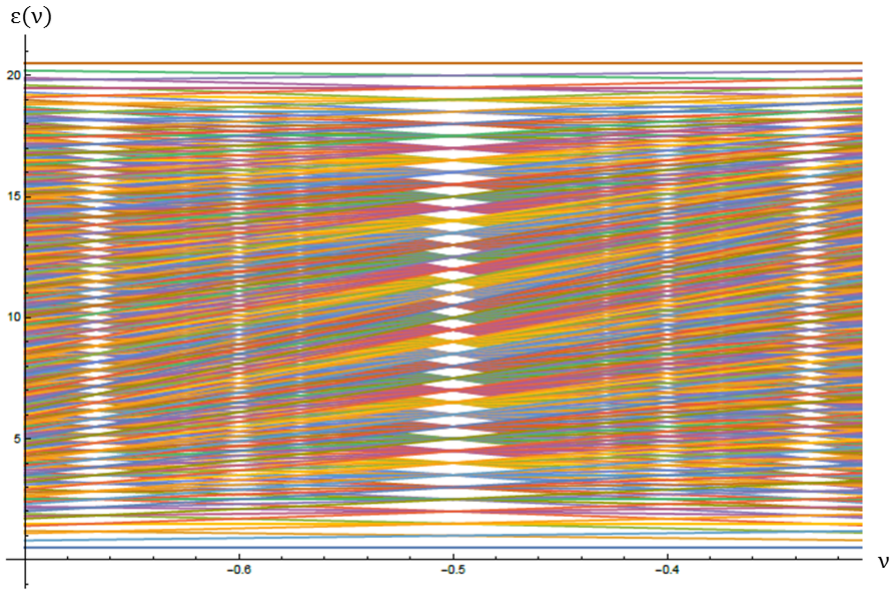

Figure 3.3: Zoomed-in plot of the expectation value spectrum of the radial motion of the Penning trap as a function of ν (3.18, 3.19) for the first twenty total quantum numbers $n_+ + n_-$. The gaps appear when ν is a rational fraction, which corresponds exactly to the classical orbits in the radial plane of the Penning trap forming closed loops [72]. The pattern is self-repeating as the scale decreases.

The plot can be extended in a straightforward way in *Mathematica* to include the expectation values for many more quantum numbers $n_+ + n_-$. Figure 3.3 shows a zoomed-in plot of a symmetric region around $\nu = -0.5$ for the expectation values of the first twenty total quantum numbers $n_+ + n_-$. It reveals more clearly the complex pattern and gaps of the spectrum, and the symmetry around this point. Such gaps correspond to rational numbers of ν, which, in the region $\nu > 0$, occur precisely when the classical radial orbits of the electron in the Penning trap are closed [72]. This can be verified by plotting $x(t)$ and $y(t)$ (1.24) for various values of ν which is written in terms of the cyclotron and magnetron frequencies as $\nu = \omega_-/(\omega_+ - \omega_-)$.

A plot of the classical orbits of the three systems also nicely illustrates how the radial motion of the three systems is linked. In Figure 3.4, the motion of an electron in the Penning trap is plotted in green, whereas the blue orbit corresponds to setting $\omega_c = 0$ to depict the 2D oscillator system. The red orbit follows from setting $\omega_z = 0$ for the Landau system.

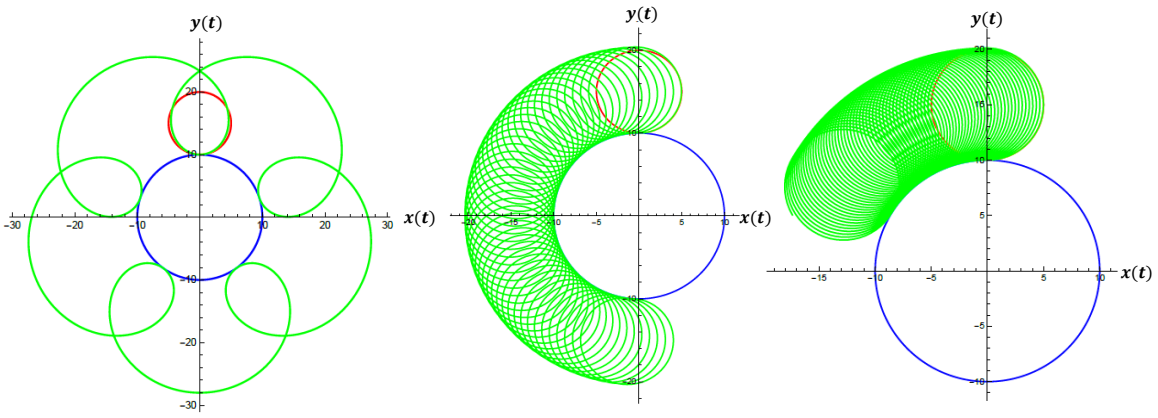

Figure 3.4: Plot of the electron orbit in the **Penning trap**, **2D harmonic oscillator** and **Landau system** as ν (3.18) and correspondingly ω_z increases in strength. From left to right: $\nu = 1/5,\ 1/40,\ 1/70$. The incomplete Penning trap orbits in the second and third plots is in consequence of the maximum number of steps being reached in the *Mathematica* calculation. It indicates how the time to complete the magnetron orbit (around the blue circle) grows with decreasing ν. In the limit $\nu \to 0$, corresponding to removing the $\vec{E}$ field from the trap completely, it is clear that the electron becomes "stuck" at the top of the blue circle; the motion in the radial plane reduces to that of the Landau system.

3.4 Transformation of the $\{x, y\}$ to the $\{+, -\}$ basis

3.4.1 Summary of systems and coordinates

In writing Hamiltonian (3.1) of the 2D oscillator in terms of classical coordinates in 3.1, the natural choice is obviously the $\{x, y\}$ basis. The quantum Hamiltonian (3.5) follows trivially upon defining the $\hat{a}_x$ and $\hat{a}_y$ mode operators. The rewriting of Hamiltonian (3.5) in terms of $\hat{a}$ and $\hat{b}$ (3.11) follows from the desire to find a basis which uniquely defines the state of the system, since the symmetry between the two axes leads to degenerate states [71]. This leads to the rewriting of $\hat{L}_z$ in a diagonal form, and the solution of the problem in terms of Fock states of the circular $\hat{a}$ and $\hat{b}$ modes.

In the Landau system above, Hamiltonian (3.15) is automatically written in terms of the circular modes above. Equal frequency contributions from the harmonic oscillator $(\hat{n}_a + \hat{n}_b)$ and angular momentum $(\hat{n}_a - \hat{n}_b)$ terms means $\hat{H}_L$ can be written in terms of one set of mode operators alone. This appeals to intuition and explains well the infinite degeneracy of Landau levels [40].

Three-dimensional (3D) confinement in the Penning trap demands the use of both $\vec{E}$ and $\vec{B}$ fields. As a result, *both* modes of "circular quanta", $\hat{n}_+$ and $\hat{n}_-$, must be used to write Hamiltonian (1.38). Consequently, the size of contribution of the harmonic oscillator term $\hbar\omega_1/2(\hat{n}_+ + \hat{n}_-)$ can *never* match that of the angular momentum contribution, $\hbar\omega_c/2(\hat{n}_+ - \hat{n}_-)$. The independent cyclotron and magnetron modes result.

3.4.2 Rotation of the coordinates and angular momentum

The basis transformation between the linear $(\hat{a}_x, \hat{a}_y)$ and circular $(\hat{a}, \hat{b})$ mode operators in 3.1, (or equivalently the operators $(\hat{a}_+, \hat{a}_-)$ defined in (1.37)) is written compactly in matrix form:

$$\begin{pmatrix} \hat{a}_+ \\ \hat{a}_- \end{pmatrix} = \frac{1}{\sqrt{2}} \begin{pmatrix} 1 & -i \\ 1 & i \end{pmatrix} \begin{pmatrix} \hat{a}_x \\ \hat{a}_y \end{pmatrix}. \tag{3.20}$$

It is instructive to form sets of Schwinger boson operators [61], as introduced in 2.3.3. For the linear ($\underline{I}$) and circular bases ($\underline{L}$):

$$\begin{aligned}
\hat{I}_0 &= \frac{\hbar}{2}\left(\hat{n}_x + \hat{n}_y\right), & \hat{L}_0 &= \frac{\hbar}{2}\left(\hat{n}_+ + \hat{n}_-\right), \\
\hat{I}_1 &= \frac{\hbar}{2}\left(\hat{a}_x^\dagger \hat{a}_y + \hat{a}_y^\dagger \hat{a}_x\right), & \hat{L}_1 &= \frac{\hbar}{2}\left(\hat{a}_+^\dagger \hat{a}_- + \hat{a}_-^\dagger \hat{a}_+\right), \\
\hat{I}_2 &= -i\frac{\hbar}{2}\left(\hat{a}_x^\dagger \hat{a}_y - \hat{a}_y^\dagger \hat{a}_x\right), & \hat{L}_2 &= -i\frac{\hbar}{2}\left(\hat{a}_+^\dagger \hat{a}_- - \hat{a}_-^\dagger \hat{a}_+\right), \\
\hat{I}_3 &= \frac{\hbar}{2}\left(\hat{n}_x - \hat{n}_y\right), & \hat{L}_3 &= \frac{\hbar}{2}\left(\hat{n}_+ - \hat{n}_-\right).
\end{aligned} \tag{3.21}$$

Expanding these Schwinger boson components in terms of position and momentum operators $\hat{x}$, $\hat{y}$, $\hat{p}_x$, and $\hat{p}_y$, establishes the following relationship between the two sets:

$$\begin{aligned}
\hat{I}_0 &= \hat{L}_0, \\
\hat{I}_1 &= \hat{L}_2, \\
\hat{I}_2 &= \hat{L}_3 = \frac{1}{2}\hat{L}_z, \\
\hat{I}_3 &= \hat{L}_1.
\end{aligned} \tag{3.22}$$

Both the second component of $\underline{I}$ and the *third* of $\underline{L}$ are identically half of the z component of angular momentum [1]. The correspondence between the sets $\underline{I}$ and $\underline{L}$ can be written in the compact form:

$$\begin{pmatrix} \hat{L}_1 \\ \hat{L}_2 \\ \hat{L}_3 \end{pmatrix} = \begin{pmatrix} 0 & 0 & 1 \\ 1 & 0 & 0 \\ 0 & 1 & 0 \end{pmatrix} \begin{pmatrix} \hat{I}_1 \\ \hat{I}_2 \\ \hat{I}_3 \end{pmatrix}, \tag{3.23}$$

which reveals the $SO(3)$ representation of the transformation matrix in (3.20) [74]. This will be discussed further in Chapter 5. For the purpose of the next Chapter, it is worthwhile restating the following: $\hat{L}_z$ can be represented as the second or third component of a set of angular momentum-like operators, depending on whether it is written in terms of the linear $\{x, y\}$, or circular $\{+, -\}$ basis respectively.

[1] The factor of 1/2 is justified in Chapter 5.

Chapter 4

Reference Frames

This chapter is motivated by a desire to interpret the *individual* x and y dynamics in the Penning trap in a consistent way. As discussed in 2.5, the $\vec{B}$ field induces velocity dependent potentials in the radial plane of the trap, so that the meaning of potential energy in this plane is ambiguous.

4.1 Classical rotating frame

It has been shown [75, 76] how the dynamics in a circular Penning trap can be more intuitively interpreted in a frame of reference rotating around the z axis. Different choices of the frequency of this rotating frame allow for useful interpretations [75], and in particular the frame rotating at $\omega_c/2$ is often used to reduce the dynamics of the radial motion to that of two simple harmonic oscillators [77].

4.1.1 Removing the effects of the magnetic field

A change of coordinates to a frame rotating around the z axis at frequency Ω is defined [75]:

$$x \to x \cos \Omega t - y \sin \Omega t, \tag{4.1}$$

$$y \to x \sin \Omega t + y \cos \Omega t, \tag{4.2}$$

where the positive rotation is in the same anticlockwise direction as that induced by the force on the electron in the magnetic field. In this frame, the Hamiltonian of the circular

Penning trap becomes [75]

$$\mathcal{H} \to \frac{1}{2m}\left(p_x^2 + p_y^2 + p_z^2\right) + \left(\frac{1}{2}\omega_c - \Omega\right)(xp_y - yp_x) + \frac{m}{2}\left(\frac{\omega_1}{2}\right)^2\left(x^2 + y^2\right) + \frac{1}{2}m\omega_z^2 z^2, \tag{4.3}$$

and the canonical momenta of the radial motions transform accordingly:

$$p_x \to m\dot{x} + my\left(\frac{1}{2}\omega_c - \Omega\right), \quad p_y \to m\dot{y} - mx\left(\frac{1}{2}\omega_c - \Omega\right). \tag{4.4}$$

By a judicious choice of $\Omega = \omega_c/2$, the angular momentum term is removed from the Hamiltonian:

$$\mathcal{H} \overset{\Omega=\omega_c/2}{\to} \mathcal{H}_\Omega = \frac{1}{2m}\left(p_x^2 + p_y^2 + p_z^2\right) + \frac{m}{2}\left(\frac{\omega_1}{2}\right)^2\left(x^2 + y^2\right) + \frac{1}{2}m\omega_z^2 z^2, \tag{4.5}$$

and from (4.4) it is clear that the canonical momenta reduce to their kinetic form [75]. Thus the rotating frame reveals an isotropic oscillator in the radial plane, along with the original axial motion, and appears to remove the coupling of the x and y motions induced by the magnetic field from the Hamiltonian.

4.1.2 Removing the effects of the electric field

Other interesting choices of the frequency Ω are the slow magnetron drift ω_- and the reduced cyclotron frequency ω_+ [75]. Plugging the former into (4.3):

$$\mathcal{H} \overset{\Omega=\omega_-}{\to} \mathcal{H}_{\omega_-} = \frac{1}{2m}\left(p_x^2 + p_y^2 + p_z^2\right) + \frac{m}{2}\left(\frac{\omega_1}{2}\right)^2\left(x^2 + y^2\right) + \frac{\omega_1}{2}(xp_y - yp_x) + \frac{1}{2}m\omega_z^2 z^2. \tag{4.6}$$

This radial part of this Hamiltonian is identical to the classical Landau Hamiltonian (3.14) with frequency $\omega_c/2$ replaced by $\omega_1/2$; the rotating frame at this frequency appears to remove any effects of the electric field, leaving only the dynamics of an electron in a magnetic field with Larmor frequency $\omega_1/2$. The choice $\Omega = \omega_+$ clearly reduces the radial part of $\mathcal{H}$ to the Landau Hamiltonian with the opposite sign of angular momentum:

$$\mathcal{H} \overset{\Omega=\omega_+}{\to} \mathcal{H}_{\omega_+} = \frac{1}{2m}\left(p_x^2 + p_y^2 + p_z^2\right) + \frac{m}{2}\left(\frac{\omega_1}{2}\right)^2\left(x^2 + y^2\right) - \frac{\omega_1}{2}(xp_y - yp_x) + \frac{1}{2}m\omega_z^2 z^2. \tag{4.7}$$

This is the effective Hamiltonian of a *positron* particle in a magnetic field with Larmor frequency $\omega_1/2$ [75].

4.2 Quantum mechanical rotating frame, $\{+,-\}$ basis

4.2.1 Removing the effects of the magnetic field

The quantum analogue of the above transformation to the rotating frame is now studied. Beginning with the quantum Hamiltonian of the Penning trap (1.38) rearranged into the sum and difference between the two oscillator modes:

$$\begin{aligned}\hat{\mathcal{H}} &= \frac{\hbar}{2}(\omega_+ - \omega_-)(\hat{a}_+^\dagger \hat{a}_+ + \hat{a}_-^\dagger \hat{a}_-) + \frac{\hbar}{2}(\omega_+ + \omega_-)(\hat{a}_+^\dagger \hat{a}_+ - \hat{a}_-^\dagger \hat{a}_-) + \hbar\omega_z(\hat{a}_z^\dagger \hat{a}_z + \frac{1}{2}) + \frac{\hbar}{2}\omega_1 \\ &= \frac{\hbar}{2}\omega_1(\hat{a}_+^\dagger \hat{a}_+ + \hat{a}_-^\dagger \hat{a}_-) + \frac{\hbar}{2}\omega_c(\hat{a}_+^\dagger \hat{a}_+ - \hat{a}_-^\dagger \hat{a}_-) + \hbar\omega_z(\hat{a}_z^\dagger \hat{a}_z + \frac{1}{2}) + \frac{\hbar}{2}\omega_1. \end{aligned} \tag{4.8}$$

From (3.21), this is rewritten in terms of the Schwinger boson operators of the $\{+,-\}$[1] basis:

$$\hat{\mathcal{H}} = \omega_1 \hat{L}_0 + \omega_c \hat{L}_3 + \hbar\omega_z \left(\hat{a}_z^\dagger \hat{a}_z + \frac{1}{2}\right) + \frac{\hbar}{2}\omega_1. \tag{4.9}$$

The analogous quantum transformation to the rotating frame discussed in 4.1 is achieved by the unitary operator

$$\hat{U}(t) = \exp\left\{\frac{i}{\hbar} 2\Omega t \hat{L}_3\right\} = \exp\left\{\frac{i}{\hbar}\Omega t \hat{L}_z\right\}. \tag{4.10}$$

Time dependent unitary transformation of the Hamiltonian follows from (2.5), so that the quantum Hamiltonian in the rotating frame becomes

$$\hat{\mathcal{H}} \to \hat{\mathcal{H}} + i\hbar \cdot \frac{i}{\hbar} 2\Omega \hat{L}_3 = \omega_1 \hat{L}_0 + \omega_c \hat{L}_3 + \hbar\omega_z \left(\hat{a}_z^\dagger \hat{a}_z + \frac{1}{2}\right) + \frac{\hbar}{2}\omega_1 - 2\Omega \hat{L}_3, \tag{4.11}$$

which follows from $\left[\hat{H}, \hat{U}(t)\right] = 0$. Again, the choice of $\Omega = \omega_c/2$ reveals

$$\hat{\mathcal{H}} \overset{\Omega=\omega_c/2}{\to} \hat{\mathcal{H}}_\Omega = \hat{\mathcal{H}} = \omega_1 \hat{L}_0 + \hbar\omega_z \left(\hat{a}_z^\dagger \hat{a}_z + \frac{1}{2}\right) + \frac{\hbar}{2}\omega_1. \tag{4.12}$$

This can be expanded out into position and momentum coordinates and identified exactly with a classical Hamiltonian in the rotating frame (4.5).

4.2.2 Removing the effects of the electric field

The other interesting choices of frequency, $\Omega = \omega_-$ and $\Omega = \omega_+$, are briefly examined in quantum form. Following from (4.11),

$$\begin{aligned}\hat{\mathcal{H}}_{\omega_-} &= \hat{\mathcal{H}} - 2(\omega_-)\hat{L}_3 \\ &= \hbar\omega_1 \left(\hat{n}_+ + \frac{1}{2}\right) + \hbar\omega_z \left(\hat{a}_z^\dagger \hat{a}_z + \frac{1}{2}\right), \end{aligned} \tag{4.13}$$

[1] The notation $\{+,-\}$ is used to indicate the $\{+,-,z\}$ basis, just as $\{x,y\}$ will be used instead of $\{x,y,z\}$ throughout this thesis. This is just for ease of reading, and does not indicate that the axial motion has been dropped.

$$\begin{aligned}\hat{\mathcal{H}}_{\omega_+} &= \hat{\mathcal{H}} - 2\left(\omega_+\right)\hat{L}_3 \\ &= \hbar\omega_1\left(\hat{n}_- + \frac{1}{2}\right) + \hbar\omega_z\left(\hat{a}_z^\dagger\hat{a}_z + \frac{1}{2}\right).\end{aligned} \tag{4.14}$$

Upon expansion, these are identical to (4.6) and (4.7) respectively.

4.2.3 States and expectation values

The above calculations so far demonstrate consistency between the rotating frames in the classical and quantum regimes. Throughout the remainder of this thesis, *the rotating frame* shall be used to refer to the frame rotating at $\omega_c/2$ explicitly.

Since (4.26) is unitary, expectation values are conserved by this transformation. Defining the solutions of the rotating frame

$$|\psi_\Omega\rangle = \hat{U}(t)|\psi\rangle, \tag{4.15}$$

the expectation value of the Hamiltonian in the frame rotating at $\omega_c/2$ is given by:

$$\begin{aligned}\langle\psi_\Omega|\hat{\mathcal{H}}_\Omega|\psi_\Omega\rangle &= \langle\psi_\Omega|\left[\hat{U}(t)\hat{\mathcal{H}}\hat{U}^\dagger(t) + i\hbar\dot{\hat{U}}(t)\hat{U}^\dagger(t)\right]|\psi_\Omega\rangle \\ &= \langle\psi_\Omega|\hat{U}(t)\hat{\mathcal{H}}\hat{U}^\dagger(t)|\psi_\Omega\rangle + i\hbar\langle\psi_\Omega|\dot{\hat{U}}(t)\hat{U}^\dagger(t)|\psi_\Omega\rangle.\end{aligned} \tag{4.16}$$

Since

$$i\hbar\dot{\hat{U}}(t)\hat{U}^\dagger(t) = -\omega_c\hat{L}_3\hat{U}(t)\hat{U}^\dagger(t), \tag{4.17}$$

and $\hat{U}(t)$ commutes with the Hamiltonian,

$$\implies \langle\psi|\hat{\mathcal{H}}_\Omega|\psi\rangle = \langle\psi|\hat{\mathcal{H}}|\psi\rangle - \omega_c\langle\psi|\hat{L}_3|\psi\rangle. \tag{4.18}$$

In terms of Fock states in the lab frame $|\psi\rangle = |n_+, n_-, n_z\rangle$:

$$\begin{aligned}\langle\psi|\hat{\mathcal{H}}|\psi\rangle &= \langle\psi|\hat{\mathcal{H}}_\Omega|\psi\rangle + \omega_c\langle\psi|\hat{L}_3|\psi\rangle \\ &= \hbar\omega_+\left(n_+ + \frac{1}{2}\right) - \hbar\omega_-\left(n_- + \frac{1}{2}\right) + \hbar\omega_z\left(n_z + \frac{1}{2}\right).\end{aligned} \tag{4.19}$$

Thus the expectation value of the Hamiltonian in the rotating frame is added to the angular momentum term $\hat{L}_3$ which was removed upon transformation, which yields the correct total energy of the system. This is elementary quantum mechanics, but the point is laboured for further discussion in 4.4.2.

The classical solution to the (radial) equations of motion in the rotating frame are undoubtedly simple harmonic oscillators with frequency $\omega_1/2$. It is also clear that the Fock states $|n_+, n_-, n_z\rangle$ are eigenstates of Hamiltonian (4.12) in the rotating frame. $\hat{\mathcal{H}}_\Omega$ is expanded into position and momentum operators:

$$\hat{\mathcal{H}}_\Omega = \frac{1}{2m}\left(\hat{p}_x^2 + \hat{p}_y^2 + \hat{p}_z^2\right) + \frac{m}{2}\left(\frac{\omega_1}{2}\right)^2\left(\hat{x}^2 + \hat{y}^2\right) + \frac{1}{2}m\omega_z^2\hat{z}^2. \tag{4.20}$$

Since this Hamiltonian is diagonal in $\hat{x}^2$, $\hat{y}^2$, $\hat{p}_x^2$ and $\hat{p}_y^2$, it *appears* as though the Fock states $|n_x, n_y, n_z\rangle$ are also eigenstates of this Hamiltonian. This implies

$$|n_x, n_y, n_z\rangle = \hat{U}^\dagger(t)|\psi\rangle, \tag{4.21}$$

for some eigenstate $|\psi\rangle$ of the Hamiltonian in the laboratory frame.

These states form the basis of discussion in the following section, where the entire calculation is reformed in the $\{x, y\}$ basis.

4.3 Hamiltonian of the Penning trap in the $\{x, y\}$ basis

In addition to the previously defined operators of the axial mode in (1.37), the operators

$$\begin{aligned}\hat{a}_x &= \frac{1}{\sqrt{2\hbar}}\left(\sqrt{\frac{m\omega_1}{2}}\hat{x} + i\sqrt{\frac{2}{m\omega_1}}\hat{p}_x\right),\\ \hat{a}_x^\dagger &= \frac{1}{\sqrt{2\hbar}}\left(\sqrt{\frac{m\omega_1}{2}}\hat{x} - i\sqrt{\frac{2}{m\omega_1}}\hat{p}_x\right),\end{aligned} \tag{4.22}$$

$$\begin{aligned}\hat{a}_y &= \frac{1}{\sqrt{2\hbar}}\left(\sqrt{\frac{m\omega_1}{2}}\hat{y} + i\sqrt{\frac{2}{m\omega_1}}\hat{p}_y\right),\\ \hat{a}_y^\dagger &= \frac{1}{\sqrt{2\hbar}}\left(\sqrt{\frac{m\omega_1}{2}}\hat{y} - i\sqrt{\frac{2}{m\omega_1}}\hat{p}_y\right),\end{aligned} \tag{4.23}$$

will now be used to write for the Penning trap. These obey the appropriate commutation relations $[\hat{a}_x, \hat{a}_x^\dagger] = [\hat{a}_y, \hat{a}_y^\dagger] = 1$, with all other commutators going to zero. The quantum Hamiltonian is thus written:

$$\boxed{\hat{\mathcal{H}} = \hbar\frac{\omega_1}{2}\left(\hat{a}_x^\dagger\hat{a}_x + \frac{1}{2}\right) + \hbar\frac{\omega_1}{2}\left(\hat{a}_y^\dagger\hat{a}_y + \frac{1}{2}\right) - i\hbar\frac{\omega_c}{2}\left(\hat{a}_x^\dagger\hat{a}_y - \hat{a}_y^\dagger\hat{a}_x\right) + \hbar\omega_z\left(\hat{a}_z^\dagger\hat{a}_z + \frac{1}{2}\right)}. \tag{4.24}$$

Referring to the Schwinger boson operators introduced in (3.21), this is equivalent to:

$$\hat{\mathcal{H}} = \omega_1\hat{I}_0 + \omega_c\hat{I}_2 + \hbar\omega_z\left(\hat{a}_z^\dagger\hat{a}_z + \frac{1}{2}\right) + \frac{\hbar}{2}\omega_1. \tag{4.25}$$

It should be borne in mind that the Hamiltonian in the form of (1.38) is identical to Hamiltonian (4.24) via the *replacement* of operators $\{\hat{a}_+, \hat{a}_-\} \to \{\hat{a}_x, \hat{a}_y\}$. The Hamiltonian itself has not been rotated or transformed. This recollects the discussion in 2.3, where the notion of dressed levels was introduced. In the present case, it is rather like the cyclotron and magnetron modes are the x and y modes dressed by the magnetic field. Of course, there is no analogous avoided crossing point for the radial motions in this case; the x and y oscillators have the same frequency, so effectively "cross" at all points. From (3.22), $\hat{I}_0 = \hat{L}_0$ and $\hat{I}_2 = \hat{L}_3$, so it is clear that the Hamiltonians written in terms of the two sets of Schwinger boson operators are likewise identical.

4.4 Quantum mechanical rotating frame, $\{x, y\}$ basis

4.4.1 Removing the magnetic field

In terms of the $\{x, y\}$ basis, analogous transformation to the rotating frame is by the $\hat{I}_2$ operator:

$$\hat{U}(t) = \exp\left\{\frac{i}{\hbar} 2\Omega t \hat{I}_2\right\} = \exp\left\{\frac{i}{\hbar}\Omega t \hat{L}_z\right\}. \tag{4.26}$$

To demonstrate consistency, this produces the same effect upon $\hat{x}$ as the classical transformation upon x:

$$\begin{aligned}
&\hat{U}(t)\,\hat{x}\,\exp\hat{U}^\dagger(t) \\
&= \exp\left\{\frac{i}{\hbar}\Omega t \hat{L}_z\right\}\left[\sqrt{\frac{\hbar}{m\omega_1}}\left(\hat{a}_x^\dagger + \hat{a}_x\right)\right]\exp\left\{-\frac{i}{\hbar}\Omega t \hat{L}_z\right\} \\
&= \sqrt{\frac{\hbar}{m\omega_1}}\left(\hat{a}_x^\dagger\,\cos\Omega t - \hat{a}_y^\dagger\,\sin\Omega t + \hat{a}_x\,\cos\Omega t - \hat{a}_y\,\sin\Omega t\right) \\
&= \hat{x}\,\cos\Omega t - \hat{y}\,\sin\Omega t.
\end{aligned} \tag{4.27}$$

This is identical, apart from the hats, to (4.1). The other position and momentum operators transform analogously. Following the prescription for time dependent unitary rotation (2.5), transformation of Hamiltonian (4.24) results in

$$\begin{aligned}
\hat{\mathcal{H}} \to\ & \hbar\frac{\omega_1}{2}\left(\hat{a}_x^\dagger\hat{a}_x + \frac{1}{2}\right) + \hbar\frac{\omega_1}{2}\left(\hat{a}_y^\dagger\hat{a}_y + \frac{1}{2}\right) \\
& - i\hbar\left(\frac{\omega_c}{2} - \Omega\right)\left(\hat{a}_x^\dagger\hat{a}_y - \hat{a}_y^\dagger\hat{a}_x\right) + \hbar\omega_z\left(\hat{a}_z^\dagger\hat{a}_z + \frac{1}{2}\right),
\end{aligned} \tag{4.28}$$

where $\Omega = \omega_c/2$ reveals

$$\hat{\mathcal{H}}_\Omega = \hbar\frac{\omega_1}{2}\left(\hat{a}_x^\dagger\hat{a}_x + \frac{1}{2}\right) + \hbar\frac{\omega_1}{2}\left(\hat{a}_y^\dagger\hat{a}_y + \frac{1}{2}\right) + \hbar\omega_z\left(\hat{a}_z^\dagger\hat{a}_z + \frac{1}{2}\right). \tag{4.29}$$

A 3D harmonic oscillator has again been obtained in the rotating frame, matching exactly (4.5) and (4.29). This problem seems resolved; this Hamiltonian (4.29) clearly admits Fock state solutions $|n_x, n_y, n_z\rangle$. It follows that dynamics of the radial system can surely be interpreted as a 2D Harmonic oscillator rotating around the z axis. The following analysis, however, refutes this idea.

4.4.2 States and expectation values

Fock states

The analysis of 4.2.3 is now repeated in the $\{x, y\}$ basis. Defining the solutions of the rotating frame

$$|\phi_\Omega\rangle = \hat{U}(t)|\phi\rangle, \tag{4.30}$$

the expectation value of the Hamiltonian in this frame is:

$$\begin{aligned}\langle\phi_\Omega|\hat{\mathcal{H}}_\Omega|\phi_\Omega\rangle &= \langle\phi_\Omega|\left[\hat{U}(t)\hat{\mathcal{H}}\hat{U}^\dagger(t) + i\hbar\dot{\hat{U}}(t)\hat{U}^\dagger(t)\right]|\phi_\Omega\rangle \\ &= \langle\phi_\Omega|\hat{U}(t)\hat{\mathcal{H}}\hat{U}^\dagger(t)|\phi_\Omega\rangle + i\hbar\langle\phi_\Omega|\dot{\hat{U}}(t)\hat{U}^\dagger(t)|\phi_\Omega\rangle. \end{aligned} \tag{4.31}$$

This time,

$$i\hbar\dot{\hat{U}}(t)\hat{U}^\dagger(t) = -\omega_c\hat{I}_2\hat{U}(t)\hat{U}^\dagger(t), \tag{4.32}$$

and again

$$\left[\hat{U}(t),\, \hat{\mathcal{H}}\right] = 0 \tag{4.33}$$

$$\implies \langle\phi_\Omega|\hat{\mathcal{H}}_\Omega|\phi_\Omega\rangle = \langle\phi|\hat{\mathcal{H}}|\phi\rangle - \omega_c\langle\phi_\Omega|\hat{I}_2|\phi_\Omega\rangle. \tag{4.34}$$

In terms of Fock states $|\phi_\Omega\rangle = |n_x, n_y, n_z\rangle$:

$$\begin{aligned}\langle\phi_\Omega|\hat{I}_2|\phi_\Omega\rangle &= \frac{-i\hbar}{2}\langle n_x, n_y, n_z|\left(\hat{a}_x^\dagger\hat{a}_y - \hat{a}_y^\dagger\hat{a}_x\right)|n_x, n_y, n_z\rangle \\ &= 0, \end{aligned} \tag{4.35}$$

so that

$$\begin{aligned}\langle\phi|\hat{\mathcal{H}}|\phi\rangle &= \langle\phi_\Omega|\hat{\mathcal{H}}_\Omega|\phi_\Omega\rangle \\ &= \hbar\frac{\omega_1}{2}\left(n_x + \frac{1}{2}\right) + \hbar\frac{\omega_1}{2}\left(n_y + \frac{1}{2}\right) + \hbar\omega_z\left(n_z + \frac{1}{2}\right). \end{aligned} \tag{4.36}$$

Assuming eigenstates in the rotating frame $|\phi_\Omega\rangle = |n_x, n_y, n_z\rangle$, and therefore $|\phi\rangle = \hat{U}^\dagger(t)|n_x, n_y, n_z\rangle$, leads to the expectation value of the Hamiltonian which *does not count the non-degenerate energy contribution of the Landau levels.* This may seem trivial. It is, after all, the reason that the $\{+,-\}$ basis is used to diagonalise this system. Yet this result is in stark contradiction to what is assumed about the eigenstates from the form of (4.29). It reveals the following:

$$\langle n_x, n_y, n_z|\hat{U}(t)\ \hat{\mathcal{H}}\ \hat{U}^\dagger(t)|n_x, n_y, n_z\rangle \neq \langle n_+, n_-, n_z|\hat{\mathcal{H}}|n_+, n_-, n_z\rangle. \tag{4.37}$$

Since the Hamiltonians (4.24) and (1.38) are identical upon replacement of operators $\{\hat{a}_x, \hat{a}_y\} \to \{\hat{a}_+, \hat{a}_-\}$, it follows that

$$|n_+, n_-, n_z\rangle \neq \hat{U}^\dagger(t)|n_x, n_y, n_z\rangle. \tag{4.38}$$

The quantum treatment reveals that the Fock states $|n_+, n_-,\rangle$ of the Penning trap are *not* rotating Fock states of the x and y modes. Transformation to the rotating frame in the

$\{+,-\}$ basis shows that the Fock states of the rotating frame are again the states $|n_+, n_-\rangle$ with additional time dependence of $\exp\{i\omega_c t/2\,(n_+ - n_-)\}$. However, the radial dynamics in the rotating frame *cannot* be split up into individual x and y motions on a quantum level. It follows that interpretation of the potential energy of the electron in the Penning trap for quantum states cannot be achieved by use of the rotating frame, as would appear logical from the classical calculation of 4.1. In the following section, the semi-classical problem is discussed.

It is interesting to consider whether there are any values of ω_c and ω_z (the "bare" frequencies) for which the Fock states $|n_x, n_y, n_z\rangle$ *can* be used to count the full energy of the system: are there trapping parameters for which expectation value of $\hat{\mathcal{H}}$ with respect to $|n_x, n_y, n_z\rangle$ is equal to that with respect to $|n_+, n_-, n_z\rangle$? The condition implies the following:

$$\begin{aligned}
\langle n_x, n_y, n_z|\hat{\mathcal{H}}|n_x, n_y, n_z\rangle &= \langle n_+, n_-, n_z|\hat{\mathcal{H}}|n_+, n_-, n_z\rangle \\
\implies \hbar\frac{\omega_1}{2}(n_x + n_y + 1) &= \hbar\frac{\omega_1}{2}(n_+ + n_- + 1) + \frac{\omega_c}{2}(n_+ - n_- + 1) \\
\implies n_x + n_y &= n_+\left(1 + \frac{\omega_c}{\omega_1}\right) + n_-\left(1 - \frac{\omega_c}{\omega_1}\right).
\end{aligned} \tag{4.39}$$

Since the total quantum number $n_x + n_y$ is always an integer value, the equality can only possibly hold when the ratio ω_c/ω_1 is also an integer: the Fock states $|n_x, n_y, n_z\rangle$ are eigenstates of the Hamiltonian in the lab frame only when

$$\frac{\omega_c}{\omega_1} = N, \qquad N = 0, 1, 2, 3, ... \tag{4.40}$$

Referring back to the spectrum of the Penning trap discussed in (3.3), it is clear that the ratio ω_c/ω_1 is connected to the variable ν along the horizontal axes of Figures 3.2 and 3.3. In fact, the condition (4.40) implies :

$$\nu = \frac{N-1}{2}; \tag{4.41}$$

The Fock states $|n_x, n_y, n_z\rangle$ are eigenstates of the quantum Hamiltonian only for half integer values along the horizontal axis of the spectrum.

In Figure 4.1, the spectrum of $\hat{\mathcal{H}}$ with respect to $|n_x, n_y, n_z\rangle$ is superposed upon the spectrum with respect to $|n_+, n_-, n_z\rangle$ for the first ten total quantum numbers $n_+ + n_-$ and $n_x + n_y$. It is clear that the two spectra coincide completely along these half integer values of ν. These are also the values for which all classical orbits in the radial plane of the Penning trap are closed [72][2].

[2]Interestingly, integer values of ν correspond to the overlap of the Penning trap and Landau system spectra.

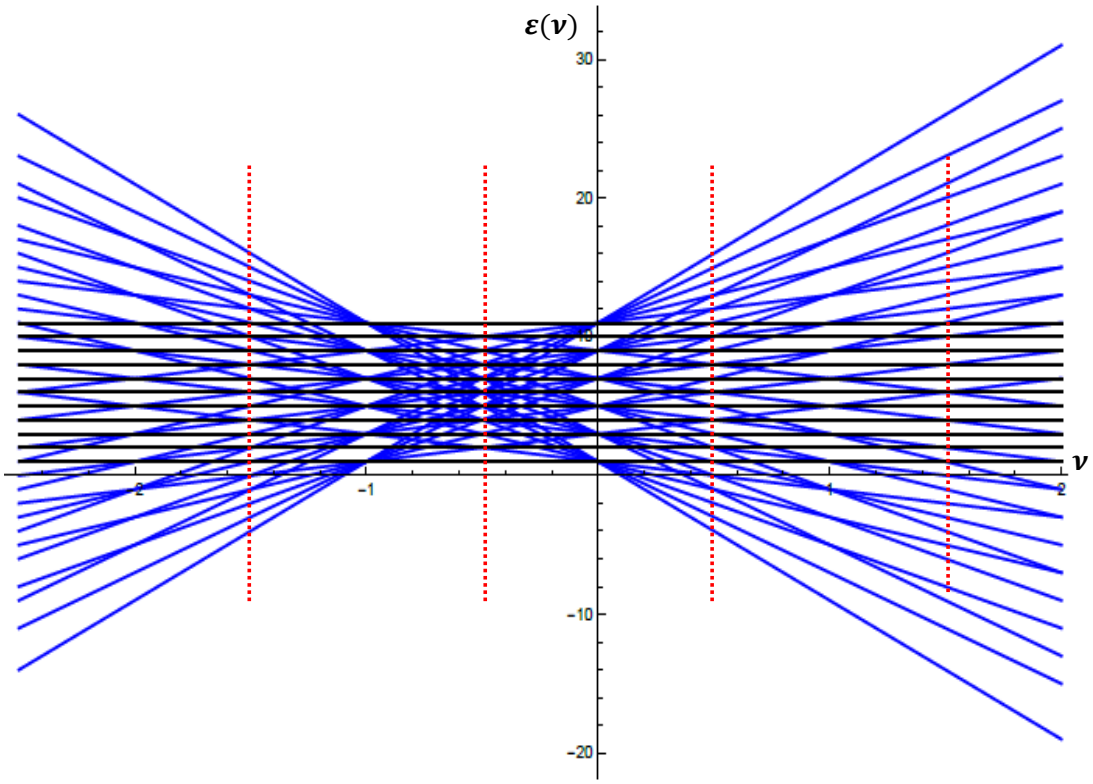

Figure 4.1: **Blue**: The expectation value spectrum of the radial motion in the Penning trap as a function of ν ((3.18), (3.19)) for the first ten total quantum numbers $n_+ + n_-$. **Black**: The expectation value spectrum of the radial motion in the Penning trap with respect to Fock states $|n_x, n_y, n_z\rangle$. **Red:** Values of ν for which the Fock states $|n_x, n_y, n_z\rangle$ are eigenstates of the Hamiltonian (4.24). These lines indicate the values of ν at which there is complete overlap of the expectation value of $\hat{\mathcal{H}}$ with respect to the two bases. At these points in the spectrum, large gaps occur, indicating closed orbits in the radial plane [72].

Coherent states

From (4.5), the classical Hamiltonian in the rotating frame, it appears that the x and y coordinates can be interpreted completely separately. This is clearly inconsistent with the quantum analysis of expectation values in 4.4.2. The semi-classical states of the Penning trap are therefore studied to reveal whether the root of this inconsistency can be traced.

The quantum Hamiltonian in the rotating frame (4.29) also admits coherent state solutions:

$$|\phi_\Omega >= |\alpha_{x_\Omega}\alpha_{y_\Omega}\alpha_{z_\Omega}\rangle, \tag{4.42}$$

where

$$\alpha_{x_\Omega} = |\alpha_{x_\Omega}| \exp i\varphi_{x_\Omega}, \;\; \alpha_{y_\Omega} = |\alpha_{y_\Omega}| \exp i\varphi_{y_\Omega}, \;\; \alpha_{z_\Omega} = |\alpha_{z_\Omega}| \exp i\varphi_{z_\Omega}. \tag{4.43}$$

The expectation value of the Hamiltonian in the lab frame with respect to these states is straightforward to compute following (4.34):

$$\begin{aligned}\langle\hat{\mathcal{H}}\rangle =& \hbar\frac{\omega_1}{2}(|\alpha_{x_\Omega}|^2 + |\alpha_{y_\Omega}|^2) + \hbar\omega_z|\alpha_{z_\Omega}|^2 \\ &+ \hbar\omega_c\,|\alpha_{x_\Omega}||\alpha_{y_\Omega}|\sin(\varphi_{y_\Omega} - \varphi_{x_\Omega}) + \frac{\hbar}{2}(\omega_1 + \omega_z).\end{aligned} \tag{4.44}$$

The energy contribution from the Landau levels can only be counted upon specifying the relative phase difference between the individual x and y motions in the rotating frame. This value is clearly maximal when $\varphi_{x_\Omega} - \varphi_{y_\Omega} = \pm\pi/2$. This corresponds precisely with the condition for maximum angular momentum in the classical 2D harmonic oscillator system (3.3), when the orbit is circular. The expectation values of the radial motions in the lab frame with respect to the states $\hat{U}^\dagger(t)|\alpha_{x_\Omega}\alpha_{y_\Omega}\alpha_{z_\Omega}\rangle$ are computed:

$$\begin{aligned}\langle\hat{x}(t)\rangle = \sqrt{\frac{\hbar}{m\omega_1}}[&|\alpha_{x_\Omega}|\,(\cos(\omega_+ t - \varphi_{x_\Omega}) + \cos(\omega_- t + \varphi_{x_\Omega})) \\ &- |\alpha_{y_\Omega}|\,(\sin(\omega_+ t - \varphi_{y_\Omega}) + \sin(\omega_- t + \varphi_{y_\Omega}))],\end{aligned} \tag{4.45}$$

$$\begin{aligned}\langle\hat{y}(t)\rangle = \sqrt{\frac{\hbar}{m\omega_1}}[&|\alpha_{x_\Omega}|\,(\sin(\omega_+ t - \varphi_{x_\Omega}) + \sin(\omega_- t + \varphi_{x_\Omega})) \\ &+ |\alpha_{y_\Omega}|\,(\cos(\omega_+ t - \varphi_{y_\Omega}) + \cos(\omega_- t + \varphi_{y_\Omega}))].\end{aligned} \tag{4.46}$$

These are compared to the classical trajectories calculated in (1.24). It is found that the solutions can *only* agree if the relation

$$\varphi_{x_\Omega} - \varphi_{y_\Omega} = \pi/2 \tag{4.47}$$

is defined. It is therefore clear that the semi-classical states of separate x and y motions, $|\alpha_{x_\Omega}\alpha_{y_\Omega}\alpha_{z_\Omega}\rangle$ are eigenstates of the Hamiltonian $\hat{\mathcal{H}}$ only for this precisely defined value of

the relative phase of the motions. In fact, the phase condition reveals that the solutions only agree when the *remaining* radial motion in the rotating frame is truly circular. In a similar way to the Fock state treatment above, general coherent states of the lab and rotating frames are compared:

$$|\alpha_+\alpha_-\alpha_z\rangle \neq \hat{U}^\dagger(t)|\alpha_{x_\Omega}\alpha_{y_\Omega}\alpha_{z_\Omega}\rangle. \tag{4.48}$$

That is, the semi-classical x and y motions in the rotating frame cannot be interpreted separately in general.

Quantum to classical

In Figure 4.2, the spectrum of the Penning trap is plotted with respect to the $|n_+, n_-, n_z\rangle$ and $|n_x, n_y, n_z\rangle$ Fock states for a total quantum number $n_+ + n_-$ of twenty. This is twice the number of levels as plotted in Figure 4.1. In comparing the two figures, it is clear that the gaps in the spectrum become much less distinct, and there is more apparent overlap between the black and blue lines in Figure 4.2. This closing of gaps and blending of the two spectra with respect to the different Fock states $|n_+, n_-, n_z\rangle$ and $|n_x, n_y, n_z\rangle$ as the total quantum number increases offers an intuitive analogy with the transition of the quantum to the classical regime. The classical transformation to the rotating frame allows interpretation of separate dynamics along the x and y axes, yet this can only happen for semi-classical states under strict phase conditions, and for Fock states for particular values of the bare frequencies.

The failings of the rotating frame in the $\{x, y\}$ basis are due to the fact that the total thermal energy of the Penning trap is not correctly "carried over" to this frame. This will be formally shown in 6.5, but it is first necessary to study the connection between the $\{x, y\}$ and $\{+, -\}$ basis in greater detail.

Since crossing points of the two spectra indicate when the Fock states $|n_x, n_y, n_z\rangle$ are eigenstates of the Hamiltonian, there may be potential uses in tuning a system to specific values of ω_c/ω_1 for a given temperature in order to access these states in the lab frame.

4.5 Alternate frame of reference for the quantum solution

The above analysis has shown that the rotating frame cannot produce a consistent quantum theory of the Penning trap in terms of quantized modes of the individual x and y directions. Another frame of reference is sought, and the calculation and discussion of this

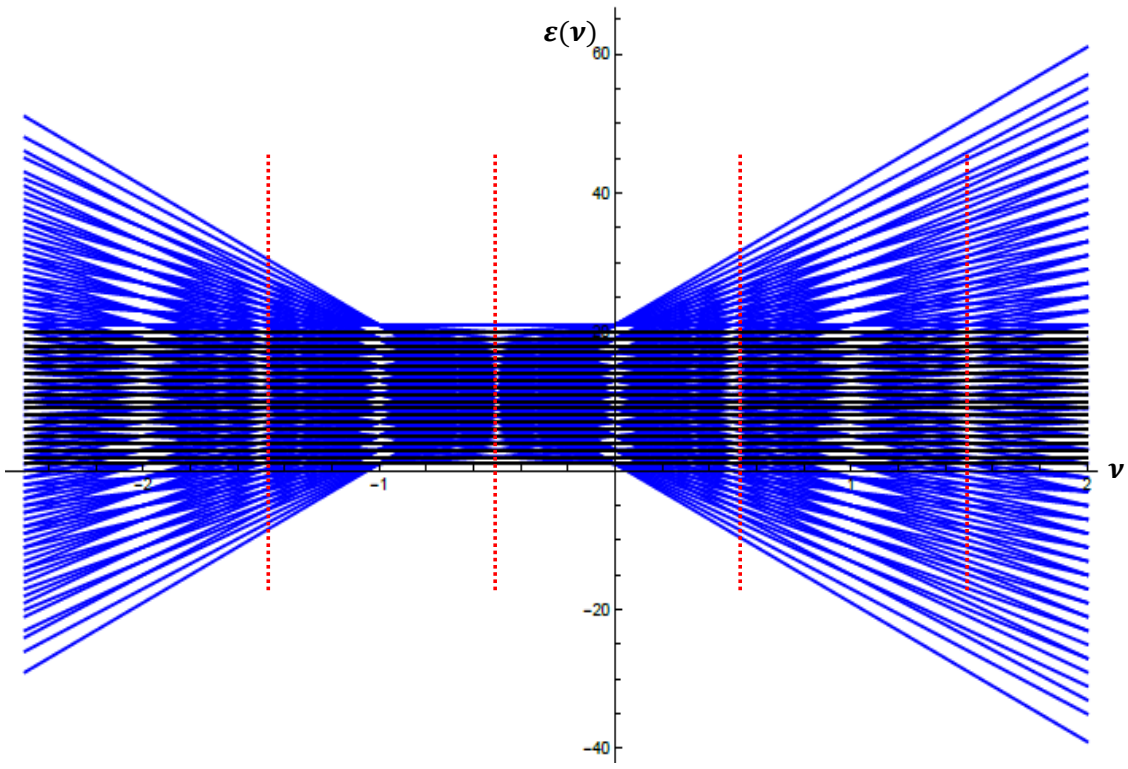

Figure 4.2: **Blue**: The expectation value spectrum of the radial motion in the Penning trap as a function of ν ((3.18), (3.19)) for the first twenty total quantum numbers $n_+ + n_-$. **Black**: The expectation value spectrum of the radial motion in the Penning trap with respect to Fock states $|n_x, n_y, n_z\rangle$. **Red:** Values of ν for which the Fock states $|n_x, n_y, n_z\rangle$ are eigenstates of the Hamiltonian (4.24). As more energy levels are considered, it is clear that the gaps in the spectrum become less distinct, and there is more apparent overlap between the spectrum with respect to $|n_+, n_-, n_z\rangle$ and $|n_+, n_-, n_z\rangle$ Fock states.

"alternate reference frame" forms the content of Chapter 6. The idea is first introduced here, as it motivates some of the discussion of Chapter 5.

Since a potential landscape along the three spatial axes $\{x, y, z\}$ is being sought, the use of the operators for these quantized modes will continue to be used, with the Hamiltonian in this basis written in the form of (4.24).

As a reminder, in terms of Schwinger boson operators of the $\{x, y\}$ basis (3.21), $\hat{\mathcal{H}}$ is written in the lab frame as a sum of the $\hat{I}_0$ and $\hat{I}_2$ components, in addition to the axial contribution. The commutation relations between the operators in the set $\underline{I}$ (and indeed every other set of angular momentum operators) dictates how each one transforms upon rotation by every other member of the set . These transformations are calculated and collected together in the following three matrices [61]

$$\begin{aligned}
\exp\left\{\frac{i}{\hbar}\phi\hat{I}_1\right\}\begin{pmatrix}\hat{I}_1\\ \hat{I}_2\\ \hat{I}_3\end{pmatrix}\exp\left\{-\frac{i}{\hbar}\phi\hat{I}_1\right\} &= \begin{pmatrix}1 & 0 & 0\\ 0 & \cos\phi & -\sin\phi\\ 0 & \sin\phi & \cos\phi\end{pmatrix}\begin{pmatrix}\hat{I}_1\\ \hat{I}_2\\ \hat{I}_3\end{pmatrix},\\
\exp\left\{\frac{i}{\hbar}\gamma\hat{I}_2\right\}\begin{pmatrix}\hat{I}_1\\ \hat{I}_2\\ \hat{I}_3\end{pmatrix}\exp\left\{-\frac{i}{\hbar}\gamma\hat{I}_2\right\} &= \begin{pmatrix}\cos\gamma & 0 & \sin\gamma\\ 0 & 1 & 0\\ -\sin\gamma & 0 & \cos\gamma\end{pmatrix}\begin{pmatrix}\hat{I}_1\\ \hat{I}_2\\ \hat{I}_3\end{pmatrix},\\
\exp\left\{\frac{i}{\hbar}\theta\hat{I}_3\right\}\begin{pmatrix}\hat{I}_1\\ \hat{I}_2\\ \hat{I}_3\end{pmatrix}\exp\left\{-\frac{i}{\hbar}\theta\hat{I}_3\right\} &= \begin{pmatrix}\cos\theta & -\sin\theta & 0\\ \sin\theta & \cos\theta & 0\\ 0 & 0 & 1\end{pmatrix}\begin{pmatrix}\hat{I}_1\\ \hat{I}_2\\ \hat{I}_3\end{pmatrix}.
\end{aligned} \tag{4.49}$$

These transformations are referred to frequently throughout the remainder of this thesis, and they are obviously not exclusive to the set $\underline{I}$. The fact that the second component $\hat{I}_2$ is identically $\hat{L}_z/2$ is, however, exclusive to this set.

4.5.1 The $\hat{I}_1$ frame

These transformations are now implemented in the following calculation:

$$\begin{aligned}
&\exp\left\{\frac{i}{\hbar}\phi\hat{I}_1\right\}\hat{\mathcal{H}}\exp\left\{-\frac{i}{\hbar}\phi\hat{I}_1\right\}\\
&= \exp\left\{\frac{i}{\hbar}\phi\hat{I}_1\right\}\left(\omega_1\hat{I}_0 + \omega_c\hat{I}_2 + \hbar\omega_z(\hat{a}_z^\dagger\hat{a}_z + \frac{1}{2}) + \frac{\hbar}{2}\omega_1\right)\exp\left\{-\frac{i}{\hbar}\phi\hat{I}_1\right\}\\
&= \omega_1\hat{I}_0 + \omega_c\left[\hat{I}_2\cos\phi - \hat{I}_3\sin\phi\right] + \hbar\omega_z(\hat{a}_z^\dagger\hat{a}_z + \frac{1}{2}) + \frac{\hbar}{2}\omega_1.
\end{aligned} \tag{4.50}$$

The choice $\phi = -\pi/2$ leads to the following:

$$\begin{aligned}\hat{\mathcal{H}}' &= \exp\left\{\frac{i}{\hbar}\left(-\frac{\pi}{2}\right)\hat{I}_1\right\}\hat{\mathcal{H}}\exp\left\{\frac{i}{\hbar}\left(\frac{\pi}{2}\right)\hat{I}_1\right\} \\ &= \omega_1\hat{I}_0 + \omega_c\hat{I}_3 + \hbar\omega_z(\hat{a}_z^\dagger\hat{a}_z + \frac{1}{2}) + \frac{\hbar}{2}\omega_1. \end{aligned} \tag{4.51}$$

In terms of creation and annihilation operators:

$$\implies \boxed{\hat{\mathcal{H}}' = \hbar\omega_+\left(\hat{n}_x + \frac{1}{2}\right) - \hbar\omega_-\left(\hat{n}_y + \frac{1}{2}\right) + \hbar\omega_z\left(\hat{n}_z + \frac{1}{2}\right)}. \tag{4.52}$$

The Hamiltonian transformed by $\hat{I}_1$ through $\pi/2$ becomes diagonal in the $\{x, y\}$ basis, from which solutions may follow naturally. What is less transparent, however, is whether or not this transformation, like the component $\hat{I}_2$, describes a rotation in space. The physical interpretation of the $\hat{I}_0$, $\hat{I}_3$ and $\hat{I}_3$ components is not yet obvious. In the following chapter, the relationship between different sets of Schwinger boson angular momentum operators, and to the canonical angular momentum operators $\{\hat{L}_x, \hat{L}_y, \hat{L}_z\}$, is thoroughly examined.

Chapter 5

The Schwinger Boson Operators

In this chapter, the role of each angular momentum operator of a given set, in terms of its effects upon spatial coordinates, is established. In order to capture the full three dimensions of the Penning trap, the analysis is extended to include three interconnecting sets of Schwinger boson operators $\{\underline{I}, \underline{J}, \underline{K}\}$. The operators of these sets are shown to provide a full mapping between the position and momentum coordinates of the three dimensional system.

5.1 The Rotation group and $SU(2)$

In his seminal work *"On Angular Momentum"* [61], Julian Schwinger has shown how "commutation relations of an arbitrary angular momentum vector can be reduced to those of a two-dimensional harmonic oscillator", leading to a method for the development of angular momentum eigenvectors. The method has since provided an indispensable tool in solving physical problems, and beautifully exploits the homomorphic mapping [78]

$$SU(2) \xrightarrow{2:1} SO(3), \tag{5.1}$$

granting insight into some of the fundamental structure of quantum theory. Questions concerning the nature of this mapping in relation to the quantum theory of the Penning trap are addressed in this chapter.

The apparently different dimensionality of the two representations of $SU(2)$ and $SO(3)$ is reconciled by considering the basic number of parameters required to define the matrices, plus the number of constraints imposed upon each in order to render them unitary and orthogonal accordingly [79]. However, in a 3D system, with three sets of creation and annihilation operators of the x, y and z directions, *three* sets of Schwinger boson operators

can be formed. The role played by each vector of each set in real 3D space is not then immediately obvious.

In this chapter, the role played by each component of a single set, in this case $\underline{I}$ of the radial plane, will first be considered. This leads to the construction of a further two such sets, $\underline{J}$ and $\underline{K}$, whereupon the now three sets are shown to relate to each other and to the orbital angular momentum components $\underline{L} \equiv \{\hat{L}_x, \hat{L}_y, \hat{L}_z\}$.

5.2 Position and momentum representation of Schwinger boson operators

In terms of both operators $\hat{a}_x$ and $\hat{a}_y$, and position and momentum coordinates $\hat{x}$, $\hat{y}$, $\hat{p}_x$, and $\hat{p}_y$, the set of Schwinger boson operator $\underline{I}$ is:

$$\begin{aligned}
\hat{I}_0 &= \frac{\hbar}{2}(\hat{n}_x + \hat{n}_y) = \frac{1}{8}m\omega_1(\hat{x}^2 + \hat{y}^2) + \frac{1}{2m\omega_1}(\hat{p}_x^2 + \hat{p}_y^2) - \frac{\hbar}{2}, \\
\hat{I}_1 &= \frac{\hbar}{2}\left(\hat{a}_x^\dagger \hat{a}_y + \hat{a}_y^\dagger \hat{a}_x\right) = \frac{1}{8}m\omega_1(2\hat{x}\hat{y}) + \frac{1}{2m\omega_1}(2\hat{p}_x\hat{p}_y), \\
\hat{I}_2 &= -i\frac{\hbar}{2}\left(\hat{a}_x^\dagger \hat{a}_y - \hat{a}_y^\dagger \hat{a}_x\right) = \frac{1}{2}(\hat{x}\hat{p}_y - \hat{y}\hat{p}_x), \\
\hat{I}_3 &= \frac{\hbar}{2}(\hat{n}_x - \hat{n}_y) = \frac{1}{8}m\omega_1(\hat{x}^2 - \hat{y}^2) + \frac{1}{2m\omega_1}(\hat{p}_x^2 - \hat{p}_y^2).
\end{aligned} \tag{5.2}$$

This expansion follows directly from (4.22) and (4.23). It is worthwhile noting that the frequency in the expansion of the operators of both mode operators $\hat{a}_x$ and $\hat{a}_y$ is $\omega_1/2$. Non-matching frequencies here would lead to significantly different expansions in terms of position and momentum operators. This is discussed further in 5.7.

The role of $\hat{I}_2$ is clear, it is (half) the canonical angular momentum of the z axis, and rotations by this operator are purely spatial. Transformation of coordinates by the other components are examined in the following section.

5.3 Role of the Schwinger boson components

Inverting the definition of the creation and annihilation operators of the x and y modes in (4.22) and (4.23):

$$\begin{aligned}
\hat{x} &= \sqrt{\frac{\hbar}{m\omega_1}}(\hat{a}_x^\dagger + \hat{a}_x), \qquad \hat{p}_x = -\frac{i}{2}\sqrt{\hbar m\omega_1}(\hat{a}_x - \hat{a}_x^\dagger), \\
\hat{y} &= \sqrt{\frac{\hbar}{m\omega_1}}(\hat{a}_y^\dagger + \hat{a}_y), \qquad \hat{p}_y = -\frac{i}{2}\sqrt{\hbar m\omega_1}(\hat{a}_y - \hat{a}_y^\dagger).
\end{aligned} \tag{5.3}$$

These are transformed by each of the vectors $\hat{I}_1$, $\hat{I}_2$ and $\hat{I}_3$:

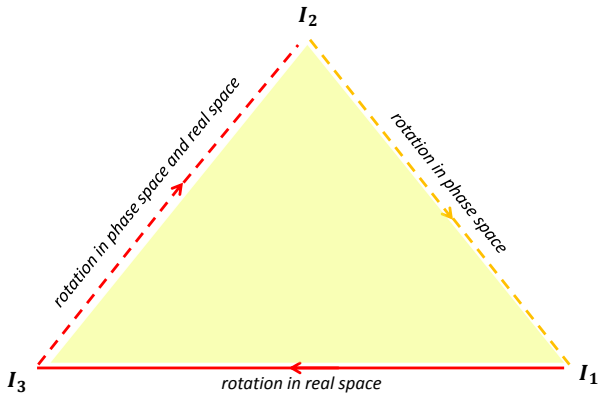

Figure 5.1: The arrows between each component of the set $\underline{I}$ indicate rotation through an angle $\pi/2$ by the operator directly opposite, with the direction implying positive sense of rotation. The caption above each line details how the three transformations are connected in terms of their effects upon spatial coordinates.

$$\begin{aligned}
\exp\left\{\frac{i}{\hbar}\phi\hat{I}_1\right\}\,\hat{x}\,\exp\left\{-\frac{i}{\hbar}\phi\hat{I}_1\right\} &= \cos\frac{\phi}{2}\hat{x} + \frac{2}{m\omega_1}\sin\frac{\phi}{2}\hat{p}_y,\\
\exp\left\{\frac{i}{\hbar}\phi\hat{I}_1\right\}\,\hat{p}_x\,\exp\left\{-\frac{i}{\hbar}\phi\hat{I}_1\right\} &= \cos\frac{\phi}{2}\hat{p}_x - \frac{1}{2}m\omega_1\sin\frac{\phi}{2}\hat{y},\\
\exp\left\{\frac{i}{\hbar}\phi\hat{I}_1\right\}\,\hat{y}\,\exp\left\{-\frac{i}{\hbar}\phi\hat{I}_1\right\} &= \cos\frac{\phi}{2}\hat{y} + \frac{2}{m\omega_1}\sin\frac{\phi}{2}\hat{p}_x,\\
\exp\left\{\frac{i}{\hbar}\phi\hat{I}_1\right\}\,\hat{p}_y\,\exp\left\{-\frac{i}{\hbar}\phi\hat{I}_1\right\} &= \cos\frac{\phi}{2}\hat{p}_y - \frac{1}{2}m\omega_1\sin\frac{\phi}{2}\hat{x}.
\end{aligned} \tag{5.4}$$

$$\begin{aligned}
\exp\left\{\frac{i}{\hbar}\gamma\hat{I}_2\right\}\,\hat{x}\,\exp\left\{-\frac{i}{\hbar}\gamma\hat{I}_2\right\} &= \cos\frac{\gamma}{2}\hat{x} - \sin\frac{\gamma}{2}\hat{y},\\
\exp\left\{\frac{i}{\hbar}\gamma\hat{I}_2\right\}\,\hat{p}_x\,\exp\left\{-\frac{i}{\hbar}\gamma\hat{I}_2\right\} &= \cos\frac{\gamma}{2}\hat{p}_x - \sin\frac{\gamma}{2}\hat{p}_y,\\
\exp\left\{\frac{i}{\hbar}\gamma\hat{I}_2\right\}\,\hat{y}\,\exp\left\{-\frac{i}{\hbar}\gamma\hat{I}_2\right\} &= \cos\frac{\gamma}{2}\hat{y} + \sin\frac{\gamma}{2}\hat{x},\\
\exp\left\{\frac{i}{\hbar}\gamma\hat{I}_2\right\}\,\hat{p}_y\,\exp\left\{-\frac{i}{\hbar}\gamma\hat{I}_2\right\} &= \cos\frac{\gamma}{2}\hat{p}_y + \sin\frac{\gamma}{2}\hat{p}_x.
\end{aligned} \tag{5.5}$$

$$\begin{aligned}
\exp\left\{\frac{i}{\hbar}\theta\hat{I}_3\right\}\,\hat{x}\,\exp\left\{-\frac{i}{\hbar}\theta\hat{I}_3\right\} &= \cos\frac{\theta}{2}\hat{x} + \frac{2}{m\omega_1}\sin\frac{\theta}{2}\hat{p}_x,\\
\exp\left\{\frac{i}{\hbar}\theta\hat{I}_3\right\}\,\hat{p}_x\,\exp\left\{-\frac{i}{\hbar}\theta\hat{I}_3\right\} &= \cos\frac{\theta}{2}\hat{p}_x - \frac{1}{2}m\omega_1\sin\frac{\theta}{2}\hat{x},\\
\exp\left\{\frac{i}{\hbar}\theta\hat{I}_3\right\}\,\hat{y}\,\exp\left\{-\frac{i}{\hbar}\theta\hat{I}_3\right\} &= \cos\frac{\theta}{2}\hat{y} - \frac{2}{m\omega_1}\sin\frac{\theta}{2}\hat{p}_y,\\
\exp\left\{\frac{i}{\hbar}\theta\hat{I}_3\right\}\,\hat{p}_y\,\exp\left\{-\frac{i}{\hbar}\theta\hat{I}_3\right\} &= \cos\frac{\theta}{2}\hat{p}_y + \frac{1}{2}m\omega_1\sin\frac{\theta}{2}\hat{y}.
\end{aligned} \tag{5.6}$$

Each set is analysed in turn:

$\hat{I}_1$ transforms spatial coordinates in one direction to momentum coordinates of a different axis, and momentum coordinates to spatial ones of the opposite axis; the first component involves a mixture of a real space and phase space transformation.

$\hat{I}_2$ transforms spatial coordinates in one direction into spatial coordinates of a different axis, and momentum coordinates to momentum ones of the different axis; the second component induces purely spatial rotations.

$\hat{I}_3$ transforms spatial coordinates in one direction into momentum coordinates of the same axis, and momentum coordinates to spatial ones of the same axis; the third component induces rotations purely in phase space.

The role of $\hat{I}_0$ should be clear, as it follows from that of $\hat{I}_3$; the "zeroth" component of the set rotates each of the position and momentum operators in phase space, but now with symmetric effects upon the $\hat{x}$ and $\hat{y}$ ($\hat{p}_x$ and $\hat{p}_y$) components. It also acts as the "total energy operator" of the system.

This makes transparent the connection between the operators of the set in terms of their effect on coordinates. Recalling the transformation matrices in (4.49), the analysis of the operators is depicted in Figure 5.1.

The operators of the set $\hat{I}_1$ each perform different types of rotations upon the $\hat{x}$ and $\hat{y}$ coordinates, but this does not reveal how the z dimension of a 3D system could be included in this formalism. This forms the topic of the next section.

5.4 The canonical angular momentum in three-dimensional space

In this section, the frequency in each of the $\hat{a}_x$, $\hat{a}_y$ and $\hat{a}_z$ operators is assumed to be the same. This is not the case for the Penning trap, as $\hat{a}_z$ contains ω_z, whereas $\hat{a}_x$ and $\hat{a}_y$ contain $\omega_1/2$ (1.37,4.22,4.23). The Schwinger boson operator sets still exist for anisotropic systems such as the Penning trap, but each component does not have the same expansion in terms of coordinates as for an isotropic system, (5.2). This is discussed more fully towards the end of this chapter, in 5.7 to 5.9 .

The three canonical angular momentum components for each axis are given by

$$\begin{aligned}\hat{L}_x &= \hat{y}\hat{p}_z - \hat{z}\hat{p}_y,\\ \hat{L}_y &= \hat{z}\hat{p}_x - \hat{x}\hat{p}_z,\\ \hat{L}_z &= \hat{x}\hat{p}_y - \hat{y}\hat{p}_x.\end{aligned} \tag{5.7}$$

In terms of Schwinger boson components of creation and annihilation operators of three isotropic oscillators of the x, y and z directions, these are given by

$$\begin{aligned}\hat{L}_x &= -i\hbar\left(\hat{a}_y^\dagger\hat{a}_z - \hat{a}_z^\dagger\hat{a}_y\right) \equiv 2\hat{K}_2,\\ \hat{L}_y &= -i\hbar\left(\hat{a}_z^\dagger\hat{a}_x - \hat{a}_x^\dagger\hat{a}_z\right) \equiv 2\hat{J}_2,\\ \hat{L}_z &= -i\hbar\left(\hat{a}_x^\dagger\hat{a}_y - \hat{a}_y^\dagger\hat{a}_x\right) \equiv 2\hat{I}_2.\end{aligned} \tag{5.8}$$

The commutation relations of the set written in this unconventional form can be tested:

$$\begin{aligned}\left[\hat{L}_x,\,\hat{L}_y\right] &= \left[-i\hbar\left(\hat{a}_y^\dagger\hat{a}_z - \hat{a}_z^\dagger\hat{a}_y\right),\,-i\hbar\left(\hat{a}_z^\dagger\hat{a}_x - \hat{a}_x^\dagger\hat{a}_z\right)\right]\\ &= -\hbar^2\left(\hat{a}_y^\dagger\hat{a}_x\hat{-a}_x^\dagger\hat{a}_y\right)\\ &= i\hbar\cdot -i\hbar\left(\hat{a}_x^\dagger\hat{a}_y - \hat{a}_y^\dagger\hat{a}_x\right)\\ &= i\hbar\hat{L}_z,\end{aligned} \tag{5.9}$$

and the other relations follow analogously. The labels $\hat{J}_2$ and $\hat{K}_2$ have been introduced in (5.8), since each of these operators forms the second component of a set $\underline{J}$ and $\underline{K}$ respectively. These sets are discussed in the following section.

5.5 The three sets of Schwinger boson operators

5.5.1 Definitions of Schwinger boson sets

The full sets of $\underline{J}$ and $\underline{K}$ operators are given by:

$$\begin{aligned}\hat{J}_0 &= \frac{\hbar}{2}\left(\hat{n}_z + \hat{n}_x\right), & \hat{K}_0 &= \frac{\hbar}{2}\left(\hat{n}_y + \hat{n}_z\right),\\ \hat{J}_1 &= \frac{\hbar}{2}\left(\hat{a}_z^\dagger\hat{a}_x + \hat{a}_x^\dagger\hat{a}_z\right), & \hat{K}_1 &= \frac{\hbar}{2}\left(\hat{a}_y^\dagger\hat{a}_z + \hat{a}_z^\dagger\hat{a}_y\right),\\ \hat{J}_2 &= -i\frac{\hbar}{2}\left(\hat{a}_z^\dagger\hat{a}_x - \hat{a}_x^\dagger\hat{a}_z\right), & \hat{K}_2 &= -i\frac{\hbar}{2}\left(\hat{a}_y^\dagger\hat{a}_z - \hat{a}_z^\dagger\hat{a}_y\right),\\ \hat{J}_3 &= \frac{\hbar}{2}\left(\hat{n}_z - \hat{n}_x\right), & \hat{K}_3 &= \frac{\hbar}{2}\left(\hat{n}_y - \hat{n}_z\right).\end{aligned} \tag{5.10}$$

Within a single set $\underline{J}$ or $\underline{K}$, these operators obey appropriate commutation relations for angular momentum algebra, (2.30). Commutation relations *between* these sets, and with operators of the set $\underline{I}$, are examined in 5.6.

5.5.2 Transformation of $\hat{a}$ and $\hat{a}^\dagger$

It is straightforward to calculate the transformation of the operators $\hat{a}_x$, $\hat{a}_y$, $\hat{a}_z$, and their self-adjoint counterparts, by the Schwinger boson operators of the appropriate set. The results for the set $\underline{I}$ are collected here [74]:

$\underline{I}$

$$\exp\left\{\frac{i}{\hbar}\phi\hat{I}_1\right\}\begin{pmatrix}\hat{a}_x^\dagger\\ \hat{a}_y^\dagger\end{pmatrix}\exp\left\{-\frac{i}{\hbar}\phi\hat{I}_1\right\}=\begin{pmatrix}\cos\frac{\phi}{2} & i\sin\frac{\phi}{2}\\ i\sin\frac{\phi}{2} & \cos\frac{\phi}{2}\end{pmatrix}\begin{pmatrix}\hat{a}_x^\dagger\\ \hat{a}_y^\dagger\end{pmatrix}, \tag{5.11}$$

$$\exp\left\{\frac{i}{\hbar}\gamma\hat{I}_2\right\}\begin{pmatrix}\hat{a}_x^\dagger\\ \hat{a}_y^\dagger\end{pmatrix}\exp\left\{-\frac{i}{\hbar}\gamma\hat{I}_2\right\}=\begin{pmatrix}\cos\frac{\gamma}{2} & -\sin\frac{\gamma}{2}\\ \sin\frac{\gamma}{2} & \cos\frac{\gamma}{2}\end{pmatrix}\begin{pmatrix}\hat{a}_x^\dagger\\ \hat{a}_y^\dagger\end{pmatrix}, \tag{5.12}$$

$$\exp\left\{\frac{i}{\hbar}\theta\hat{I}_3\right\}\begin{pmatrix}\hat{a}_x^\dagger\\ \hat{a}_y^\dagger\end{pmatrix}\exp\left\{-\frac{i}{\hbar}\theta\hat{I}_3\right\}=\begin{pmatrix}\exp\left(i\frac{\theta}{2}\right) & 0\\ 0 & \exp\left(-i\frac{\theta}{2}\right)\end{pmatrix}\begin{pmatrix}\hat{a}_x^\dagger\\ \hat{a}_y^\dagger\end{pmatrix}. \tag{5.13}$$

Analogous results for the set $\underline{J}$ and $\underline{K}$ are given in A. The relative position of the pairs of operators within each 2×1 matrix is crucial for the consistency of all the results of this chapter, and indeed throughout the remainder of this thesis.

5.6 Rotation matrices and commutation maps

The calculation for commutation of every component of each set by every other is lengthy, as indeed are the results written out in full. Instead, following from Figure 5.1, the results have been collected into a "commutation map" to highlight the interconnectivity of the three sets. Before discussing this, an example calculation is detailed in order to clarify the meaning of the lines and arrows on the map.

Beginning with the commutation relation of $\hat{I}_1$ and $\hat{J}_1$:

$$\begin{aligned}\left[\hat{I}_1,\,\hat{J}_1\right] &= \left[\frac{\hbar}{2}\left(\hat{a}_x^\dagger\hat{a}_y+\hat{a}_y^\dagger\hat{a}_x\right),\,\frac{\hbar}{2}\left(\hat{a}_z^\dagger\hat{a}_x+\hat{a}_x^\dagger\hat{a}_z\right)\right]\\ &= \frac{\hbar^2}{4}\left(-\hat{a}_z^\dagger\hat{a}_y+\hat{a}_y^\dagger\hat{a}_z\right)\\ &= i\frac{\hbar}{2}\cdot -i\frac{\hbar}{2}\left(\hat{a}_y^\dagger\hat{a}_z-\hat{a}_z^\dagger\hat{a}_y\right)\\ &= i\frac{\hbar}{2}\hat{K}_2.\end{aligned} \tag{5.14}$$

From this calculation, a line is formed:

$$\hat{I}_1 \xrightarrow{\hat{J}_1} \hat{K}_2, \tag{5.15}$$

and a glossary of these lines corresponding to commutation relations is built up, where, instead of writing the transformation operator above the line, each is colour coded for ease of reading. Additionally, the direction of the **black** arrow on each line indicates whether the resultant operator is positive or negative through commutation; the line

$$\hat{I}_1 \xleftarrow{\hat{K}_1} \hat{J}_2 \tag{5.16}$$

indicates $\left[\hat{I}_1,\, \hat{K}_1\right] = -\frac{i\hbar}{2}\hat{J}_2$. Some of the commutation relations are non-cyclic. For example,

$$\left[\hat{K}_3,\, \hat{I}_2\right] = \frac{i\hbar}{2}\hat{I}_1, \tag{5.17}$$

but

$$\left[\hat{I}_1,\, \hat{I}_2\right] = i\hbar\hat{I}_3. \tag{5.18}$$

Relations such as this are indicated by arrows at the start *and* end of each line, pointing in the direction in which the result occurs. Lines with only *one* black arrow in the center (i.e none at the ends) indicate that the commutation relations are fully cyclic. This is discussed further at the end of the section.

A last point which should be mentioned is that the commutation relations occurring within each set i.e. $\hat{I}_2 \longrightarrow \hat{I}_1 \longrightarrow \hat{I}_3$ are indicated by the yellow shading enclosed in the area bordered by these lines, which also means that these results are twice the value of those indicated by other lines. This is due to the fact that

$$\left[\hat{I}_1,\, \hat{I}_2\right] = i\hbar\hat{I}_3, \tag{5.19}$$

but

$$\left[\hat{I}_2,\, \hat{J}_1\right] = i\frac{\hbar}{2}\hat{K}_1; \tag{5.20}$$

each set individually obeys the angular momentum commutation relations, but transformations *between sets* $\underline{I}$, $\underline{J}$ and $\underline{K}$ must pick up an extra factor of $1/2$.

There are a few things to note about Figure 5.2. Firstly, commutation relations which are cyclic, i.e. those indicated by only one black arrow in the centre of the line, additionally indicate the *transformation* of one component to another. For example, referring to the result of (5.14):

$$\exp\left\{\frac{i}{\hbar}\phi\hat{J}_1\right\}\,\hat{I}_1\,\exp\left\{-\frac{i}{\hbar}\phi\hat{J}_1\right\} = \cos\frac{\phi}{2}\hat{I}_1 + \sin\frac{\phi}{2}\hat{K}_2 \overset{\phi=\pi}{\Longrightarrow} \hat{K}_2. \tag{5.21}$$

Therefore all *cyclic* relations on the map additionally indicate transformation through an angle of π, unless the transformations are within a *single* set, in which case the angle must be $\pi/2$ for complete transformation:

$$\exp\left\{\frac{i}{\hbar}\phi\hat{I}_2\right\}\,\hat{I}_1\,\exp\left\{-\frac{i}{\hbar}\phi\hat{I}_2\right\} = \cos\phi\hat{I}_1 + \sin\phi\hat{I}_3 \overset{\phi=\frac{\pi}{2}}{\Longrightarrow} \hat{I}_3. \tag{5.22}$$

This should be read as "$\hat{I}_2$ transforms $\hat{I}_1$ to $\hat{I}_3$" for correspondence with the map. Details of transformation of one component to another for non-cyclic cases cannot be described

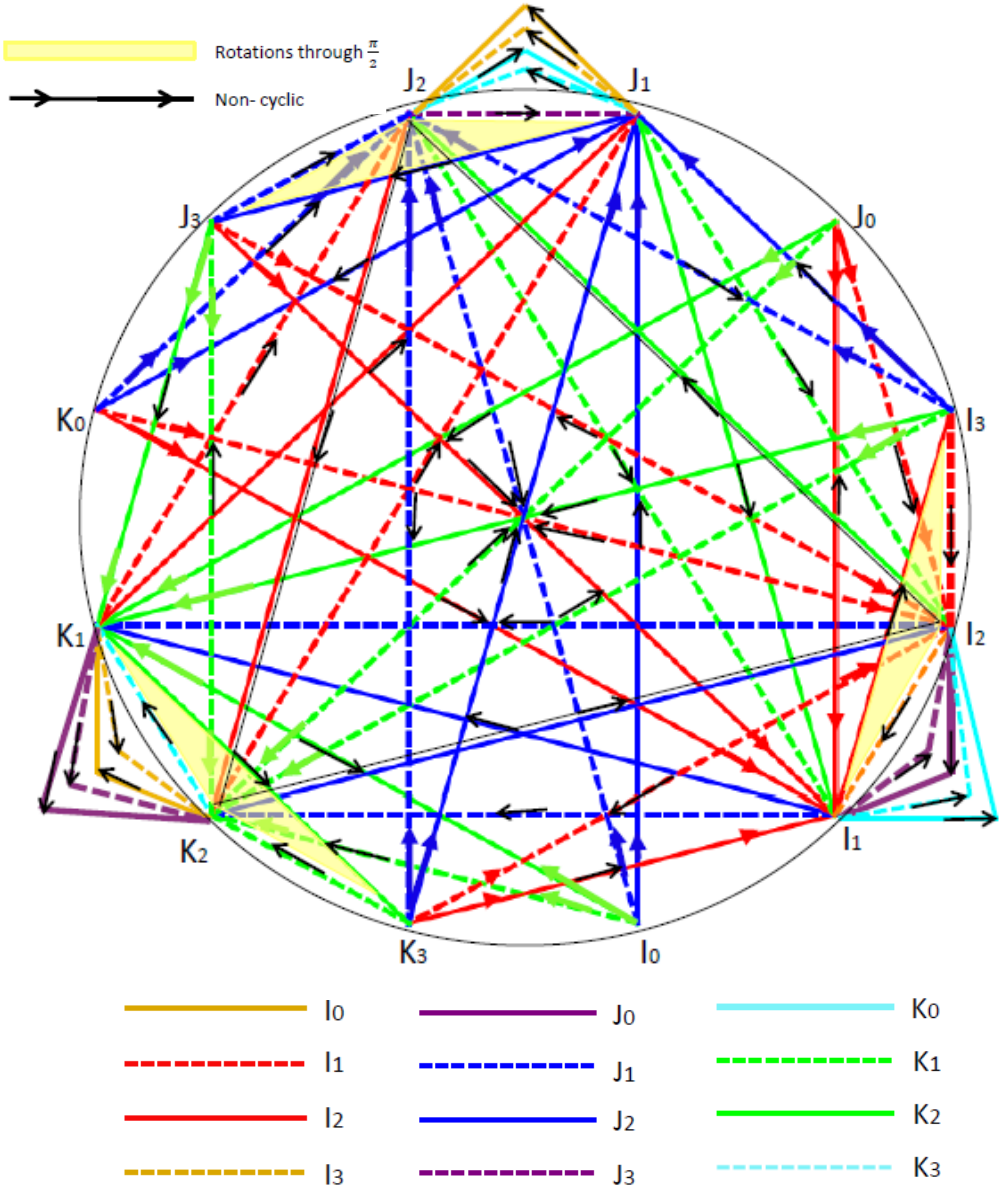

Figure 5.2: Graphical form of the commutation relations of a set of twelve Schwinger boson angular momentum components by each other member of the set. For example, the green dashed line $\hat{J}_1 \longrightarrow \hat{I}_2$ details the calculation $\left[\hat{J}_1, \hat{K}_1\right] = i\hbar/2\,\hat{I}_2$. The black arrows in the middle of each line represents the sense of positive commutation, and lines with additional arrows at either end detail non-cyclic commutation relations. The areas shaded in yellow indicate twice the value of the other commutation relations, e.g. $\left[\hat{I}_2, \hat{I}_3\right] = i\hbar\hat{I}_1$, since these relations are calculated for operators within a single set $\underline{I}$, $\underline{J}$ or $\underline{K}$.

in a simple form of a map, and must be written out in full. For example,

$$\exp\left\{\frac{i}{\hbar}\phi\hat{I}_1\right\}\hat{K}_3\exp\left\{-\frac{i}{\hbar}\phi\hat{I}_1\right\} = \hat{K}_3 - \frac{1}{2}\sin\phi\hat{I}_2 - \frac{1}{2}(\cos\phi - 1)\hat{I}_3. \tag{5.23}$$

These occur specifically when transforming "from" a zeroth or third component by any first or second component operator of a different set. The complete set of transformations resulting from these non-cyclic cases are given in Appendix B.

A final point worth noting is that a component describing a real angular momentum in space can only be transformed to other canonical angular momentum components by real space transformations (solid lines). This is significant because it means that our zeroth, first, and third components can never be transformed to one pointing along a real axis.

5.6.1 Testing the formalism

In order to show how all of the $\underline{I}$, $\underline{J}$, and $\underline{K}$ operators can be used simultaneously in a consistent way, an example calculation for a simple system is given in this section.

Beginning with the Hamiltonian of a 3D isotropic harmonic oscillator system:

$$\hat{H}_{xyz} = \hbar\omega\left(\hat{n}_x + \frac{1}{2}\right) + \hbar\omega\left(\hat{n}_y + \frac{1}{2}\right) + \hbar\omega\left(\hat{n}_z + \frac{1}{2}\right). \tag{5.24}$$

This is expanded in the following way:

$$\hat{H}_{xyz} = \omega\frac{\hbar}{2}\left(\hat{a}_x^\dagger\hat{a}_x + \hat{a}_y^\dagger\hat{a}_y\right) + \omega\frac{\hbar}{2}\left(\hat{a}_z^\dagger\hat{a}_z + \hat{a}_x^\dagger\hat{a}_x\right) + \omega\frac{\hbar}{2}\left(\hat{a}_y^\dagger\hat{a}_y + \hat{a}_z^\dagger\hat{a}_z\right) + \hbar\omega\frac{3}{2}, \tag{5.25}$$

to allow rewriting in terms of $\underline{I}$, $\underline{J}$ and $\underline{K}$ operators:

$$\hat{H}_{xyz} = \omega(\hat{I}_0 + \hat{J}_0 + \hat{K}_0) + \hbar\omega\frac{3}{2}. \tag{5.26}$$

This is now rotated around the arbitrarily chosen z axis:

$$\begin{aligned}
&\exp\left\{\frac{i}{\hbar}\phi\hat{I}_2\right\}\hat{H}_{xyz}\exp\left\{-\frac{i}{\hbar}\phi\hat{I}_2\right\} \\
&= \omega\left(\hat{I}_0 + \hat{J}_0 - \frac{1}{2}\sin\phi\hat{I}_1 + \frac{1}{2}(\cos\phi - 1)\hat{I}_3 + \hat{K}_0 + \frac{1}{2}\sin\phi\hat{I}_1 - \frac{1}{2}(\cos\phi - 1)\hat{I}_3\right) + \hbar\omega\frac{3}{2} \\
&= \omega(\hat{I}_0 + \hat{J}_0 + \hat{K}_0) + \hbar\omega\frac{3}{2}.
\end{aligned} \tag{5.27}$$

Thus, as it should, rotation around the z axis by any angle leaves this fully isotropic oscillator system unchanged. The results obtained so far in this chapter have shed some light upon the role of the components of a set of Schwinger boson angular momentum vectors, and have highlighted the intricate connections between three sets of Schwinger boson angular momentum vectors.

5.7 Canonical angular momentum for anisotropic systems

It has been discussed that the second component operators from each set as defined in (5.2) and (5.10) refer to the operators $\frac{1}{2}\hat{L}_z$, $\frac{1}{2}\hat{L}_y$ and $\frac{1}{2}\hat{L}_x$. This is true only when the operators $\hat{a}_x^\dagger$, $\hat{a}_y^\dagger$, $\hat{a}_z^\dagger$, and their conjugate counterparts, are the creation and annihilation operators of quantum oscillators of the *same frequency*.

For example, consider a 3D classical system of a particle of mass m harmonically oscillating with a *different* frequency along each axis, with Hamiltonian

$$H_A = \frac{1}{2m}\left(p_x^2 + p_y^2 + p_z^2\right) + \frac{1}{2}m\omega_x^2 x^2 + \frac{1}{2}m\omega_y^2 y^2 + \frac{1}{2}m\omega_z^2 z^2; \tag{5.28}$$

$$\omega_x \neq \omega_y \neq \omega_z. \tag{5.29}$$

This is written in quantum form

$$\hat{H}_A = \hbar\omega_x\left(\hat{a}_x^\dagger\hat{a}_x + \frac{1}{2}\right) + \hbar\omega_y\left(\hat{a}_y^\dagger\hat{a}_y + \frac{1}{2}\right) + \hbar\omega_z\left(\hat{a}_z^\dagger\hat{a}_z + \frac{1}{2}\right), \tag{5.30}$$

where

$$\begin{aligned}
\hat{a}_x &= \frac{1}{\sqrt{2\hbar}}\left(\sqrt{m\omega_x}x + i\sqrt{\frac{1}{m\omega_x}}p_x\right), \quad \hat{a}_x^\dagger = \frac{1}{\sqrt{2\hbar}}\left(\sqrt{m\omega_x}x - i\sqrt{\frac{1}{m\omega_x}}p_x\right), \\
\hat{a}_y &= \frac{1}{\sqrt{2\hbar}}\left(\sqrt{m\omega_y}y + i\sqrt{\frac{1}{m\omega_y}}p_y\right), \quad \hat{a}_y^\dagger = \frac{1}{\sqrt{2\hbar}}\left(\sqrt{m\omega_y}y - i\sqrt{\frac{1}{m\omega_y}}p_y\right), \\
\hat{a}_z &= \frac{1}{\sqrt{2\hbar}}\left(\sqrt{m\omega_z}z + i\sqrt{\frac{1}{m\omega_z}}p_z\right), \quad \hat{a}_z^\dagger = \frac{1}{\sqrt{2\hbar}}\left(\sqrt{m\omega_z}z - i\sqrt{\frac{1}{m\omega_z}}p_z\right).
\end{aligned} \tag{5.31}$$

Now, the classical canonical momentum along each axis is given by [37],

$$\vec{L} = \vec{r} \times \vec{p}, \tag{5.32}$$

resulting in the individual quantum components

$$\begin{aligned}
\hat{L}_x &= \hat{y}\hat{p}_z - \hat{z}\hat{p}_y, \\
\hat{L}_y &= \hat{z}\hat{p}_x - \hat{x}\hat{p}_z, \\
\hat{L}_z &= \hat{x}\hat{p}_y - \hat{y}\hat{p}_x.
\end{aligned} \tag{5.33}$$

In terms of the operators in (5.31), these are now written:

$$\begin{aligned}
\hat{L}_x &= -i\frac{\hbar}{2}\left(\left(\sqrt{\frac{\omega_z}{\omega_y}} + \sqrt{\frac{\omega_y}{\omega_z}}\right)(\hat{a}_y^\dagger\hat{a}_z - \hat{a}_z^\dagger\hat{a}_y) + \left(\sqrt{\frac{\omega_z}{\omega_y}} - \sqrt{\frac{\omega_y}{\omega_z}}\right)(\hat{a}_y\hat{a}_z - \hat{a}_y^\dagger\hat{a}_z^\dagger)\right) \equiv 2\hat{\mathcal{K}}_2, \\
\hat{L}_y &= -i\frac{\hbar}{2}\left(\left(\sqrt{\frac{\omega_x}{\omega_z}} + \sqrt{\frac{\omega_z}{\omega_x}}\right)(\hat{a}_z^\dagger\hat{a}_x - \hat{a}_x^\dagger\hat{a}_z) + \left(\sqrt{\frac{\omega_x}{\omega_z}} - \sqrt{\frac{\omega_z}{\omega_x}}\right)(\hat{a}_z\hat{a}_x - \hat{a}_z^\dagger\hat{a}_x^\dagger)\right) \equiv 2\hat{\mathcal{J}}_2, \\
\hat{L}_z &= -i\frac{\hbar}{2}\left(\left(\sqrt{\frac{\omega_y}{\omega_x}} + \sqrt{\frac{\omega_x}{\omega_y}}\right)(\hat{a}_x^\dagger\hat{a}_y - \hat{a}_y^\dagger\hat{a}_x) + \left(\sqrt{\frac{\omega_y}{\omega_x}} - \sqrt{\frac{\omega_x}{\omega_y}}\right)(\hat{a}_x\hat{a}_y - \hat{a}_x^\dagger\hat{a}_y^\dagger)\right) \equiv 2\hat{\mathcal{I}}_2,
\end{aligned} \tag{5.34}$$

where the notation $\hat{\mathcal{I}}_2$, $\hat{\mathcal{J}}_2$, $\hat{\mathcal{K}}_2$ has been adopted for these anisotropic components. It can be shown that appropriate commutation relations between them are preserved.

The canonical angular momentum operators of each axis written in the position and momentum representation in (5.33) are unchanged in this case of anisotropic oscillation. However, anisotropic confinement results in a change of the second component operators of the sets $\underline{I}$, $\underline{J}$ and $\underline{K}$ to $\hat{\mathcal{I}}_2$, $\hat{\mathcal{J}}_2$ and $\hat{\mathcal{K}}_2$ defined above.

Another way of looking at this is that the operators $\hat{I}_2$, $\hat{J}_2$ and $\hat{K}_2$ no longer point along the three real axes for the anisotropic system, but that the direction in which they point had been displaced.

An intriguing question arises: how do the operators $\hat{I}_2$, $\hat{J}_2$ and $\hat{K}_2$ map to $\hat{\mathcal{I}}_2$, $\hat{\mathcal{J}}_2$ and $\hat{\mathcal{K}}_2$ as the confinement of a trapped particle along each axis changes? In other words, how does $\hat{H}_{xyz}$ in (5.24) map to $\hat{H}_A$ in (5.30)?

It is important to recognise that all operators of the sets $\underline{I}$, $\underline{J}$ and $\underline{K}$ defined in 5.5 still "exist" for an anisotropic system such as $\hat{H}_A$, but they no longer play the same role as for the isotropic case $\hat{H}_{xyz}$. For a completely anisotropic system, rotations around the real x, y and z axes are effectively conducted by the operators $2\hat{\mathcal{K}}_2$, $2\hat{\mathcal{J}}_2$ and $2\hat{\mathcal{I}}_2$ respectively. Calculation of this is detailed in 5.9.

5.8 Squeezing the axes

5.8.1 Mapping of creation and annihilation operators

Squeezing operators are introduced for the x, y and z modes [41][1]:

$$\begin{aligned}
\hat{S}(\zeta_x) &= \exp\left\{-\frac{\zeta_x}{2}\hat{a}_x^{\dagger 2} + \frac{\zeta_x^*}{2}\hat{a}_x^2\right\}; \quad \zeta_x = r_x \exp(i\phi_x), \\
\hat{S}(\zeta_y) &= \exp\left\{-\frac{\zeta_y}{2}\hat{a}_y^{\dagger 2} + \frac{\zeta_y^*}{2}\hat{a}_y^2\right\}; \quad \zeta_y = r_y \exp(i\phi_y), \\
\hat{S}(\zeta_z) &= \exp\left\{-\frac{\zeta_z}{2}\hat{a}_z^{\dagger 2} + \frac{\zeta_z^*}{2}\hat{a}_z^2\right\}; \quad \zeta_z = r_z \exp(i\phi_z).
\end{aligned} \tag{5.35}$$

It is straightforward to show that they act on their appropriate $\hat{a}$ and $\hat{a}^\dagger$ as follows [41]:

$$\begin{aligned}
\hat{S}(\zeta_x)\hat{a}_x\hat{S}^\dagger(\zeta_x) &= \hat{a}_x \cosh(r_x) + \hat{a}_x^\dagger \sinh(r_x)\exp(i\phi_x), \\
\hat{S}(\zeta_x)\hat{a}_x^\dagger\hat{S}^\dagger(\zeta_x) &= \hat{a}_x^\dagger \cosh(r_x) + \hat{a}_x \sinh(r_x)\exp(-i\phi_x),
\end{aligned} \tag{5.36}$$

[1]The notation here has been chosen in an effort to reduce clutter in calculations. The argument of each operator, i.e. ζ_x, ζ_y and ζ_z additionally indicates the Hilbert space in which it acts. In this sense, the notation $\hat{S}(\zeta_x)$, $\hat{S}(\zeta_y)$, $\hat{S}(\zeta_z)$ is shorthand for $\hat{S}_x(\zeta_x)$, $\hat{S}_y(\zeta_y)$ and $\hat{S}_z(\zeta_z)$ respectively.

$$\hat{S}(\zeta_y)\hat{a}_y\hat{S}^\dagger(\zeta_y) = \hat{a}_y\cosh(r_y) + \hat{a}_y^\dagger\sinh(r_y)\exp(i\phi_y),$$
$$\hat{S}(\zeta_y)\hat{a}_y^\dagger\hat{S}^\dagger(\zeta_y) = \hat{a}_y^\dagger\cosh(r_y) + \hat{a}_y\sinh(r_y)\exp(-i\phi_y), \tag{5.37}$$

$$\hat{S}(\zeta_z)\hat{a}_z\hat{S}^\dagger(\zeta_z) = \hat{a}_z\cosh(r_z) + \hat{a}_z^\dagger\sinh(r_z)\exp(i\phi_z),$$
$$\hat{S}(\zeta_z)\hat{a}_z^\dagger\hat{S}^\dagger(\zeta_z) = \hat{a}_z^\dagger\cosh(r_z) + \hat{a}_z\sinh(r_z)\exp(-i\phi_z). \tag{5.38}$$

Setting $\phi_x = \phi_y = \phi_z = 0$ and taking, for example, the operators of the x mode for the isotropic system ($\omega_x = \omega_y = \omega_z = \omega$), the squeezing operators have the following effect:

$$\hat{S}(\zeta_x)\hat{a}_x(\omega)\hat{S}^\dagger = \frac{1}{\sqrt{2\hbar}}\left(\sqrt{m\omega}\exp(\zeta_x)\hat{x} + \frac{i}{\sqrt{m\omega}}\exp(-\zeta_x)\hat{p}_x\right),$$
$$\hat{S}(\zeta_x)\hat{a}_x^\dagger(\omega)\hat{S}^\dagger(\zeta_x) = \frac{1}{\sqrt{2\hbar}}\left(\sqrt{m\omega}\exp(\zeta_x)\hat{x} - \frac{i}{\sqrt{m\omega}}\exp(-\zeta_x)\hat{p}_x\right). \tag{5.39}$$

Comparing this to (5.31), it is clear that the squeezing operator $\hat{S}(\zeta_x)$ maps the isotropic (ω) to anisotropic (ω_x) forms of $\hat{a}_x$ if the following is defined:

$$\zeta_x = \ln\left(\sqrt{\frac{\omega_x}{\omega}}\right). \tag{5.40}$$

The analogous result must hold for the y and z mode operators:

$$\zeta_y = \ln\left(\sqrt{\frac{\omega_y}{\omega}}\right), \quad \zeta_z = \ln\left(\sqrt{\frac{\omega_z}{\omega}}\right). \tag{5.41}$$

In mapping from the isotropic to anisotropic Hamiltonians (5.24)→(5.30), it is clear that the squeezing parameters of the different axes are related to each other through the frequency ω.

5.8.2 Mapping of the second component operators

This section focuses how the mappings of the second components $\hat{I}_2 \longrightarrow \hat{\mathcal{I}}_2$, $\hat{J}_2 \longrightarrow \hat{\mathcal{J}}_2$ and $\hat{K}_2 \longrightarrow \hat{\mathcal{K}}_2$ are achieved as confinement along each axis changes.

$\hat{I}_2 \longrightarrow \hat{\mathcal{I}}_2$**:**

Applying $\hat{S}(\zeta_x)$ and $\hat{S}(\zeta_y)$ to the operator $\hat{I}_2$:

$$\begin{aligned}
\hat{I}_2 \longrightarrow & -i\frac{\hbar}{2}\,\hat{S}(\zeta_y)\hat{S}(\zeta_x)\,\left(\hat{a}_x^\dagger\hat{a}_y - \hat{a}_y^\dagger\hat{a}_x\right)\,\hat{S}^\dagger(\zeta_x)\hat{S}^\dagger(\zeta_y) \\
&= -i\frac{\hbar}{2}\,\Big[\Big(\hat{a}_x^\dagger\cosh(\zeta_x) + \hat{a}_x\sinh(\zeta_x)\Big)\Big(\hat{a}_y\cosh(\zeta_y) + \hat{a}_y^\dagger\sinh(\zeta_y)\Big) \\
&\quad - \Big(\hat{a}_y^\dagger\cosh(\zeta_y) + \hat{a}_y\sinh(\zeta_y)\Big)\Big(\hat{a}_x\cosh(\zeta_x) + \hat{a}_x^\dagger\sinh(\zeta_x)\Big)\Big] \\
&= -i\frac{\hbar}{2}\,\Big(\hat{a}_x^\dagger\hat{a}_y\left[\cosh(\zeta_x)\cosh(\zeta_y) - \sinh(\zeta_x)\sinh(\zeta_y)\right] \\
&\quad -\hat{a}_y^\dagger\hat{a}_x\left[\cosh(\zeta_x)\cosh(\zeta_y) - \sinh(\zeta_x)\sinh(\zeta_y)\right] \\
&\quad +\hat{a}_x\hat{a}_y\left[\sinh(\zeta_x)\cosh(\zeta_y) - \sinh(\zeta_y)\cosh(\zeta)\right] \\
&\quad -\hat{a}_x^\dagger\hat{a}_y^\dagger\left[\sinh(\zeta_x)\cosh(\zeta_y) - \sinh(\zeta_y)\cosh(\zeta_x)\right]\Big)\,. \qquad (5.42)
\end{aligned}$$

Making use of the identities

$$\begin{aligned}
&\cosh(\zeta_x - \zeta_y) = \cosh(\zeta_x)\cosh(\zeta_y) - \sinh(\zeta_x)\sinh(\zeta_y), \\
&\sinh(\zeta_x - \zeta_y) = \sinh(\zeta_x)\cosh(\zeta_y) - \sinh(\zeta_y)\cosh(\zeta_x), \qquad (5.43)
\end{aligned}$$

reveals:

$$\begin{aligned}
&\hat{S}(\zeta_y)\hat{S}(\zeta_x)\,\hat{I}_2\,\hat{S}^\dagger(\zeta_x)\hat{S}^\dagger(\zeta_y) \\
&\qquad = -i\frac{\hbar}{2}\,\Big(\Big(\hat{a}_x^\dagger\hat{a}_y - \hat{a}_y^\dagger\hat{a}_x\Big)\left[\cosh(\zeta_x - \zeta_y)\right] \\
&\qquad\quad + \Big(\hat{a}_x\hat{a}_y - \hat{a}_x^\dagger\hat{a}_y^\dagger\Big)\left[\sinh(\zeta_x - \zeta_y)\right]\Big)\,. \qquad (5.44)
\end{aligned}$$

Comparing this to the definition of $\hat{\mathcal{I}}_2$ which follows from (5.34):

$$\hat{\mathcal{I}}_2 = -i\frac{\hbar}{4}\left(\left(\sqrt{\frac{\omega_y}{\omega_x}} + \sqrt{\frac{\omega_x}{\omega_y}}\right)\left(\hat{a}_x^\dagger\hat{a}_y - \hat{a}_y^\dagger\hat{a}_x\right) + \left(\sqrt{\frac{\omega_y}{\omega_x}} - \sqrt{\frac{\omega_x}{\omega_y}}\right)\left(\hat{a}_x\hat{a}_y - \hat{a}_x^\dagger\hat{a}_y^\dagger\right)\right), \qquad (5.45)$$

it is clear that the component $\hat{I}_2$ is mapped to $\hat{\mathcal{I}}_2$ by the application of the squeezing operators $\hat{S}(\zeta_x)$ and $\hat{S}(\zeta_y)$ if

$$\begin{aligned}
\cosh(\zeta_x - \zeta_y) = \frac{1}{2}\left(\sqrt{\frac{\omega_y}{\omega_x}} + \sqrt{\frac{\omega_x}{\omega_y}}\right), \qquad \sinh(\zeta_x - \zeta_y) = \frac{1}{2}\left(\sqrt{\frac{\omega_y}{\omega_x}} - \sqrt{\frac{\omega_x}{\omega_y}}\right) \\
\Longrightarrow (\zeta_x - \zeta_y) = \tanh^{-1}\left[\frac{\sqrt{\frac{\omega_y}{\omega_x}} - \sqrt{\frac{\omega_x}{\omega_y}}}{\sqrt{\frac{\omega_y}{\omega_x}} + \sqrt{\frac{\omega_x}{\omega_y}}}\right]. \qquad (5.46)
\end{aligned}$$

$\hat{J}_2 \longrightarrow \hat{\mathcal{J}}_2$**:**

Following from the above analysis, the transformation from $\hat{J}_2$ to $\hat{\mathcal{J}}_2$:

$$\hat{\mathcal{J}}_2 = -i\frac{\hbar}{4}\left(\left(\sqrt{\frac{\omega_x}{\omega_z}} + \sqrt{\frac{\omega_z}{\omega_x}}\right)\left(\hat{a}_z^\dagger\hat{a}_x - \hat{a}_x^\dagger\hat{a}_z\right) + \left(\sqrt{\frac{\omega_x}{\omega_z}} - \sqrt{\frac{\omega_z}{\omega_x}}\right)\left(\hat{a}_z\hat{a}_x - \hat{a}_z^\dagger\hat{a}_x^\dagger\right)\right), \qquad (5.47)$$

is achieved by squeezing operators for the x and z modes if

$$\cosh(\zeta_z - \zeta_x) = \frac{1}{2}\left(\sqrt{\frac{\omega_x}{\omega_z}} + \sqrt{\frac{\omega_z}{\omega_x}}\right), \qquad \sinh(\zeta_z - \zeta_x) = \frac{1}{2}\left(\sqrt{\frac{\omega_x}{\omega_z}} - \sqrt{\frac{\omega_z}{\omega_x}}\right)$$
$$\implies (\zeta_z - \zeta_x) = \tanh^{-1}\left[\frac{\sqrt{\frac{\omega_x}{\omega_z}} - \sqrt{\frac{\omega_z}{\omega_x}}}{\sqrt{\frac{\omega_x}{\omega_z}} + \sqrt{\frac{\omega_z}{\omega_x}}}\right]. \tag{5.48}$$

$\hat{K}_2 \longrightarrow \hat{\mathcal{K}}_2$**:**

Accordingly, the transformation from $\hat{K}_2$ to $\hat{\mathcal{K}}_2$:

$$\hat{\mathcal{K}}_2 = -i\frac{\hbar}{4}\left(\left(\sqrt{\frac{\omega_z}{\omega_y}} + \sqrt{\frac{\omega_y}{\omega_z}}\right)(\hat{a}_y^\dagger \hat{a}_z - \hat{a}_z^\dagger \hat{a}_y) + \left(\sqrt{\frac{\omega_z}{\omega_y}} - \sqrt{\frac{\omega_y}{\omega_z}}\right)(\hat{a}_y \hat{a}_z - \hat{a}_y^\dagger \hat{a}_z^\dagger)\right), \tag{5.49}$$

is achieved by application of the squeezing operators $\hat{S}(\zeta_y)$ and $\hat{S}(\zeta_z)$ if

$$\cosh(\zeta_y - \zeta_z) = \frac{1}{2}\left(\sqrt{\frac{\omega_z}{\omega_y}} + \sqrt{\frac{\omega_y}{\omega_z}}\right), \qquad \sinh(\zeta_y - \zeta_z) = \frac{1}{2}\left(\sqrt{\frac{\omega_z}{\omega_y}} - \sqrt{\frac{\omega_y}{\omega_z}}\right)$$
$$\implies (\zeta_y - \zeta_z) = \tanh^{-1}\left[\frac{\sqrt{\frac{\omega_z}{\omega_y}} - \sqrt{\frac{\omega_y}{\omega_z}}}{\sqrt{\frac{\omega_z}{\omega_y}} + \sqrt{\frac{\omega_y}{\omega_z}}}\right]. \tag{5.50}$$

5.8.3 Conservation of commutation relations

As the confinement along each axis changes from ω, the following can now be identified:

$$\begin{aligned}
\hat{L}_z &\longrightarrow \hat{S}(\zeta_y)\hat{S}(\zeta_x)\,\hat{L}_z\,\hat{S}^\dagger(\zeta_x)\hat{S}^\dagger(\zeta_y),\\
\hat{L}_x &\longrightarrow \hat{S}(\zeta_z)\hat{S}(\zeta_y)\,\hat{L}_x\,\hat{S}^\dagger(\zeta_y)\hat{S}^\dagger(\zeta_z),\\
\hat{L}_y &\longrightarrow \hat{S}(\zeta_x)\hat{S}(\zeta_z)\,\hat{L}_y\,\hat{S}^\dagger(\zeta_z)\hat{S}^\dagger(\zeta_x),
\end{aligned} \tag{5.51}$$

as $\hat{H}_{xyz} \to \hat{H}_A$. Conservation of commutation relations between $\hat{L}_x$, $\hat{L}_y$ and $\hat{L}_z$ is straightforward to check:

$$\begin{aligned}
\left[\hat{L}_x, \hat{L}_y\right] &\longrightarrow \left[\hat{S}(\zeta_z)\hat{S}(\zeta_y)\,\hat{L}_x\,\hat{S}^\dagger(\zeta_y)\hat{S}^\dagger(\zeta_z),\ \hat{S}(\zeta_x)\hat{S}(\zeta_z)\,\hat{L}_y\,\hat{S}^\dagger(\zeta_z)\hat{S}^\dagger(\zeta_x)\right]\\
&= \hat{S}(\zeta_z)\hat{S}(\zeta_y)\,\hat{L}_x\,\hat{S}^\dagger(\zeta_y)\hat{S}^\dagger(\zeta_z)\cdot\hat{S}(\zeta_x)\hat{S}(\zeta_z)\,\hat{L}_y\,\hat{S}^\dagger(\zeta_z)\hat{S}^\dagger(\zeta_x)\\
&\quad - \hat{S}(\zeta_x)\hat{S}(\zeta_z)\,\hat{L}_y\,\hat{S}^\dagger(\zeta_z)\hat{S}^\dagger(\zeta_x)\cdot\hat{S}(\zeta_z)\hat{S}(\zeta_y)\,\hat{L}_x\,\hat{S}^\dagger(\zeta_y)\hat{S}^\dagger(\zeta_z).
\end{aligned} \tag{5.52}$$

Making use of the unitary property of squeezing operators $\hat{S}\cdot\hat{S}^\dagger = \hat{1}$ [41]:

$$\begin{aligned}
\left[\hat{L}_x, \hat{L}_y\right] &\longrightarrow \hat{S}(\zeta_z)\hat{S}(\zeta_y)\hat{S}(\zeta_x)\,\hat{L}_x\ \cdot\ \hat{L}_y\,\hat{S}^\dagger(\zeta_y)\hat{S}^\dagger(\zeta_z)\hat{S}^\dagger(\eta_z)\\
&\quad - \hat{S}(\zeta_x)\hat{S}(\zeta_z)\hat{S}(\zeta_y)\,\hat{L}_y\ \cdot\ \hat{L}_x\,\hat{S}^\dagger(\zeta_x)\hat{S}^\dagger(\zeta_y)\hat{S}^\dagger(\zeta_z)\\
&= \hat{S}(\zeta_z)\hat{S}(\zeta_y)\hat{S}(\zeta_x)\left[\hat{L}_x, \hat{L}_y\right]\hat{S}^\dagger(\zeta_x)\hat{S}^\dagger(\zeta_y)\hat{S}^\dagger(\zeta_z)
\end{aligned} \tag{5.53}$$

Now, since $\left[\hat{L}_x,\, \hat{L}_y\right] = i\hbar\hat{L}_z$ and $\hat{S}(\zeta_z)\hat{L}_z\hat{S}^\dagger(\zeta_z) = \hat{L}_z$ ($\hat{L}_z$ contains no $\hat{a}_z$ or $\hat{a}_z^\dagger$ operators):

$$\left[\hat{L}_x,\, \hat{L}_y\right] \longrightarrow i\hbar\hat{L}_z. \tag{5.54}$$

In conclusion, the squeezing operators $\hat{S}(\zeta_x)$, $\hat{S}(\zeta_y)$, and $\hat{S}(\zeta_z)$, map the isotropic to anisotropic forms of $\hat{L}_x$, $\hat{L}_y$, $\hat{L}_z$ as confinement along an axis changes, i.e. they map components $\hat{K}_2/2$, $\hat{J}_2/2$, $\hat{I}_2/2$ to $\hat{\mathcal{K}}_2/2$, $\hat{\mathcal{J}}_2/2$, $\hat{\mathcal{I}}_2/2$.

5.8.4 Zeroth, first and third anisotropic components

Since the second component operators of the anisotropic sets $\underline{\mathcal{I}}$, $\underline{\mathcal{J}}$ and $\underline{\mathcal{K}}$ are produced from the isotropic ones by squeezing operators, it follows that other components of the sets, e.g. $\hat{\mathcal{I}}_1$, $\hat{\mathcal{I}}_3$, $\hat{\mathcal{I}}_0$, $\hat{\mathcal{K}}_1$, $\hat{\mathcal{K}}_2$ etc. are mapped analogously.

Beginning, for example, with the set $\underline{I}$:

$$\begin{aligned}
\hat{\mathcal{I}}_0 = \hat{S}(\zeta_y)\hat{S}(\zeta_x)\hat{I}_0\hat{S}^\dagger(\zeta_x)\hat{S}^\dagger(\zeta_y) &= \frac{\hbar}{4}\Bigg(\hat{n}_x\cosh(2\zeta_x) + \frac{1}{2}\left(\hat{a}_x^\dagger\hat{a}_x^\dagger + \hat{a}_x\hat{a}_x\right)\sinh(2\zeta_y) + \sinh^2(\zeta_x) \\
&\quad + \left(\hat{n}_y\cosh(2\zeta_y) + \frac{1}{2}\left(\hat{a}_y^\dagger\hat{a}_y^\dagger + \hat{a}_y\hat{a}_y\right)\sinh(2\zeta_y) + \sinh^2(\zeta_y)\right)\Bigg), \\
\hat{\mathcal{I}}_1 = \hat{S}(\zeta_y)\hat{S}(\zeta_x)\hat{I}_1\hat{S}^\dagger(\zeta_x)\hat{S}^\dagger(\zeta_y) &= \frac{\hbar}{4}\left(\left(\hat{a}_x^\dagger\hat{a}_y + \hat{a}_y^\dagger\hat{a}_x\right)\cosh(\zeta_x+\zeta_y) + \left(\hat{a}_x\hat{a}_y + \hat{a}_x^\dagger\hat{a}_y^\dagger\right)\sinh(\zeta_x+\zeta_y)\right), \\
\hat{\mathcal{I}}_2 = \hat{S}(\zeta_y)\hat{S}(\zeta_x)\hat{I}_2\hat{S}^\dagger(\zeta_x)\hat{S}^\dagger(\zeta_y) &= \frac{-i\hbar}{4}\left(\left(\hat{a}_x^\dagger\hat{a}_y - \hat{a}_y^\dagger\hat{a}_x\right)\cosh(\zeta_x-\zeta_y) + \left(\hat{a}_x\hat{a}_y - \hat{a}_x^\dagger\hat{a}_y^\dagger\right)\sinh(\zeta_x-\zeta_y)\right), \\
\hat{\mathcal{I}}_3 = \hat{S}(\zeta_y)\hat{S}(\zeta_x)\hat{I}_3\hat{S}^\dagger(\zeta_x)\hat{S}^\dagger(\zeta_y) &= \frac{\hbar}{4}\Bigg(\hat{n}_x\cosh(2\zeta_x) + \frac{1}{2}\left(\hat{a}_x^\dagger\hat{a}_x^\dagger + \hat{a}_x\hat{a}_x\right)\sinh(2\zeta_x) + \sinh^2(\zeta_x) \\
&\quad - \left(\hat{n}_y\cosh(2\zeta_y) + \frac{1}{2}\left(\hat{a}_y^\dagger\hat{a}_y^\dagger + \hat{a}_y\hat{a}_y\right)\sinh(2\zeta_y) + \sinh^2(\zeta_y)\right)\Bigg).
\end{aligned} \tag{5.55}$$

Conservation of commutation relations follows naturally:

$$\begin{aligned}
\left[\hat{\mathcal{I}}_1,\, \hat{\mathcal{I}}_2\right] &= \left[\hat{S}(\zeta_y)\hat{S}(\zeta_x)\hat{I}_1\hat{S}^\dagger(\zeta_x)\hat{S}^\dagger(\zeta_y),\, \hat{S}(\zeta_y)\hat{S}(\zeta_x)\hat{I}_2\hat{S}^\dagger(\zeta_x)\hat{S}^\dagger(\zeta_y)\right] \\
&= \hat{S}(\zeta_y)\hat{S}(\zeta_x)\hat{I}_1\hat{S}^\dagger(\zeta_x)\hat{S}^\dagger(\zeta_y)\cdot\hat{S}(\zeta_y)\hat{S}(\zeta_x)\hat{I}_2\hat{S}^\dagger(\zeta_x)\hat{S}^\dagger(\zeta_y) \\
&\quad - \hat{S}(\zeta_y)\hat{S}(\zeta_x)\hat{I}_2\hat{S}^\dagger(\zeta_x)\hat{S}^\dagger(\zeta_y)\cdot\hat{S}(\zeta_y)\hat{S}(\zeta_x)\hat{I}_1\hat{S}^\dagger(\zeta_x)\hat{S}^\dagger(\zeta_y) \\
&= \hat{S}(\zeta_x)\hat{S}(\zeta_y)\left[\hat{I}_1,\, \hat{I}_2\right]\hat{S}(\zeta_x)\hat{S}(\zeta_y) \\
&= i\hbar\,\hat{S}(\zeta_x)\hat{S}(\zeta_y)\hat{I}_3\hat{S}(\zeta_x)\hat{S}(\zeta_y) \\
&= i\hbar\,\hat{\mathcal{I}}_3.
\end{aligned} \tag{5.56}$$

Following this example, it is clear that the anisotropic components of the other sets are

given by:

$$\begin{aligned}
\hat{\mathcal{J}}_0 &= \hat{S}(\zeta_x)\hat{S}(\zeta_z)\hat{J}_0\hat{S}^\dagger(\zeta_z)\hat{S}^\dagger(\zeta_x),\\
\hat{\mathcal{J}}_1 &= \hat{S}(\zeta_x)\hat{S}(\zeta_z)\hat{J}_1\hat{S}^\dagger(\zeta_z)\hat{S}^\dagger(\zeta_x),\\
\hat{\mathcal{J}}_2 &= \hat{S}(\zeta_x)\hat{S}(\zeta_z)\hat{J}_2\hat{S}^\dagger(\zeta_z)\hat{S}^\dagger(\zeta_x),\\
\hat{\mathcal{J}}_3 &= \hat{S}(\zeta_x)\hat{S}(\zeta_z)\hat{J}_3\hat{S}^\dagger(\zeta_z)\hat{S}^\dagger(\zeta_x).
\end{aligned} \tag{5.57}$$

$$\begin{aligned}
\hat{\mathcal{K}}_0 &= \hat{S}(\zeta_z)\hat{S}(\zeta_y)\hat{K}_0\hat{S}^\dagger(\zeta_y)\hat{S}^\dagger(\zeta_z),\\
\hat{\mathcal{K}}_1 &= \hat{S}(\zeta_z)\hat{S}(\eta_y)\hat{K}_1\hat{S}^\dagger(\zeta_y)\hat{S}^\dagger(\zeta_z),\\
\hat{\mathcal{K}}_2 &= \hat{S}(\zeta_z)\hat{S}(\zeta_y)\hat{K}_2\hat{S}^\dagger(\zeta_y)\hat{S}^\dagger(\zeta_z),\\
\hat{\mathcal{K}}_3 &= \hat{S}(\zeta_z)\hat{S}(\zeta_y)\hat{K}_3\hat{S}^\dagger(\zeta_y)\hat{S}^\dagger(\zeta_z).
\end{aligned} \tag{5.58}$$

It is straightforward to check that the conditions imposed upon ζ_x, ζ_y and ζ_z in (5.46), (5.48) and (5.50) ensure that the commutation relations between *all* operators of the sets $\underline{\mathcal{I}}$, $\underline{\mathcal{J}}$ and $\underline{\mathcal{J}}$ are identical to those for the components of $\underline{I}$, $\underline{J}$ and $\underline{K}$. It follows that the commutation map in Figure (5.2) remains unchanged for the anisotropic sets.

5.9 The role of the anisotropic Schwinger boson operators

The aim of this section is to clarify how the anisotropic components act upon real space and momentum coordinates. Calculations are performed using the set $\underline{\mathcal{I}}$, from which analogous results follow for the other sets $\underline{\mathcal{J}}$ and $\underline{\mathcal{K}}$.

It is known that the component $2\hat{\mathcal{I}}_2$ is identically the canonical angular momentum of the z axis (indeed this motivated the present discussion), but it is not easy to see from (5.55) how this component acts upon a spatial coordinate. This is calculated explicitly here:

$$\begin{aligned}
\exp\left\{\frac{i}{\hbar}\gamma\hat{\mathcal{I}}_2\right\}\hat{x}\,\exp\left\{-\frac{i}{\hbar}\gamma\hat{\mathcal{I}}_2\right\} &= \exp\left\{\frac{i}{\hbar}\gamma\hat{\mathcal{I}}_2\right\}\left(\sqrt{\frac{\hbar}{2m\omega_x}}(\hat{a}_x^\dagger+\hat{a}_x)\right)\exp\left\{-\frac{i}{\hbar}\gamma\hat{\mathcal{I}}_2\right\}\\
&= \sqrt{\frac{\hbar}{2m\omega_x}}\left((\hat{a}_x^\dagger+\hat{a}_x)\cos\frac{\gamma}{2}-(\hat{a}_y^\dagger+\hat{a}_y)\sin\frac{\gamma}{2}\exp(\zeta_y-\zeta_x)\right)\\
&= \hat{x}\cos\frac{\gamma}{2}-\hat{y}\sqrt{\frac{\omega_y}{\omega_x}}\sin\frac{\gamma}{2}\exp(\zeta_y-\zeta_x).
\end{aligned} \tag{5.59}$$

Now, since $\exp(A)=\cosh(A)-\sinh(A)$, from (5.46):

$$\exp(\zeta_y-\zeta_x)=\frac{1}{2}\left(\sqrt{\frac{\omega_y}{\omega_x}}+\sqrt{\frac{\omega_x}{\omega_y}}\right)-\frac{1}{2}\left(\sqrt{\frac{\omega_y}{\omega_x}}-\sqrt{\frac{\omega_x}{\omega_y}}\right)=\sqrt{\frac{\omega_x}{\omega_y}}, \tag{5.60}$$

$$\implies \exp\left\{\frac{i}{\hbar}\gamma\hat{\mathcal{I}}_2\right\}\hat{x}\,\exp\left\{-\frac{i}{\hbar}\gamma\hat{\mathcal{I}}_2\right\}=\hat{x}\cos\frac{\gamma}{2}-\hat{y}\sin\frac{\gamma}{2}. \tag{5.61}$$

Thus, the anisotropic component $\hat{\mathcal{I}}_2$ rotates the radial coordinates around the z axis, identically to the transformation of the *isotropic* system by $\hat{I}_2$ in (5.5).

The zeroth, first and third components of the anisotropic sets have been found to perform similar transformations to those of the isotropic system, with the results modified by the degree of freedom introduced by the squeezing parameters. For example:

$$\begin{aligned}\exp\left\{\frac{i}{\hbar}\phi\hat{\mathcal{I}}_1\right\}\hat{x}\exp\left\{-\frac{i}{\hbar}\phi\hat{\mathcal{I}}_1\right\} &= \exp\left\{\frac{i}{\hbar}\phi\hat{\mathcal{I}}_1\right\}\left(\sqrt{\frac{\hbar}{2m\omega_x}}(\hat{a}_x^\dagger+\hat{a}_x)\right)\exp\left\{-\frac{i}{\hbar}\phi\hat{\mathcal{I}}_1\right\}\\ &= \sqrt{\frac{\hbar}{2m\omega_x}}\left((\hat{a}_x^\dagger+\hat{a}_x)\cos\frac{\phi}{2}-i(\hat{a}_y-\hat{a}_y^\dagger)\sin\frac{\phi}{2}\exp(-(\zeta_y+\zeta_x))\right)\\ &= \hat{x}\cos\frac{\phi}{2}+\frac{1}{m}\hat{p}_y\sin\frac{\phi}{2}\frac{1}{\sqrt{\omega_x\omega_y}}\exp(-(\zeta_y+\zeta_x)).\end{aligned} \tag{5.62}$$

For a given angle ϕ, the resulting contribution of the $\hat{p}_y$ coordinate differs from transformation of $\hat{x}$ by $\hat{I}_1$ for the isotropic system, (5.4).

5.10 Summary and application in the Penning trap

This chapter has investigated in detail the role of a set of Schwinger boson operators in 3D space. The above calculations demonstrate how many such sets may be formed simultaneously to completely characterise all rotations in phase space or real space upon position and momentum coordinates. In a system where the confinement along each spatial trapping axis is different, it was shown how there exists analogous operators mapped from the standard ones by squeezing operators. These "anisotropic components" play the same role as their isotropic counterparts for the isotropic system. Both the isotropic and anisotropic sets can be applied simultaneously to a set of system coordinates when the squeezing parameters mapping from one set to the other are strictly defined. The role played by each operator will depend upon the relative confinement of a trapped particle along the three real axes.

This builds up a rather large glossary of possible unitary transformations, the results of which are straightforward to read off or derive from the commutation map in Figure 5.2. In pursuit of interpreting the individual x and y potentials on a quantum level, the investigation sheds light upon the connection between quantum unitary operations and physical transformations in space. This is of significance for the investigation of the potential landscape of an electron in the Penning trap, and the question of whether or not this can be modified by a mode coupling electric potential as suggested in Chapter 2.

The results from this chapter necessarily motivate further questions on the subject. It is interesting to examine the limits of the squeezing transformations; can they effectively

map between confinement in 2D and 3D systems? This question is addressed in 8.6, where such a limit result is shown to be analogous to driving the Penning trap to the ultra-elliptical regime [29].

Chapter 6

Quantum Mechanics of the Penning Trap

Following the analysis of the previous chapters, the quantum theory of the Penning trap in the basis $\{x, y, z\}$ can now be fully addressed. The relationship to the more conventional $\{+, -, z\}$ basis is discussed towards the end of this chapter. This is in an effort to examine the manipulation of the potential energy of the electron in the trap, following the discussion in Chapter 2.

6.1 The Schrödinger Equation

6.1.1 Transformation of coordinates

From Hamiltonian (1.16), the time independent Schrödinger equation of the circular Penning trap is

$$\begin{aligned}\hat{\mathcal{H}}\psi = E\psi = \Bigg[&-\frac{\hbar^2}{2m}\left(\frac{\partial^2}{\partial\hat{x}^2}+\frac{\partial^2}{\partial\hat{y}^2}+\frac{\partial^2}{\partial\hat{z}^2}\right)\\ &+\frac{1}{2}m\left(\frac{\omega_1}{2}\right)^2(\hat{x}^2+\hat{y}^2)+\frac{1}{2}m\omega_z^2\hat{z}^2\\ &-i\hbar\frac{\omega_c}{2}\left(\hat{x}\frac{\partial}{\partial\hat{y}}-\hat{y}\frac{\partial}{\partial\hat{x}}\right)\Bigg]\psi.\end{aligned} \tag{6.1}$$

The appropriate transformation to render this separable is the following rotation of position and and momentum operators:

$$\hat{x}\to\frac{1}{\sqrt{2}}\left(\hat{x}-\frac{2}{m\omega_1}\hat{p}_y\right),\quad \hat{y}\to\frac{1}{\sqrt{2}}\left(\hat{y}-\frac{2}{m\omega_1}\hat{p}_x\right), \tag{6.2}$$

$$\hat{p}_x\to\frac{1}{\sqrt{2}}\left(p_x+\frac{m\omega_1}{2}y\right),\quad \hat{p}_y\to\frac{1}{\sqrt{2}}\left(\hat{p}_y+\frac{m\omega_1}{2}\hat{x}\right). \tag{6.3}$$

This follows from the result in (5.4) detailing the transformation of coordinates by the $\hat{I}_1$ operator through $\phi = -\pi/2$. It is analogous to defining the canonically conjugate variables in (1.34) [15].

The transformation produces a new Hamiltonian, $\hat{\mathcal{H}} \to \hat{\mathcal{H}}'$ which results in the Schrödinger equation:

$$\begin{aligned}\hat{\mathcal{H}}'\psi' = E\psi' = \Bigg[&\left(-\frac{\hbar^2}{2m_x}\frac{\partial^2}{\partial\hat{x}^2} + \frac{1}{2}m_x\omega_+^2\hat{x}^2\right) \\ &- \left(-\frac{\hbar^2}{2m_y}\frac{\partial^2}{\partial\hat{y}^2} + \frac{1}{2}m_y\omega_-^2\hat{y}^2\right) \\ &+ \left(-\frac{\hbar^2}{2m}\frac{\partial^2}{\partial\hat{z}^2} + \frac{1}{2}m\omega_z^2\hat{z}^2\right)\Bigg]\psi',\end{aligned} \tag{6.4}$$

where effective masses for the x and y motions are defined:

$$m_x = \frac{1}{2}\frac{\omega_1}{\omega_+}m, \quad m_y = \frac{1}{2}\frac{\omega_1}{\omega_-}m. \tag{6.5}$$

In this way, the transformed Schrödinger equation is written in the correct canonical form of three independent harmonic oscillators. The transformed Hamiltonian details a harmonic oscillator of frequency ω_+ along the x axis where the electron has effective mass m_x, and a negative one with frequency ω_- along y with effective mass m_y. The axial motion remains unchanged.

6.1.2 Solutions of the Schrödinger equation

The total wavefunction of $\hat{\mathcal{H}}'$ is written:

$$\psi' = \psi'_x(x)\psi'_y(y)\psi_z(z), \tag{6.6}$$

where [59]

$$\begin{aligned}\psi'_x(x) &= \sum_{n=0}^{\infty}\psi'_n(x,\, m_x,\, \omega_+), \\ \psi'_y(y) &= \sum_{n=0}^{\infty}\psi'_n(y,\, m_y,\, \omega_-), \\ \psi_z(z) &= \sum_{n=0}^{\infty}\psi_n(z);\end{aligned} \tag{6.7}$$

$$\begin{aligned}\psi'_n(x,\, m_x,\, \omega_+) = \Bigg(&\left(\frac{m_x\omega_+}{\pi\hbar}\right)^{\frac{1}{4}}\frac{1}{2^{\frac{n}{2}}\sqrt{n!}} \\ &\times \exp\left\{-\frac{m_x\omega_+x^2}{2\hbar}\right\} H_n\left[x\sqrt{\frac{m_x\omega_+}{\hbar}}\right]\Bigg),\end{aligned} \tag{6.8}$$

$$\psi'_n(y,\, m_y,\, \omega_-) = \left(\left(\frac{m_y\omega_-}{\pi\hbar} \right)^{\frac{1}{4}} \frac{1}{2^{\frac{n}{2}}\sqrt{n!}} \times \exp\left\{ -\frac{m_y\omega_- y^2}{2\hbar} \right\} H_n\left[y\sqrt{\frac{m_y\omega_-}{\hbar}} \right] \right), \tag{6.9}$$

$$\psi_n(z) = \left(\frac{m\omega_z}{\pi\hbar} \right)^{\frac{1}{4}} \frac{1}{2^{\frac{n}{2}}\sqrt{n!}} \exp\left\{ -\frac{m\omega_z z^2}{2\hbar} \right\} H_n\left[z\sqrt{\frac{m\omega_z}{\hbar}} \right]. \tag{6.10}$$

Following from the definitions of m_x and m_y, these wavefunctions further simplify by noting

$$m_x\omega_+ = m_y\omega_- = m\frac{\omega_1}{2}. \tag{6.11}$$

In this way, the radial wavefunctions in this rotated frame are solutions of the isotropic harmonic oscillator of frequency $\omega_1/2$. It is quite remarkable that although the solution of the Schrödinger equation in this frame have such simple form, the Hamiltonian $\hat{\mathcal{H}}'$ itself must involve the separate effective masses and frequencies for each direction.

6.2 The quantum operator transformation

As introduced in 4.5.1, the creation and annihilation operator analogue of the transformation defined by (6.2) and (6.3) is unitary rotation by the operator

$$\hat{U}_1 = \exp\left\{ -\frac{i\pi}{4}(\hat{a}_x^\dagger\hat{a}_y + \hat{a}_y^\dagger\hat{a}_x) \right\} = \exp\left\{ -\frac{i}{\hbar}\frac{\pi}{2}\hat{I}_1 \right\}, \tag{6.12}$$

where $\hat{I}_1 = \frac{\hbar}{2}\left(\hat{a}_x^\dagger\hat{a}_y + \hat{a}_y^\dagger\hat{a}_x\right)$.

It is interesting to note that (6.12) is noneother than a two-mode symmetric beamsplitter operator [79]. The operator $\hat{I}_1$ itself shall be accordingly referred to as *the beamsplitter operator*, or simply $\hat{I}_1$, and the frame obtained through this transformation as *the* $\hat{I}_1$ *frame*.

As a reminder, applying this transformation to the quantum Hamiltonian (4.24) yields:

$$\hat{\mathcal{H}}' = \hbar\omega_+\left(\hat{a}_x^\dagger\hat{a}_x + \frac{1}{2}\right) - \hbar\omega_-\left(\hat{a}_y^\dagger\hat{a}_y + \frac{1}{2}\right) + \hbar\omega_z\left(\hat{a}_z^\dagger\hat{a}_z + \frac{1}{2}\right). \tag{6.13}$$

When expanded out, this is exactly the same as the position and momentum representation of the Hamiltonian (6.4) in this frame.

6.2.1 Solutions of the Penning trap in the $\{x, y\}$ basis

Defining $|\psi\rangle$ as a general solution of $\hat{\mathcal{H}}$ in the lab frame, solutions in the $\hat{I}_1$ frame are accordingly given by

$$|\psi'\rangle = \hat{U}_1|\psi\rangle. \tag{6.14}$$

Fock states

The transformed Hamiltonian $\hat{\mathcal{H}}'$ admits Fock state solutions of the form

$$|\psi'\rangle = |n_x, n_y, n_z\rangle. \tag{6.15}$$

It is straightforward to perform the inverse transformation of this solution to find $|\psi\rangle$, the corresponding solution in the lab frame.

$$\begin{aligned}
|\psi\rangle &= \hat{U}_1^\dagger |n_x, n_y, n_z\rangle \\
&= \hat{U}_1^\dagger \left[\frac{1}{\sqrt{n_x!\, n_y!\, n_z!}} (\hat{a}_x^\dagger)^{n_x} (\hat{a}_y^\dagger)^{n_y} (\hat{a}_z^\dagger)^{n_z} \right] |0_x 0_y 0_z\rangle \\
&= \hat{U}_1^\dagger \left[\frac{1}{\sqrt{n_x!\, n_y!\, n_z!}} (\hat{a}_x^\dagger)^{n_x} (\hat{a}_y^\dagger)^{n_y} (\hat{a}_z^\dagger)^{n_z} \right] \hat{U}_1 \hat{U}_1^\dagger |0_x 0_y 0_z\rangle.
\end{aligned} \tag{6.16}$$

Now,

$$\begin{aligned}
\hat{U}_1^\dagger |0_x 0_y 0_z\rangle &= \sum_{l=0} \frac{1}{l!} \left(\frac{i\pi}{4} (\hat{a}_x^\dagger \hat{a}_y + \hat{a}_y^\dagger \hat{a}_x) \right)^l |0_x 0_y 0_z\rangle \\
&= |0_x 0_y 0_z\rangle,
\end{aligned} \tag{6.17}$$

since only the $l = 0$ term of this expansion survives. The calculation then follows in a straightforward way:

$$\begin{aligned}
\hat{U}_1^\dagger |n_x, n_y, n_z\rangle &= \frac{1}{\sqrt{n_x!\, n_y!\, n_z!}} \hat{U}_1^\dagger \left[(\hat{a}_x^\dagger)^{n_x} \right] \hat{U}_1 \hat{U}_1^\dagger \left[(\hat{a}_y^\dagger)^{n_y} \right] \hat{U}_1 \hat{U}_1^\dagger \left[(\hat{a}_z^\dagger)^{n_z} \right] \hat{U}_1 |0_x 0_y 0_z\rangle \\
&= \frac{1}{\sqrt{n_x!\, n_y!\, n_z!}} \left[\hat{U}_1^\dagger \hat{a}_x^\dagger \hat{U}_1 \right]^{n_x} \left[\hat{U}_1^\dagger \hat{a}_y^\dagger \hat{U}_1 \right]^{n_y} \hat{U}_1^\dagger \left[\hat{a}_z^\dagger \right]^{n_z} \hat{U}_1 |0_x 0_y 0_z\rangle \\
\implies \hat{U}_1^\dagger |n_x, n_y, n_z\rangle &= \frac{1}{\sqrt{n_x!\, n_y!\, n_z!}} \left[\frac{\hat{a}_x^\dagger + i\hat{a}_y^\dagger}{\sqrt{2}} \right]^{n_x} \left[\frac{i\hat{a}_x^\dagger + \hat{a}_x^\dagger}{\sqrt{2}} \right]^{n_y} \left[\hat{a}_z^\dagger \right]^{n_z} |0_x 0_y 0_z\rangle.
\end{aligned} \tag{6.18}$$

The last line of the calculation follows from 5.5.2, the *reverse* $\hat{I}_1$ transformation of $\hat{a}_x^\dagger$ and $\hat{a}_y^\dagger$ through an angle $\phi = -\pi/2$ [74]:

$$\exp\left\{ \frac{i}{\hbar} \left(\frac{\pi}{2} \right) \hat{I}_1 \right\} \begin{pmatrix} \hat{a}_x^\dagger \\ \hat{a}_y^\dagger \end{pmatrix} \exp\left\{ -\frac{i}{\hbar} \left(\frac{\pi}{2} \right) \hat{I}_1 \right\} = \frac{1}{\sqrt{2}} \begin{pmatrix} 1 & i \\ i & 1 \end{pmatrix} \begin{pmatrix} \hat{a}_x^\dagger \\ \hat{a}_y^\dagger \end{pmatrix}. \tag{6.19}$$

A few specific examples of $|\psi\rangle$, the Fock state solution in the lab frame:

$$\begin{aligned}
&\hat{U}_1^\dagger |0_x 0_y 0_z\rangle = |0_x 0_y 0_z\rangle \\
&\hat{U}_1^\dagger |1_x 0_y 0_z\rangle = \frac{1}{\sqrt{2}} \left(|1_x 0_y 0_z\rangle + i|0_x 1_y 0_z\rangle \right) \\
&\hat{U}_1^\dagger |2_x 2_y 0_z\rangle = \frac{1}{4} \left(\sqrt{3}(|0_x 4_y 0_z\rangle + |4_x 0_y 0_z\rangle) - \sqrt{2}|2_x 2_y 0_z\rangle \right), \\
&\ldots
\end{aligned} \tag{6.20}$$

It is clear that the Fock state solutions in the $\hat{I}_1$ frame are none other than superpositions of states of the same total quantum number in the laboratory frame.

The relationship between the above lab frame states $|\psi\rangle$ of the $\{x, y\}$ basis, and the solutions in terms of the more conventional Penning trap basis $\{+, -\}$ in 1.3.2, is straightforward. The expectation values of Hamiltonian $\hat{\mathcal{H}}'$ in the above states (6.20) are found to be:

$$\begin{aligned}
\langle 0_x 0_y 0_z|\hat{U}_1\ \hat{\mathcal{H}}\ \hat{U}_1^\dagger|0_x 0_y 0_z\rangle &= \hbar\frac{\omega_1}{2} = \langle 0_+ 0_- 0_z|\hat{\mathcal{H}}|0_+ 0_- 0_z\rangle,\\
\langle 1_x 0_y 0_z|\hat{U}_1\ \hat{\mathcal{H}}\ \hat{U}_1^\dagger|1_x 0_y 0_z\rangle &= \hbar\left(\frac{\omega_1}{2} + \omega_+\right)\\
&= \langle 1_+ 0_- 0_z|\hat{\mathcal{H}}|1_+ 0_- 0_z\rangle,\\
\langle 2_x 2_y 0_z|\hat{U}_1\ \hat{\mathcal{H}}\ \hat{U}_1^\dagger|2_x 2_y 2_z\rangle &= 5\hbar\frac{\omega_1}{2} = \langle 2_+ 2_- 0_z|\hat{\mathcal{H}}|2_+ 2_- 0_z\rangle.
\end{aligned} \tag{6.21}$$

That is, the expectation value of the state $\hat{U}_1^\dagger|n_x, n_y, n_z\rangle$ in the lab frame matches exactly the energy of the state $|n_+, n_-, n_z\rangle$ in the same frame, where $n_+ = n_x,\ n_- = n_y$:

$$\langle n_x, n_y, n_z|\hat{U}_1\ \hat{\mathcal{H}}\ \hat{U}_1^\dagger|n_x, n_y, n_z\rangle = \langle n_+, n_-, n_z|\hat{\mathcal{H}}|n_+, n_-, n_z\rangle. \tag{6.22}$$

Following this, it seems plausible that the general relationship between the eigenstates of the Penning trap Hamiltonian in terms of the $\{x, y\}$ (4.24) and $\{+, -\}$ (1.38) bases is given by:

$$|n_+, n_-, n_z\rangle \stackrel{?}{=} \frac{1}{\sqrt{n_x!\, n_y!\, n_z!}}\left[\frac{\hat{a}_x^\dagger + i\hat{a}_y^\dagger}{\sqrt{2}}\right]^{n_x}\left[\frac{i\hat{a}_x^\dagger + \hat{a}_x^\dagger}{\sqrt{2}}\right]^{n_y}\left[\hat{a}_z^\dagger\right]^{n_z}|0_x 0_y 0_z\rangle, \tag{6.23}$$

where $n_+ = n_x,\ n_- = n_y$. This is discussed further in 6.4.

Coherent states

Hamiltonian (6.13) is used to determine the time dependence of the operators in the $\hat{I}_1$ frame:

$$\begin{aligned}
i\hbar\partial_t\hat{a}_x^\dagger &= [\hat{a}_x^\dagger,\ \hat{\mathcal{H}}'] = -\hbar\omega_+\hat{a}_x^\dagger \Longrightarrow \hat{a}_x^\dagger(t) = e^{i\omega_+ t}\hat{a}_x^\dagger,\\
i\hbar\partial_t\hat{a}_y^\dagger &= [\hat{a}_y^\dagger,\ \hat{\mathcal{H}}'] = \hbar\omega_-\hat{a}_y^\dagger \Longrightarrow \hat{a}_y^\dagger(t) = e^{-i\omega_- t}\hat{a}_y^\dagger,\\
i\hbar\partial_t\hat{a}_z^\dagger &= [\hat{a}_z^\dagger,\ \hat{\mathcal{H}}'] = -\hbar\omega_z\hat{a}_z^\dagger \Longrightarrow \hat{a}_z^\dagger(t) = e^{i\omega_z t}\hat{a}_x^\dagger,
\end{aligned} \tag{6.24}$$

where $\hat{a}_x^\dagger = \hat{a}_x^\dagger(0)$, $\hat{a}_y^\dagger = \hat{a}_y^\dagger(0)$, $\hat{a}_z^\dagger = \hat{a}_z^\dagger(0)$. $\hat{\mathcal{H}}'$ therefore admits time dependent coherent state solutions [41]

$$|\alpha_x^{'}(t)\alpha_y^{'}(t)\alpha_z(t)\rangle = |\alpha_x^{'}e^{-i\omega_+ t}\alpha_y^{'}e^{i\omega_- t}\alpha_z e^{-i\omega_z t}\rangle; \tag{6.25}$$

$$|\alpha_x^{'}(t)\alpha_y^{'}(t)\alpha_z(t)\rangle = \hat{D}(\alpha_x^{'}(t))\hat{D}(\alpha_y^{'}(t))\hat{D}(\alpha_z(t))|0_x0_y0_z\rangle, \tag{6.26}$$

where $\hat{D}(\alpha(t))$ is the general time dependent displacement defined in (1.43). The form of these solutions in the lab frame is straightforward to determine following the Fock state treatment above:

$$\begin{aligned}
&\hat{U}_1^\dagger|\alpha_x^{'}(t)\alpha_y^{'}(t)\alpha_z(t)\rangle \\
&\quad= \hat{U}_1^\dagger\left[\hat{D}(\alpha_x^{'}(t))\hat{D}(\alpha_y^{'}(t))\hat{D}(\alpha_z(t))\right]|0_x0_y0_z\rangle \\
&\quad= \hat{U}_1^\dagger\left[\hat{D}(\alpha_x^{'}(t))\hat{D}(\alpha_y^{'}(t))\hat{D}(\alpha_z(t))\right]\hat{U}_1\hat{U}_1^\dagger|0_x0_y0_z\rangle \\
&\quad= \hat{U}_1^\dagger\left[\hat{D}(\alpha_x^{'}(t))\hat{D}(\alpha_y^{'}(t))\hat{D}(\alpha_z(t))\right]\hat{U}_1|0_x0_y0_z\rangle \\
&\quad= \hat{U}_1^\dagger\left[\exp\left\{\alpha_x^{'}(t)\hat{a}_x^\dagger - \alpha_x^{'*}(t)\hat{a}_x + \alpha_y^{'}(t)\hat{a}_y^\dagger - \alpha_y^{'*}(t)\hat{a}_y + \alpha_z(t)\hat{a}_z^\dagger - \alpha_z^*(t)\hat{a}_z\right\}\right]\hat{U}_1|0_x0_y0_z\rangle \\
&\quad= \exp\left\{\hat{U}_1^\dagger\left[\alpha_x^{'}(t)\hat{a}_x^\dagger - \alpha_x^{'*}(t)\hat{a}_x + \alpha_y^{'}(t)\hat{a}_y^\dagger - \alpha_y^{'*}(t)\hat{a}_y + \alpha_z(t)\hat{a}_z^\dagger - \alpha_z^*(t)\hat{a}_z\right]\hat{U}_1\right\}|0_x0_y0_z\rangle \\
&\quad= \exp\left\{\alpha_x\hat{a}_x^\dagger - \alpha_x^*\hat{a}_x + \alpha_y\hat{a}_y^\dagger - \alpha_y^*\hat{a}_y + \alpha_z\hat{a}_z^\dagger + \alpha_z^*\hat{a}_z\right\}|0_x0_y0_z\rangle \\
&\quad\equiv |\alpha_x(t)\alpha_y(t)\alpha_z(t)\rangle,
\end{aligned} \tag{6.27}$$

where

$$\alpha_x(t) = \frac{\alpha_x^{'}(t) + i\alpha_y^{'}(t)}{\sqrt{2}}, \quad \alpha_y(t) = \frac{\alpha_y^{'}(t) + i\alpha_x^{'}(t)}{\sqrt{2}}, \tag{6.28}$$

and

$$\alpha_x^{'}(t) = \exp(-i\omega_+t) \quad \alpha_y^{'}(t) = \exp(i\omega_-t) \quad \alpha_z(t) = \exp(-i\omega_zt). \tag{6.29}$$

Thus, the Hamiltonian in the lab frame (4.24) admits coherent state solutions with complex amplitudes modified from those in the $\hat{I}_1$ frame.

The expectation values of the radial coordinates for these coherent states are calculated:

$$\begin{aligned}
\langle\hat{x}(t)\rangle = \sqrt{\frac{2\hbar}{m\omega_1}}\Big(&|\alpha_x^{'}|\cos(\omega_+t - \varphi_{x'}) \\
&-|\alpha_y^{'}|\sin(\omega_-t + \varphi_{y'})\Big),
\end{aligned} \tag{6.30}$$

$$\begin{aligned}
\langle\hat{y}(t)\rangle = \sqrt{\frac{2\hbar}{m\omega_1}}\Big(&|\alpha_y^{'}|\cos(\omega_-t + \varphi_{y'}) \\
&+|\alpha_x^{'}|\sin(\omega_+t - \varphi_{x'})\Big).
\end{aligned} \tag{6.31}$$

These are found to be identical to the classical results in (1.24) if

$$|\alpha_y^{'}| = \sqrt{\frac{m\omega_1}{2\hbar}}|A_-|, \quad \varphi_{y'} = \varphi_-, \tag{6.32}$$

$$|\alpha_x^{'}| = \sqrt{\frac{m\omega_1}{2\hbar}}|A_+|, \quad \varphi_{x'} = -(\varphi_+ + \frac{\pi}{2}). \tag{6.33}$$

In 4.4.2, it was shown that the x and y coherent state solutions resulting from the rotating frame transformation required strict conditions upon the relative phase of the x and y motions (4.47) in order to agree with the classical solutions. The above solution following the beamsplitter transformation is more general.

6.3 The $\{x, y\}$ to the $\{+, -\}$ basis (revisited)

This chapter has abandoned the conventional cyclotron and magnetron mode description of the Penning trap (1.37, 1.38), in order to examine the individual x and y motions.

Formally discussed in Chapter 1, the construction of the operators $\hat{a}_+$ and $\hat{a}_-$ in (1.37) via the formation of canonically conjugate pairs q_+, p_+ and q_-, p_- decouples the radial motion in the Penning trap. This method of decoupling is referred to as the *replacement of operators* $\{\hat{a}_x, \hat{a}_y\}$.

Likewise, transformation to the $\hat{I}_1$ frame as proposed in this chapter decouples the Hamiltonian written in the $\{x, y\}$ basis. This method is the *rotation to the* $\hat{I}_1$ *frame*.

The aim of this section is to highlight the differences and similarities between these two formulations.

In Chapter 3, it was discussed how the change of basis from linear $\{x, y\}$ to circular $\{+, -\}$ mode operators, or coordinates, involves the unitary rotation (3.20). It was also revealed how the $SO(3)$ representation of this transformation affects the Schwinger boson angular momentum vectors of the set $\underline{L}$ of the $\{+, -\}$ basis. This rotation is responsible for the seemingly inconsistent expectation value results for transformation to the rotating frame in Chapter 4 in the two bases: the change of coordinates $\{x, y\} \longrightarrow \{+, -\}$ involves the coupling term in the Hamiltonian (4.24) changing from a *second* to a *third* component of angular momentum.

6.3.1 An alternative definition of $\hat{a}_+$ and $\hat{a}_-$

It is clear that transformation of $\hat{\mathcal{H}}$ to a diagonal basis is not unique. In fact, choosing the following definition of $\hat{a}_+$ and $\hat{a}_-$:

$$\begin{pmatrix} \hat{a}_+ \\ \hat{a}_- \end{pmatrix} = \frac{1}{\sqrt{2}} \begin{pmatrix} 1 & -i \\ -i & 1 \end{pmatrix} \begin{pmatrix} \hat{a}_x \\ \hat{a}_y \end{pmatrix} \tag{6.34}$$

achieves such a diagonal form of the Penning trap Hamiltonian; the resulting Hamiltonian is in fact identical to (1.38). Comparison to (5.11) reveals this is exactly the $\hat{I}_1$ rotation of $\hat{a}_x$ and $\hat{a}_y$ through $\pi/2$. If this formulation of the cyclotron and magnetron mode operators is used rather than than those conventionally used for the Penning trap and Landau systems as shown in (3.20) [15], the only difference is the resulting rotation of the set $\underline{I}$ Schwinger boson components. The $SO(3)$ representation of the (2×2) matrix in (6.34) is given by [74]:

$$\begin{pmatrix} 1 & 0 & 0 \\ 0 & 0 & -1 \\ 0 & 1 & 0 \end{pmatrix}. \tag{6.35}$$

Comparing to (4.49), this is exactly the rotation matrix of a general set of Schwinger boson angular momentum components by the first component of the set, through an angle $\pi/2$. Collecting all this together, the Hamiltonian (4.24) can be diagonalised by forming the following operators:

$$\begin{pmatrix} \hat{a}_+ \\ \hat{a}_- \end{pmatrix} = \exp\left\{\frac{i}{\hbar}\left(\frac{\pi}{2}\right)\hat{I}_1\right\}\begin{pmatrix} \hat{a}_x \\ \hat{a}_y \end{pmatrix}\exp\left\{-\frac{i}{\hbar}\left(\frac{\pi}{2}\right)\hat{I}_1\right\}, \tag{6.36}$$

$$\begin{pmatrix} \hat{a}_+^\dagger \\ \hat{a}_-^\dagger \end{pmatrix} = \exp\left\{\frac{i}{\hbar}\left(\frac{\pi}{2}\right)\hat{I}_1\right\}\begin{pmatrix} \hat{a}_x^\dagger \\ \hat{a}_y^\dagger \end{pmatrix}\exp\left\{-\frac{i}{\hbar}\left(\frac{\pi}{2}\right)\hat{I}_1\right\}, \tag{6.37}$$

which rotates the set of Schwinger boson vectors $\underline{I}$ in the following way to form new ones $\underline{L}$:

$$\begin{pmatrix} \hat{L}_1 \\ \hat{L}_2 \\ \hat{L}_3 \end{pmatrix} = \exp\left\{\frac{i}{\hbar}\left(\frac{\pi}{2}\right)\hat{I}_1\right\}\begin{pmatrix} \hat{I}_1 \\ \hat{I}_2 \\ \hat{I}_3 \end{pmatrix}\exp\left\{\frac{i}{\hbar}\left(\frac{\pi}{2}\right)\hat{I}_1\right\} = \begin{pmatrix} 1 & 0 & 0 \\ 0 & 0 & -1 \\ 0 & 1 & 0 \end{pmatrix}\begin{pmatrix} \hat{I}_1 \\ \hat{I}_2 \\ \hat{I}_3 \end{pmatrix}. \tag{6.38}$$

Examining again the Fock state solutions of the Penning trap in (6.18), and substituting in the definitions of $\hat{a}_+^\dagger$ and $\hat{a}_-^\dagger$ from (6.37):

$$\hat{U}_1^\dagger|n_x, n_y, n_z\rangle = \frac{1}{\sqrt{n_x!\, n_y!\, n_z!}}\left[\hat{a}_+^\dagger\right]^{n_x}\left[\hat{a}_-^\dagger\right]^{n_y}\left[\hat{a}_z^\dagger\right]^{n_z}|0_x 0_y 0_z\rangle. \tag{6.39}$$

This makes clear the connection between the two methods of solving the problem, i.e. by *replacement* or *rotation* of coordinates.

6.3.2 The circular mode operators vs. the beamsplitter mode operators

The mapping of $\hat{a}_x$ and $\hat{a}_y$ to cyclotron and magnetron mode operators in (3.20) simultaneously rotates all three operators of a Schwinger boson set $\underline{I}$ as shown in (3.23), since

this mapping is formed of a *superposition* of $SU(2)$ matrices. In contrast, since $\hat{a}_+$ and $\hat{a}_-$ formed from the $\hat{I}_1$ rotation relies upon the Pauli matrix σ_1 alone, as shown in (6.36), only the operators $\hat{I}_2$ and $\hat{I}_3$ are rotated by this transformation. For the purposes of studying the quantum theory of the Penning trap, both rotations achieve the desired goal of turning a second into a third component angular momentum operator; both choices enable $\hat{\mathcal{H}}$ to be rewritten in diagonal form. In examining the method of solving $\hat{\mathcal{H}}$ by rotation to the $\hat{I}_1$ frame, however, the basis of $\{\hat{a}_+, \hat{a}_-\}$ constructed via rotation by the $\hat{I}_1$ operator offers a more direct correspondence.

In summary, the operators of the cyclotron and magnetron modes can be formed by at least two different combinations of $\hat{a}_x$ and $\hat{a}_y$. The conventional method [14] discussed in Chapter 1 decouples the x and y coordinates before forming quantum mode operators, whereas the formation of $\hat{a}_+$ and $\hat{a}_-$ introduced in 6.3.1 decouples *after* forming creation and annihilation operators. In both cases, the "beamsplitter" transformation is involved. Upon examination, it is now also transparent that this same rotation is responsible for decoupling the classical equations of motion in 1.2.1. It is now clear that decoupling should take place after quantization of the modes by the methods discussed in this present chapter, so to keep track of the individual x and y degrees of freedom more consistently. In addition, performing this beamsplitter operation within the formalism of angular momentum algebra in the quantum regime provides an elegant method for this.

For the remainder of this thesis, the connection between the $\{+,-\}$ and $\{x,y\}$ basis is given by the definition in (6.37) and accordingly, (6.38). All of the results can be found completely analogously for the more conventional mapping [15] established in 3.4.2.

6.4 The two basis sets

The overlap of $\hat{U}_1^\dagger|n_x,n_y,n_z\rangle$ with Fock states $|n_+,n_-,n_z\rangle$ follows from (6.39):

$$\begin{aligned}
&\langle n_+,n_-,n_z|\hat{U}_1^\dagger|n_x,n_y,n_z\rangle \\
&\qquad = \frac{1}{\sqrt{n_+!n_-!n_z!n_x!n_y!n_z!}}\langle 0_+0_-0_z|\,(\hat{a}_+)^{n_+}\,(\hat{a}_-)^{n_-}\,(\hat{a}_z)^{n_z}\left(\hat{a}_+^\dagger\right)^{n_x}\left(\hat{a}_-^\dagger\right)^{n_y}\left(\hat{a}_z^\dagger\right)^{n_z}|0_x0_y0_z\rangle \\
&\qquad = \frac{1}{\sqrt{n_+!n_-!n_x!n_y!}}\langle 0_+0_-|\,(\hat{a}_+)^{n_+}\,(\hat{a}_-)^{n_-}\left(\hat{a}_+^\dagger\right)^{n_x}\left(\hat{a}_-^\dagger\right)^{n_y}|0_x0_y\rangle.
\end{aligned} \tag{6.40}$$

Now, if $n_+ = n_x$ and $n_- = n_y$:

$$\begin{aligned}\langle n_+, n_-, n_z|\hat{U}_1^\dagger|n_x, n_y, n_z\rangle &= \frac{1}{n_+!n_-!}\langle 0_+0_-|\left(\hat{n}_+ + 1\right)^{n_+}\left(\hat{n}_- + 1\right)^{n_-}|0_x0_y\rangle \\ &= \frac{1}{n_+!n_-!}\langle 0_+0_-|0_x0_y\rangle. \end{aligned} \tag{6.41}$$

Since $\langle 0_+0_-|0_x0_y\rangle \neq n_+!n_-!$ for general values of n_+ and n_-,

$$\langle n_+, n_-, n_z|\hat{U}_1^\dagger|n_x, n_y, n_z\rangle \neq 1. \tag{6.42}$$

Although the expectation value of the Hamiltonian $\hat{\mathcal{H}}$ with respect to both the states $|n_+, n_-, n_z\rangle$ and $\hat{U}_1^\dagger|n_x, n_y, n_z\rangle$ is the same (6.22), it is not true that the *states* are the same, but only that they are degenerate with each other, for $n_+ = n_x$ and $n_- = n_y$.

6.5 Thermal states and the total energy

Now that the connection between the two bases $\{x, y\}$ and $\{+, -\}$ has been well established, it is appropriate to revisit the discussion of the thermal energy in the Penning trap.

From 1.4.1, the density matrix of the Penning trap $\hat{\rho}_{\pm,z}$ in (1.67) is necessarily a function of the $\hat{n}_+$, $\hat{n}_-$ and $\hat{n}_z$ operators. In this way, the total energy of the Penning trap is completely governed by its thermal environment, the *real* energy of the Penning trap. The question of how this translates to the liner modes in the rotating and $\hat{I}_1$ frames can now be addressed.

6.5.1 The thermal energy in the rotating frame

The total thermal density matrix is transformed to the rotating frame of the Penning trap in the following way:

$$\begin{aligned}\hat{U}(t)\hat{\rho}_{\pm,z}\hat{U}^\dagger(t) &= \exp\left\{\frac{i}{\hbar}\left(\omega_c t\right)\hat{L}_3\right\}\hat{\rho}_{\pm,z}\exp\left\{\frac{i}{\hbar}\left(-\omega_c t\right)\hat{L}_3\right\} \\ &= \hat{\rho}_{\pm,z}, \end{aligned} \tag{6.43}$$

since $\left[\hat{L}_3,\, \hat{n}_+\right] = \left[\hat{L}_3,\, \hat{n}_-\right] = 0$. Using (6.34):

$$\begin{aligned}\hbar\hat{n}_+ &= \hat{I}_0 + \hat{I}_2, \\ \hbar\hat{n}_- &= \hat{I}_0 - \hat{I}_2, \end{aligned} \tag{6.44}$$

so that the individual density matrices of the cyclotron and magnetron modes are written in the $\{x, y\}$ basis:

$$\hat{\rho}_+ = \frac{\exp(-\beta\omega_+ \left(\hat{I}_0 + \hat{I}_2 + \frac{1}{2}\right))}{Tr[\exp(-\beta\hbar\omega_+ \left(\hat{n}_+ + \frac{1}{2}\right))]},$$
$$\hat{\rho}_- = \frac{\exp(-\beta\omega_z \left(\hat{I}_0 - \hat{I}_2 + \frac{1}{2}\right))}{Tr[\exp(-\beta\hbar\omega_z \left(\hat{n}_- + \frac{1}{2}\right))]}. \tag{6.45}$$

These are the $\{x, y\}$ basis representations of the thermal density matrices of the system in both the laboratory and $\hat{I}_1$ frames. The presence of the $\hat{I}_2$ operator shows how the thermal energy, the real total energy of the system, *cannot* be described via the harmonic motion in the x and y directions in either the lab or rotating frames of the Penning trap.

6.5.2 The thermal energy in the $\hat{I}_1$ frame

Making use of the fact that $\hat{L}_1 = \hat{I}_1$ (6.38), the density matrix of the Penning trap is transformed to the $\hat{I}_1$ frame in the following way:

$$\begin{aligned}\hat{U}_1\hat{\rho}_{\pm,z}\hat{U}_1^\dagger &= \exp\left\{\frac{i}{\hbar}\left(-\frac{\pi}{2}\right)\hat{L}_1\right\}\hat{\rho}_{\pm,z}\exp\left\{\frac{i}{\hbar}\left(-\frac{\pi}{2}\right)\hat{L}_1\right\} \\ &= \frac{\exp(-\beta\omega_+ \left(\hat{L}_0 - \hat{L}_2 + \frac{1}{2}\right))}{Tr[\exp(-\beta\hbar\omega_+ \left(\hat{n}_+ + \frac{1}{2}\right))]} \bigotimes \frac{\exp(-\beta\omega_z \left(\hat{L}_0 + \hat{L}_2 + \frac{1}{2}\right))}{Tr[\exp(-\beta\hbar\omega_z \left(\hat{n}_- + \frac{1}{2}\right))]} \bigotimes \hat{\rho}_z. \end{aligned} \tag{6.46}$$

Identifying the following from (6.38):

$$\hat{L}_0 - \hat{L}_2 = \hat{I}_0 + \hat{I}_3 = \hbar\hat{n}_x,$$
$$\hat{L}_0 + \hat{L}_2 = \hat{I}_0 - \hat{I}_3 = \hbar\hat{n}_y, \tag{6.47}$$

the density matrix of the Penning trap in the $\hat{I}_1$ frame is given by

$$\hat{\rho}'_{\pm,z} = \frac{\exp(-\beta\hbar\omega_+ \left(\hat{n}_x + \frac{1}{2}\right))}{Tr[\exp(-\beta\hbar\omega_+ \left(\hat{n}_x + \frac{1}{2}\right))]} \bigotimes \frac{\exp(-\beta\hbar\omega_z \left(\hat{n}_y + \frac{1}{2}\right))}{Tr[\exp(-\beta\hbar\omega_z \left(\hat{n}_y + \frac{1}{2}\right))]} \bigotimes \frac{\exp(-\beta\hbar\omega_z \left(\hat{n}_z + \frac{1}{2}\right))}{Tr[\exp(-\beta\hbar\omega_z \left(\hat{n}_z + \frac{1}{2}\right))]}, \tag{6.48}$$

where in the partition functions of the x and y modes, $\hat{n}_+$ and $\hat{n}_-$ can be used interchangeably with $\hat{n}_x$ and $\hat{n}_y$ respectively.

In conclusion to the study of the individual quantum energy of the x and y motions in the Penning trap: it is only in the $\hat{I}_1$ frame, and *not*, as seems intuitive from the straightforward classical transformations, in the rotating frame, that individual behaviour of the x and y motions can be identified. In this former frame, the effects of the magnetic vector potential $\vec{A}$ upon the energy is manifest as effective masses in the harmonic oscillator

potentials of the x and y modes. Within these oscillator potentials, the wavefunction of the electron in both directions behaves identically to one of an electron of original mass m in a harmonic oscillator of frequency $\omega_1/2$. In terms of "where" these potentials exist, this follows from the analysis of Chapter 5: the $\hat{I}_1$ frame has is removed from the lab by a phase space and real space transformation. It is straightforward to verify [61]

$$\exp\left\{\frac{i}{\hbar}\theta\hat{I}_1\right\} = \exp\left\{\frac{i}{\hbar}\left(\frac{\pi}{2}\right)\hat{I}_3\right\}\exp\left\{\frac{i}{\hbar}\theta\hat{I}_2\right\}\exp\left\{\frac{i}{\hbar}\left(-\frac{\pi}{2}\right)\hat{I}_3\right\}, \tag{6.49}$$

so that the $\hat{I}_1$ transformation through an angle $-\pi/2$ can be interpreted as a $-\pi/4$ rotation around the z axis which has itself been rotated by $\pi/4$ in phase space.

Chapter 7

Sideband Coupling in the $\{x, y\}$ Basis

This chapter revisits the calculation from Chapter 2 of coupling the axial and cyclotron modes of the Penning trap. It demonstrates the robustness of the dressed-atom formalism [57] in the $\{x, y\}$ basis, and shows how use of the $\hat{I}_1$ frame enables experimental access to the individual x and y motions in the trap.

7.1 The coupling potential in the $\hat{I}_1$ frame

As deduced from Chapters 4 and 6, the appropriate frame of reference in which the Penning trap Hamiltonian is diagonal in the $\{x, y\}$ basis, is the $\hat{I}_1$ frame. It is therefore necessary to transform the coupling potential in (2.2) to this frame before analysing its effects upon the individual x and y degrees of freedom.

From the operators $\hat{a}_x$, $\hat{a}_y$, $\hat{a}_z$ of the Penning trap (4.22, 4.23, 1.37), the $\hat{x}$, and $\hat{z}$ coordinates are given by:

$$\hat{x} = \sqrt{\frac{\hbar}{m\omega_1}}\left(\hat{a}_x^\dagger + \hat{a}_x\right), \quad \hat{z} = \sqrt{\frac{\hbar}{2m\omega_z}}\left(\hat{a}_z^\dagger + \hat{a}_z\right), \tag{7.1}$$

so that, from (2.2), the quantized coupling potential is written:

$$\hat{V}_p(t) = -\epsilon_p \cos(\omega_p t)\frac{\hbar}{m}\frac{1}{\sqrt{2\omega_1\omega_z}}\left[\hat{a}_x^\dagger\hat{a}_z^\dagger + \hat{a}_x^\dagger\hat{a}_z + \hat{a}_z^\dagger\hat{a}_x + \hat{a}_x\hat{a}_z\right]. \tag{7.2}$$

Transformation of $\hat{V}_p(t)$ by $\hat{U}_1$ in (6.12) produces:

$$\begin{aligned}\hat{V}_p'(t) \equiv \hat{U}_1\,\hat{V}_p(t)\,\hat{U}_1^\dagger = -\epsilon_p\,\cos(\omega_p t)\frac{\hbar}{m}\frac{1}{\sqrt{2\omega_1\omega_z}}\Bigg[&\left(\frac{\hat{a}_x^\dagger - i\hat{a}_y^\dagger}{\sqrt{2}}\right)\hat{a}_z^\dagger + \left(\frac{\hat{a}_x^\dagger - i\hat{a}_y^\dagger}{\sqrt{2}}\right)\hat{a}_z \\ &+\hat{a}_z^\dagger\left(\frac{\hat{a}_x + i\hat{a}_y}{\sqrt{2}}\right) + \left(\frac{\hat{a}_x + i\hat{a}_y}{\sqrt{2}}\right)\hat{a}_z\Bigg].\end{aligned} \tag{7.3}$$

The total Hamiltonian in the $\hat{I}_1$ frame is given straightforwardly by

$$\hat{\mathcal{H}}_p^{'} = \hat{\mathcal{H}}^{'} + q\hat{V}_p^{'}(t). \tag{7.4}$$

Following from 2.2, the frame of reference in which the explicit time dependence of the potential $\hat{V}_p^{'}(t)$ in (7.4) can be eliminated is defined by the unitary operator

$$\hat{U}_p^{'}(t) = \exp\left\{-i\frac{\omega_p}{2}\left(\hat{n}_z - \hat{n}_x\right)t\right\} \equiv \exp\left\{-\frac{i}{\hbar}(\omega_p t)\hat{J}_3\right\}. \tag{7.5}$$

This is itself obtained straightforwardly by rotation of (2.6) by $\hat{U}_1$. Explicitly, Hamiltonian (7.4) in this rotating frame becomes

$$\begin{aligned}
\hat{\mathcal{H}}_{pt}^{'} =& \hat{U}_p^{'}(t)\hat{\mathcal{H}}_p^{'}\hat{U}_p^{'\dagger}(t) + i\hbar\dot{\hat{U}}_p^{'}(t)\hat{U}_p^{'\dagger}(t) \\
=& \hbar\omega_+\left(\hat{n}_x + \frac{1}{2}\right) + \hbar\omega_z\left(\hat{n}_z + \frac{1}{2}\right) - \hbar\omega_-\left(\hat{n}_y + \frac{1}{2}\right) + \hbar\frac{\omega_p}{2}(\hat{n}_z - \hat{n}_x) \\
&+ e\frac{\hbar}{2m}\frac{1}{\sqrt{\omega_1\omega_z}}\epsilon_p\cos(\omega_p t)\left\{\hat{a}_x\hat{a}_z + \hat{a}_x^\dagger\hat{a}_z e^{i\omega_p t} + \hat{a}_z^\dagger\hat{a}_x e^{-i\omega_p t} + \hat{a}_x^\dagger\hat{a}_z^\dagger\right. \\
&\left. + i\hat{a}_y\hat{a}_z e^{i\frac{\omega_p}{2}t} - i\hat{a}_y^\dagger\hat{a}_z e^{i\frac{\omega_p}{2}t} + i\hat{a}_z^\dagger\hat{a}_y e^{-i\frac{\omega_p}{2}t} - i\hat{a}_y^\dagger\hat{a}_z^\dagger e^{-i\frac{\omega_p}{2}t}\right\}.
\end{aligned} \tag{7.6}$$

The cosine function is again expanded and ω_p from (2.9) inserted, in parallel with the calculation of 2.2. At this point the secular approximation [58] is made so that the coupling potential in this frame reduces to

$$\hat{V}_p'(t) = -\frac{\hbar}{4m}\frac{1}{\sqrt{\omega_1\omega_z}}\epsilon_p\{\hat{a}_z^\dagger\hat{a}_x + \hat{a}_x^\dagger\hat{a}_z\}. \tag{7.7}$$

The total Hamiltonian (7.6) accordingly becomes

$$\hat{\mathcal{H}}_{pt}^{'} = \omega_0\hat{J}_0 + \delta\hat{J}_3 + 2\xi\hat{J}_1 + \frac{\hbar\omega_0}{2} - \hbar\omega_-\left(\hat{n}_y + \frac{1}{2}\right). \tag{7.8}$$

where ξ and ω_0 are defined in (2.12) and (2.13) respectively, and the operators of the set $\underline{J}$ are given in (5.10).

7.2 Dressing the energy levels

7.2.1 Interpretation I: the dressed frame

As in the $\{+,-\}$ basis, writing Hamiltonian (7.8) in diagonal form has two interpretations. The first of these is transformation to the dressed frame, by application of operator:

$$\hat{U}_2 = \exp\left\{\frac{\theta}{2}(\hat{a}_z^\dagger\hat{a}_x - \hat{a}_x^\dagger\hat{a}_z)\right\} = \exp\left\{\frac{i}{\hbar}\theta\hat{J}_2\right\}, \tag{7.9}$$

where θ is again given in (2.15). This produces

$$\begin{aligned}\hat{\mathbb{H}}' &= \hat{U}_2 \hat{\mathcal{H}}'_{pt} \hat{U}_2^\dagger \\ &= \hbar \begin{pmatrix} \hat{a}_z^\dagger & \hat{a}_x^\dagger & \hat{a}_y^\dagger \end{pmatrix} \begin{pmatrix} \left(\frac{\omega_0+\Delta}{2}\right) & 0 & 0 \\ 0 & \left(\frac{\omega_0-\Delta}{2}\right) & 0 \\ 0 & 0 & -\omega_- \end{pmatrix} \begin{pmatrix} \hat{a}_z \\ \hat{a}_x \\ \hat{a}_y \end{pmatrix} + \hbar \frac{(\omega_1+\omega_z)}{2}, \end{aligned} \tag{7.10}$$

where Δ is defined in (2.17).

7.2.2 Interpretation II: dressed states

The Hamiltonian $\hat{\mathcal{H}}'_{pt}$ *rewritten* in terms of the dressed basis is given by

$$\boxed{\hat{\mathcal{H}}'_{pt} = \hbar\varepsilon_\alpha \left(\hat{n}'_\alpha + \frac{1}{2}\right) + \hbar\varepsilon_\beta \left(\hat{n}'_\beta + \frac{1}{2}\right) - \hbar\omega_- \left(\hat{a}_y^\dagger \hat{a}_y + \frac{1}{2}\right)}, \tag{7.11}$$

where

$$\begin{aligned} \hat{a}_\alpha^{\dagger\prime} &= \cos\frac{\theta}{2}\hat{a}_z^\dagger + \sin\frac{\theta}{2}\hat{a}_x^\dagger, \quad & \hat{a}'_\alpha &= \cos\frac{\theta}{2}\hat{a}_z + \sin\frac{\theta}{2}\hat{a}_x, \\ \hat{a}_\beta^{\dagger\prime} &= \cos\frac{\theta}{2}\hat{a}_x^\dagger - \sin\frac{\theta}{2}\hat{a}_z^\dagger, \quad & \hat{a}'_\beta &= \cos\frac{\theta}{2}\hat{a}_x - \sin\frac{\theta}{2}\hat{a}_z, \end{aligned} \tag{7.12}$$

and ε_α, ε_β are given in (2.25).

7.2.3 The avoided crossing

Referring to the coupled Hamiltonian (7.8) before dressing, the magnetron motion is again dropped to form:

$$\begin{aligned}\hat{\mathcal{H}}'_d &= \hat{\mathcal{H}}'_{pt} - \hat{\mathcal{H}}_- \\ &= \omega_0 \hat{J}_0 + \delta \hat{J}_3 + 2\xi \hat{J}_1 + \frac{\hbar\omega_0}{2}. \end{aligned} \tag{7.13}$$

The quantum numbers $N' = n_z + n_x$ and $l' = n_z - n_x$ are defined so that:

$$\begin{aligned} \hat{J}_0|n_x, n_z\rangle &= \frac{\hbar}{2} N' |n_x, n_z\rangle, \\ \hat{J}_3|n_x, n_z\rangle &= \frac{\hbar}{2} l' |n_x, n_z\rangle, \end{aligned} \tag{7.14}$$

where $N' = 0, 1, 2, 3, ...,$ and $l' = -N', -N'+2, ..., N'-2, N'$. The expectation value of $\hat{\mathcal{H}}'_d$ in the Fock state $|n_x, n_z\rangle$ is given by:

$$\langle \hat{\mathcal{H}}'_d \rangle = \frac{\hbar\omega_0}{2}(N'+1) + \frac{\hbar\delta}{2} l'. \tag{7.15}$$

Similarly rewriting Hamiltonian (7.11) in terms of the dressed modes:

$$\begin{aligned}\hat{\mathcal{H}}'_{pt} &= \frac{(\varepsilon_\alpha + \varepsilon_\beta)}{2}\left(\hat{n}'_\alpha + \hat{n}'_\beta\right) + \frac{(\varepsilon_\alpha - \varepsilon_\beta)}{2}\left(\hat{n}'_\alpha - \hat{n}'_\beta\right) + \frac{\hbar\omega_0}{2} - \hbar\omega_-(\hat{a}_y^\dagger \hat{a}_y + \frac{1}{2}) \\ &= \omega_0 \hat{J}_0^{\alpha\beta'} + \Delta \hat{J}_3^{\alpha\beta'} + \frac{\hbar\omega_0}{2} - \hbar\omega_- \left(\hat{a}_y^\dagger \hat{a}_y + \frac{1}{2}\right), \end{aligned} \tag{7.16}$$

and defining $\hat{\mathcal{H}}'_d$ by removing the magnetron Hamiltonian:

$$\hat{\mathcal{H}}'_d = \omega_0 \hat{J}_0^{\alpha\beta'} + \Delta \hat{J}_3^{\alpha\beta'} + \frac{\hbar\omega_0}{2}. \tag{7.17}$$

$\hat{J}_0^{\alpha\beta'}$ and $\hat{J}_3^{\alpha\beta'}$ are the zeroth and third components of the set of Schwinger boson algebra of the dressed modes of the coupled x and z motions, in the $\hat{I}_1$ frame.

Again, the effects of dressing are seen in Figure 2.2, where, for calculation in this basis, the quantum numbers N, l should be replaced by N', l'. The only difference in this calculation from that in Chapter 2 has been the transformation to the $\hat{I}_1$ frame in 7.1. Accordingly, all results throughout the remainder of this chapter are directly applicable to the calculation in the $\{+, -\}$ basis.

7.3 Solutions of the coupled Penning trap

7.3.1 The wavefunction

The expansion of the coupled Hamiltonian (7.10) in the dressed frame is:

$$\begin{aligned}\hat{\mathbb{H}}' = &\left(\frac{1}{2}m_-\omega_{\mathbb{H}_x}^2\hat{x}^2 + \frac{1}{2m_-}\hat{p}_x^2\right) + \left(\frac{1}{2}m_+\omega_{\mathbb{H}_z}^2\hat{z}^2 + \frac{1}{2m_+}\hat{p}_z^2\right) \\ &- \left(\frac{1}{2}m_y\omega_-^2\hat{y}^2 + \frac{1}{2m_y}\hat{p}_y^2\right). \end{aligned} \tag{7.18}$$

This results in the Schrödinger equation:

$$\begin{aligned}E_{\mathbb{H}}\,\psi'_{\mathbb{H}} = \Bigg[&\left(-\frac{\hbar^2}{2m_-}\frac{\partial^2}{\partial\hat{x}^2} + \frac{1}{2}m_-\omega_{\mathbb{H}_x}^2\hat{x}^2\right) \\ &+ \left(-\frac{\hbar^2}{2m_+}\frac{\partial^2}{\partial\hat{z}^2} + \frac{1}{2}m_+\omega_{\mathbb{H}_z}^2\hat{z}^2\right) \\ &- \left(-\frac{\hbar^2}{2m_y}\frac{\partial^2}{\partial\hat{y}^2} + \frac{1}{2}m_y\omega_-^2\hat{y}^2\right)\Bigg]\psi'_{\mathbb{H}}, \end{aligned} \tag{7.19}$$

where

$$\begin{aligned}\omega_{\mathbb{H}_z} &= \epsilon_\alpha, \\ \omega_{\mathbb{H}_x} &= \epsilon_\beta, \end{aligned} \tag{7.20}$$

$$m_- = \frac{1}{2}\frac{\omega_1}{\omega_{\mathbb{H}_x}}m, \quad m_+ = \frac{\omega_z}{\omega_{\mathbb{H}_z}}m, \quad m_y = \frac{1}{2}\frac{\omega_1}{\omega_-}m. \tag{7.21}$$

In a similar way to the wavefunctions of the uncoupled trap in the $\hat{I}_1$ frame (6.11), following from the definitions of $m_{\mathbb{H}_z}$, $m_{\mathbb{H}_x}$, m_y, the mass and frequency terms combine in the following way:

$$m_y\omega_- = m\frac{\omega_1}{2}, \quad m_-\omega_{\mathbb{H}_x} = m\frac{\omega_1}{2}, \quad m_+\omega_{\mathbb{H}_z} = m\omega_z. \tag{7.22}$$

The n components of the wavefunctions are therefore given by:

$$\psi'_{\mathbb{H}_n}(x,\, m_-,\, \omega_{\mathbb{H}_x}) = \left(\left(\frac{m\omega_1}{2\pi\hbar}\right)^{\frac{1}{4}} \frac{1}{2^{\frac{n}{2}}\sqrt{n!}} \times \exp\left(-\frac{m\omega_1 x^2}{4\hbar}\right) H_n\left[x\sqrt{\frac{m\omega_1}{4\hbar}}\right]\right), \tag{7.23}$$

$$\psi'_{\mathbb{H}_n}(z,\, m_+,\, \omega_{\mathbb{H}_z}) = \left(\left(\frac{m\omega_z}{\pi\hbar}\right)^{\frac{1}{4}} \frac{1}{2^{\frac{n}{2}}\sqrt{n!}} \times \exp\left(-\frac{m\omega_z x^2}{2\hbar}\right) H_n\left[x\sqrt{\frac{m\omega_z}{\hbar}}\right]\right), \tag{7.24}$$

$$\psi'_n(y,\, m_y,\, \omega_-) = \left(\left(\frac{m\omega_1}{2\pi\hbar}\right)^{\frac{1}{4}} \frac{1}{2^{\frac{n}{2}}\sqrt{n!}} \times \exp\left(-\frac{m\omega_1 x^2}{4\hbar}\right) H_n\left[x\sqrt{\frac{m\omega_1}{4\hbar}}\right]\right), \tag{7.25}$$

where the total solution is given by a product of the sum of these functions, as in 6.1.2. In fact, the solution reduces *exactly* to that of the uncoupled Hamiltonian in the $\hat{I}_1$ frame. This is rather striking: the wavefunctions of the coupled system in the dressed frame are identical to those admitted by a 3D harmonic oscillator with frequencies ω_z and two of frequency $\omega_1/2$. In this way, no effects of the coupling can be seen in these solutions.

7.3.2 Fock states

The eigenstates in the lab frame must be calculated via the three inverse unitary operators, $\hat{U}_2^{-1}$, $\hat{U}'_p(t)^{-1}$, and $\hat{U}_1^{-1}$. Hamiltonian (7.10) immediately admits both Fock state and coherent state solutions in the dressed frame.

Denoting solutions in the dressed frame

$$|\psi_{\mathbb{H}}> = \hat{U}_2\hat{U}'_p(t)\hat{U}_1|\psi_p>, \tag{7.26}$$

those in the lab frame are given by

$$|\psi_p> = \hat{U}_1^\dagger\hat{U}_p^{\dagger'}(t)\hat{U}_2^\dagger|\psi_{\mathbb{H}}> . \tag{7.27}$$

Fock state solutions in the lab frame are straightforward to calculate:

$$
\begin{aligned}
|\psi_p\rangle &= \hat{U}_1^\dagger \hat{U}_p^{\dagger'}(t)\hat{U}_2^\dagger \left[\frac{1}{\sqrt{n_x!\,n_y!\,n_z!}}(\hat{a}_x^\dagger)^{n_x}(\hat{a}_y^\dagger)^{n_y}(\hat{a}_z^\dagger)^{n_z}\right]|0_x0_y0_z\rangle \\
&= \frac{1}{\sqrt{n_x!\,n_y!\,n_z!}}\hat{U}_1^\dagger \hat{U}_p^{\dagger'}(t)\hat{U}_2^\dagger \left[(\hat{a}_x^\dagger)^{n_x}(\hat{a}_y^\dagger)^{n_y}(\hat{a}_z^\dagger)^{n_z}\right]\hat{U}_2\hat{U}_p'(t)\hat{U}_1\cdot\hat{U}_1^\dagger \hat{U}_p^{\dagger'}(t)\hat{U}_2^\dagger|0_x0_y0_z\rangle \\
&= \frac{1}{\sqrt{n_x!\,n_y!\,n_z!}}\hat{U}_1^\dagger \hat{U}_p^{\dagger'}(t)\hat{U}_2^\dagger \left[(\hat{a}_x^\dagger)^{n_x}(\hat{a}_y^\dagger)^{n_y}(\hat{a}_z^\dagger)^{n_z}\right]\hat{U}_2\hat{U}_p'(t)\hat{U}_1|0_x0_y0_z\rangle \\
&= \frac{1}{\sqrt{n_x!\,n_y!\,n_z!}}\hat{U}_1^\dagger \hat{U}_p^{\dagger'}(t)\hat{U}_2^\dagger \left[\hat{a}_x^\dagger\right]^{n_x}\hat{U}_2\hat{U}_p'(t)\hat{U}_1\cdot\hat{U}_1^\dagger \hat{U}_p^{\dagger'}(t)\hat{U}_2^\dagger \left[\hat{a}_y^\dagger\right]^{n_y}\hat{U}_2\hat{U}_p'(t)\hat{U}_1\times \\
&\qquad\qquad \times \hat{U}_1^\dagger \hat{U}_p^{\dagger'}(t)\hat{U}_2^\dagger \left[\hat{a}_z^\dagger\right]^{n_z}\hat{U}_2\hat{U}_p'(t)\hat{U}_1|0_x0_y0_z\rangle \\
&= \frac{1}{\sqrt{n_x!\,n_y!\,n_z!}}\left[\hat{U}_1^\dagger \hat{U}_p^{\dagger'}(t)\hat{U}_2^\dagger \left[\hat{a}_x^\dagger\right]\hat{U}_2\hat{U}_p'(t)\hat{U}_1\right]^{n_x}\left[\hat{U}_1^\dagger \hat{U}_p^{\dagger'}(t)\hat{U}_2^\dagger \left[\hat{a}_y^\dagger\right]\hat{U}_2\hat{U}_p'(t)\hat{U}_1\right]^{n_y}\times \\
&\qquad\qquad \times \left[\hat{U}_1^\dagger \hat{U}_p^{\dagger'}(t)\hat{U}_2^\dagger \left[\hat{a}_z^\dagger\right]\hat{U}_2\hat{U}_p'(t)\hat{U}_1\right]^{n_z}|0_x0_y0_z\rangle \\
&= \frac{1}{\sqrt{n_x!n_y!n_z!}}\left[\frac{(\hat{a}_x^\dagger + i\hat{a}_y^\dagger)}{\sqrt{2}}e^{-(\frac{i\omega_p t}{2})}\cos\frac{\theta}{2} - \hat{a}_z^\dagger e^{(\frac{i\omega_p t}{2})}\sin\frac{\theta}{2}\right]^{n_x}\left[\frac{(\hat{a}_y^\dagger + i\hat{a}_x^\dagger)}{\sqrt{2}}\right]^{n_y}\times \\
&\qquad\qquad \times \left[\hat{a}_z^\dagger e^{(\frac{i\omega_p t}{2})}\cos\frac{\theta}{2} + \frac{(\hat{a}_x^\dagger + i\hat{a}_y^\dagger)}{\sqrt{2}}e^{-(\frac{i\omega_p t}{2})}\sin\frac{\theta}{2}\right]^{n_z}|0_x0_y0_z\rangle. \qquad (7.28)
\end{aligned}
$$

Adopting the notation

$$
|\psi_p\rangle_{n_xn_yn_z} = \hat{U}_1^\dagger \hat{U}_p^{\dagger'}(t)\hat{U}_2^\dagger|n_x, n_y, n_z\rangle, \qquad (7.29)
$$

the first few quantum states in the lab frame are given by:

$$
\begin{aligned}
|\psi_p\rangle_{0_x0_y0_z} &= |0_x0_y0_z\rangle, \\
|\psi_p\rangle_{1_x0_y0_z} &= \frac{1}{\sqrt{2}}\,e^{-\frac{i\omega_p t}{2}}\cos\frac{\theta}{2}(|1_x0_y0_z\rangle + i|0_x1_y0_z\rangle) - e^{\frac{i\omega_p t}{2}}\sin\frac{\theta}{2}|0_x0_y1_z\rangle, \\
|\psi_p\rangle_{0_x1_y0_z} &= \frac{1}{\sqrt{2}}(i|1_x0_y0_z\rangle + |0_x1_y0_z\rangle), \\
|\psi_p\rangle_{0_x0_y1_z} &= \frac{1}{\sqrt{2}}\,e^{-\frac{i\omega_p t}{2}}\sin\frac{\theta}{2}(|1_x0_y0_z\rangle + i|0_x1_y0_z\rangle) + e^{\frac{i\omega_p t}{2}}\cos\frac{\theta}{2}|0_x0_y1_z\rangle, \\
|\psi_p\rangle_{2_x0_y0_z} &= e^{-i\omega_p t}\cos^2\frac{\theta}{2}\left(\frac{1}{2}(|2_x0_y0_z\rangle - |0_x2_y0_z\rangle) + \frac{i}{\sqrt{2}}|1_x1_y0_z\rangle\right) - \cos\frac{\theta}{2}\sin\frac{\theta}{2}\left(|1_x0_y1_z\rangle + i|0_x1_y1_z\rangle\right) \\
&\quad + e^{i\omega_p t}\sin^2\frac{\theta}{2}|0_x0_y2_z\rangle, \qquad (7.30)
\end{aligned}
$$

with θ given in (2.15).

Accordingly, the general solutions in lab frame in the $\{+, -\}$ basis is

$$
\begin{aligned}
&\frac{1}{\sqrt{n_+!n_-!n_z!}}\left[\hat{a}_+^\dagger e^{-(\frac{i\omega_p t}{2})}\cos\frac{\theta}{2} - \hat{a}_z^\dagger e^{(\frac{i\omega_p t}{2})}\sin\frac{\theta}{2}\right]^{n_+}\left[\hat{a}_-^\dagger\right]^{n_-}\times \\
&\qquad\qquad \times\left[\hat{a}_z^\dagger e^{(\frac{i\omega_p t}{2})}\cos\frac{\theta}{2} + \hat{a}_+^\dagger e^{-(\frac{i\omega_p t}{2})}\sin\frac{\theta}{2}\right]^{n_z}|0_+0_-0_z\rangle, \qquad (7.31)
\end{aligned}
$$

so that these first few Fock states are given by

$$
\begin{aligned}
&|0_+0_-0_z\rangle, \\
&e^{-\frac{i\omega_p t}{2}} \cos\frac{\theta}{2}|1_+0_-0_z\rangle - e^{\frac{i\omega_p t}{2}} \sin\frac{\theta}{2}|0_+0_-1_z\rangle, \\
&|0_+1_-0_z\rangle, \\
&e^{\frac{-i\omega_p t}{2}} \sin\frac{\theta}{2}|1_+0_-0_z\rangle + e^{\frac{i\omega_p t}{2}} \cos\frac{\theta}{2}|0_+0_-1_z\rangle, \\
&e^{-i\omega_p t} \cos^2\frac{\theta}{2}|2_+0_-0_z\rangle - \sqrt{2}\cos\frac{\theta}{2}\sin\frac{\theta}{2}|1_+0_-1_z\rangle + e^{i\omega_p t}\sin^2\frac{\theta}{2}|0_+0_-2_z\rangle.
\end{aligned} \tag{7.32}
$$

In this way, entangled states of the axial and cyclotron modes are straightforward to compute, where the angle θ depends directly on the strength of the coupling field in (2.1).

7.3.3 Coherent states

From the above calculation in (7.28), the time dependent coherent states in the lab frame follow naturally.

Denoting time dependent coherent states of the dressed frame:

$$
|\beta_x(t),\, \beta_y(t),\, \beta_z(t)\rangle = |\beta_x e^{-i\omega_{\mathbb{H}_x} t},\, \beta_y e^{i\omega_- t},\, \beta_z e^{-i\omega_{\mathbb{H}_z} t}\rangle, \tag{7.33}
$$

application of the inverse unitary transformations results in:

$$
\hat{U}_1^\dagger \hat{U}_p^{\dagger\prime}(t)\hat{U}_2^\dagger|\beta_x(t)\beta_y(t)\beta_z(t)\rangle = |\beta_{px}(t)\beta_{py}(t)\beta_{pz}(t)\rangle, \tag{7.34}
$$

where

$$
\begin{aligned}
\beta_{px}(t) = \frac{1}{\sqrt{2}}\Big(&e^{-\frac{i\omega_p t}{2}} A(\chi)\beta_x(t) + i\beta_y(t) \\
&+e^{-\frac{i\omega_p t}{2}}\sqrt{1 - A(\chi)^2}\beta_z(t)\Big),
\end{aligned} \tag{7.35}
$$

$$
\begin{aligned}
\beta_{py}(t) = \frac{1}{\sqrt{2}}\Big(&e^{-\frac{i\omega_p t}{2}} A(\chi)\beta_x(t) + \beta_y(t) \\
&+e^{-\frac{i\omega_p t}{2}}\sqrt{1 - A(\chi)^2} i\beta_z(t)\Big),
\end{aligned} \tag{7.36}
$$

$$
\begin{aligned}
\beta_{pz}(t) = \Big(&-e^{\frac{i\omega_p t}{2}}\sqrt{1 - A(\chi)^2}\beta_x(t) \\
&+e^{\frac{i\omega_p t}{2}} A(\chi)\beta_z(t)\Big);
\end{aligned} \tag{7.37}
$$

$$
A(\chi) = \cos\frac{\theta}{2} = \sqrt{\frac{1 + \sqrt{\chi^2 + 1}}{2\sqrt{\chi^2 + 1}}}, \quad \chi = \frac{2\xi}{\delta}. \tag{7.38}
$$

Analogous results again hold for the $\{+, -\}$ basis.

The straightforward production of solutions illustrates the successful formulation of the mode coupling calculation in quantum form. Additionally, the careful considerations of the linear and circular bases of mode operators in previous chapters enables a logical mapping between calculations involving them.

Chapter 8

Quantum Theory of the Elliptical Penning Trap

This chapter presents a detailed quantum solution of the ideal elliptical Penning trap, and the straightforward extenstion to the ultra-elliptical regime of the Geonium Chip [29]. It demonstrates how the carefully constructed formalism of the previous chapters can be combined in a useful and consistent way.

8.1 Quantum Hamiltonian of the ideal elliptical trap

As a reminder, from 1.5 the classical Hamiltonian of the ideal elliptical Penning trap is given by

$$\begin{aligned}\mathcal{H}_\epsilon = &\frac{1}{2m}(p_x^2+p_y^2+p_z^2)+\frac{\omega_c}{2}(xp_y-yp_x)\\ &+\frac{1}{8}m\omega_1^2(x^2+y^2)+\frac{1}{4}m\epsilon\omega_z^2\left(x^2-y^2\right)+\frac{1}{2}m\omega_z^2z^2,\end{aligned} \tag{8.1}$$

where the ellipticity parameter ϵ arises from the asymmetry between the electric field curvature in the x and y directions (1.78). In terms of the creation and annihilation operators of the $\{x,y\}$ basis (4.22, 4.23), this additional asymmetric contribution is written:

$$\hat{x}^2-\hat{y}^2=\frac{\hbar}{m\omega_1}\left(\hat{a}_x^\dagger\hat{a}_x^\dagger+\hat{a}_x\hat{a}_x-(\hat{a}_y^\dagger\hat{a}_y^\dagger+\hat{a}_y\hat{a}_y)+2(\hat{n}_x-\hat{n}_y)\right). \tag{8.2}$$

The whole quantum Hamiltonian of the ideal elliptical Penning trap is therefore given by adding this to the Hamiltonian in the $\{x, y\}$ basis (4.24).

$$\begin{aligned}\hat{\mathcal{H}}_\epsilon = &\hbar\frac{\omega_1}{2}\left(\hat{a}_x^\dagger\hat{a}_x + \frac{1}{2}\right) + \hbar\frac{\omega_1}{2}\left(\hat{a}_y^\dagger\hat{a}_y + \frac{1}{2}\right) \\ &- i\hbar\frac{\omega_c}{2}(\hat{a}_x^\dagger\hat{a}_y - \hat{a}_y^\dagger\hat{a}_x) + \hbar\omega_z\left(\hat{a}_z^\dagger\hat{a}_z + \frac{1}{2}\right) \\ &+ \frac{1}{4}m\epsilon\omega_z^2\left(\frac{\hbar}{m\omega_1}\left(\hat{a}_x^\dagger\hat{a}_x^\dagger + \hat{a}_x\hat{a}_x - (\hat{a}_y^\dagger\hat{a}_y^\dagger + \hat{a}_y\hat{a}_y) + 2(\hat{n}_x - \hat{n}_y)\right)\right). \end{aligned} \tag{8.3}$$

In terms of Schwinger boson operators of the set $\underline{I}$ (5.2), $\hat{\mathcal{H}}_\epsilon$ is written

$$\begin{aligned}\hat{\mathcal{H}}_\epsilon = &\omega_1\hat{I}_0 + \omega_c\hat{I}_2 + \hbar\omega_z\left(\hat{a}_z^\dagger\hat{a}_z + \frac{1}{2}\right) \\ &+ \frac{1}{4}m\epsilon\omega_z^2\left(\frac{\hbar}{m\omega_1}\left(\hat{a}_x^\dagger\hat{a}_x^\dagger + \hat{a}_x\hat{a}_x - (\hat{a}_y^\dagger\hat{a}_y^\dagger + \hat{a}_y\hat{a}_y) + 2(\hat{n}_x - \hat{n}_y)\right)\right) + \hbar\frac{\omega_1}{2}. \end{aligned} \tag{8.4}$$

The elliptical term is of a similar form to the anisotropic angular momentum component $\hat{\mathcal{I}}_3$ encountered in Chapter 5. In fact, it is exactly this operator (5.55) in the limit of infinite squeezing of both modes $\zeta_x \to \infty$, $\zeta_y \longrightarrow \infty$. It is clear that this component reduces to $\hat{I}_3$ upon application of reverse squeezing operators, and so the method of solving $\hat{\mathcal{H}}_\epsilon$ must involve transformations of this kind.

8.2 Solving the Elliptical Hamiltonian

8.2.1 Transformation to the $\hat{I}_{1_\phi}$ frame

It has been found that the angular momentum term $\hat{I}_2$ should be removed from the elliptical Hamiltonian *before* application of squeezing operators. Since this follows from transformation by the $\hat{I}_1$ operator as discussed in Chapter 6, the calculation proceeds as follows:

Defining rotation by $\hat{I}_1$ through an arbitrary angle ϕ as

$$\hat{U}_{1_\phi} = \exp\left\{\frac{i}{\hbar}\phi\hat{I}_1\right\}, \tag{8.5}$$

this is applied to $\hat{\mathcal{H}}_\epsilon$ and the terms collected:

$$\begin{aligned}&\hat{U}_{1_\phi}\hat{\mathcal{H}}_\epsilon\hat{U}_{1_\phi}^\dagger \\ &= \omega_1\hat{I}_0 + \hbar\frac{\omega_1}{2} + \hbar\omega_z\left(\hat{a}_z^\dagger\hat{a}_z + \frac{1}{2}\right) + \hat{I}_2\left[\omega_c\cos\phi + \frac{\epsilon\omega_z^2}{\omega_1}\sin\phi\right] \\ &\quad + \hat{I}_3\left[\frac{\epsilon\omega_z^2}{\omega_1}\cos\phi - \omega_c\sin\phi\right] + \frac{\hbar}{4}\frac{\epsilon\omega_z^2}{\omega_1}\left(\hat{a}_x^\dagger\hat{a}_x^\dagger + \hat{a}_x\hat{a}_x - \hat{a}_y^\dagger\hat{a}_y^\dagger - \hat{a}_y\hat{a}_y\right). \end{aligned} \tag{8.6}$$

Elimination of $\hat{I}_2$ follows from setting

$$\omega_c\cos\phi + \frac{\epsilon\omega_z^2}{\omega_1}\sin\phi = 0 \tag{8.7}$$

$$\implies \phi = \arctan\left[-\frac{\omega_1\omega_c}{\epsilon\omega_z^2}\right]. \tag{8.8}$$

Labelling

$$\chi = -\frac{\omega_1\omega_c}{\epsilon\omega_z^2}, \tag{8.9}$$

and noting

$$\cos\phi = \frac{1}{\sqrt{1+\chi^2}}, \;\; \sin\phi = \frac{\chi}{\sqrt{1+\chi^2}}, \tag{8.10}$$

results in

$$\begin{aligned}
\hat{\mathcal{H}}'_\epsilon &= \exp\left\{\frac{i}{\hbar}\phi\hat{I}_1\right\}\hat{\mathcal{H}}_\epsilon \exp\left\{-\frac{i}{\hbar}\phi\hat{I}_1\right\} \\
&= \omega_1\hat{I}_0 + \hbar\omega_z\left(\hat{a}_z^\dagger\hat{a}_z + \frac{1}{2}\right) \\
&\quad + \hat{I}_3\left[\frac{\epsilon\omega_z^2}{\omega_1}\sqrt{1+\chi^2}\right] + \frac{\hbar}{4}\frac{\epsilon\omega_z^2}{\omega_1}\left(\hat{a}_x^\dagger\hat{a}_x^\dagger + \hat{a}_x\hat{a}_x - \hat{a}_y^\dagger\hat{a}_y^\dagger - \hat{a}_y\hat{a}_y\right) \\
&= \frac{\hbar\omega_1}{2}(\hat{n}_x + \hat{n}_y) + \hbar\omega_z\left(\hat{a}_z^\dagger\hat{a}_z + \frac{1}{2}\right) + \frac{\hbar}{2}(\hat{n}_x - \hat{n}_y)\left(\frac{1}{\omega_1}\sqrt{\epsilon^2\omega_z^4 + \omega_1^2\omega_c^2}\right) \\
&\quad + \frac{\hbar}{4}\frac{\epsilon\omega_z^2}{\omega_1}\left(\hat{a}_x^\dagger\hat{a}_x^\dagger + \hat{a}_x\hat{a}_x - \hat{a}_y^\dagger\hat{a}_y^\dagger - \hat{a}_y\hat{a}_y\right) + \hbar\frac{\omega_1}{2}.
\end{aligned} \tag{8.11}$$

8.2.2 Applying squeezing operators

A diagonal form of $\hat{\mathcal{H}}_\epsilon$ can now be achieved by application of squeezing operators for each mode to $\hat{\mathcal{H}}'_\epsilon$. The squeezing operators $\hat{S}(\zeta_x)$ and $\hat{S}(\zeta_y)$ in (5.35) are applied to (8.11) to

produce:

$$
\begin{aligned}
\hat{\mathcal{H}}_\zeta &= \hat{S}(\zeta_x)\hat{S}(\zeta_y)\hat{\mathcal{H}}'_\epsilon\hat{S}^\dagger(\zeta_y)\hat{S}^\dagger(\zeta_y) \\
&= \hbar\hat{n}_x\left[\cosh(2r_x)\left(\frac{\omega_1}{2}+\frac{1}{2\omega_1}\sqrt{\epsilon^2\omega_z^4+\omega_1^2\omega_c^2}\right)+\frac{1}{2}\frac{\epsilon\omega_z^2}{\omega_1}\sinh(2r_x)\cos(\phi_x)\right] \\
&\quad \hbar\left[\sinh^2(r_x)\left(\frac{\omega_1}{2}+\frac{1}{2\omega_1}\sqrt{\epsilon^2\omega_z^4+\omega_1^2\omega_c^2}\right)+\frac{1}{4}\frac{\epsilon\omega_z^2}{\omega_1}\sinh(2r_x)\cos(\phi_x)\right] \\
&\quad +\hbar\hat{n}_y\left[\cosh(2r_y)\left(\frac{\omega_1}{2}-\frac{1}{2\omega_1}\sqrt{\epsilon^2\omega_z^4+\omega_1^2\omega_c^2}\right)-\frac{1}{2}\frac{\epsilon\omega_z^2}{\omega_1}\sinh(2r_y)\cos(\phi_y)\right] \\
&\quad +\hbar\left[\sinh^2(r_y)\left(\frac{\omega_1}{2}-\frac{1}{2\omega_1}\sqrt{\epsilon^2\omega_z^4+\omega_1^2\omega_c^2}\right)-\frac{1}{4}\frac{\epsilon\omega_z^2}{\omega_1}\sinh(2r_y)\cos(\phi_y)\right] \\
&\quad +\hbar\hat{a}_x^\dagger\hat{a}_x^\dagger\left[\frac{1}{2}\sinh(2r_x)\exp(i\phi_x)\left(\frac{\omega_1}{2}+\frac{1}{2\omega_1}\sqrt{\epsilon^2\omega_z^4+\omega_1^2\omega_c^2}\right)\right. \\
&\qquad \left.+\frac{1}{4}\frac{\epsilon\omega_z^2}{\omega_1}\left(\cosh^2(r_x)+\sinh^2(r_x)\exp(2i\phi_x)\right)\right] \\
&\quad +\hbar\hat{a}_x\hat{a}_x\left[\frac{1}{2}\sinh(2r_x)\exp(-i\phi_x)\left(\frac{\omega_1}{2}+\frac{1}{2\omega_1}\sqrt{\epsilon^2\omega_z^4+\omega_1^2\omega_c^2}\right)\right. \\
&\qquad \left.+\frac{1}{4}\frac{\epsilon\omega_z^2}{\omega_1}\left(\cosh^2(r_x)+\sinh^2(r_x)\exp(-2i\phi_x)\right)\right] \\
&\quad +\hbar\hat{a}_y^\dagger\hat{a}_y^\dagger\left[\frac{1}{2}\sinh(2r_y)\exp(i\phi_y)\left(\frac{\omega_1}{2}-\frac{1}{2\omega_1}\sqrt{\epsilon^2\omega_z^4+\omega_1^2\omega_c^2}\right)\right. \\
&\qquad \left.-\frac{1}{4}\frac{\epsilon\omega_z^2}{\omega_1}\left(\cosh^2(r_y)+\sinh^2(r_y)\exp(2i\phi_y)\right)\right] \\
&\quad +\hbar\hat{a}_y\hat{a}_y\left[\frac{1}{2}\sinh(2r_y)\exp(-i\phi_y)\left(\frac{\omega_1}{2}-\frac{1}{2\omega_1}\sqrt{\epsilon^2\omega_z^4+\omega_1^2\omega_c^2}\right)\right. \\
&\qquad \left.-\frac{1}{4}\frac{\epsilon\omega_z^2}{\omega_1}\left(\cosh^2(r_y)+\sinh^2(r_y)\exp(-2i\phi_y)\right)\right] \\
&\quad +\hbar\omega_z\left(\hat{a}_z^\dagger\hat{a}_z+\frac{1}{2}\right)+\hbar\frac{\omega_1}{2}. \qquad (8.12)
\end{aligned}
$$

Achieving a diagonal form of $\hat{\mathcal{H}}_\zeta$ requires setting:

$$
\begin{aligned}
&(i)\ \frac{1}{2}\sinh(2r_x)\exp(i\phi_x)\left(\frac{\omega_1}{2}+\frac{1}{2\omega_1}\sqrt{\epsilon^2\omega_z^4+\omega_1^2\omega_c^2}\right)=-\frac{1}{4}\frac{\epsilon\omega_z^2}{\omega_1}\left(\cosh^2(r_x)+\sinh^2(r_x)\exp(2i\phi_x)\right), \\
&(ii)\ \frac{1}{2}\sinh(2r_x)\exp(-i\phi_x)\left(\frac{\omega_1}{2}+\frac{1}{2\omega_1}\sqrt{\epsilon^2\omega_z^4+\omega_1^2\omega_c^2}\right)=-\frac{1}{4}\frac{\epsilon\omega_z^2}{\omega_1}\left(\cosh^2(r_x)+\sinh^2(r_x)\exp(-2i\phi_x)\right), \qquad (8.13)
\end{aligned}
$$

$$
\begin{aligned}
&(iii)\ \frac{1}{2}\sinh(2r_y)\exp(i\phi_y)\left(\frac{\omega_1}{2}-\frac{1}{2\omega_1}\sqrt{\epsilon^2\omega_z^4+\omega_1^2\omega_c^2}\right)=\frac{1}{4}\frac{\epsilon\omega_z^2}{\omega_1}\left(\cosh^2(r_y)+\sinh^2(r_y)\exp(2i\phi_y)\right), \\
&(iv)\ \frac{1}{2}\sinh(2r_y)\exp(-i\phi_y)\left(\frac{\omega_1}{2}-\frac{1}{2\omega_1}\sqrt{\epsilon^2\omega_z^4+\omega_1^2\omega_c^2}\right)=\frac{1}{4}\frac{\epsilon\omega_z^2}{\omega_1}\left(\cosh^2(r_y)+\sinh^2(r_y)\exp(-2i\phi_y)\right). \qquad (8.14)
\end{aligned}
$$

In this way, all $\hat{a}^\dagger\hat{a}^\dagger$ and $\hat{a}\hat{a}$ terms are removed from (8.12). For the pairs of conditions (i) and (ii), (iii) and (iv) to hold simultaneously:

$$
\phi_x = \phi_y = 0, \qquad (8.15)
$$

so that (i) becomes identical to (ii), (iii) to (iv), and the notation $r_x \to \zeta_x$, $r_y \to \zeta_y$ is adopted. At this point the constants [15]

$$\kappa = \frac{\epsilon\omega_z^2}{2\omega_1} \tag{8.16}$$

and

$$K(\kappa) = \frac{\omega_c}{2\kappa}\left[\sqrt{1+\frac{4\kappa^2}{\omega_c^2}} - 1\right] \tag{8.17}$$

are introduced, so that (i) is rewritten:

$$(i) \quad \sinh(2\zeta_x)\left(\omega_+ + \kappa K(\kappa)\right) = -\kappa\cosh(2\zeta_x). \tag{8.18}$$

Thus the conditions (i) and (ii) reduce to

$$\begin{aligned} \tanh(2\zeta_x) &= -\frac{\kappa}{\omega_+ + \kappa K(\kappa)}, \\ \implies 2\zeta_x = \tanh^{-1}(\gamma_x); \qquad \gamma_x &= -\frac{\kappa}{\omega_+ + \kappa K(\kappa)}. \end{aligned} \tag{8.19}$$

Now,

$$\cosh(2\zeta_x) = \frac{1}{\sqrt{1-\gamma_x^2}}, \qquad \sinh(2\zeta_x) = \frac{\gamma_x}{\sqrt{1-\gamma_x^2}}, \tag{8.20}$$

so that the first line of (8.12) becomes:

$$\begin{aligned} &\hbar\hat{n}_x\left[\frac{1}{\sqrt{1-\gamma_x^2}}\left(\omega_+ + \kappa K(\kappa)\right) + \kappa\frac{\gamma_x}{\sqrt{1-\gamma_x^2}}\right] \\ &= \hbar\hat{n}_x\frac{1}{\sqrt{1-\gamma_x^2}}\left[\omega_+ + \kappa K(\kappa) + \kappa\gamma_x\right] \\ &= \hbar\hat{n}_x\left(\omega_+ + \kappa K(\kappa)\right)\sqrt{1-\gamma_x^2} \\ &= \hbar\hat{n}_x\sqrt{\left(\omega_+ + \kappa K(\kappa)\right)^2 - \gamma_x^2\left(\omega_+ + \kappa K(\kappa)\right)^2} \\ &= \hbar\hat{n}_x\sqrt{\left(\omega_+ + \kappa K(\kappa)\right)^2 - \kappa^2}. \end{aligned} \tag{8.21}$$

Identifying [15]

$$K(\kappa)^2 = 1 - \frac{\omega_c}{\kappa}K(\kappa), \tag{8.22}$$

(8.21) is written

$$\begin{aligned} &\hbar\hat{n}_x\sqrt{\omega_+^2 + \kappa^2\left(1 - \frac{\omega_c}{\kappa}K(\kappa)\right) + 2\omega_+\kappa K(\kappa) - \kappa^2} \\ &= \hbar\hat{n}_x\sqrt{\omega_+^2 + \kappa K(\kappa)(2\omega_+ - \omega_c)} \\ &= \hbar\hat{n}_x\sqrt{\omega_+^2 + \kappa K(\kappa)(\omega_c + \omega_1 - \omega_c)} \\ &= \hbar\hat{n}_x\sqrt{\omega_+^2 + \omega_1\kappa K(\kappa)}. \end{aligned} \tag{8.23}$$

In a similar way, condition (iii) simplifies to:

$$(iii) \quad \sinh(2\zeta_y)\left(\omega_- + \kappa K(\kappa)\right) = -\kappa\cosh(2\zeta_y), \tag{8.24}$$

so that diagonal form in the y degree of freedom is achieved by setting

$$\begin{aligned} \tanh(2\zeta_y) &= -\frac{\kappa}{\omega_- + \kappa K(\kappa)} \\ \implies 2\zeta_y = \tanh^{-1}(\gamma_y); \qquad \gamma_y &= -\frac{\kappa}{\omega_- + \kappa K(\kappa)}. \end{aligned} \tag{8.25}$$

The third line of (8.12) therefore becomes:

$$\begin{aligned} &-\hbar\hat{n}_y\left[\frac{1}{\sqrt{1-\gamma_y^2}}\left(\omega_- + \kappa K(\kappa)\right) + \kappa\frac{\gamma_y}{\sqrt{1-\gamma_y^2}}\right] \\ &= -\hbar\hat{n}_y\frac{1}{\sqrt{1-\gamma_y^2}}\left[\omega_- + \kappa K(\kappa) + \kappa\gamma_y\right] \\ &= -\hbar\hat{n}_y\left(\omega_- + \kappa K(\kappa)\right)\sqrt{1-\gamma_y^2} \\ &= -\hbar\hat{n}_y\sqrt{\left(\omega_- + \kappa K(\kappa)\right)^2 - \gamma_y^2\left(\omega_- + \kappa K(\kappa)\right)^2} \\ &= -\hbar\hat{n}_y\sqrt{\left(\omega_- + \kappa K(\kappa)\right)^2 - \kappa^2} \\ &= -\hbar\hat{n}_y\sqrt{\omega_-^2 + \kappa K(\kappa)(2\omega_- - \omega_c)} \\ &= -\hbar\hat{n}_y\sqrt{\omega_-^2 + \kappa K(\kappa)(\omega_c - \omega_1 - \omega_c)} \\ &= -\hbar\hat{n}_y\sqrt{\omega_-^2 - \omega_1\kappa K(\kappa)}. \end{aligned} \tag{8.26}$$

The total ground state energy of (8.12) is collected to produce:

$$\begin{aligned} &\hbar\left[\left(\frac{1}{2}(\cosh(2r_x)-1)\right)\left(\omega_+ + \kappa K(\kappa)\right) + \frac{1}{2}\kappa\sinh(2r_x)\right] + \hbar\frac{\omega_1}{2} \\ &+\hbar\left[-\left(\frac{1}{2}(\cosh(2r_y)-1)\right)\left(\omega_- + \kappa K(\kappa)\right) - \frac{1}{2}\kappa\sinh(2r_y)\right] + \hbar\frac{\omega_1}{2} \\ &= \frac{\hbar}{2}\left[\frac{1}{\sqrt{1-\gamma_x^2}}\left(\left(\omega_+ + \kappa K(\kappa)\right) + \kappa\gamma_x\right)\right. \\ &\quad \left.-\frac{1}{\sqrt{1-\gamma_y^2}}\left(\left(\omega_- + \kappa K(\kappa)\right) + \kappa\gamma_y\right) + \left(\omega_- + \kappa K(\kappa) - \omega_+ - \kappa K(\kappa)\right)\right] + \hbar\frac{\omega_1}{2} \\ &= \hbar\left[\sqrt{\omega_+^2 + \omega_1\kappa K(\kappa)} - \sqrt{\omega_-^2 - \omega_1\kappa K(\kappa)}\right]. \end{aligned} \tag{8.27}$$

Identifying the frequencies [15]

$$\begin{aligned} \tilde{\omega}_+ &= \sqrt{\omega_+^2 + \kappa\omega_1\cdot K(\kappa)} = \sqrt{\frac{1}{2}(\omega_c^2 - \omega_z^2) + \frac{1}{2}\sqrt{\omega_c^2\omega_1^2 + \epsilon^2\omega_z^2}}, \\ \tilde{\omega}_- &= \sqrt{\omega_-^2 - \kappa\omega_1\cdot K(\kappa)} = \sqrt{\frac{1}{2}(\omega_c^2 - \omega_z^2) - \frac{1}{2}\sqrt{\omega_c^2\omega_1^2 + \epsilon^2\omega_z^2}}, \end{aligned} \tag{8.28}$$

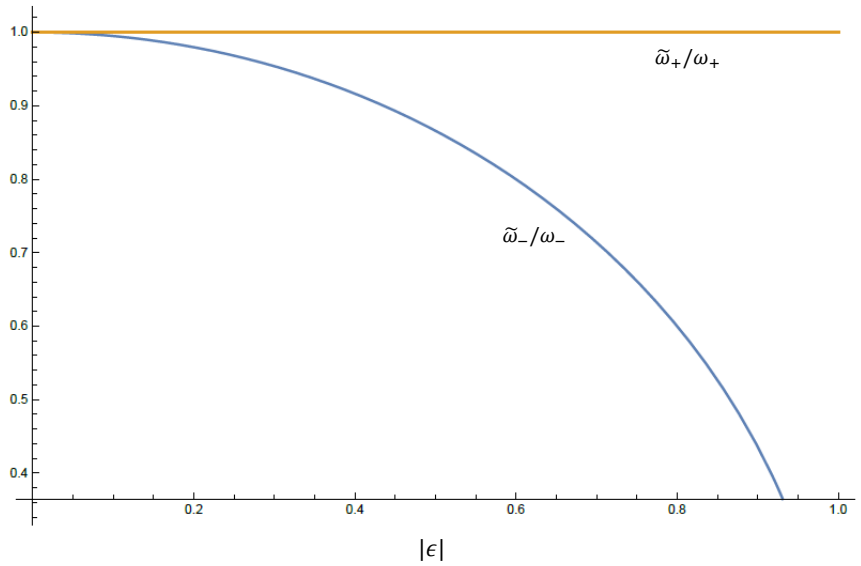

Figure 8.1: Plot of the variation of the generalised cyclotron (red) and magnetron (blue) mode frequencies as a function of ellipticity as given in (8.28) [15].

reduces (8.12) to:

$$\boxed{\hat{\mathcal{H}}_\zeta = \hbar\tilde{\omega}_+\left(\hat{n}_x + \frac{1}{2}\right) - \hbar\tilde{\omega}_-\left(\hat{n}_y + \frac{1}{2}\right) + \hbar\omega_z\left(\hat{n}_z + \frac{1}{2}\right)}. \tag{8.29}$$

This is an analogous quantum treatment of Kretzschmar's canonical transformations in [15], producing identical mode frequencies. As identified in his paper, the frequency of the cyclotron is little affected by a changing ellipticity parameter, whereas that of the magnetron decreases rapidly as $|\epsilon| \to 1$. This can be seen explicitly in Figure 8.1, where $\tilde{\omega}_+(\epsilon)$ and $\tilde{\omega}_-(\epsilon)$ are plotted.

8.2.3 Solutions of the elliptical Penning trap

The solutions of $\hat{\mathcal{H}}_\zeta$ appear trivial, but it is worthwhile to discuss how they appear in the laboratory frame.

Fock states

Consider first the simplest solution, the Fock states $|n_x, n_y, n_z\rangle$. This is interpreted in the following way: in a frame of reference transformed from the lab by the operator $\hat{U}_{1_\phi}$, duly called the $\hat{I}_{1_\phi}$ frame, the elliptical Hamiltonian admits squeezed number state solutions

$\hat{S}^\dagger(\zeta_x)\hat{S}^\dagger(\zeta_y)|n_x, n_y, n_z\rangle$ [80]. As discussed in 6.2.1, Fock state and coherent state solutions in the lab frame of the circular Penning trap in the $\{x, y\}$ basis can be found.

Seeking an analogous result for the elliptical trap, solutions in the lab are given by:

$$\begin{aligned}
&\hat{U}^\dagger_{1_\phi}\hat{S}^\dagger(\zeta_x)\hat{S}^\dagger(\zeta_y)|n_x, n_y, n_z\rangle \\
&= \hat{U}^\dagger_{1_\phi}\hat{S}^\dagger(\zeta_x)\hat{S}^\dagger(\zeta_y)\left[\frac{1}{\sqrt{n_x!\, n_y!\, n_z!}}(\hat{a}_x^\dagger)^{n_x}(\hat{a}_y^\dagger)^{n_y}(\hat{a}_z^\dagger)^{n_z}\right]|0_x 0_y 0_z\rangle \\
&= \hat{U}^\dagger_{1_\phi}\hat{S}^\dagger(\zeta_x)\hat{S}^\dagger(\zeta_y)\left[\frac{1}{\sqrt{n_x!\, n_y!\, n_z!}}(\hat{a}_x^\dagger)^{n_x}(\hat{a}_y^\dagger)^{n_y}(\hat{a}_z^\dagger)^{n_z}\right]\hat{S}(\zeta_y)\hat{S}(\zeta_x)\hat{U}_{1_\phi}\cdot\hat{U}^\dagger_{1_\phi}\hat{S}^\dagger(\zeta_x)\hat{S}^\dagger(\zeta_y)|0_x 0_y 0_z\rangle.
\end{aligned} \tag{8.30}$$

After some calculation, this produces

$$\begin{aligned}
&\frac{1}{\sqrt{n_x!\, n_y!}}\left[\left(\cos\frac{\phi}{2}\hat{a}_x^\dagger - i\sin\frac{\phi}{2}\hat{a}_y^\dagger\right)\cosh(\zeta_x) - \left(\cos\frac{\phi}{2}\hat{a}_x + i\sin\frac{\phi}{2}\hat{a}_y\right)\sinh(\zeta_x)\right]^{n_x}\times \\
&\times\left[\left(\cos\frac{\phi}{2}\hat{a}_y^\dagger - i\sin\frac{\phi}{2}\hat{a}_x^\dagger\right)\cosh(\zeta_y) - \left(\cos\frac{\phi}{2}\hat{a}_y + i\sin\frac{\phi}{2}\hat{a}_x\right)\sinh(\zeta_y)\right]^{n_y}\hat{U}^\dagger_{1_\phi}|-\zeta_x, -\zeta_y, n_z\rangle.
\end{aligned} \tag{8.31}$$

The states do not simplify further, as the $\hat{U}_{1_\phi}$ operator acting on $\hat{S}(\zeta_x)$ and $\hat{S}(\zeta_y)$ does *not* produce squeeze operators. In this way, solutions of the elliptical trap in the lab frame in this basis are not as straightforward to interpret as those for the radially symmetric trap. The conclusion is that the $\hat{I}_{1_\phi}$ frame is the appropriate frame of reference in which to study the elliptical trap. An analogous treatment in the $\{+, -\}$ basis is examined in 8.3.2.

Coherent states

$\hat{\mathcal{H}}_\zeta$ also admits coherent state solutions of the form $|\alpha_x, \alpha_y, \alpha_z\rangle$. Again, this can be interpreted in the following way: the elliptical Hamiltonian in the $\hat{I}_{1_\phi}$ frame admits coherent squeezed states of the form [41]:

$$\hat{S}^\dagger(\zeta_x)\hat{S}^\dagger(\zeta_y)|\alpha_x, \alpha_y, \alpha_z\rangle = \hat{D}(\alpha_x\cosh(r_x) - \alpha_x^*\sinh(r_x))\hat{D}(\alpha_y\cosh(r_y) - \alpha_y^*\sinh(r_y))|\zeta_x, \zeta_y\alpha_z\rangle. \tag{8.32}$$

Again, since the $\hat{U}_{1_\phi}$ operator does not transform the squeezing operators to a simple form, the conclusion from above holds: the $\hat{I}_{1_\phi}$ frame is the most suitable for studying the quantum elliptical trap.

8.3 The elliptical Penning trap in the $\{+,-\}$ basis

The above calculation can of course be performed in the $\{+,-\}$ basis. In term of creation and annihilation operators of the cyclotron and magnetron modes (6.36, 6.37), the ideal elliptical Penning trap Hamiltonian is written[1]:

$$\begin{aligned}\hat{\mathcal{H}}_\epsilon = &\hbar\omega_+\left(\hat{a}_+^\dagger\hat{a}_+ + \frac{1}{2}\right) - \hbar\omega_-\left(\hat{a}_-^\dagger\hat{a}_- + \frac{1}{2}\right) + \hbar\omega_z\left(\hat{a}_z^\dagger\hat{a}_z + \frac{1}{2}\right)\\ &+ \frac{1}{4}m\epsilon\omega_z^2\left(\frac{\hbar}{m\omega_1}\left(\hat{a}_+^\dagger\hat{a}_+^\dagger + \hat{a}_+\hat{a}_+ - (\hat{a}_-^\dagger\hat{a}_-^\dagger + \hat{a}_-\hat{a}_-) + 2i(\hat{a}_+^\dagger\hat{a}_- - \hat{a}_-^\dagger\hat{a}_+)\right)\right). \quad (8.33)\end{aligned}$$

Only the elliptical term in this Hamiltonian is non-diagonal. However, similarly to Hamiltonian (8.3), $\hat{\mathcal{H}}_\epsilon$ in this $\{+,-\}$ basis must first be transformed by its appropriate beamsplitter operator, $\hat{L}_1$ (3.21).

Transformation to the $\hat{L}_{1_\theta}$ frame

The calculation proceeds as follows:

$$\begin{aligned}&\exp\left\{\frac{i}{\hbar}\theta\hat{L}_1\right\}\hat{\mathcal{H}}_\epsilon\exp\left\{-\frac{i}{\hbar}\theta\hat{L}_1\right\}\\ &= \omega_1\hat{L}_0 + \omega_c\left[\cos\theta\hat{L}_3 + \sin\theta\hat{L}_3\right] + \hbar\omega_z(\hat{a}_z^\dagger\hat{a}_z + \frac{1}{2})\\ &\quad + \frac{1}{4}\frac{\epsilon\omega_z^2}{\omega_1}\left(\hat{a}_+^\dagger\hat{a}_+^\dagger + \hat{a}_+\hat{a}_+ - \hat{a}_-^\dagger\hat{a}_-^\dagger - \hat{a}_-\hat{a}_- + 4\left[\hat{L}_3\sin\theta - \hat{L}_2\cos\theta\right]\right)\\ &= \omega_1\hat{L}_0 + \hbar\omega_z(\hat{a}_z^\dagger\hat{a}_z + \frac{1}{2}) + \hat{L}_3\left[\omega_c\cos\theta + \frac{\epsilon\omega_z^2}{\omega_1}\sin\theta\right]\\ &\quad - \hat{L}_2\left[\frac{\epsilon\omega_z^2}{\omega_1}\cos\theta - \omega_c\sin\theta\right] + \frac{\hbar}{4}\frac{\epsilon\omega_z^2}{\omega_1}\left(\hat{a}_+^\dagger\hat{a}_+^\dagger + \hat{a}_+\hat{a}_+ - \hat{a}_-^\dagger\hat{a}_-^\dagger - \hat{a}_-\hat{a}_-\right) + \hbar\frac{\omega_1}{2}. \quad (8.34)\end{aligned}$$

$\hat{L}_2$ is eliminated by setting

$$\frac{\epsilon\omega_z^2}{\omega_1}\cos\theta - \omega_c\sin\theta = 0 \quad (8.35)$$

$$\implies \theta = \arctan\left[\frac{\epsilon\omega_z^2}{\omega_1\omega_c}\right]. \quad (8.36)$$

Denoting

$$\gamma = \frac{\epsilon\omega_z^2}{\omega_1\omega_c}, \quad (8.37)$$

[1] The calculation has also proven consistent in the $\{+,-\}$ basis defined by the more conventional operators in (3.20).

leads to

$$\begin{aligned}
&\exp\left\{\frac{i}{\hbar}\theta\hat{L}_1\right\}\hat{\mathcal{H}}_\epsilon\exp\left\{-\frac{i}{\hbar}\theta\hat{L}_1\right\}\\
&=\omega_1\hat{L}_0+\hbar\omega_z(\hat{a}_z^\dagger\hat{a}_z+\frac{1}{2})\\
&\quad+\hat{L}_3\left[\omega_c\sqrt{1+\gamma^2}\right]+\frac{\hbar}{4}\frac{\epsilon\omega_z^2}{\omega_1}\left(\hat{a}_+^\dagger\hat{a}_+^\dagger+\hat{a}_+\hat{a}_+-\hat{a}_-^\dagger\hat{a}_-^\dagger-\hat{a}_-\hat{a}_-\right)\\
&=\frac{\hbar\omega_1}{2}(\hat{n}_++\hat{n}_-)+\hbar\omega_z(\hat{a}_z^\dagger\hat{a}_z+\frac{1}{2})+\frac{\hbar}{2}(\hat{n}_+-\hat{n}_-)\left(\frac{1}{\omega_1}\sqrt{\epsilon^2\omega_z^4+\omega_1^2\omega_c^2}\right)\\
&\quad+\frac{\hbar}{4}\frac{\epsilon\omega_z^2}{\omega_1}\left(\hat{a}_+^\dagger\hat{a}_+^\dagger+\hat{a}_+\hat{a}_+-\hat{a}_-^\dagger\hat{a}_-^\dagger-\hat{a}_-\hat{a}_-\right)+\hbar\frac{\omega_1}{2}.
\end{aligned}\tag{8.38}$$

The calculation has so far been completely analogous to that in the $\{x,y\}$ basis, with the only difference being between the parameters γ and χ (8.37, 8.9), and the angles ϕ and θ (8.10, 8.36). In fact,

$$\gamma=-\frac{1}{\chi},\qquad\theta=-\frac{1}{\gamma}.\tag{8.39}$$

8.3.1 Squeezing in the $\{+,-\}$ basis

Squeezing operators of the cyclotron and magnetron modes are written:

$$\begin{aligned}
\hat{S}(\zeta_+)&=\exp\left\{-\frac{\zeta_+}{2}\hat{a}_+^{\dagger2}+\frac{\zeta_+^*}{2}\hat{a}_+^2\right\};\quad\zeta_+=r_+\exp(i\phi_+),\\
\hat{S}(\zeta_-)&=\exp\left\{-\frac{\zeta_-}{2}\hat{a}_-^{\dagger2}+\frac{\zeta_-^*}{2}\hat{a}_-^2\right\};\quad\zeta_-=r_-\exp(i\phi_-),
\end{aligned}\tag{8.40}$$

which transform the operators $\hat{a}_+$, $\hat{a}_-$, $\hat{a}_+^\dagger$, $\hat{a}_-^\dagger$ completely analogously to (5.36). Since (8.38) is identical to (8.11) upon replacement of operators $\hat{a}_+$ to $\hat{a}_x$ and $\hat{a}_-$ to $\hat{a}_y$, applying $\hat{S}(\zeta_+)$ and $\hat{S}(\zeta_-)$ to (8.38) produces a diagonal Hamiltonian if the following parameters are set:

$$\phi_+=\phi_-=0,\tag{8.41}$$

$$\zeta_+=\zeta_x\tag{8.42}$$

$$\zeta_-=\zeta_y.\tag{8.43}$$

The result in this basis is likewise [15]

$$\hat{\mathcal{H}}_\zeta=\hbar\tilde{\omega}_+\left(\hat{n}_++\frac{1}{2}\right)-\hbar\tilde{\omega}_-\left(\hat{n}_-+\frac{1}{2}\right)+\hbar\omega_z\left(\hat{n}_z+\frac{1}{2}\right),\tag{8.44}$$

where $\tilde{\omega}_+$ and $\tilde{\omega}_-$ are defined in (8.28).

8.3.2 Solutions of the elliptical Penning trap in the $\{+,-\}$ basis

As in the case of the $\{x,y\}$ basis, the operator $\hat{U}_{1_\theta} = \exp\{i/\hbar\,\theta\hat{L}_1\}$ acting on the squeezed number states and coherent squeezed states of $\{+,-\}$ does not produce further squeezed states.

One interpretation is that the operators $\hat{a}_+$ and $\hat{a}_-$ are *replaced* by the combinations $\hat{\tilde{a}}_+ = \cos(\theta/2)\hat{a}_+ + i\,\sin(\theta/2)\hat{a}_-$ and $\hat{\tilde{a}}_- = \cos(\theta/2)\hat{a}_- + i\,\sin(\theta/2)\hat{a}_+$ before application of squeezing operators. In this way, there are squeezed number states and coherent squeezed states of some basis $\{\tilde{+},\tilde{-}\}$ in the lab frame. This interpretation is more similar to the classical approach in [15].

Calculation of, for example, trajectories of the electron are straightforward to compute from the quantum mechanical analysis. Consider a radial solution of the elliptical Penning trap in the $\hat{L}_{1_\theta}$ frame

$$|\alpha_+(t),\alpha_-(t)\rangle,$$
$$\alpha_+(t) = \exp(i(\theta_+ - \tilde{\omega}_+ t)) \quad \alpha_-(t) = \exp(i(\theta_- + \tilde{\omega}_- t)). \tag{8.45}$$

Making use of (1.39), the expectation value of the electron along the x axis in the lab is given by

$$\begin{aligned}
\langle\hat{x}(t)\rangle &= \sqrt{\frac{\hbar}{2m\omega_1}}\langle\alpha_+(t),\alpha_-(t)|\hat{S}(\zeta_+)\hat{S}(\zeta_-)\hat{U}_{1_\theta}\left(\hat{a}_+^\dagger + \hat{a}_+ + \hat{a}_-^\dagger + \hat{a}_-\right)\hat{U}_{1_\theta}\hat{S}^\dagger(\zeta_+)\hat{S}^\dagger(\zeta_-)|\alpha_+(t),\alpha_-(t)\rangle \\
&= \alpha_+\left(\exp\left(-i(\tilde{\omega}_+ t - \theta_+)\right)\left[\cosh(\zeta_+)\exp\left(\frac{i\theta}{2}\right) + \sinh(\zeta_+)\exp\left(\frac{-i\theta}{2}\right)\right]\right. \\
&\quad \left. + \exp\left(i(\tilde{\omega}_+ t - \theta_+)\right)\left[\cosh(\zeta_+)\exp\left(\frac{-i\theta}{2}\right) + \sinh(\zeta_+)\exp\left(\frac{i\theta}{2}\right)\right]\right) \\
&\quad + \alpha_-\left(\exp\left(-i(\tilde{\omega}_- t + \theta_-)\right)\left[\cosh(\zeta_-)\exp\left(\frac{i\theta}{2}\right) + \sinh(\zeta_-)\exp\left(\frac{-i\theta}{2}\right)\right]\right. \\
&\quad \left. + \exp\left(-i(\tilde{\omega}_- t + \theta_-)\right)\left[\cosh(\zeta_-)\exp\left(\frac{-i\theta}{2}\right) + \sinh(\zeta_-)\exp\left(\frac{i\theta}{2}\right)\right]\right).
\end{aligned} \tag{8.46}$$

The variables ζ_+, ζ_- and θ are given in (8.42, 8.43, 8.36), with arbitrary θ_+ and θ_-. After fairly lengthy calculation, this, and $\langle\hat{y}(t)\rangle$, can be found to agree with the position space trajectory in the literature (1.85) [15].

8.4 Mode coupling in the elliptical Penning trap

In Chapters 2 and 7, coupling of the axial and cyclotron modes is achieved by the time dependent potential of (2.2).

In order that the effects of $\hat{V}_p(t)$ upon the x and y modes in the elliptical trap can be interpreted, the Hamiltonian needs to be written in diagonal form in this basis. As

discussed above, this is achieved by transforming to the $\hat{I}_{1_\phi}$ frame and after squeezing by the operators $\hat{S}(\zeta_x)$ and $\hat{S}(\zeta_y)$. In the following calculation, the coupling potential must be transformed by these operators in succession before the formation of dressed levels can be discussed.

8.4.1 Applying $\hat{U}_{1_\phi}$, $\hat{S}(\zeta_x)$, $\hat{S}(\zeta_y)$ to the coupling potential

The only difference between the time dependent cyclotron-axial coupling field for the radially symmetric trap (2.2) and one required for the elliptical trap, is the frequency of the field: $\omega_p \longrightarrow \tilde{\omega}_p$. The resulting potential is defined

$$\tilde{V}_p(t) = -\epsilon_p \cos(\tilde{\omega}_p t)(xz). \tag{8.47}$$

Quantized and re-expressed in terms of the creation and annihilation operators for the three oscillator modes using the expansion of $\hat{x}$ and $\hat{z}$ in (1.39), this is first transformed by $\hat{U}_{1_\phi}$ to become:

$$\begin{aligned}
&\hat{U}_{1_\phi}\hat{\tilde{V}}_p(t)\hat{U}^\dagger_{1_\phi} \\
&= -\epsilon_p \cos(\tilde{\omega}_p t)\frac{\hbar}{m}\frac{1}{\sqrt{2\omega_1\omega_z}}\left[\left(\cos\frac{\phi}{2}\hat{a}^\dagger_x + i\sin\frac{\phi}{2}\hat{a}^\dagger_y\right)\hat{a}^\dagger_z + \left(\cos\frac{\phi}{2}\hat{a}^\dagger_x + i\sin\frac{\phi}{2}\hat{a}^\dagger_y\right)\hat{a}_z\right. \\
&\left.+\hat{a}^\dagger_z\left(\cos\frac{\phi}{2}\hat{a}_x - i\sin\frac{\phi}{2}\hat{a}_y\right) + \left(\cos\frac{\phi}{2}\hat{a}_x - i\sin\frac{\phi}{2}\hat{a}_y\right)\hat{a}_z\right].
\end{aligned} \tag{8.48}$$

Applying $\hat{S}(\zeta_x)$ and $\hat{S}(\zeta_y)$ to this:

$$\begin{aligned}
\hat{V}_{\zeta p}(t) &= \hat{S}(\zeta_x)\hat{S}(\zeta_y)\hat{U}_{1_\phi}\hat{\tilde{V}}_p(t)\hat{U}^\dagger_{1_\phi}\hat{S}^\dagger(\zeta_y)\hat{S}^\dagger(\zeta_x) \\
&= -\epsilon_p \cos(\tilde{\omega}_p t)\frac{\hbar}{m}\frac{1}{\sqrt{2\omega_1\omega_z}}\left[\cos\frac{\phi}{2}\left(\cosh(\zeta_x)+\sinh(\zeta_x)\right)\left(\hat{a}^\dagger_z\hat{a}^\dagger_x + \hat{a}^\dagger_z\hat{a}_x\right.\right. \\
&\quad \left.+\hat{a}^\dagger_x\hat{a}_z + \hat{a}_z\hat{a}_x\right) \\
&\quad \left.+i\sin\frac{\phi}{2}\left(\cosh(\zeta_y)-\sinh(\zeta_y)\right)\left(\hat{a}^\dagger_z\hat{a}^\dagger_y + \hat{a}^\dagger_y\hat{a}_z - \hat{a}^\dagger_z\hat{a}_y - \hat{a}_z\hat{a}_y\right)\right].
\end{aligned} \tag{8.49}$$

The total Hamiltonian in this frame is now given by

$$\begin{aligned}
&\hat{\mathcal{H}}_\zeta + q\hat{V}_{\zeta p}(t) \\
&\equiv \hat{S}(\zeta_x)\hat{S}(\zeta_y)\hat{U}_{1_\phi}\left(\hat{\mathcal{H}}_\epsilon + q\hat{\tilde{V}}_p(t)\right)\hat{U}^\dagger_{1_\phi}\hat{S}^\dagger(\zeta_y)\hat{S}^\dagger(\zeta_x)
\end{aligned} \tag{8.50}$$

Transforming to a frame rotating at $\tilde{\omega}_p$ by use of

$$\hat{\tilde{U}}'_p(t) = \exp\left\{-\frac{i}{\hbar}(\tilde{\omega}_p t)\hat{J}_3\right\}, \tag{8.51}$$

and defining

$$\tilde{\omega}_p = \tilde{\omega}_+ - \omega_z + \delta, \tag{8.52}$$

a secular approximation [58] results in the rotated and squeezed coupling potential:

$$\hat{\tilde{U}}_p'(t)\hat{V}_{\zeta p}(t)\hat{\tilde{U}}_p'^{\dagger}(t) = -\frac{\hbar}{2m}\frac{1}{\sqrt{2\omega_1\omega_z}}\cos\frac{\phi}{2}\exp(\zeta_x)\epsilon_p\{\hat{a}_z^{\dagger}\hat{a}_x + \hat{a}_x^{\dagger}\hat{a}_z\}. \tag{8.53}$$

The coupled, elliptical Hamiltonian (8.50) in this squeezed and rotated frame is therefore given by:

$$\begin{aligned}\hat{\mathcal{H}}_{\zeta pt} &= \hat{\tilde{U}}_p'(t)\left(\hat{\mathcal{H}}_\zeta + q\hat{V}_{\zeta p}(t)\right)\hat{\tilde{U}}_p'^{\dagger}(t) + i\hbar\dot{\hat{\tilde{U}}}_p'(t)\hat{\tilde{U}}_p'^{\dagger}(t)\\ &= \tilde{\omega}_0\hat{J}_0 + \delta\hat{J}_3 + 2\tilde{\xi}\hat{J}_1 + \frac{\hbar\tilde{\omega}_0}{2} - \hbar\tilde{\omega}_-\left(\hat{n}_y + \frac{1}{2}\right),\end{aligned} \tag{8.54}$$

where $\tilde{\xi}$ is defined

$$\tilde{\xi} = \frac{e}{2m}\frac{1}{\sqrt{2\omega_1\omega_z}}\cos\frac{\phi}{2}\exp(\zeta_x)\,\epsilon_p, \tag{8.55}$$

$\tilde{\omega}_0 = \tilde{\omega}_+ + \omega_z$, and the other constants are collected together for convenience:

$$\begin{aligned}\tanh(2\zeta_x) &= -\frac{\kappa}{\omega_+ + \kappa K(\kappa)},\\ \zeta_x = \frac{1}{2}\tanh^{-1}(\gamma_x); \qquad \gamma_x &= -\frac{\kappa}{\omega_+ + \kappa K(\kappa)},\\ \phi &= \arctan\left[-\frac{\omega_1\omega_c}{\epsilon\omega_z^2}\right].\end{aligned} \tag{8.56}$$

8.4.2 Dressing in the elliptical trap

The dressed frame

Once again, an operator constructed from $\hat{J}_2$ serves to diagonalise the coupled Hamiltonian (8.54):

$$\hat{U}_{2_\epsilon} = \exp\left\{\frac{i}{\hbar}\tilde{\theta}\hat{J}_2\right\} = \exp\left\{\frac{\tilde{\theta}}{2}(\hat{a}_z^{\dagger}\hat{a}_x - \hat{a}_x^{\dagger}\hat{a}_z)\right\}. \tag{8.57}$$

Analogously to the rotation angle for mode coupling in the symmetric trap, (8.36):

$$\tilde{\theta} = \arctan\left[\frac{2\tilde{\xi}}{\delta}\right]. \tag{8.58}$$

This produces

$$\mathbb{H}_\zeta = \hat{U}_{2_\epsilon}\hat{\mathcal{H}}_{\zeta pt}\hat{U}_{2_\epsilon}^{\dagger} = \hbar\tilde{\omega}_{\mathbb{H}_x}\left(\hat{n}_x + \frac{1}{2}\right) + \hbar\tilde{\omega}_{\mathbb{H}_z}\left(\hat{n}_z + \frac{1}{2}\right) - \hbar\tilde{\omega}_-\left(\hat{n}_y + \frac{1}{2}\right). \tag{8.59}$$

The eigenfrequencies are given by

$$\tilde{\omega}_{\mathbb{H}_z} = \frac{\tilde{\omega}_0 + \tilde{\Delta}}{2}, \qquad \tilde{\omega}_{\mathbb{H}_x} = \frac{\tilde{\omega}_0 - \tilde{\Delta}}{2}, \tag{8.60}$$

where

$$\tilde{\Delta} = \sqrt{4\tilde{\xi}^2 + \delta^2}. \tag{8.61}$$

Dressed states

The operators of the dressed states of the coupled elliptical trap are straightforwardly given by

$$\begin{aligned}\hat{a}^\dagger_{\alpha\zeta} &= \cos\frac{\tilde{\theta}}{2}\hat{a}^\dagger_z + \sin\frac{\tilde{\theta}}{2}\hat{a}^\dagger_x, \quad \hat{a}_{\alpha\zeta} = \cos\frac{\tilde{\theta}}{2}\hat{a}_z + \sin\frac{\tilde{\theta}}{2}\hat{a}_x,\\ \hat{a}^\dagger_{\beta\zeta} &= \cos\frac{\tilde{\theta}}{2}\hat{a}^\dagger_x - \sin\frac{\tilde{\theta}}{2}\hat{a}^\dagger_z, \quad \hat{a}_{\beta\zeta} = \cos\frac{\tilde{\theta}}{2}\hat{a}_x - \sin\frac{\tilde{\theta}}{2}\hat{a}_z,\end{aligned} \tag{8.62}$$

so that (8.54) is rewritten

$$\boxed{\hat{\mathcal{H}}_{\zeta pt} = \tilde{\varepsilon}_\alpha\left(\hat{\alpha}^\dagger_\zeta\hat{\alpha}_\zeta + \frac{1}{2}\right) + \tilde{\varepsilon}_\beta\left(\hat{\beta}^\dagger_\zeta\hat{\beta}_\zeta + \frac{1}{2}\right) - \hbar\omega_-\left(\hat{a}^\dagger_y\hat{a}_y + \frac{1}{2}\right)}, \tag{8.63}$$

where

$$\tilde{\varepsilon}_\alpha = \tilde{\omega}_{\mathbb{H}_z}, \quad \tilde{\varepsilon}_\beta = \tilde{\omega}_{\mathbb{H}_x}. \tag{8.64}$$

The effects of dressing can again be seen in Figure 2.2, where the quantum numbers N, l should this time be replaced by quantum numbers of some squeezed modes, N'_ζ, l'_ζ.

8.5 The quantum ultra-elliptical trap

As discussed in 1.6.2, the Geonium Chip trap can be driven into the ultra-elliptical regime [29] by careful modification of the tuning ratios of the chip electrodes (1.83).

8.5.1 Driving to the ultra-elliptical regime

Considering again the problem as presented in the $\{x, y\}$ basis, suppose now that the ellipticity parameter is a function of time, $\epsilon \to \epsilon(t)$, resulting in the Hamiltonian

$$\begin{aligned}\hat{\mathcal{H}}_{\epsilon(t)} = \frac{1}{2m}(\hat{p}_x^2 + \hat{p}_y^2 + \hat{p}_z^2) + \frac{\omega_c}{2}(\hat{x}\hat{p}_y - \hat{y}\hat{p}_x)\\ + \frac{1}{8}m\omega_1^2(\hat{x}^2 + \hat{y}^2) + \frac{1}{4}m\,\epsilon(t)\omega_z^2\left(\hat{x}^2 - \hat{y}^2\right) + \frac{1}{2}m\omega_z^2\hat{z}^2.\end{aligned} \tag{8.65}$$

It was discussed in detail throughout 8.2 how the elliptical Hamiltonian in the quantum form of (8.3) is solved by application of three operators, $\hat{U}_{1_\phi}$, $\hat{S}(\zeta_x)$, $\hat{S}(\zeta_y)$, where, from (8.19), (8.25) and (8.8), ϕ, ζ_x, and ζ_y are functions of the ellipticity parameter. Explicitly:

$$\begin{aligned}\zeta_x(\epsilon) &= \tanh^{-1}\left(\frac{-\epsilon\omega_z^2/2\omega_1}{\omega_+ + \frac{\omega_c}{2}\left(\sqrt{1 + \frac{\epsilon^2\omega_z^2}{\omega_1^2\omega_c^2}} - 1\right)}\right),\\ \zeta_y(\epsilon) &= \tanh^{-1}\left(\frac{-\epsilon\omega_z^2/2\omega_1}{\omega_- + \frac{\omega_c}{2}\left(\sqrt{1 + \frac{\epsilon^2\omega_z^2}{\omega_1^2\omega_c^2}} - 1\right)}\right),\\ \phi(\epsilon) &= \arctan\left(-\frac{\omega_1\omega_c}{\epsilon\omega_z^2}\right).\end{aligned} \tag{8.66}$$

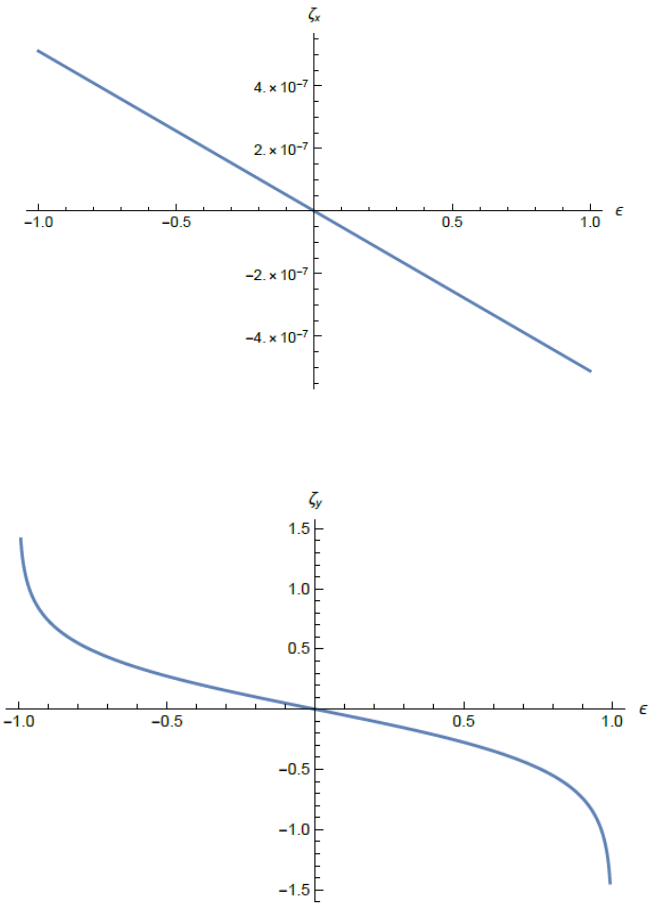

Figure 8.2: The squeezing parameters $\zeta_x(\epsilon)$ (upper) and $\zeta_y(\epsilon)$ (lower) as given in (8.66). The values are plotted for a magnetic field $B = 0.5T$ and ring voltage $V_r = -1V$ in the Geonium Chip trap. The values ζ_x and ζ_y correspond exactly to ζ_+ and ζ_- (8.42, 8.43) when the calculation is performed in the $\{+, -\}$ basis.

If ϵ is now increased slowly enough in time, it follows that the solutions of the trap are given by these same three operators acting on some eigenstate of a diagonal Hamiltonian with continually increasing values of ϕ, ζ_x, and ζ_y. The squeezing of the modes with ellipticity allows for a rather attractive interpretation of the quantum elliptical Penning trap; we can readily imagine the physical squeezing of the orbits with increasing ϵ, the reduction of the motion to a narrow ellipse along an axis. Plotting the squeezing parameters $\zeta_x(\epsilon)$ and $\zeta_y(\epsilon)$ from (8.66) nicely illustrates how the physical orbits of the cyclotron and magnetron motions are so differently affected by increasing ellipticity. As shown in Figure 8.2, ζ_x (and therefore ζ_+) varies little with ϵ, whereas ζ_y (and ζ_-) tends to $\pm\infty$ as $\epsilon \to \pm 1$. Thus the cyclotron orbit is largely unaffected by the ellipticity, whereas the magnetron motion is squeezed to a line along the x (y) axis when $\epsilon \to 1$ ($\epsilon \to -1$), as shown in Figure 1.9.

As discussed in 1.6.2, the ellipticity must be varied such that an optimal tuning ration, T_c^{opt} is maintained; time dependence of $\epsilon(t)$ should therefore be chosen so that a curve in Figure 1.10 is followed exactly. Since $\epsilon(t)$ must be a function of the tuning ratios T_g, T_e and T_c in (1.83), it follows that the solutions of the trap must be given by squeezed states, where the degree of squeezing depends directly on these ratios. The careful preparation of robust squeezed states by this mechanism is considered below.

8.5.2 Cooling the magnetron motion

Also discussed in 1.6.2, experimental adiabaticity demands that the magnetron motion is continually cooled as the trap is driven towards the ultra-elliptical regime to limit the size of the semi-major axis of its orbit [29].

Axial-magnetron coupling for the circular trap can be achieved by the field $E_m(t) = Re(\epsilon_m e^{i\omega_m t})(x\hat{e}_z + z\hat{e}_x)$, resulting in the same potential as in (2.2), but with the subscript change $p \to m$:

$$V_m(t) = -\epsilon_m \cos(\omega_m t)(xz). \tag{8.67}$$

It was shown in 8.4 that the cyclotron-axial coupling potentials for the radially symmetric and elliptical traps differ only by the choice of frequency $\omega_p \leftrightarrow \tilde{\omega}_p$, and the calculation for coupling the axial and magnetron motions proves completely analogous. Moreover, since at every stage of mode coupling, the required coupling frequency will be different from the previous one as the ellipticity varies, the coupling potential and frequency are denoted as

explicit functions of ϵ:

$$\begin{aligned} V_m(t) &\longrightarrow V_m(\epsilon,\, t), \\ \omega_m &\longrightarrow \tilde{\omega}_m(\epsilon). \end{aligned} \tag{8.68}$$

Details are given for the elliptical axial-magnetron mode coupling calculation, bearing in mind that setting $\epsilon = 0$ will reduce it to the result for the radially symmetric trap. Quantisation and transformation by the operators $\hat{U}_{1_{\phi(\epsilon)}}$, $\hat{S}(\zeta_x(\epsilon))$ and $\hat{S}(\zeta_y(\epsilon))$ in succession results in

$$\begin{aligned} \hat{V}_{\zeta m}(\epsilon,t) =& \hat{S}(\zeta_x(\epsilon))\hat{S}(\zeta_y(\epsilon))\hat{U}_{1_{\phi(\epsilon)}}\hat{\tilde{V}}_m(\epsilon,t)\hat{U}^\dagger_{1_{\phi(\epsilon)}}\hat{S}^\dagger(\zeta_y(\epsilon))\hat{S}^\dagger(\zeta_x(\epsilon)) \\ =& -\epsilon_m\, \cos(\tilde{\omega}_m(\epsilon)t)\frac{\hbar}{m}\frac{1}{\sqrt{2\omega_1\omega_z}}\left[\cos\frac{\phi(\epsilon)}{2}\,(\cosh(\zeta_x(\epsilon))+\sinh(\zeta_x(\epsilon)))\left(\hat{a}_z^\dagger\hat{a}_x^\dagger+\hat{a}_z^\dagger\hat{a}_x\right.\right. \\ &\left.+\hat{a}_x^\dagger\hat{a}_z+\hat{a}_z\hat{a}_x\right) \\ &\left.+i\sin\frac{\phi(\epsilon)}{2}\,(\,\cosh(\zeta_y(\epsilon))-\sinh(\zeta_y(\epsilon))\,)\left(\hat{a}_z^\dagger\hat{a}_y^\dagger+\hat{a}_y^\dagger\hat{a}_z-\hat{a}_z^\dagger\hat{a}_y-\hat{a}_z\hat{a}_y\right)\right]. \end{aligned} \tag{8.69}$$

The total Hamiltonian is now given by

$$\hat{\mathcal{H}}_{\zeta m}(\epsilon) = \hat{\mathcal{H}}_\zeta + q\hat{V}_{\zeta m}(\epsilon,\, t). \tag{8.70}$$

The explicit time dependence of the additional potential $\hat{V}_{\zeta m}$ can be removed by transforming Hamiltonian (8.70) by unitary operator

$$\hat{U}_m(t) = \exp\left\{-\frac{i}{\hbar}(\tilde{\omega}_m(\epsilon)t)\hat{K}_3\right\}. \tag{8.71}$$

Accordingly, (8.69) becomes in this rotating frame:

$$\begin{aligned} &\hat{U}_m(t)\hat{V}_{\zeta m}(\epsilon,t)\hat{U}_m^\dagger(t) \\ &= -\epsilon_m\, \cos(\tilde{\omega}_m(\epsilon)t)\frac{\hbar}{m}\frac{1}{\sqrt{2\omega_1\omega_z}}\left[\cos\frac{\phi(\epsilon)}{2}\,(\cosh(\zeta_x(\epsilon))+\sinh(\zeta_x(\epsilon)))\left(\left(\hat{a}_z^\dagger\hat{a}_x^\dagger+\hat{a}_z^\dagger\hat{a}_x\right)e^{i\frac{\tilde{\omega}_m(\epsilon)}{2}t}\right.\right. \\ &\quad\left.+\left(\hat{a}_x^\dagger\hat{a}_z+\hat{a}_z\hat{a}_x\right)e^{-i\frac{\tilde{\omega}_m(\epsilon)}{2}t}\right) \\ &\quad\left.+i\sin\frac{\phi(\epsilon)}{2}\,(\,\cosh(\zeta_y(\epsilon))-\sinh(\zeta_y(\epsilon))\,)\left(\hat{a}_z^\dagger\hat{a}_y^\dagger+\hat{a}_y^\dagger\hat{a}_z e^{-i\tilde{\omega}_m(\epsilon)t}-\hat{a}_z^\dagger\hat{a}_y e^{i\tilde{\omega}_m(\epsilon)t}-\hat{a}_z\hat{a}_y\right)\right]. \end{aligned} \tag{8.72}$$

Expansion of $\cos(\tilde{\omega}_m(\epsilon)t)$ into exponential form results in two stationary terms in (8.72), so that a secular approximation [58], and the choice of coupling frequency

$$\tilde{\omega}_m(\epsilon) = \tilde{\omega}_-(\epsilon) + \omega_z + \delta \tag{8.73}$$

results in the total Hamiltonian:

$$\begin{aligned}\hat{\mathcal{H}}_{\zeta mt}(\epsilon) &= \hat{U}_m(t)\hat{\mathcal{H}}_{\zeta m}(\epsilon)\hat{U}_m^\dagger(t) + i\hbar\dot{\hat{U}}_m(t)\hat{U}_m^\dagger(t) \\ &= \tilde{\omega}_{0,m}(\epsilon)\hat{K}_0 + \delta\hat{K}_3 - 2\tilde{\xi}_m(\epsilon)\hat{K}_2 + \frac{\hbar\tilde{\omega}_{0,m}(\epsilon)}{2} + \hbar\tilde{\omega}_+\left(\hat{a}_x^\dagger\hat{a}_x + \frac{1}{2}\right),\end{aligned} \tag{8.74}$$

where

$$\tilde{\omega}_{0,m}(\epsilon) = \omega_z - \tilde{\omega}_-(\epsilon), \tag{8.75}$$

$$\tilde{\xi}_m(\epsilon) = \frac{e}{2m}\frac{1}{\sqrt{2\omega_1\omega_z}}\sin\frac{\phi(\epsilon)}{2}\exp(-\zeta_y(\epsilon))\,\epsilon_m, \tag{8.76}$$

and $\zeta_y(\epsilon)$, $\phi(\epsilon)$ are given in (8.66).

Solving the axial-magnetron coupled Hamiltonian

Hamiltonian (8.74) is solved by application of $\hat{U}_{m,1}(\epsilon)$, defined

$$\hat{U}_{m,1}(\epsilon) = \exp\left\{\frac{i}{\hbar}\tilde{\theta}_m(\epsilon)\hat{K}_1\right\}, \tag{8.77}$$

where

$$\tilde{\theta}_m(\epsilon) = \arctan\left[\frac{2\tilde{\xi}_m(\epsilon)}{\delta}\right]. \tag{8.78}$$

$$\begin{aligned}\implies \hat{\mathbb{H}}(\epsilon) &= \hat{U}_{m,1}(\epsilon)\,\hat{\mathcal{H}}_{\zeta mt}(\epsilon)\,\hat{U}_{m,1}^\dagger(\epsilon) \\ &= \hbar\tilde{\omega}_+\left(\hat{n}_x + \frac{1}{2}\right) + \hbar\frac{1}{2}\left(\tilde{\omega}_{0,m}(\epsilon) + \sqrt{4\tilde{\xi}_m^2(\epsilon) + \delta^2}\right)\left(\hat{n}_y + \frac{1}{2}\right) \\ &\quad + \hbar\frac{1}{2}\left(\tilde{\omega}_{0,m}(\epsilon) - \sqrt{4\tilde{\xi}_m^2(\epsilon) + \delta^2}\right)\left(\hat{n}_z + \frac{1}{2}\right).\end{aligned} \tag{8.79}$$

The dressed states interpretation is detailed in Appendix C.

8.5.3 Preparation of squeezed states

The results from 8.5.1 and 8.5.2 are now combined to describe the necessary process of increasing the ellipticity and coupling the magnetron motion in alternate stages [29].

Suppose that the radially symmetric Penning trap is prepared in some eigenstate $|\psi\rangle$. Following a curve in Figure 1.10 which maintains an optimal tuning ratio, the voltage ratios are adjusted to produce an ellipticity value ϵ_1. From 8.2.3, the solution of the trap is now given by

$$\hat{U}_{1_{\phi(\epsilon_1)}}^\dagger\hat{S}^\dagger(\zeta_x(\epsilon_1))\hat{S}^\dagger(\zeta_y(\epsilon_1))|\psi\rangle \equiv |\phi\rangle, \tag{8.80}$$

where $\zeta_x(\epsilon)$, $\zeta_y(\epsilon)$ and $\phi(\epsilon)$ are given in (8.66). The magnetron and axial modes are now coupled by $V_m(\epsilon_1, t)$ in (8.67), and the eigenstate of the Hamiltonian becomes

$$\hat{U}_m^\dagger(t)\hat{U}_{m,1}^\dagger(\epsilon_1)|\phi\rangle \equiv |\Theta\rangle. \tag{8.81}$$

Again the voltage ratios are adjusted, producing a new ellipticity parameter $\epsilon_2 + \epsilon_1$, resulting in the eigenstate

$$\hat{U}_{1_{\phi(\epsilon_2)}}^\dagger \hat{S}^\dagger(\zeta_x(\epsilon_2))\hat{S}^\dagger(\zeta_y(\epsilon_2))|\Theta\rangle \equiv |\Upsilon\rangle. \tag{8.82}$$

Assuming that the process ends with mode coupling, it continues k times until the desired ellipticity value $\epsilon_k + \epsilon_{k-1} + ... + \epsilon_1$ is reached, resulting in the eigenstates

$$\begin{aligned}&\hat{U}_m^\dagger(t)\hat{U}_{m,1}^\dagger(\epsilon_k) \cdot \hat{U}_{1_{\phi(\epsilon_k)}}^\dagger \hat{S}^\dagger(\zeta_x(\epsilon_k))\hat{S}^\dagger(\zeta_y(\epsilon_k)) \; ... \; \hat{U}_m^\dagger(t)\hat{U}_{m,1}^\dagger(\epsilon_2)\cdot \\ &\cdot \hat{U}_{1_{\phi(\epsilon_2)}}^\dagger \hat{S}^\dagger(\zeta_x(\epsilon_2))\hat{S}^\dagger(\zeta_y(\epsilon_2)) \cdot \hat{U}_m^\dagger(t)\hat{U}_{m,1}^\dagger(\epsilon_1) \cdot \hat{U}_{1_{\phi(\epsilon_1)}}^\dagger \hat{S}^\dagger(\zeta_x(\epsilon_1))\hat{S}^\dagger(\zeta_y(\epsilon_1))|\psi\rangle.\end{aligned} \tag{8.83}$$

8.5.4 Achieveing quantum adiabaticity

Of course, for the final state of the electron to match that in (8.83) after the complex sequence of elliptical driving and mode coupling, each stage of the experimental process must satisfy the quantum adiabaticity theorem. First derived in 1928 by Born and Fock [81], the theorem states that, during its evolution by a Hamiltonian $\hat{H}(t)$, a quantum state prepared in an initial eigenstate $|n(0)\rangle$ remains close to the instantaneous eigenstate $|n(t)\rangle$ as time evolves [82]. A detailed calculation of the criteria for ensuring quantum adiabaticity are not included due to time constraints, but a general discussion is provided below.

The theorem is more easily applied to the present case when formulated in the parameter domain [83, 84] rather than the time domian. In consequence of this, for the squeezing parts of the evolution driven by $\hat{\mathcal{H}}_{\epsilon(t)}$ in (8.65), the parameter path between between an initial value ϵ_I to a final value ϵ_F must be followed infinitely slowly [82]; from Figure 1.10, this *path* refers to each section of a segmented line along which the system is being driven. This requires that the voltage ratios controlling progression along this path are adjusted accordingly. For the mode coupling stages of the process, the problem can be described by analogy with the Landau-Zener (LZ) model [85, 86]. The word "adiabatic" is from the Greek α (not), $\delta\iota\alpha$ (through), $\beta\alpha\iota\nu\iota\nu$ (to pass) [82]. In the present case it refers to avoiding the gap in energy levels created by the coupling field strength $\tilde{\xi}_m(\epsilon)$ (8.76). This is depicted in Figure 8.3 where only the lowest split energy levels of the combined axial and magnetron modes are included. Although a very simplified representation of

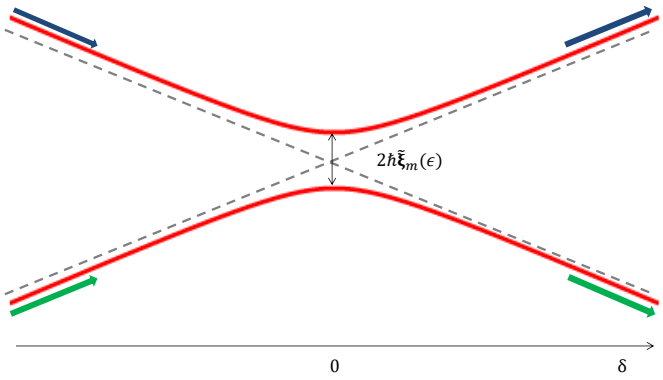

Figure 8.3: An avoided crossing between the $n_y = 1$, $n_z = 0$ and $n_y = 0$, $n_z = 1$ levels can be used to discuss quantum adiabaticity requirements for the axial-magnetron coupling stages of driving to the ultra-elliptical regime [29]. A large enough gap between the dressed levels (or an instantaneous switching on of the coupling field) means that the system either follows the blue or green paths as the gap at $\delta = 0$ is created, so that the electron remains in an adiabatic state. Explicit calculation of the adiabatic modes is given in Appendix C.

the system, it illustrates the adiabaticity condition as applied to this process. During the coupling stages, the ellipticity is assumed to be held at a constant value. Referring to Figure 8.2, the system will remain in an adiabatic state (red line) by following either the path indicated by the blue or green arrows as the gap at $\delta = 0$ is created when the coupling field in (8.67) is first switched on. Avoiding transition between the adiabatic states requires that the time associated with such a transition $\to \infty$. This can be satisfied by achieving a large enough gap $\tilde{\xi}_m(\epsilon)$, as provided by the field strength (8.67). The size of this gap depends on ϵ, and as can be seen in (8.83), is taken care of mathematically by the changing values of ϵ in the sequence of $\hat{U}^{\dagger}_{m,1}(\epsilon)$ operations. The experimental method as discussed in [29] addresses this by observation of the dependence $\tilde{\omega}_- \equiv \tilde{\omega}_-(\epsilon)$ which must change for each stage of the process.

8.6 The infinitely squeezed harmonic oscillator

In Chapter 5, squeezing transformations were shown to map between 3D isotropic trapping systems, and 3D anisotropic systems, with restrictions placed upon the squeezing parameters (5.46, 5.48, 5.50) in order to preserve commutation relations. The connection between this and the present analysis of the quantum elliptical Penning trap is if course

no coincidence; this section briefly highlights and explores this correspondence.

8.6.1 Squeezing in the infinite limit

In the limit $\epsilon \to 1$ of the Penning trap, the squeezing parameter in the y direction, $\zeta_y \to -\infty$, as can be seen in Figure 8.2. In this limit, the trapping frequency along this direction, $\tilde{\omega}_-$, simultaneously $\to 0$ [15] as plotted in Figure 8.1. The correspondence between the relative size of the squeezing parameters $\zeta_{x(+)}$, $\zeta_{y(-)}$, and that between the generalised frequency of the modes $\tilde{\omega}_+$ and $\tilde{\omega}_-$ is in agreement with the analysis of Chapter 5; it was predicted exactly by (5.46), and ensures that commutation relations are conserved. The driving of the Penning trap to the ultra-elliptical regime supports the idea from Chapter 5 that the operator methods devised can be used to map between 2D and 3D trapping systems, as the real valued plots of the magnetron orbit in Figure 1.9 show how the system becomes quasi-2D[2] in the limit $\epsilon \to 1$ [29]. Such agreement between the two is satisfying, given that the results of Chapter 5 are derived only from conservation of angular momentum commutation relations as trapping frequencies are changed. The results of this chapter in conjunction with those of Chapter 5 should greatly assist future theoretical and experimental exploration of the ultra-elliptical trap, whether in the quantum regime or otherwise.

8.6.2 The effective mass of the electron

In Chapter 6, effective masses were introduced along the x and y directions in the $\hat{I}_1$ frame (6.5) to interpret the effects of the magnetic field upon the potential energy of the electron in the trap. In the present case of the elliptical trap, these effective masses become

$$\tilde{m}_x = \frac{1}{2}\frac{\omega_1}{\tilde{\omega}_+}m, \quad \tilde{m}_y = \frac{1}{2}\frac{\omega_1}{\tilde{\omega}_-}m, \tag{8.84}$$

so that the elliptical Hamiltonian (8.29) can be expanded out as

$$\hat{\mathcal{H}}_\zeta = \frac{1}{2\tilde{m}_x}\hat{p}_x^2 - \frac{1}{2\tilde{m}_y}\hat{p}_y^2 + \frac{1}{2m}\hat{p}_z^2 + \frac{1}{2}\tilde{m}_x\hat{x}^2 - \frac{1}{2}\tilde{m}_y\hat{y}^2 + \frac{1}{2}m\hat{z}^2. \tag{8.85}$$

Now, as $\epsilon \to 1$ and $\tilde{\omega}_- \to 0$, it is clear that the effective mass in the y direction, $\tilde{m}_y$, will become unbounded. An infinite effective mass in a harmonic oscillator potential indicates zero motion along this axis, and so in this sense the system truly becomes 2D in the ultra-elliptical limit.

[2] The discussion of the behavoiur of the electron in the x and y motions here is in the $\hat{I}_{1_\phi}$ frame.

Chapter 9

Landau-Zener-Stückelberg Interferometry in the Penning Trap

This chapter returns again to the appearance of avoided crossings of the coupled Penning trap, as shown in Figure 2.2. It is shown how a coupling potential with a sum of carefully chosen frequency components leads to interference patterns of Penning trap observables. Moreover, the calculation demonstrates how enhanced quantum control is achievable by adopting the dressed-atom formalism [57] for the Penning trap. Calculations are performed in the conventional $\{+,-\}$ basis since the discussion does not require knowledge of individual x and y dynamics.

9.1 Landau-Zener-Stückelberg interferometry: an introduction

Let us refer to the calculation of cyclotron-axial mode coupling in Chapter 2. The coupled Hamiltonian (2.11), before dressing, is written in the following form

$$\hat{\mathcal{H}}_{pt} = \omega_0 \hat{T}_0 + \delta \hat{T}_3 + 2\xi \hat{T}_1 - \hbar\omega_- \left(\hat{a}_-^\dagger \hat{a}_- + \frac{1}{2} \right), \tag{9.1}$$

where ω_0 is given in (2.13) and ξ is the renormalized field strength of the coupling field (2.1), with units Hz (2.12). Operators of the set $\underline{T}$ are defined in (2.29). Consider the structure of (9.1). The $+$ and z contributions in $\hat{\mathcal{H}}_{pt}$ reveal a form reminiscent of the

Hamiltonian of a TLS [87]:

$$H_{\mathrm{TLS}} = \begin{bmatrix} \varepsilon_0(t) & \Delta \\ \Delta & \varepsilon_1(t) \end{bmatrix}. \tag{9.2}$$

$\varepsilon_0(t)$ and $\varepsilon_1(t)$ are the energy levels of two diabatic states, and Δ is the coupling strength between them. Such a Hamiltonian forms the basis of Landau-Zener-Stückelberg (LZS) interferometry [88, 89]. In this latter system, the phase accumulated between successive driven transitions of a TLS at an avoided crossing, LZ transitions [85, 86], may lead to constructive or destructive interference. As a result, physical observables have periodic dependence on the parameters of the system, and an interference pattern can be built up as these parameters are varied [90]. Fourier transforms of these patterns can extract information on the energy level spectrum [87]. Additionally, they can provide a tool with which to study the interaction of the system with the trapping fields and with the environment, and offer possibility of "fast and reliable control of a quantum system" [90]. Such capabilities in the Penning trap have obvious appeal.

9.2 The coupling field

In order to induce transitions between the dressed levels of (9.1), it must be modified to include periodic time dependence proportional to the $\hat{T}_1$ term. For this purpose, an electric field comprised of three separate components is defined:

$$\begin{aligned} \vec{E}_{\mathrm{LZS}}(t) = &\frac{A}{2}\cos(\omega_p t)(x\hat{e}_z + z\hat{e}_x) \\ &+ \frac{B}{2}\cos(\omega_n t)(x\hat{e}_z + z\hat{e}_x) \\ &+ \frac{B}{2}\cos(\omega_q t)(x\hat{e}_z + z\hat{e}_x). \end{aligned} \tag{9.3}$$

The associated potential of $\vec{E}_{\mathrm{LZS}}(t)$ is

$$V_{\mathrm{LZS}}(t) = -\left(A\cos(\omega_p t) + B(\cos(\omega_n t) + \cos(\omega_q t))\right)(xz), \tag{9.4}$$

which is identical to (2.2) but for the replacement of the time dependence with three separate terms. Recall the definition of the quantum coordinates $\hat{x}$ and $\hat{z}$ in terms of creation and annihilation operators of the cyclotron and axial modes (1.39), and the definition $\omega_p = \omega_+ - \omega_z + \delta$. As will be shown, the frequencies ω_n and ω_q in (9.4) will act to drive the sidebands of the coupling established by the ω_p contribution in this potential.

In a frame of reference rotating at ω_p defined by the unitary operator $\hat{U}_p(t)$ in (2.6),

the Hamiltonian of the electron in the presence of (9.3) becomes

$$\begin{aligned}\hat{\mathcal{H}}_{\mathrm{LZS}} =&\hat{U}_p(t)\left(\hat{\mathcal{H}}+q\hat{V}_{\mathrm{LZS}}(t)\right)\hat{U}_p^{\dagger}(t)+i\hbar\hat{\dot{U}}_p(t)\hat{U}_p^{\dagger}(t)\\ =&\omega_0\hat{T}_0+\delta\hat{T}_3-\hbar\omega_-\left(\hat{a}_-^{\dagger}\hat{a}_-+\frac{1}{2}\right)\\ &+\frac{e\hbar}{2m\sqrt{\omega_1\omega_z}}\left(A\cos(\omega_p t)+B(\cos(\omega_n t)+\cos(\omega_q t))\right)\times\\ &\times\left\{\hat{a}_+\hat{a}_z+\hat{a}_+^{\dagger}\hat{a}_z e^{i\omega_p t}+\hat{a}_z^{\dagger}\hat{a}_+ e^{-i\omega_p t}+\hat{a}_+^{\dagger}\hat{a}_z^{\dagger}\right.\\ &\left.+\hat{a}_-\hat{a}_z e^{i\frac{\omega_p}{2}t}+\hat{a}_-^{\dagger}\hat{a}_z e^{i\frac{\omega_p}{2}t}+\hat{a}_z^{\dagger}\hat{a}_- e^{-i\frac{\omega_p}{2}t}+\hat{a}_-^{\dagger}\hat{a}_z^{\dagger}e^{-i\frac{\omega_p}{2}t}\right\}.\end{aligned}\tag{9.5}$$

The cosine function is expanded into exponential form, and in this frame, the potential energy contributed by (9.3) becomes

$$\begin{aligned}\hat{U}_p(t)\left(q\hat{V}_{\mathrm{LZS}}(t)\right)\hat{U}_p^{\dagger}(t)=\frac{e\hbar}{2m\sqrt{\omega_1\omega_z}}&\left[\hat{a}_+^{\dagger}\hat{a}_z^{\dagger}\left(A(e^{i\omega_p t}+e^{-i\omega_p t})+B(e^{i\omega_n t}+e^{-i\omega_n t}+e^{i\omega_q t}+e^{-i\omega_q t})\right)\right.\\ &+\hat{a}_-^{\dagger}\hat{a}_z^{\dagger}\,e^{-i\frac{\omega_p}{2}t}\left(A(e^{i\omega_p t}+e^{-i\omega_p t})+B(e^{i\omega_n t}+e^{-i\omega_n t}+e^{i\omega_q t}+e^{-i\omega_q t})\right)\\ &+\hat{a}_+^{\dagger}\hat{a}_z\,e^{i\omega_p t}\left(A(e^{i\omega_p t}+e^{-i\omega_p t})+B(e^{i\omega_n t}+e^{-i\omega_n t}+e^{i\omega_q t}+e^{-i\omega_q t})\right)\\ &+\hat{a}_-^{\dagger}\hat{a}_z\,e^{i\frac{\omega_p}{2}t}\left(A(e^{i\omega_p t}+e^{-i\omega_p t})+B(e^{i\omega_n t}+e^{-i\omega_n t}+e^{i\omega_q t}+e^{-i\omega_q t})\right)\\ &+\hat{a}_z^{\dagger}\hat{a}_+\,e^{-i\omega_p t}\left(A(e^{i\omega_p t}+e^{-i\omega_p t})+B(e^{i\omega_n t}+e^{-i\omega_n t}+e^{i\omega_q t}+e^{-i\omega_q t})\right)\\ &+\hat{a}_z^{\dagger}\hat{a}_-\,e^{-i\frac{\omega_p}{2}t}\left(A(e^{i\omega_p t}+e^{-i\omega_p t})+B(e^{i\omega_n t}+e^{-i\omega_n t}+e^{i\omega_q t}+e^{-i\omega_q t})\right)\\ &+\hat{a}_+\hat{a}_z\,\left(A(e^{i\omega_p t}+e^{-i\omega_p t})+B(e^{i\omega_n t}+e^{-i\omega_n t}+e^{i\omega_q t}+e^{-i\omega_q t})\right)\\ &\left.+\hat{a}_-\hat{a}_z\,e^{i\frac{\omega_p}{2}t}\left(A(e^{i\omega_p t}+e^{-i\omega_p t})+B(e^{i\omega_n t}+e^{-i\omega_n t}+e^{i\omega_q t}+e^{-i\omega_q t})\right)\right],\end{aligned}\tag{9.6}$$

Inserting the frequencies

$$\omega_n=\omega_p+\varphi,\qquad \omega_q=\omega_p-\varphi,\tag{9.7}$$

$$
\begin{aligned}
\hat{U}_p(t)\left(q\hat{V}_{\mathrm{LZS}}(t)\right)\hat{U}_p^\dagger(t) = \frac{e\hbar}{4m\sqrt{\omega_1\omega_z}}\Big[&\hat{a}_+^\dagger\hat{a}_z^\dagger\left(A(e^{i\omega_p t}+e^{-i\omega_p t})\right.\\
&\left.+B(e^{i(\omega_p+\varphi)t}+e^{-i(\omega_p+\varphi)t}+e^{i(\omega_p-\varphi)t}+e^{-i(\omega_p-\varphi)t})\right)\\
&+\hat{a}_-^\dagger\hat{a}_z^\dagger\left(A(e^{i\omega_p t/2}+e^{-i3\omega_p t/2})\right.\\
&\left.+B(e^{i(\omega_p/2+\varphi)t}+e^{-i(3\omega_p/2+\varphi)t}+e^{i(\omega_p/2-\varphi)t}+e^{-i(3\omega_p/2-\varphi)t})\right)\\
&+\hat{a}_+^\dagger\hat{a}_z\left(A(e^{2i\omega_p t}+\underbrace{e^0}_{RWA})\right.\\
&\left.+B(e^{i(2\omega_p+\varphi)t}+\underbrace{e^{-i\varphi t}}_{RWA}+e^{i(2\omega_p-\varphi)t}+\underbrace{e^{i\varphi t}}_{RWA})\right)\\
&+\hat{a}_-^\dagger\hat{a}_z\left(A(e^{3i\omega_p t/2}+e^{-i\omega_p t/2})\right.\\
&\left.+B(e^{i(3\omega_p/2+\varphi)t}+e^{-i(\omega_p/2+\varphi)t}+e^{i(3\omega_p/2-\varphi)t}+e^{-i(\omega_p/2-\varphi)t})\right)\\
&+\hat{a}_z^\dagger\hat{a}_+\left(A(\underbrace{e^0}_{RWA}+e^{-2i\omega_p t})\right.\\
&\left.+B(\underbrace{e^{i\varphi t}}_{RWA}+e^{-i(2\omega_p+\varphi)t}+\underbrace{e^{-i\varphi t}}_{RWA}+e^{-i(2\omega_p-\varphi)t})\right)\\
&+\hat{a}_z^\dagger\hat{a}_-\left(A(e^{i\omega_p t/2}+e^{-3i\omega_p t/2})\right.\\
&\left.+B(e^{i(\omega_p/2+\varphi)t}+e^{-i(3\omega_p/2+\varphi)t}+e^{i(\omega_p/2-\varphi)t}+e^{-i(3\omega_p/2-\varphi)t})\right)\\
&+\hat{a}_+\hat{a}_z\left(A(e^{i\omega_p t}+e^{-i\omega_p t})\right.\\
&\left.+B(e^{i(\omega_p+\varphi)t}+e^{-i(\omega_p+\varphi)t}+e^{i(\omega_p-\varphi)t}+e^{-i(\omega_p-\varphi)t})\right)\\
&+\hat{a}_-\hat{a}_z\left(A(e^{3i\omega_p t/2}+e^{-i\omega_p t/2})\right.\\
&\left.+B(e^{i(3\omega_p/2+\varphi)t}+e^{-i(\omega_p/2+\varphi)t}+e^{i(3\omega_p/2-\varphi)t}+e^{-i(\omega_p/2-\varphi)t})\right)\Big].
\end{aligned}
\tag{9.8}
$$

Now, the frequency φ is chosen such that

$$
\varphi \ll \omega_+ \quad \text{and} \quad \varphi \ll \omega_z. \tag{9.9}
$$

Once again, the only terms not oscillating at $\omega_p \sim$ GHz frequencues are those captioned "RWA". Making the now familiar secular approximation [58] reduces (9.8) to

$$
\begin{aligned}
\hat{U}_p(t)\left(q\hat{V}_{\mathrm{LZS}}(t)\right)\hat{U}_p^\dagger(t) &= \frac{e\hbar}{4m\sqrt{\omega_1\omega_z}}\left[\hat{a}_+^\dagger\hat{a}_z\left(A+B\left(e^{-i\varphi t}+e^{i\varphi t}\right)\right)+\hat{a}_z^\dagger\hat{a}_+\left(A+B\left(e^{i\varphi t}+e^{-i\varphi t}\right)\right)\right]\\
&= \frac{e\hbar}{m\sqrt{\omega_1\omega_z}}\left(\frac{A}{4}+\frac{B}{2}\cos(\varphi t)\right)\left(\hat{a}_z^\dagger\hat{a}_+ + \hat{a}_+^\dagger\hat{a}_z\right).
\end{aligned}
\tag{9.10}
$$

From (9.5), the Hamiltonian of the Penning trap with the applied coupling field $\vec{E}_{\mathrm{LZS}}(t)$ in (9.3) in a frame rotating at ω_p becomes

$$\begin{aligned}\hat{\mathcal{H}}_{\mathrm{LZS}} = \omega_0\hat{T}_0 + \delta\hat{T}_3 + \frac{\hbar\omega_0}{2} - \hbar\omega_-\left(\hat{a}_-^\dagger\hat{a}_- + \frac{1}{2}\right) \\ + \frac{e}{m}\frac{1}{\sqrt{\omega_1\omega_z}}\left(\frac{A}{2} + B\cos(\varphi t)\right)\hat{T}_1.\end{aligned} \tag{9.11}$$

This is rewritten

$$\boxed{\hat{\mathcal{H}}_{\mathrm{LZS}} = \omega_0\left(\hat{T}_0 + \frac{\hbar}{2}\right) + \delta\hat{T}_3 - \varepsilon(t)\hat{T}_1 - \hbar\omega_-\left(\hat{a}_-^\dagger\hat{a}_- + \frac{1}{2}\right)}, \tag{9.12}$$

where

$$\varepsilon(t) = -\left(\chi_0 + \chi\cos(\varphi t)\right), \tag{9.13}$$

and

$$\chi_0 = \frac{e}{m}\frac{1}{\sqrt{\omega_1\omega_z}}\frac{A}{2}, \qquad \chi = \frac{e}{m}\frac{1}{\sqrt{\omega_1\omega_z}}B. \tag{9.14}$$

The offset χ_0 and amplitude χ of the "driving field"[1] $\varepsilon(t)$ are therefore directly controlled through A and B, the amplitudes of the applied field $\vec{E}_{\mathrm{LZS}}(t)$ in (9.3).

9.3 The Landau-Zener-Stückelberg Hamiltonian

In order that it is written in a more conventional form [90], Hamiltonian (9.12) is rotated through $\pi/2$ by $\hat{T}_2$ to reveal:

$$\begin{aligned}\hat{\mathcal{H}}''_{\mathrm{LZS}} &= \exp\left\{\frac{i}{\hbar}\left(\frac{\pi}{2}\right)\hat{T}_2\right\} H_{\mathrm{LZS}} \exp\left\{\frac{i}{\hbar}\left(-\frac{\pi}{2}\right)\hat{T}_2\right\} \\ &= \omega_0\left(\hat{T}_0 + \frac{\hbar}{2}\right) - \delta\hat{T}_1 - \varepsilon(t)\hat{T}_3 - \hbar\omega_-\left(\hat{a}_y^\dagger\hat{a}_y + \frac{1}{2}\right).\end{aligned} \tag{9.15}$$

A 2D Hamiltonian of the cyclotron and axial modes is then defined

$$\hat{\mathcal{H}}(t) = \hat{\mathcal{H}}''_{\mathrm{LZS}} - \hat{\mathcal{H}}_-, \tag{9.16}$$

$$\implies \boxed{\hat{\mathcal{H}}(t) = \omega_0\left(\hat{T}_0 + \frac{\hbar}{2}\right) - \delta\hat{T}_1 - \varepsilon(t)\hat{T}_3}. \tag{9.17}$$

The quantum numbers N and l and the action of the operators $\hat{T}_0$ and $\hat{T}_3$ on Fock states $|n_+, n_z\rangle$ are detailed in (2.35) and (2.36) respectively.

The validity of dropping the magnetron contribution follows from the separable nature of the Penning trap Hamiltonian in (1.38), since the coupled energy levels are unaffected by this degree of freedom. In contrast to an analogous Hamiltonian constructed from Pauli operators [60], as in (9.2), $\hat{\mathcal{H}}(t)$ contains both the potential *and* kinetic energy contributions of the system.

[1] The units of ε are Hz, but this is a convenient term to use.

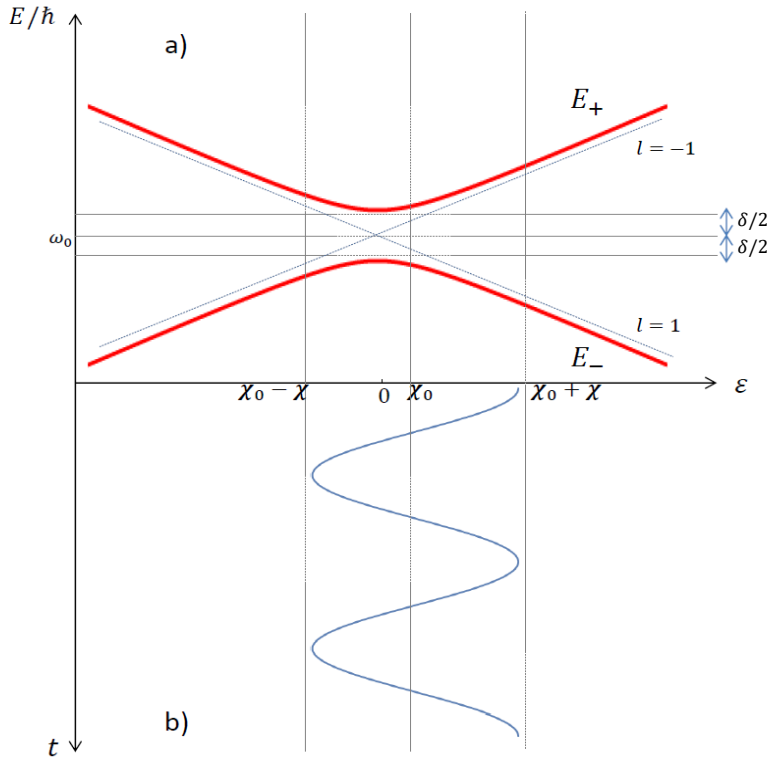

Figure 9.1: a) Energy levels of $\hat{\mathcal{H}}(t)$ in (9.17) vs. the bias ε for $N = 1$. The red curves show the *adiabatic* energy levels $E_{\pm}$, with an avoided crossing of size δ. The dashed blue lines represent the *diabatic* energy levels $l = 1, -1$ which correspond to the Fock states $|n_+, n_z\rangle = |0, 1\rangle$ and $|n_+, n_z\rangle = |1, 0\rangle$ respectively. b) The bias signal $\varepsilon(t)$ with amplitude χ and offset χ_0. The diagram has been copied from a similar one in [90].

9.3.1 Cooling to the state $N = 1$

For the states with total quantum number $N = 1$, there are two possible values of l:

$$\begin{aligned} |n_+, n_z\rangle = |1, 0\rangle \ : \quad & l = -1, \\ |n_+, n_z\rangle = |0, 1\rangle \ : \quad & l = 1. \end{aligned} \tag{9.18}$$

Therefore the levels $N = 1$, $l = 1$ and $N = 1$, $l = -1$ correspond to the first excited states of the coupled modes, the dressed modes.

The instantaneous eigenvalues of $\hat{\mathcal{H}}(t)$ in the state $N = 1$ are

$$E_\pm(t) = \hbar\omega_0 \pm \hbar\frac{\Omega(t)}{2}, \tag{9.19}$$

$$\Omega(t) = \sqrt{\delta^2 + \varepsilon(t)^2}. \tag{9.20}$$

Of course, there are an infinite number of ladder states for Hamiltonian (9.17); for each level N there are N avoided crossings in the adiabatic levels of $\hat{\mathcal{H}}(t)$, resulting in a total of $\sum_{N=0} N$ avoided crossings in the entire spectrum. This is discussed fully in 9.6.

The following two sections consider only the sub-levels of $N = 1$, an ideal TLS. For the purpose of the current stage of the calculation, it is assumed that the electron is prepared in the pure state $N = 1$, so that the rest of the spectrum can be effectively ignored.

9.4 Adiabatic-impulse model

There are many theoretical approaches to solving this problem [91, 92, 93, 94, 95], but the most intuivive one is chosen [90], the adiabatic-impulse model [96, 97, 98]. As the name suggests, the model is based upon treating two distinct types of evolution of the system: adiabatic evolution far from the crossing points, and instantaneous transition between E_+ and E_- at the point of minimum separation. This transition occurs at times t_1 and t_2, where [90]

$$\varphi t_1 = \arccos\left(\frac{\chi_0}{\chi}\right), \qquad \varphi t_2 = \pi - \varphi t_1, \tag{9.21}$$

as indicated in Figure 9.2. In terms of the amplitudes of the bare potential V_{LZS}, $\chi_0/\chi = A/2B$. It should be noted that setting $\chi_0 = A = 0$ results in other interesting population dynamics and phase effects in the system, as has been studied for periodically driven two state systems [99]. However, it does not produce the interference patterns of observables, since these rely on being able to change both the offset χ_0 and amplitude χ of the driving field.

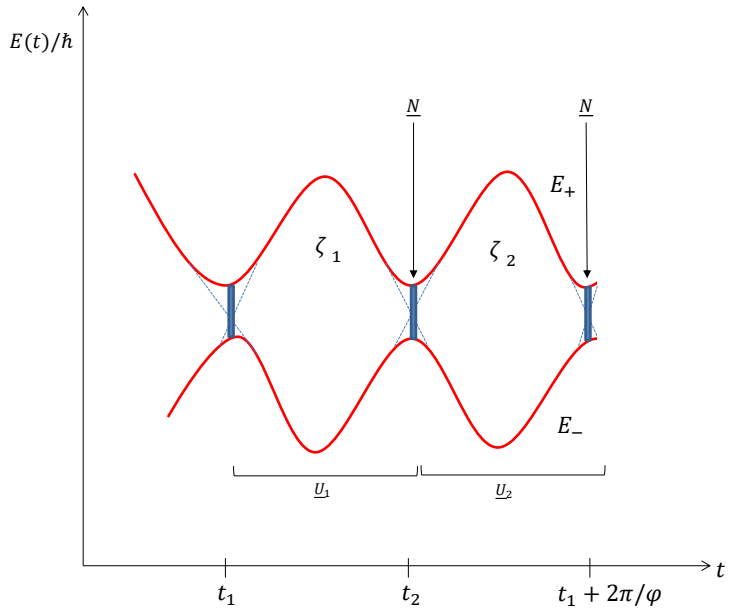

Figure 9.2: Evolution of the energy levels of adiabatic (red) and daibatic (blue) states in time during one period of the driving $\varepsilon(t)$. The phases acquired, ζ_1 and ζ_2, are equal to the area under the curves between crossing points. The matrices $\underline{\mathbf{U}}$ and $\underline{\mathbf{N}}$ (9.26, 9.39) can be used to determine the adiabatic and non-adiabatic evolution of the system [90].

Of course, the reality is that the population mixing does not occur so suddenly, but the model has been found to provide an accurate description of the evolution as long as the system follows a linear transition as it passes through the avoided crossing points [85, 86].

9.4.1 Adiabatic evolution

Far from the points of minimum separation, the wavefunction $\psi(t)$ satisfying the Schrödinger equation $\hat{\mathcal{H}}\psi = E\psi$ is written in the adiabatic basis [90]

$$\psi(t) = \sum_{\pm} b_{\pm}(t)\varphi_{\pm}(t) = \sum_{\pm} c_{\pm}(t)\varphi_{\pm}(t) \exp\left\{\mp\left(\zeta + \frac{\pi}{4}\right)\right\}, \tag{9.22}$$

$$\zeta = \frac{1}{2}\int \Omega(t)\, dt. \tag{9.23}$$

In the adiabatic approximation, $c_{\pm}$ are time independent coefficients between crossing points, so the adiabatic evolution from an initial time t_i to a final time t_f is simply given by [90]

$$\mathbf{b}(t_f) = \underline{\mathbf{U}}(t_f, t_i)\mathbf{b}(t_i), \tag{9.24}$$

where [90]

$$\mathbf{b}(t) = \begin{pmatrix} b_+(t) \\ b_-(t) \end{pmatrix}, \tag{9.25}$$

$$\underline{\mathbf{U}}(t_f, t_i) = \begin{pmatrix} \exp\{-i\zeta(t_f,t_i)\} & 0 \\ 0 & \exp\{i\zeta(t_f,t_i)\} \end{pmatrix} = \exp\{-i\zeta(t_f,t_i)\sigma_z\}, \tag{9.26}$$

$$\zeta(t_f, t_i) = \frac{1}{2}\int_{t_i}^{t_f} \Omega(t)\, dt. \tag{9.27}$$

In Figure 9.2, during the adiabatic stages of evolution over one period of the driving $\varepsilon(t)$, the phases acquired are

$$\zeta_1 = \frac{1}{2}\int_{t_1}^{t_2} \Omega(t)\, dt\,, \qquad \zeta_2 = \frac{1}{2}\int_{t_2}^{t_1+\frac{2\pi}{\varphi}} \Omega(t)\, dt\,, \tag{9.28}$$

which correspond to the areas between the energy levels during these adiabatic stages. The matrices $\underline{\mathbf{U}}_1$ and $\underline{\mathbf{U}}_2$ in the same figure correspond to $\underline{\mathbf{U}}(t_2, t_1)$ and $\underline{\mathbf{U}}(t_1 + 2\pi/\varphi, t_2)$ respectively.

9.4.2 Single passage: a Landau-Zener transition

In Figure 9.2, energy of the diabatic energy levels, shown in blue, are given by $\omega_0 \pm \varepsilon(t)/2$. In the non-adiabatic regions near t_1 and t_2 where the time obeys

$$t = t_{1,2} + t', \quad \varphi|t'| \ll 1, \tag{9.29}$$

the evolution of the driving frequency can be written [90]

$$\varepsilon(t_{1,2} + t') \approx \pm v t', \tag{9.30}$$

where

$$v = \chi\,\varphi|\cos(\varphi t_{1,2})| = \chi\,\varphi\sqrt{1 - \left(\frac{\chi_0}{\chi}\right)^2}. \tag{9.31}$$

The Hamiltonian (9.17) in this region becomes linear:

$$\hat{\mathcal{H}}(t') = \omega_0\hat{T}_0 - \delta\hat{T}_1 \mp v t'\hat{T}_3. \tag{9.32}$$

Apart from the $\hat{T}_0$ term which simply acts to shift the energy levels by a constant, this is exactly the LZ Hamiltonian [85, 86].

If the lower energy level E_- is initially occupied, the transition probability to the upper level E_+ is calculated as [40]

$$P_+ = P_{LZ} = \exp(-2\pi\eta), \tag{9.33}$$

$$\eta = \frac{\delta^2}{4v}. \tag{9.34}$$

As the driving velocity v increases from 0: the adiabatic limit, to ∞: the sudden-change limit [90], the probability of transition from the lower to upper adiabatic state varies from 0 to 1 [40].

The upper limit of of this transition time is given by [99]

$$t_{LZ} = \frac{2}{\delta}\sqrt{\eta}\max(1, \sqrt{\eta}), \tag{9.35}$$

but it is generally shorter than this. The applicability of the adiabatic-impulse model in the Penning trap depends upon the lengthscales l over which the diabatic and adiabatic evolution occur: $l_{adiabatic} \gg l_{diabatic}$. This requirement is fulfiled by large δ/φ and/ or large χ/φ [99], resulting in the combined condition:

$$\boxed{\delta^2 + \chi^2 \gg \varphi^2}. \tag{9.36}$$

In [100], multiphoton fringes are produced by this approach when analogous parameters of the Penning trap obey

$$\chi \lesssim \varphi \lesssim \delta. \tag{9.37}$$

In order to keep track of the relative phase of the wavefunction between the lower and upper adiabatic states, the LZ transition can be described by the non-adiabatic evolution matrix [90]:

$$\mathbf{b}(t_{1,2} + 0) = \underline{\mathbf{N}}\,\mathbf{b}(t_{1,2} - 0), \tag{9.38}$$

$$\underline{\mathbf{N}} = \begin{pmatrix} \sqrt{1 - P_{LZ}}\exp\{-i\tilde{\varphi}_S\} & -\sqrt{P_{LZ}} \\ \sqrt{P_{LZ}} & \sqrt{1 - P_{LZ}}\exp\{i\tilde{\varphi}_S\} \end{pmatrix}, \tag{9.39}$$

where

$$\tilde{\varphi}_S = \varphi_S - \frac{\pi}{2}, \tag{9.40}$$

the Stokes phase [101] is given by

$$\varphi_S = \frac{\pi}{4} + \eta\,(\ln\eta - 1) + \arg\Gamma(1 - i\eta), \tag{9.41}$$

and Γ is the gamma function $\Gamma(x) = (x-1)!$.

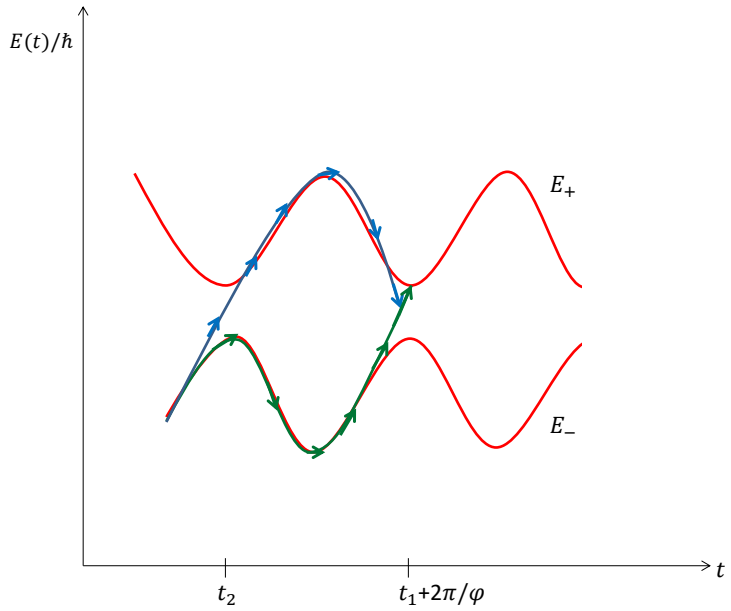

Figure 9.3: Transition from the lower to upper adiabatic energy level during the first (blue) and second (green) passages of the avoided crossing [90]. The interference between the two possible transitions is captured by the Stückelberg phase [85, 89] in the total transition probability after time $t_1 + 2\pi/\varphi$ in (9.42).

9.4.3 Double passage: The Stückelberg phase

Figure 9.3 shows the different possible paths from the lower to upper adiabatic energy level as electron is driven through the avoided crossing points. The total probability of transition after $t_1 + 2\pi/\varphi$, which corresponds to one period of the driving field, is given by [85, 89, 102]:

$$\boxed{P_+ = 4P_{LZ}(1 - P_{LZ})\sin^2(\phi_{St})}, \tag{9.42}$$

$$\phi_{St} = \zeta_2 + \tilde{\varphi}_s. \tag{9.43}$$

The probability P_+ is therefore an oscillating function of the *Stückelberg phase*, ϕ_{St}. The two parts of the phase correspond to the component ζ_2 (9.28) acquired during adiabatic evolution, and $\tilde{\varphi}_s$ (9.40) contributing from adiabatic transition [90]. There are cases in which the Stückelberg oscillations are averaged out [103], and the average probability is given by

$$\overline{P}_+ = 2P_{LZ}(1 - P_{LZ}). \tag{9.44}$$

This averaged value is simply the sum of the probabilities of the first and second transitions.

For systems where LZS interferometry *does* occur (the conditions for this are discussed in 9.5.1), from (9.42), interference between the transitions means that the total excitation probability after double passage may vary from 0, corresponding to destructive interference, to $4P_{LZ}$, in the case of constructive interference [90].

9.5 Multiple passages

9.5.1 Conditions for Landau-Zener-Stückelberg interference

The relevant time scales of the problem must first be considered when studying the system as avoided crossings are passed periodically. The time between such events is of the order of half the driving period [90], $T/2 = \pi/\varphi$. When successive transitions do not overlap and the phase coherence is preserved, corresponding to a long dephasing time T_2, LZS interference can occur [90]. This condition is written:

$$\boxed{t_{LZ} < \frac{T}{2} < T_2.} \tag{9.45}$$

$T/2 \ll T_2$: zero decoherence

The effects of decoherence are discussed in 9.8.1, but for now, assuming zero decoherence (setting $T_2 \gg T/2$), the condition for LZS interferometry from (9.45) becomes

$$\max\left(1, \sqrt{\eta}\right) < \frac{\pi\delta}{2\varphi\sqrt{\eta}}. \tag{9.46}$$

There are two ways in which this inequality may be satisfied:

$\boxed{1 > \sqrt{\eta}}$: This results in two conditions:

$$\chi^2 - \chi_0^2 > \frac{\varphi^2}{\pi^4}, \tag{9.47}$$

$$\chi^2 - \chi_0^2 > \frac{\delta^4}{16\varphi^2}, \tag{9.48}$$

$$\implies \delta \sim \varphi, \quad \chi^2 - \chi_0^2 \sim \delta^2 \tag{9.49}$$

Thus the driving frequency φ should be of the same order of the detuning δ and the difference in the strengths of A and B in (9.4).

$\boxed{1 < \sqrt{\eta}}$: In terms of Penning trap parameters, this requires

$$\delta > \frac{2\varphi}{\pi}, \tag{9.50}$$

$$\chi^2 - \chi_0^2 < \frac{\delta^4}{16\varphi^2}. \tag{9.51}$$

These latter conditions agree with those aimed at in (9.37), so the regime $1 < \sqrt{\eta}$ will be adopted in what follows.

9.5.2 Evolution of the driven two-level system

It has been shown [90] that if the driving is applied for a time t, corresponding to n full periods of $\varepsilon(t)$, the solution is given by combining the matrices $\underline{\mathbf{U}}$ and $\underline{\mathbf{N}}$, corresponding to the adiabatic and non-adiabatic parts of evolution, in the following way:

For $t - \frac{2\pi n}{\varphi} \in (t_1, t_2)$, corresponding to the time falling in the first half of a period of $\varepsilon(t)$:

$$\underline{\mathbf{U}}\left(t, t_1 + \frac{2\pi n}{\varphi}\right)(\underline{\mathbf{N}}\,\underline{\mathbf{U}}_2\,\underline{\mathbf{N}}\,\underline{\mathbf{U}}_1)^n\,, \tag{9.52}$$

and for $t - \frac{2\pi n}{\varphi} \in (t_2, t_1 + \frac{2\pi}{\varphi})$, when the time falls in the second half,

$$\underline{\mathbf{U}}\left(t, t_2 + \frac{2\pi n}{\varphi}\right)\underline{\mathbf{N}}\,\underline{\mathbf{U}}_1\,(\underline{\mathbf{N}}\,\underline{\mathbf{U}}_2\,\underline{\mathbf{N}}\,\underline{\mathbf{U}}_1)^n\,. \tag{9.53}$$

As a reminder,

$$\begin{aligned}
\underline{\mathbf{U}}_1 &= \underline{\mathbf{U}}(t_2, t_1) = \exp\left\{-i\zeta(t_2, t_1)\sigma_z\right\}, \\
\underline{\mathbf{U}}_2 &= \underline{\mathbf{U}}\left(t_1 + \frac{2\pi}{\varphi}, t_2\right) = \exp\left\{-i\zeta\left(t_1 + \frac{2\pi}{\varphi}, t_2\right)\underline{\sigma}_z\right\},
\end{aligned} \tag{9.54}$$

as indicated in Figure 9.3.

The evolution matrices

Closely following [90], the evolution matrices and conditions for LZS interference are found in terms of parameters of the Penning trap.

For a one period oscillation, the evolution matrix is clearly given by [90, 99]

$$\underline{\mathbf{N}}\,\underline{\mathbf{U}}_2\,\underline{\mathbf{N}}\,\underline{\mathbf{U}}_1 = \begin{pmatrix} \nu & -\gamma^* \\ \gamma & \nu^* \end{pmatrix}, \tag{9.55}$$

where

$$\begin{aligned}\nu &= (1-P_{LZ})e^{-i\zeta_+} - P_{LZ}e^{-i\zeta_-},\\ \gamma &= \sqrt{P_{LZ}(1-P_{LZ})}e^{i\tilde{\varphi}_S}\left(e^{-i\zeta_+} + e^{-i\zeta_-}\right),\\ \zeta_+ &= \zeta_1 + \zeta_2 + 2\tilde{\varphi}_S,\\ \zeta_- &= \zeta_1 - \zeta_2.\end{aligned} \tag{9.56}$$

Its n^{th} power is given by [104, 99]

$$(\underline{\mathbf{N}}\,\underline{\mathbf{U}}_2\,\underline{\mathbf{N}}\,\underline{\mathbf{U}}_1)^n = \begin{pmatrix} u_{11} & -u_{21}^* \\ u_{21} & u_{11}^* \end{pmatrix}, \tag{9.57}$$

where the elements are

$$\begin{aligned}u_{11} &= \cos(n\phi) + i\Im(\nu)\frac{\sin(n\phi)}{\sin(\phi)},\\ u_{21} &= \gamma\frac{\sin(n\phi)}{\sin(\phi)},\\ \cos\phi &= \Re(\nu).\end{aligned} \tag{9.58}$$

Since the probability of occupation of the upper level, P_+, is given by $|b_+(t)|^2$ at time t, for $t - \frac{2\pi n}{\varphi} \in (t_1, t_2)$, (9.52) reveals [90]:

$$P_+^{(I)}(n) = |\gamma|^2\frac{\sin^2(n\phi)}{\sin^2(\phi)}. \tag{9.59}$$

Similarly for $t - \frac{2\pi n}{\varphi} \in (t_2, t_1 + \frac{2\pi}{\varphi})$, (9.53) results in [90]:

$$P_+^{(II)}(n) = 2Q_1\frac{\sin^2(n\phi)}{\sin^2(\phi)} + Q_2\frac{sin(2n\phi)}{\sin(\phi)} + P_{LZ}\cos(2n\phi), \tag{9.60}$$

where

$$\begin{aligned}Q_1 &= P_{LZ}\left[P_{LZ}\sin^2(\zeta_-) + (1-P_{LZ})(1+\cos(\zeta_+)\cos(\zeta_-)\right],\\ Q_2 &= 2P_{LZ}(1-P_{LZ})\cos(\zeta_1+\tilde{\varphi}_S)\cos(\zeta_2+\tilde{\varphi}_S).\end{aligned} \tag{9.61}$$

Time averaging over $n \gg 1$ periods results in [90]:

$$\overline{P_+^{(1)}} = \frac{|\gamma|^2}{2\sin^2(\phi)} = \frac{1}{2}\frac{|\gamma|^2}{|\gamma|^2 + (\Im(\nu))^2}, \tag{9.62}$$

$$\overline{P_+^{(II)}} = \frac{Q_1}{\sin^2(\phi)}. \tag{9.63}$$

From (9.62), P_+ is maximal when $\Im(\nu) = 0$, which leads to the general resonance condition [90]:

$$\boxed{(1-P_{LZ})\sin(\zeta_+) - P_{LZ}\sin(\zeta_-) = 0}. \tag{9.64}$$

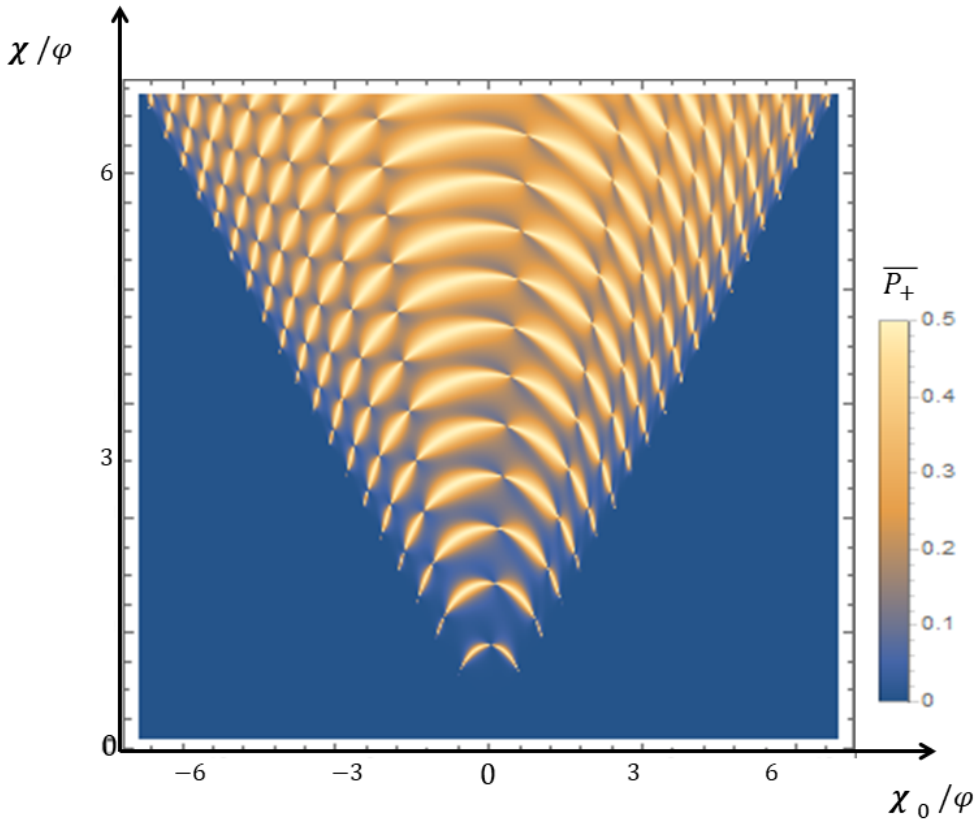

Figure 9.4: The time averaged occupation probability $\overline{P_+}$ of the upper adiabatic energy level E_+ as given in (9.68) for the Penning trap for the pure state $N = 1$. A value of $\varphi = 0.32\,\delta$ is chosen, and the range of both χ and χ_0 are $\pm 7\delta$, corresponding to the regime $\chi\varphi \lesssim \delta^2$ (9.37). The arcs around $\chi = \chi_0 = 0$ are described by the resonance condition in (9.65) for the slow passage limit. Experimentally, the peaks in probability should correspond to the frequency measurement of the upper adiabatic state $E_+/\hbar = \omega_0 + \sqrt{\delta^2 + (\chi + \chi_0)^2}/2$ as the voltages A and B are varied in (9.4). The plot is replicated from [90] with parameters adapted to the Penning trap.

In the *slow limit*, when $2\pi\eta \gg 1$, the resonance condition becomes [90]

$$\zeta_+ = \zeta_1 + \zeta_2 + 2\tilde{\varphi}_S = k\pi, \tag{9.65}$$

and for the *fast limit*, corresponding to $2\pi\eta \ll 1$ [90]:

$$\zeta_1 - \zeta_2 = k\pi \tag{9.66}$$

for any integer k, and $\tilde{\varphi}_S \approx -\pi/2$.

9.5.3 The slow-passage limit $\eta \gg 1$, $P_{LZ} \ll 1$

In terms of Penning trap parameters, this regime is described by

$$\delta^4 \gg 16\varphi^2(\chi^2 - \chi_0^2). \tag{9.67}$$

In this limit, the difference between $\overline{P_+^{(I)}}$ and $\overline{P_+^{(II)}}$, due to the application time of the driving field falling in the first, or second half of a cycle, can be ignored [90]. The lowest approximation in P_{LZ} of $\overline{P_+^{(II)}}$ gives [88, 89]

$$\boxed{\overline{P_+} = \frac{P_{LZ}\left(1 + \cos(\zeta_+)\cos(\zeta_-)\right)}{\sin^2(\zeta_+) + 2P_{LZ}\left(1 + \cos(\zeta_+)\cos(\zeta_-)\right)}}. \tag{9.68}$$

If the system is initially in the lower energy level, this gives the average occupation probability of the upper level [90]. The maximum value of $\overline{P_+}$ is 1/2, and occurs when $\sin(\zeta_+) = 0$. This is exactly the resonance condition in the slow limit given in (9.65), and as can be seen in Figure (9.4), it describes arcs around the point $\chi = \chi_0 = 0$ [90]. The width of the resonance lines is determined by the numerator in (9.68) [90]. When

$$\cos(\zeta_+)\cos(\zeta_-) = -1, \tag{9.69}$$

the width of the line is zero. The ratio χ/φ determines the position of the resonances, but it does not depend on the gap δ [105]. Only the region $\chi < |\chi_0|$ is valid; if the offset χ_0 is grater than the driving amplitude χ, then no avoided crossings are encountered, and the theory inapplicable.

If $\chi_0 = 0$, corresponding to setting $A = 0$ in the applied field (9.3), the resonance condition is simplified to [90]

$$\frac{2\chi}{\varphi} = k\pi. \tag{9.70}$$

9.5.4 Collective conditions and other regimes

The collected conditions necessary for producing Figure 9.4 for the $N = 1$ level of the Penning trap are:

$$\begin{aligned}
\text{Adiabatic impulse condition} &: \delta^2 + \chi^2 \gg \varphi^2 \\
\text{LZS Interference} &: \chi^2 - \chi_0^2 < \frac{\delta^4}{16\varphi^2} \text{ and } \delta > \frac{2\varphi}{\pi}, \\
\text{Slow Driving regime} &: \delta^4 \gg 16\varphi^2(\chi^2 - \chi_0^2), \\
\text{Observation of fringes} &: \chi \lesssim \varphi \lesssim \delta.
\end{aligned} \tag{9.71}$$

As discussed, there are other approaches to solving this problem, such as Floquet theory [106, 95, 107], which more readily allows for the inclusion of dissipative processes in the system [90]. There are also many regimes and conditions, such as the fast passage limit [108], within the adiabatic-impulse approach which could be worth further investigation for the Penning trap. This is beyond the scope of this thesis.

The analysis has so far ignored some rather significant features in the Penning trap. The first of these is that the level occupation of the system is governed by the temperature of the trap, as in (1.71). The spectrum of both the uncoupled and coupled systems must therefore include a thermal distribution of energy levels, with the above calculation only applying to the $N = 1$ level. This is discussed in the following two sections, and the remaining "neglected features" are addressed in 9.8.

9.6 Generalisation to N levels: the coupled harmonic oscillator spectrum

Unless cooling to the exact state $N = 1$ is achieved, the driving $\varepsilon(t)$ must necessarily involve avoided crossings between the l levels of other values of N.

The expectation values of the $\hat{\mathcal{H}}(t)$ with respect to the Fock states $|n_+, n_z\rangle$ is given by

$$\begin{aligned}\frac{1}{\hbar}\langle n_+, n_z|\hat{\mathcal{H}}(t)|n_+, n_z\rangle &= \frac{\omega_0}{2}\left[n_z + n_+ - \frac{\varepsilon(t)}{\omega_0}(n_z - n_+) + 1\right] \\ &= \frac{\omega_0}{2}\left[N - \frac{\varepsilon(t)}{\omega_0}\, l + 1\right]. \end{aligned} \tag{9.72}$$

For a given instant in time, the diabatic energy of the system is defined

$$\begin{aligned}\frac{1}{\hbar}E_{diabatic} &= \frac{1}{\hbar}\overline{\langle n_+, n_z|\hat{\mathcal{H}}(t)|n_+, n_z\rangle} \\ &= \frac{\omega_0}{2}\left(N + 1 - \frac{\varepsilon}{\omega_0}\, l\right), \end{aligned} \tag{9.73}$$

for $N = 0, 1, 2, ...,\ l = -N, -N+2, ...0..., N-2, N$.

The ladder of states in Figure 9.5 shows a plot of (9.73) for $N = 6$. At $\varepsilon = 0$, there is no splitting between the different l levels, since there is no component $\hat{T}_3$ in the Hamiltonian (9.17). As ε increases, the $\hat{T}_3$ component contributes $-\hbar/2\,|\varepsilon|(n_z - n_+)$ to the expectation value, so that for a given $N = n_+ + n_z$, each level is split into $N + 1$ sub-levels.

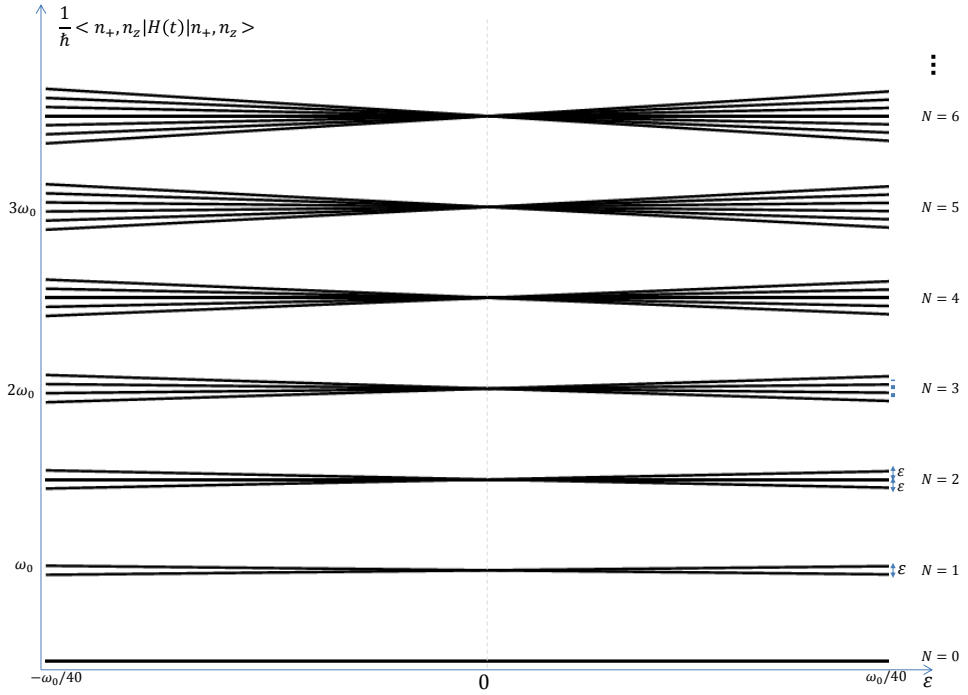

Figure 9.5: The first seven diabatic energy levels of $\hat{\mathcal{H}}(t)$ (9.17). There is no splitting at $\varepsilon = 0$, since the $\hat{T}_3$ component in $\hat{\mathcal{H}}(t)$ vanishes. Away from the origin, the splitting between each adjacent level is given by $|\varepsilon|$. The figure is drawn to scale: the maximum strength of ε in this plot is $\pm\omega_0/40$.

9.6.1 The zoomed-out spectrum

Figure 9.6 shows the diabatic energy levels of the first seven quantum numbers N for a driving field strength $|\varepsilon| = \omega_0/4$, which is $\times 10$ the strength of ε in Figure 9.5[2]. At this strength, various crossing points of l sub-levels can be seen. The spectrum in Figure 9.7 now shows a zoomed-out plot of 9.6, where the relative strength ε has been increased to $\pm 3\omega_0/2$. Comparison of the three Figures 9.5, 9.6 and 9.7 shows how the relative size of the intrinsic frequency ω_0 and the strength of the field ε, determines the overall spectrum of the coupled levels. Increasing ε effectively zooms-out upon a the spectrum of a cranked oscillator [72].

[2]Figure 9.6 is in fact identical to the spectrum of the cranked harmonic oscillator, as discussed in 3.3, around the point $\nu = -0.5$. The difference between the cranked oscillator spectrum and the present case is that this is a plot of the *diabatic* levels of the system; the $\hat{T}_1$ component in Hamiltonian (9.17) will lift the degeneracy at every crossing point in the spectrum when the adiabatic levels are plotted.

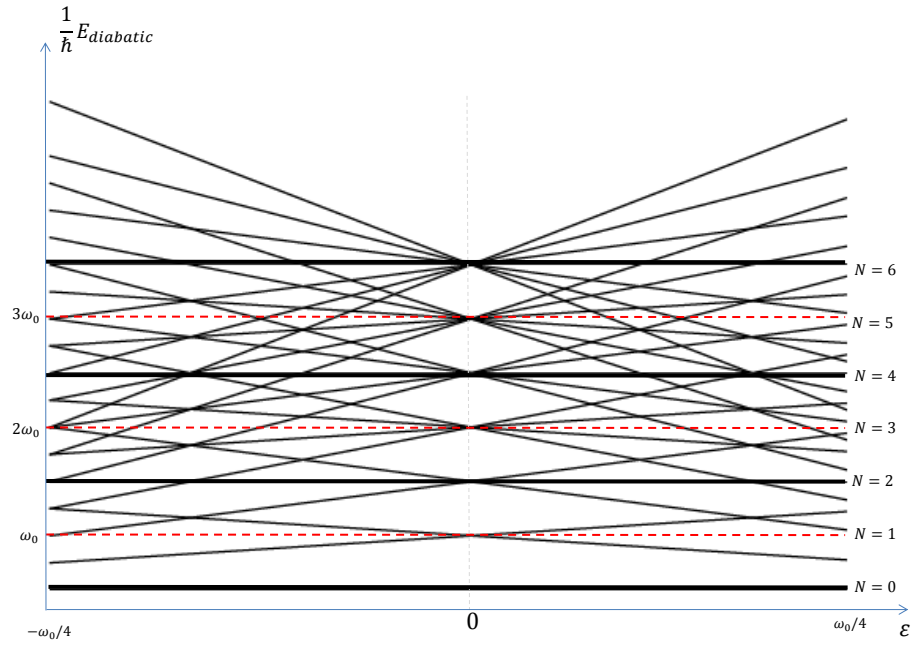

Figure 9.6: Increasing the relative strength of ε to $\pm\omega_0/4$ reveals how the splitting of the l sub-levels from the first seven N levels cross.

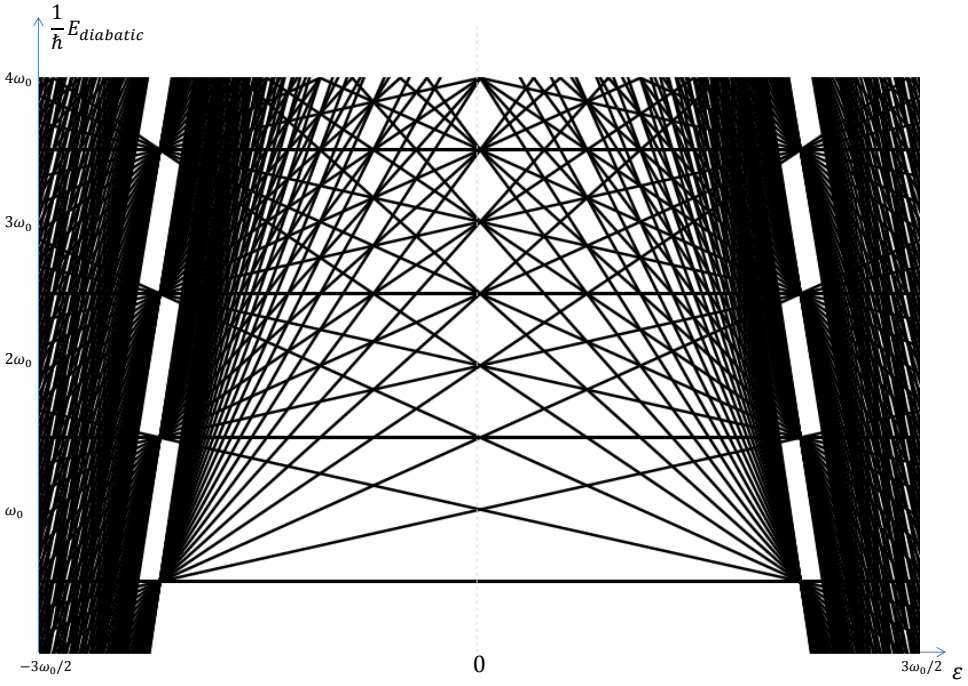

Figure 9.7: The first seven diabatic energy levels for $|\varepsilon| = \pm 3\omega_0/2$. The spectrum is revealed to be exactly that of the cranked harmonic oscillator, as discussed in 3.3, where $\varepsilon = 0$ corresponds exactly to the point $\nu = -0.5$ about which the levels of a 2D harmonic oscillator are split.

Labelling the Fock states of the adiabatic basis $|n_\nu, n_\mu\rangle$, the adiabatic energy is defined[3]

$$\begin{aligned}\frac{1}{\hbar}E_{adiabatic} &= \frac{1}{\hbar}\overline{\langle n_\nu, n_\mu|\hat{\mathcal{H}}(t)|n_\nu, n_\mu\rangle} \\ &= \frac{\omega_0}{2}\left(N+1-\sqrt{\left(\frac{\varepsilon}{\omega_0}\right)^2+\left(\frac{\delta}{\omega_0}\right)^2}\,l\right). \end{aligned} \tag{9.74}$$

Figure 9.8 shows a plot of $2E_{adiabatic}/\hbar\omega_0$ for a fixed field strength ε, and snapshots of the spectrum of $N = 6$ as the avoided crossing of size δ is increased in steps from zero to $\delta = 9\omega_0/10$.

[3]The eigenvalues of $|n_\nu, n_\mu\rangle$ correspond to $E_\pm$ in (9.19) when $N = 1$.

It is clear from these "snapshots" that the avoided crossing between the l sub-levels only occur at the point $\varepsilon = 0$. This result is helpful; it indicates that the crossing of l from different values of N is not relevant in the present system. In this way, each manifold of N levels can be considered independent in the LZS driving calculation.

9.7 The thermal state of the system

As discussed in 1.4.1, the state of the Penning trap must be described by a statistical weighting of states through the density operator $\hat{\rho}_{\pm,z}$ (1.67). From this, the probability of the electron being in a particular Fock state is calculated from the product of the diagonal elements of the individual $\hat{\rho}_+$, $\hat{\rho}_-$ and $\hat{\rho}_z$ matrices [41]. In Chapter 2, the probabilities of excitation of Fock states $|n_+, n_z\rangle$ after mode coupling was shown to follow directly from the eigenvalues of the dressed modes in the lab frame.

Calculating the effects of the LZS coupling field in (9.3) is separated into two parts. The first involves setting $\chi = 0$ ($B = 0$ in (9.3)), so that the field couples the modes exactly as in Chapter 2; the only difference in the statistical results from Hamiltonian 2.34 is then the replacement $2\xi \to -\delta$ and $\delta + \varphi \to \chi_0$ from the previous chapter to the present one. Once the statistical properties of the system have been established, the driving between the dressed levels is "switched on" with $|\chi| > 0$. The probability amplitudes resulting from LZS interferometry for an multi-anticrossing system [87], for each separate manifold of N levels, should then be considered.

In this way, the final results are a convolution of the probabilities of being in the dressed levels with total quantum number $n_\nu + n_\mu$, with the probabilities resulting from LZS driving around an $(n_\nu + n_\mu)$-level anticrossing system [87].

9.7.1 Statistical properties of the uncoupled system, $\chi_0 = \chi = 0$

It is worthwhile to first discuss the statistical properties of each manifold of N levels before *any* coupling field is applied.

For the uncoupled system held at temperature $T = 1/k_B\beta$, the probability of the electron occupying the state $|n_+, n_z\rangle$ is given by [41]

$$\begin{aligned} P(n_+, n_z) &= P(n_+)P(n_z) \\ &= \exp(-\beta\hbar\omega_+ n_+)(1 - \exp(-\beta\hbar\omega_+)) \cdot \exp(-\beta\hbar\omega_z n_z)(1 - \exp(-\beta\hbar\omega_z)). \end{aligned} \tag{9.75}$$

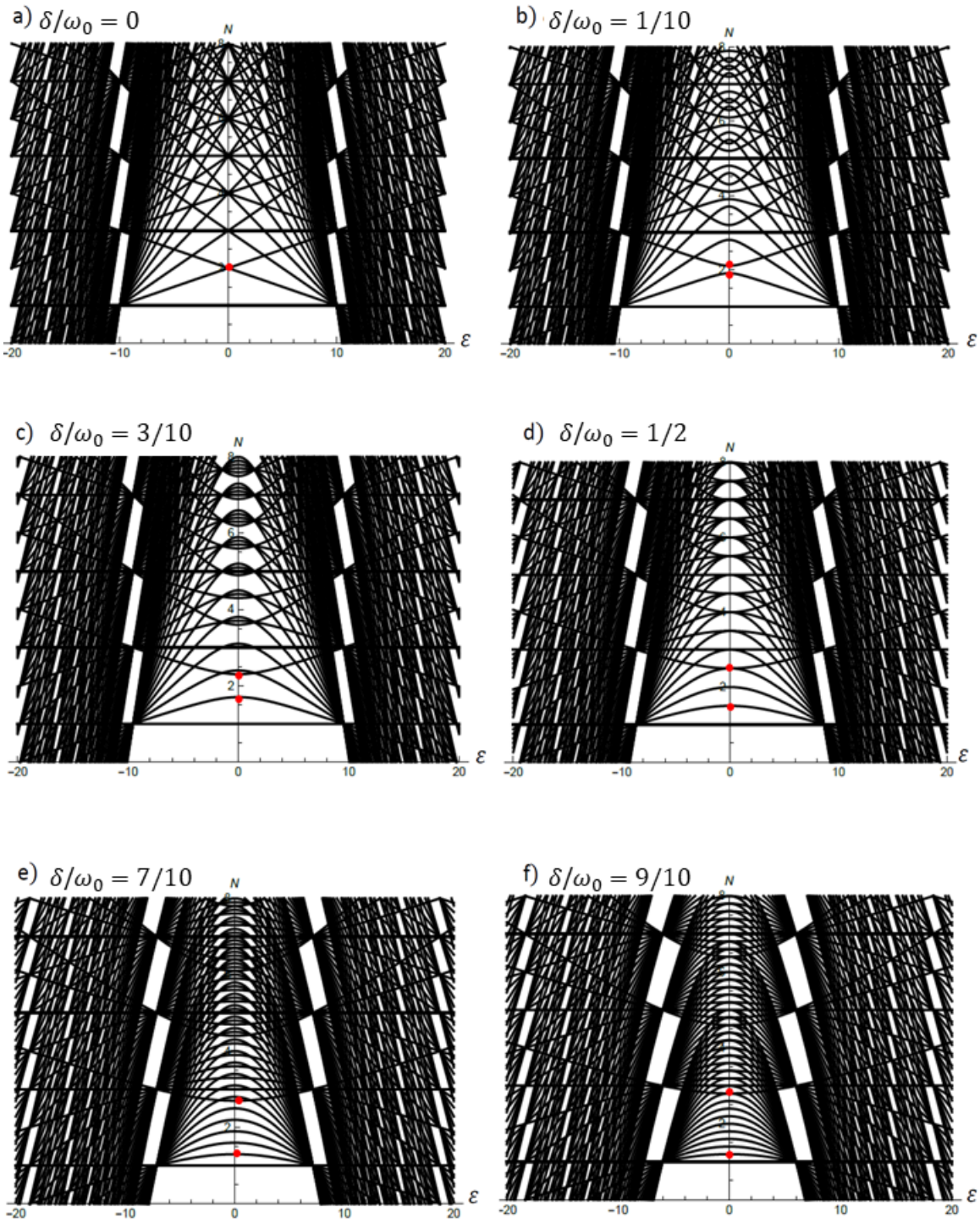

Figure 9.8: Renormalised values of the adiabatic spectrum (9.74) are plotted for increasing values of δ/ω_0 from a) to f), where the values $\omega_0 = 10$ and $|\varepsilon| = 20$ have been arbitrarily chosen. The red dots enable the splitting between two levels to be traced from a) to f). Of course, δ will be fixed for given experiment, but the purpose of the snapshots is to illustrate that the only avoided crossings between the l sub-levels occurs at $\varepsilon = 0$. In this way, other "crossing points" of the spectrum can be effectively ignored.

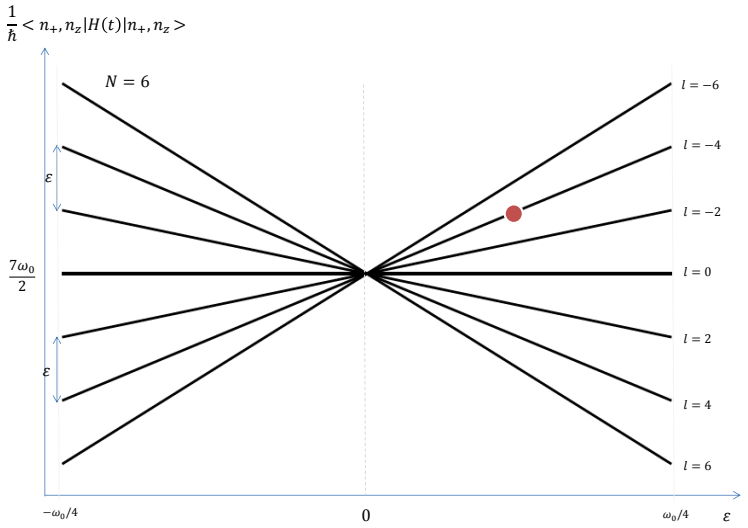

Figure 9.9: Zoomed in plot of the manifold of $N = 6$ diabatic energy levels of Hamiltonian (9.17), with the axes drawn to scale.

This determines the probability of occupation of *each* l level of the spectrum before coupling is applied. The total probability of the collection of l sub-levels belonging to a particular N must now be found. As an example, the level $N = 6$ is considered. Referring to Figure 9.9, this is comprised of sub-levels $(n_+ = 6, n_z = 0)$, $(n_+ = 5, n_z = 1)$, $(n_+ = 4, n_z = 2)$,...$(n_+ = 0, n_z = 6)$. The probability of the electron occupying any of these levels is given by the sum of the individual probabilities $P(n_+, n_z)$:

$$P(N = 6) = P(6_+, 0_z) + P(5_+, 1_z) + P(4_+, 2_z) + P(3_+, 3_z) + P(2_+, 4_z) + P(1_+, 5_z) + P(6_+, 0_z), \tag{9.76}$$

which is straightforward to calculate from (9.75). The probability of occupation of a general level N follows from this:

$$\begin{aligned} P(N) = (1 - \exp(-\beta\hbar\omega_+))(1 - \exp(-\beta\hbar\omega_z)) \, [&\exp(-\beta\hbar\omega_+ N) \\ &+ \exp(-\beta\hbar((N-1)\omega_+ + \omega_z)) + \exp(-\beta\hbar((N-2)\omega_+ + 2\omega_z)) + ... \\ &... + \exp(-\beta\hbar((N-N)\omega_+ + N\omega_z))] \\ &= (1 - \exp(-\beta\hbar\omega_+))(1 - \exp(-\beta\hbar\omega_z)) \sum_k^N \exp\left[-\beta\hbar((N-k)\omega_+ + k\omega_z)\right]. \end{aligned} \tag{9.77}$$

Plots of this $P(N)$ are shown in Figures 9.10 and 9.11 for $T = 4.2\,\mathrm{K}$ and $T = 80\,\mathrm{mK}$ respectively. From comparison of the scale of the y axis, it is clear that just as a lower temperature of the trap guarantees lower average quantum numbers $\overline{n}_+$ and $\overline{n}_z$, so too

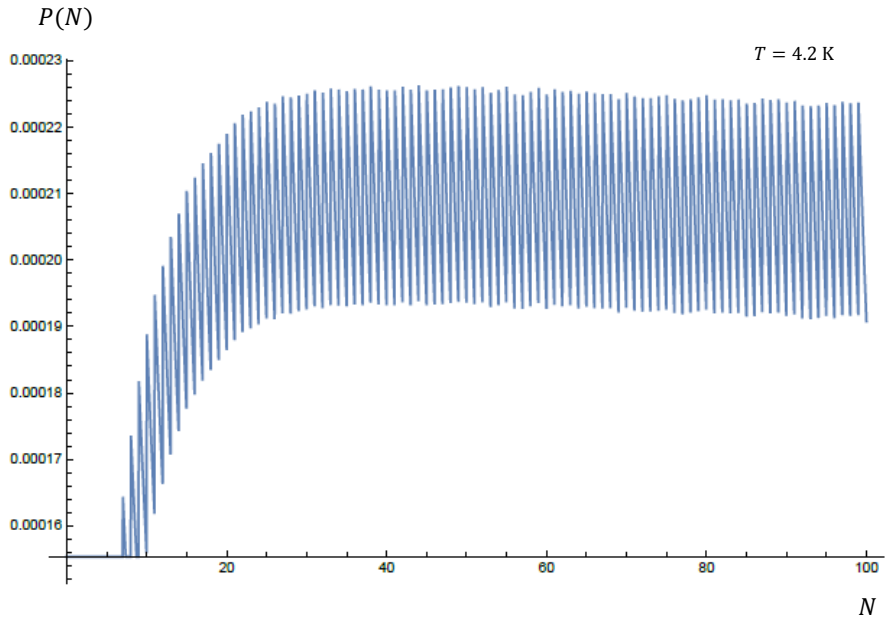

Figure 9.10: Plot of $P(N)$ (9.77), the probability of each manifold of N levels, where $T = 4.2\,\mathrm{K}$.

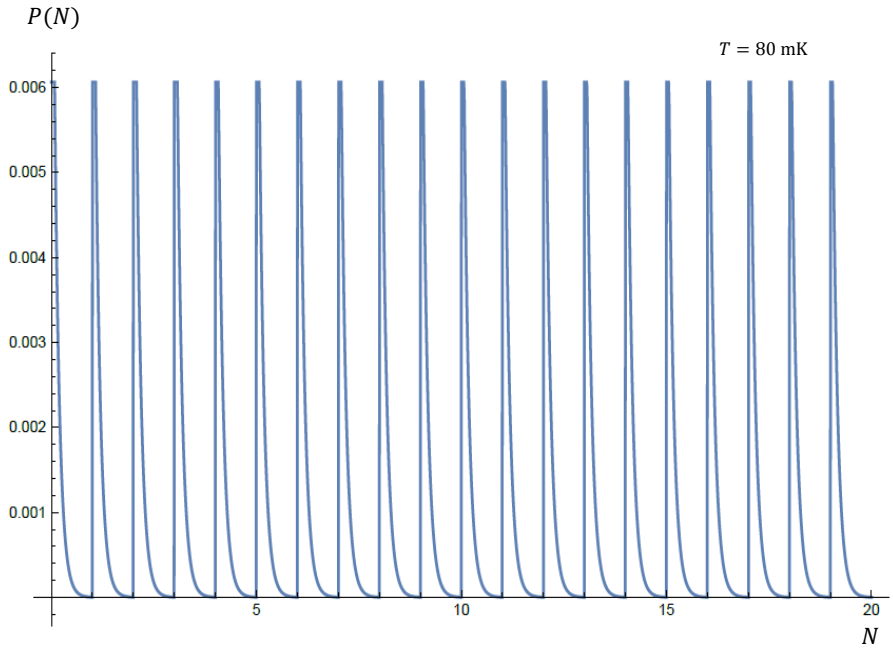

Figure 9.11: Plot of $P(N)$ (9.77), the probability of each manifold of N levels, where $T = 80\,\mathrm{mK}$.

must the probability of occupation $P(N)$ increase for lower values of N as the temperature is lowered.

9.7.2 Statistical properties of the coupled system, $|\chi_0| > 0$, $\chi = 0$

Once coupled, the probability of occupying Fock states $|n_+, n_z\rangle$ are determined by the following thermal probability distributions

$$\begin{aligned} P_c(n_z, n_+) &= P(n_\nu, n_\mu) \\ &= \exp(-\beta\hbar\varepsilon_+ n_+)(1-\exp(-\beta\hbar\varepsilon_+)) \cdot \exp(-\beta\hbar\varepsilon_z n_z)(1-\exp(-\beta\hbar\varepsilon_z)), \end{aligned} \tag{9.78}$$

where the subscript c has been used to denote that the modes have been coupled, and the frequencies of the dressed modes are given by

$$\begin{aligned} \varepsilon_+ &= \frac{1}{2}\left(\omega_0 + \sqrt{\delta^2+\chi_0^2}\right), \\ \varepsilon_z &= \frac{1}{2}\left(\omega_0 - \sqrt{\delta^2+\chi_0^2}\right). \end{aligned} \tag{9.79}$$

In analogy to (9.77), the probability of occupation of levels N becomes after coupling:

$$P_c(N) = (1-\exp(-\beta\hbar\varepsilon_+))(1-\exp(-\beta\hbar\varepsilon_z)) \sum_k^N \exp\left[-\beta\hbar((N-k)\varepsilon_+ + k\varepsilon_z)\right]. \tag{9.80}$$

Now, the $\pm$ signs implied by the square root in (9.79) result in negative statistics for the system if either the positive square root is taken in ε_z, or the negative one in ε_+. Since these statistics must describe real observables of the system, it follows that the negative root must be taken in ε_z and the positive one in ε_+ when calculating statistical values. In this way, the average occupation numbers of the cyclotron and axial modes after coupling are found to be the same:

$$\overline{n}_+ = \frac{1}{\exp\left[\beta\hbar\frac{1}{2}\left(\omega_0 + \sqrt{\delta^2+\chi_0^2}\right)\right]-1} = \overline{n}_z, \tag{9.81}$$

where the positive root is taken. Following this, $P_c(N)$ is plotted in Figures 9.12 and 9.13 for a value $\chi_0 = 0.2\,\delta$. It is clear that the probability of occupation of a lower N for the coupled system is greatly enhanced from the uncoupled case for both $T = 4.2\,\mathrm{K}$ and $T = 80\,\mathrm{mK}$. Moreover, the probability of occupation of each level l for a given N becomes identical:

$$P_c(n_+, n_z) = P_c(n_+ - 1, n_z + 1) = ... = P_c(n_+ - N, n_z + N), \tag{9.82}$$

which is consistent with the fact that $\overline{n}_+ = \overline{n}_z$ after coupling.

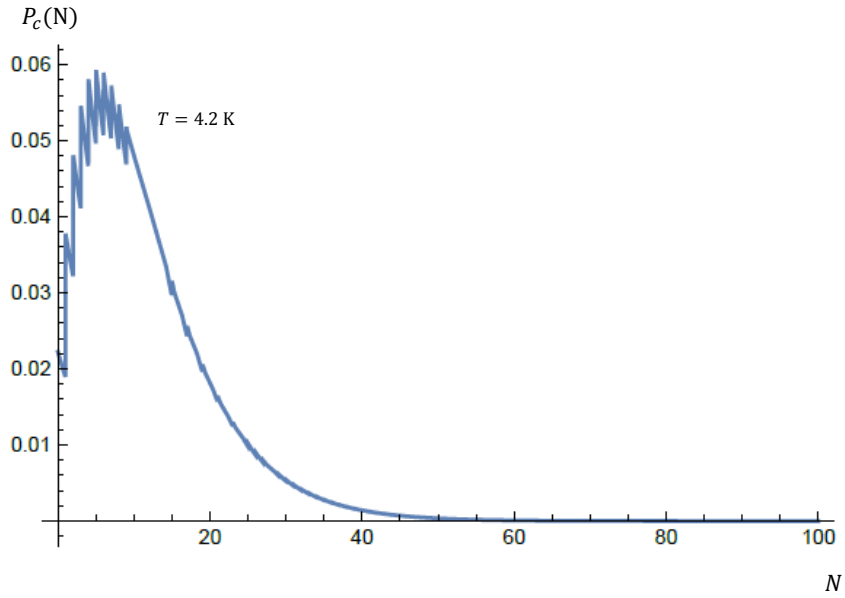

Figure 9.12: Plot of $P_c(N)$ (9.80), the probability of each manifold of N levels after coupling, where $T = 4.2\,\mathrm{K}$, and $\chi_0 = 0.2\,\delta$.

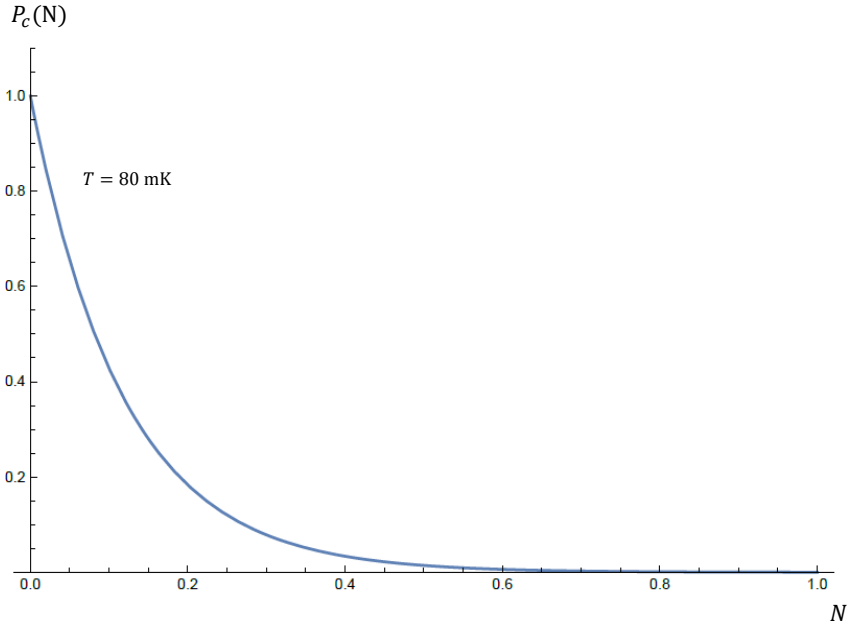

Figure 9.13: Plot of $P_c(N)$ (9.80), the probability of each manifold of N levels after coupling, where $T = 80\,\mathrm{mK}$, and $\chi_0 = 0.2\,\delta$.

9.7.3 Landau-Zener-Stückelberg interference for the coupled oscillator spectrum, $|\chi_0| > 0$, $|\chi| > 0$

A careful analysis of LZS driving for *multi*-anticrossing systems is beyond the scope of this thesis. In [87], an analytical method of studying the dynamics of such a system is proposed, where driving by a single large-amplitude triangle pulse is considered. This is a useful starting point for the Penning trap calculation, and their results for a three-level system are in agreement with the interference patterns observed experimentally [109].

Following this, suppose that the occupation probability of a given l level within a particular N manifold after a period of LZS driving is then given by some function $P_{\mathrm{LZS}}(N, l)$. Then the total probability $P_T(N, l)$ of occupation of a level (N, l) (or equivalently (n_+, n_z)) after a period of LZS driving in the Penning trap is given by

$$P_T(N, l) = P_c(N)\, P_{\mathrm{LZS}}(N, l). \tag{9.83}$$

This is simply a product of the probability arising from mode coupling with $\chi = 0$ (9.80), and that of LZS driving in an N-level system. In this way, *each* pair of (N, l) levels, equivalent to pairs of (n_+, n_z) levels of the spectrum, generates a unique interference pattern.

It is clear from Figure 9.13 that mK temperatures guarantee a lower occupation number N after coupling. Thus only the lowest levels in the spectrum would be involved when the driving field is switched on, $|\chi| > 0$. In the limit $T \to 0$, the occupation probability of the upper adiabatic level in (9.68) would be more readily applicable in the Penning trap. However, the following subsection discusses how it may be possible to effectively ignore all but the $N = 1$ level of the spectrum when measurements are made, despite the finite temperature of the system.

9.7.4 Proposed detection of Landau-Zener-Stückelberg interference in the Penning trap

An LZS interference pattern for a TLS is generated by effective measurement of the population of the upper adiabatic level as the offset χ_0 and amplitude χ of the driving field are varied, as in Figure 9.4. In terms of the applied potential for the Penning trap, this involves varying A (the offset) and B (the amplitude) in (9.3) respectively. Suppose again that the electron is in the pure state $N = 1$ before the coupling field is applied. A measurement of the frequency corresponding to the upper adiabatic energy level, $\omega_0 + \sqrt{\delta^2 + (\chi + \chi_0)^2}/2$, would indicate maximum probability of occupation of the dressed $N = 1, l = -1$ level. If

the measurement of the axial frequency was repeated several times, a probability of measuring this value for a given A and B field strength could be found. In this way, repeated measurements of the axial frequency for each value of A and B would enable the build up of an LZS interference pattern such as that shown in Figure 9.4.

As discussed, the Penning trap is not a TLS. However, measurement of the average quantum number of the modes [46] after a period of driving could generate exact interference patterns of such a system.

The procedure is as follows. The LZS driving field is applied for a given period of time[4], and the average quantum numbers of the two modes, $\overline{n}_+$ and $\overline{n}_z$, measured when the field is switched off. The average quantum number $\overline{n}$ of a general mode is related to the probability distribution $P(n)$ in a thermal state by the following relation [41]:

$$P(n) = \frac{\overline{n}^n}{(\overline{n}+1)^{n+1}}. \tag{9.84}$$

In this way, a measurement of $\overline{n}_+$ and $\overline{n}_z$ in the Penning trap produces a distribution $P(n_+)P(n_z)$. This is none other than an experimentally obtained distribution $P_T(N,l)$ (9.83). The process is repeated for new values of the field strength B and offset A in (9.4), and a new distribution $P_T(N,l)$ produced. A single value for a *specific* N and l, plotted at each new value $\{A,B\}$, builds up a density plot $P_T(N,l)$.

For example, $P(n_+=1)$ and $P(n_z=0)$ could be determined, through (9.84), from a measurement of $\overline{n}_+$ and $\overline{n}_z$. As A and B change, these values are again measured, and $P(n_+=1)\cdot P(n_z=0)$ recorded on a density plot of A vs. B, until a continuation of the process builds up the graph. This is exactly a plot of $P_T(N=1,l=-1)$, and a such can be compared directly to the theoretically obtained distribution $P_T(N=1,l=-1)=P_c(N=1)P_{\mathrm{LZS}}(N=1,l=-1)$ (9.83). Now, the distribution $P_{\mathrm{LZS}}(N=1,l=-1)$ is exactly $\overline{P_+}$ in (9.68) from conventional LZS theory for a TLS. Meanwhile, $P_c(N=1)$ is a single value directly determined from (9.80), and as such can be factored out of the plotted values. In this way, it is proposed that the interference pattern in Figure 9.4 could be exactly generated by the axial and cyclotron levels in the Penning trap, coupled by the potential in (9.4).

9.8 Further considerations

Some further deviations from the standard theory of LZS driving are now briefly discussed.

[4]The period of driving must be long enough such that the theory in 9.4 and 9.5 is applicable.

9.8.1 Decoherence

In the above analysis, it was assumed that the transition time between two levels, given by half the period of the driving cycle, is much less than the coherence time of the system, (9.45). In the strong decoherence limit, there will be no resulting LZS interference [90, 110]. As the coherence time (or driving frequency φ) increases, resultant interference patters will then depend upon how many adiabatic transitions can take place within this time. For example, if transitions resulting from different driving cycles are separated by more than the coherence time, then they act as independent contributions to a given pattern [90]. In this way, the coherence of the system, an essential ingredient in quantum information processing [111], can be probed [110].

9.8.2 The elliptical trap

In 8.4 it was shown how the mode coupling calculation of Chapter 2 is modified for the elliptical Penning trap. It follows that the LZS driving field in (9.4) can also be suitably adapted by the replacement $\omega_+ \to \tilde{\omega}_+$ in each frequency defined in 9.7. The resultant LZS driving is then between energy levels of the squeezed Fock states which form the adiabatic basis of the system. This would again allow for study of LZS interference beyond conventional theory.

Further theory of detection of any LZS interference in the Penning trap must be an ongoing topic of investigation. Quite apart from the resulting experimental possibilities of the theory, the system itself presents quite a novel theoretical problem in quantum optics which seems worthy of further study. In particular, it would be interesting to address the coupled x and z levels discussed in Chapter 7 with a driving field, and to investigate whether this enabled a type of spatial interference in the trap.

Chapter 10

Manipulating the Potential Landscape

This thesis has explored a dressed-atom approach [57] in the quantum theory of the Penning trap, motivated by the mode coupling calculation introduced in Chapter 2. In particular, a parallel between this calculation, and the ability to spatially vary the trapping potential in an atom trap with RF-induced coupling [60], was drawn. This chapter re-examines this apparent parallelism.

10.1 Comparison of RF dressing in atom traps and mode coupling in Penning traps: continued

This section follows from 2.5, addressing some of the main challenges in pursuing modification of the potential landscape in a Penning trap through sideband coupling. Chapter 7 repeated the sideband coupling calculation in the $\{x, y\}$ basis, and it is in this basis that the present considerations are discussed. In this section, the effective field strength ξ (2.12) used throughout both Chapter 2 and 7 becomes $\xi(\hat{x}, \hat{z})$,

$$\xi \rightarrow \xi(\hat{x}, \hat{z}), \tag{10.1}$$

to indicate a proposed variation in space. Appropriate forms of this field strength are discussed in later sections.

10.1.1 Rotation around $\hat{J}_2$

A few things are noted from analysis of the creation of a double well in the dressed-atom calculation in 2.4.1 [62]. Analogous attempts in the Penning trap through the effective

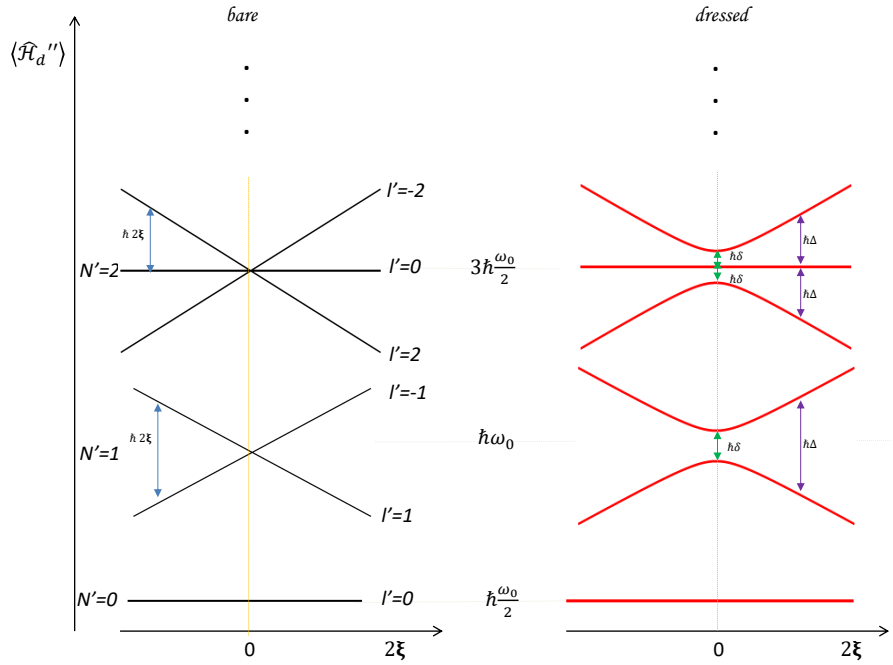

Figure 10.1: The bare and dressed potentials of the coupled cyclotron and axial energy levels in a frame rotated through an angle $-\pi/2$ around $\hat{I}_1$, $-\omega_p t$ around $\hat{J}_3$ and $-\pi/2$ around $\hat{J}_2$. The size of the splitting Δ is defined in (2.17).

field strength $\xi(\hat{x},\hat{z})$ require that this term is present in both the diabatic and adiabatic energy levels of the coupled Hamiltonian (7.13): the amplitude of the $\hat{J}_3$ eigenvalue must be proportional to $\xi(\hat{x},\hat{z})$ before dressing. One way to ensure a $\xi(\hat{x},\hat{z})\cdot\hat{J}_3$ term in this Hamiltonian requires that a contribution of $(\hat{n}_z-\hat{n}_x)$ "survives" the secular approximation of the coupling potential in (7.3). For a general harmonic oscillator with principle quantum number n, the oppositely rotating time dependence of $\hat{a}^\dagger$ and $\hat{a}$ will always ensure that $\hat{n}$ has no time dependence in a Hamiltonian. In this way, a remaining $(\hat{n}_z-\hat{n}_x)$ term in the coupling potential 7.3 would demand zero time dependence of the coupling field: only a *static* electric field could produce $\xi(\hat{x},\hat{z})\hat{J}_3$ in Hamiltonian 7.13. By this approach, the only way of having spatial control of the potentials is the addition of more electrodes contributing the desired static potential energy.

There is of course another approach. A $-\pi/2$ rotation of $\hat{\mathcal{H}}_d'$ around the local y axis results in:

$$\begin{aligned}\hat{\mathcal{H}}_d'' &= \exp\left\{\frac{i}{\hbar}\left(-\frac{\pi}{2}\right)\hat{J}_2\right\}\left(\omega_0\hat{J}_0+\delta\hat{J}_3+2\xi\hat{J}_1+\frac{\hbar\omega_0}{2}\right)\exp\left\{\frac{i}{\hbar}\left(\frac{\pi}{2}\right)\hat{J}_2\right\}\\ &= \omega_0\hat{J}_0+\delta\hat{J}_1-2\xi\hat{J}_3+\frac{\hbar\omega_0}{2}.\end{aligned} \tag{10.2}$$

Figure 10.1 shows a plot of the bare and dressed potentials of this Hamiltonian. In

comparison to the analogous plot of the levels before the $-\pi/2$ rotation around $\hat{J}_2$ (Figure 2.2), it is clear that the roles of δ and 2ξ have been swapped. In addition, the z mode now corresponds to the lower diabatic and adiabatic states, due to the negative contribution of $\hat{J}_3$ in (10.2).

10.1.2 The unknown form of $\xi(\hat{x}, \hat{z})$

The form of $\xi(\hat{x}, \hat{z})$ in the Geonium Chip would be controlled by the configuration of the MW generators and transmission lines. This configuration must be set by what is required to manipulate the potential energy of the electron in the trap in a desired way. Furthermore, the frame transformations between the lab, in which the physical field is produced, and the frame of the Hamiltonian $\mathcal{H}_d''$, are numerous: it has been rotated through $-\pi/2$ around $\hat{I}_1$, $-\omega_p t$ around $\hat{J}_3$ and $-\pi/2$ around $\hat{J}_2$. It is necessary to analyse how the generalised coordinates $\hat{x}$, $\hat{z}$, $\hat{p}_x$ and $\hat{p}_z$ transform under these various operations.

Transformation of coordinates

Combined transformation of the quantum coordinates of the Penning trap by $-\pi/2$ around $\hat{I}_1$, $-\omega_p t$ around $\hat{J}_3$ and a general angle θ around $\hat{J}_2$ are detailed in Appendix D. At this point, the careful distinction made between transformation to a new reference frame, and dressing of energy levels within an original frame, becomes crucial. The first two rotations, by $\hat{I}_1$ and $\hat{J}_3$, are interpreted as transformations upon the canonical coordinates of the system. In a frame further rotated through $-\pi/2$ by $\hat{J}_2$, the dressed levels on the right hand side of Figure 10.1 occur. In this way, the effective rotation through θ by $\hat{J}_2$ should *not* be incorporated into the total rotation of the coordinate system. As now shown, the results of Chapter 5 enable an elegant interpretation of the effects of the $-\pi/2$ rotation upon the system coordinates.

Since the harmonic oscillators of the x and z modes are not isotropic, transformation around $\hat{J}_2$ is *not* around the real y axis in the Penning trap. In 5.9, it was shown how such a rotation in real space could only be achieved by $\hat{\mathcal{J}}_2$, the anisotropic form of $\hat{J}_2$, equivalent to $\hat{L}_y/2$. From (5.57), the inverse mapping $\hat{\mathcal{J}}_2 \to \hat{J}_2$ is given by

$$\hat{J}_2 = \hat{S}^\dagger(\zeta_x)\hat{S}^\dagger(\zeta_z)\hat{\mathcal{J}}_2\hat{S}(\zeta_z)\hat{S}(\zeta_x). \tag{10.3}$$

Using the operator theorem $\exp(\chi\hat{O})f[\hat{A}]\exp(-\chi\hat{O}) = f[\exp(\chi\hat{O})\hat{A}\exp(-\chi\hat{O})]$ [41], transformation of a general operator $\hat{A}$ through an angle Φ by $\hat{J}_2$ can be rewritten in the

following way:

$$\begin{aligned}
&\exp\left\{\frac{i}{\hbar}\Phi\hat{J}_2\right\}\hat{A}\exp\left\{-\frac{i}{\hbar}\Phi\hat{J}_2\right\}\\
&=\exp\left\{\frac{i}{\hbar}\Phi\left(\hat{S}^\dagger(\zeta_x)\hat{S}^\dagger(\zeta_z)\hat{\mathcal{J}}_2\hat{S}(\zeta_z)\hat{S}(\zeta_x)\right)\right\}\hat{A}\exp\left\{-\frac{i}{\hbar}\Phi\left(\hat{S}^\dagger(\zeta_x)\hat{S}^\dagger(\zeta_z)\hat{\mathcal{J}}_2\hat{S}(\zeta_z)\hat{S}(\zeta_x)\right)\right\}\\
&=\hat{S}^\dagger(\zeta_x)\hat{S}^\dagger(\zeta_z)\exp\left\{\frac{i}{\hbar}\Phi\hat{\mathcal{J}}_2\right\}\left(\hat{S}(\zeta_z)\hat{S}(\zeta_x)\,\hat{A}\,\hat{S}^\dagger(\zeta_x)\hat{S}^\dagger(\zeta_z)\right)\exp\left\{-\frac{i}{\hbar}\Phi\hat{\mathcal{J}}_2\right\}\hat{S}(\zeta_z)\hat{S}(\zeta_x).
\end{aligned}\tag{10.4}$$

From (5.36) it is straightforward to calculate

$$\begin{aligned}
\hat{S}(\zeta_x)\hat{S}(\zeta_z)\,\hat{x}\,\hat{S}^\dagger(\zeta_z)\hat{S}^\dagger(\zeta_x)&=\exp(\zeta_x)\,\hat{x},\\
\hat{S}(\zeta_x)\hat{S}(\zeta_z)\,\hat{z}\,\hat{S}^\dagger(\zeta_z)\hat{S}^\dagger(\zeta_x)&=\exp(\zeta_z)\,\hat{z}.
\end{aligned}\tag{10.5}$$

Now, following the results of 5.9:

$$\begin{aligned}
\exp\left\{\frac{i}{\hbar}\left(-\frac{\pi}{2}\right)\hat{\mathcal{J}}_2\right\}\hat{x}\exp\left\{\frac{i}{\hbar}\left(\frac{\pi}{2}\right)\hat{\mathcal{J}}_2\right\}&=\frac{1}{\sqrt{2}}\left(\hat{x}-\hat{z}\right),\\
\exp\left\{\frac{i}{\hbar}\left(-\frac{\pi}{2}\right)\hat{\mathcal{J}}_2\right\}\hat{z}\exp\left\{\frac{i}{\hbar}\left(\frac{\pi}{2}\right)\hat{\mathcal{J}}_2\right\}&=\frac{1}{\sqrt{2}}\left(\hat{z}+\hat{x}\right),
\end{aligned}\tag{10.6}$$

so that the total transformation of $\hat{x}$ and $\hat{z}$ around $\hat{J}_2$ through $\Phi=-\pi/2$ results in the mapping

$$\begin{aligned}
\hat{x}&\to\frac{1}{\sqrt{2}}\left(\hat{x}-\exp(\zeta_x-\zeta_z)\hat{z}\right),\\
\hat{z}&\to\frac{1}{\sqrt{2}}\left(\hat{z}+\exp(\zeta_z-\zeta_x)\hat{x}\right),
\end{aligned}\tag{10.7}$$

and $\hat{y}$ remains unchanged. Likewise, transformation of the respective momentum components is calculated as

$$\begin{aligned}
\hat{p}_x&\to\frac{1}{\sqrt{2}}\left(\hat{p}_x-\exp(\zeta_z-\zeta_x)\hat{p}_z\right),\\
\hat{p}_z&\to\frac{1}{\sqrt{2}}\left(\hat{p}_z+\exp(\zeta_x-\zeta_z)\hat{p}_x\right).
\end{aligned}\tag{10.8}$$

From (5.48), for the present case where $\omega_x\equiv\omega_1/2$, the squeezing parameters are defined by

$$(\zeta_z-\zeta_x)=\tanh^{-1}\left[\frac{\sqrt{\frac{\omega_1}{2\omega_z}}-\sqrt{\frac{2\omega_z}{\omega_1}}}{\sqrt{\frac{\omega_1}{2\omega_z}}+\sqrt{\frac{2\omega_z}{\omega_1}}}\right].\tag{10.9}$$

For a Penning trap with $V_r=1\,\mathrm{V}$, $|\vec{B}|=0.5\,\mathrm{T}$, $\exp(\zeta_z-\zeta_x)\approx 19$. As $\omega_1/2\to\omega_z$ for isotropic trapping in the xz plane, $\exp(\zeta_z-\zeta_x)\to 1$, and the transformations in (10.7) and (10.8) reduce to a $-\pi/4$ rotation around the real y axis.

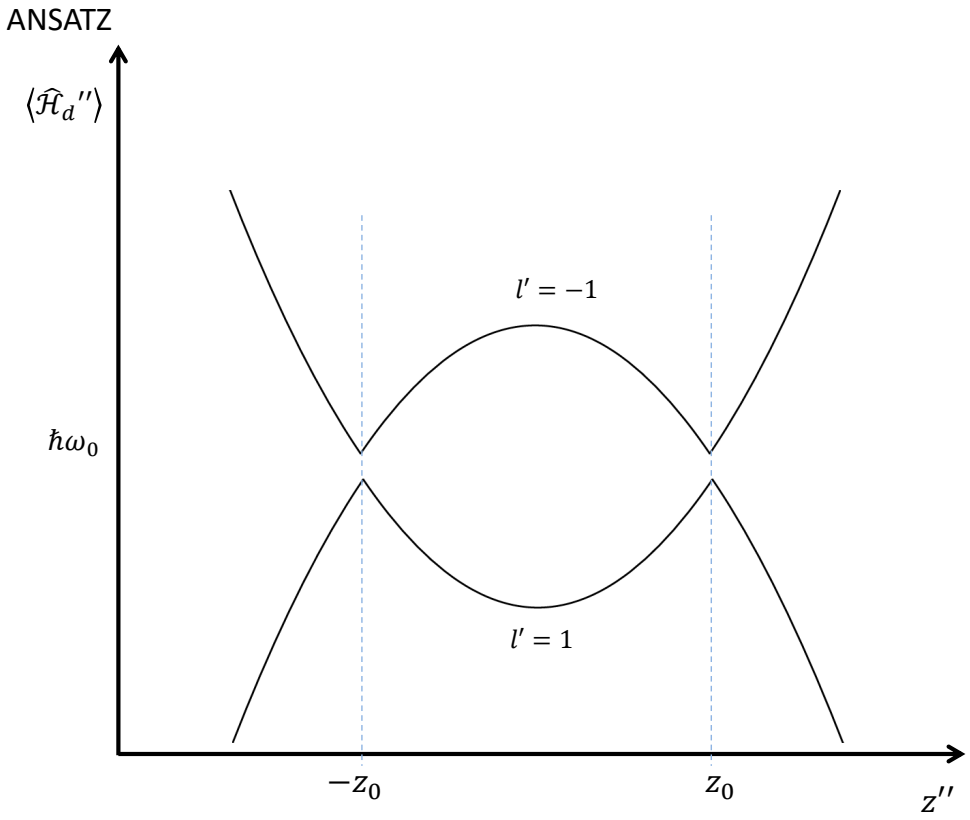

Figure 10.2: A field strength $\xi(z_0) = \xi(-z_0) = 0$ in the frame of $\hat{\mathcal{H}}_d''$ in (10.2) would result in a double well structure of the adiabatic $N' = 1$ levels.

$\xi(\hat{x}, \hat{z})$ in the laboratory

Let's denote the z coordinate in the "dressed frame" by z''. Supposing the coupling strength ξ could be equal to zero at two points along the $\hat{z}''$ axis within the trapping region, at some coordinates z_0 and $-z_0$, then the adiabatic levels of $N = 1$ in the frame of $\hat{\mathcal{H}}_d''$ (10.2) would assume the shape in Figure 10.2. Such a $\xi(\hat{z}'')$ in this frame could result from a sinusoidal function. As an example, the bare and dressed levels for the field strength $\xi(\hat{z}'') = A/2\cos(k\hat{z}'')$ are shown in Figure 10.3.

Of course, $\xi(\hat{z}'')$ must be transformed back the laboratory frame in order to determine the form of the electric field which would generate these adiabatic potentials. Using the results of (10.7), the resulting potential as would be generated in the lab is non-physical; it violates Maxwell's equation $\vec{\nabla} \cdot \vec{E} = 0$ [38].

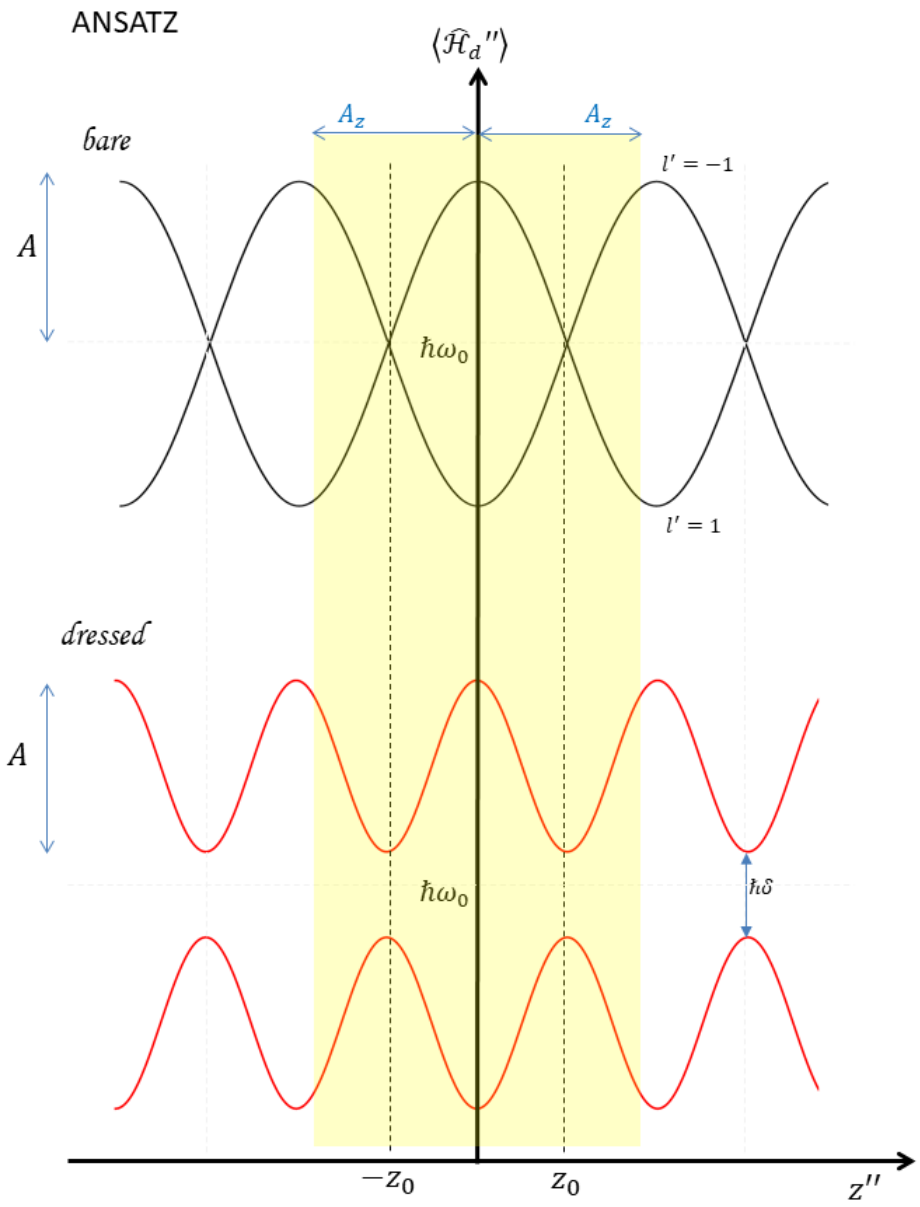

Figure 10.3: The bare and dressed energy levels of the $N' = 1$ cyclotron-axial coupled Hamiltonian in the frame of reference of $\hat{\mathcal{H}}_d''$ (10.2), where the spatial dependence of the coupling field strength in this frame is given by an ansatz field strength $\xi(\hat{z}'') = A/2\cos(k\hat{z}'')$. The amplitude of the electron's motion along this axis is indicated by the yellow region, where A_z is defined in (1.26). The depth of the well could be controlled by A, and the separation of the central maxima by $z_0 = \pi/k$. The size of the avoided crossing is given by δ. The electron would encounter the double well of the upper adiabatic energy as shown in the diagram only if the amplitude of motion was approximately the same size of half the wavelength of $\xi(\hat{z}'')$, i.e. if $A_z \gtrsim \pi/k$. Increasing this amplitude, or increasing the wavenumber k, would expose the electron to an increasing number of energy wells.

10.1.3 The potential energy

A further complication is that both potential *and* kinetic energy terms are contained in the Schwinger boson operator set $\underline{J}$. In reference to the ansatz for $\xi(\hat{z}'')$ plotted in Figure 10.3, both the diabatic and adiabatic energy levels represent the total energy of $l = 1$ and $l = -1$ for this field strength. To modify the potential energy along the z and/ or x axis alone, the resulting coupling term should be a function of $\hat{z}$ and/ or $\hat{x}$ operators *only*. For a coupling potential of the form $\hat{x}\hat{z}$, this implies that all four of the following terms should be present in the Hamiltonian:

$$\hat{a}_z^\dagger \hat{a}_x + \hat{a}_x^\dagger \hat{a}_z + \hat{a}_z^\dagger \hat{a}_x^\dagger + \hat{a}_z \hat{a}_x. \tag{10.10}$$

From (2), when this term is rotated around the $\hat{J}_2$ axis, it produces the following:

$$\begin{aligned} \xrightarrow{\Phi \hat{J}_2} & \cos\Phi \left(\hat{a}_z^\dagger \hat{a}_x + \hat{a}_x^\dagger \hat{a}_z \right) + \sin\Phi \left(\hat{a}_z^\dagger \hat{a}_z - \hat{a}_x^\dagger \hat{a}_x \right) \\ & + \left(\cos^2 \frac{\Phi}{2} - \sin^2 \frac{\Phi}{2} \right) \left(\hat{a}_z^\dagger \hat{a}_x^\dagger + \hat{a}_z \hat{a}_x \right) \\ & + \cos\frac{\Phi}{2} \sin\frac{\Phi}{2} \left(\hat{a}_z^\dagger \hat{a}_z^\dagger + \hat{a}_z \hat{a}_z - \left(\hat{a}_x^\dagger \hat{a}_x^\dagger + \hat{a}_x \hat{a}_x \right) \right). \end{aligned} \tag{10.11}$$

In terms of the mode operators (1.37, 4.22, 4.23), $\hat{x}^2$ and $\hat{z}^2$ are written

$$\hat{x}^2 = \frac{\hbar}{m\omega_1} \left(\hat{a}_x^\dagger \hat{a}_x^\dagger + \hat{a}_x \hat{a}_x + 2 \left(\hat{n}_x + \frac{1}{2} \right) \right), \tag{10.12}$$

$$\hat{z}^2 = \frac{\hbar}{2m\omega_z} \left(\hat{a}_z^\dagger \hat{a}_z^\dagger + \hat{a}_z \hat{a}_z + 2 \left(\hat{n}_z + \frac{1}{2} \right) \right). \tag{10.13}$$

It is clear from (10.11) that a $\pi/2$ rotation around $\hat{J}_2$ transforms (10.10) to a sum of $\hat{z}^2$ and $-\hat{x}^2$, in the same way $\hat{J}_1 \xrightarrow{(\pi/2)\hat{J}_2} \hat{J}_3$.

The anisotropic Schwinger boson operators

The sum of operators in (10.10) is none other than operator $\hat{\mathcal{J}}_1$ (5.57) further squeezed in the limit $\zeta_x \to \infty$, $\zeta_x \to \infty$. Likewise, an infinitely squeezed $\hat{\mathcal{J}}_3$ would reveal a sum of $\hat{x}^2$ and $\hat{z}^2$.

In the Penning trap, the set $\underline{\mathcal{J}}$ is formed with the squeezing parameters strictly given by (10.9). Denoting the set $\underline{\mathcal{J}}$ in the infinitely squeezed limit as $\underline{\mathcal{J}}_\infty$, the "correct" operator to use for the transformation $\hat{x}\hat{z} \to \hat{x}^2 - \hat{z}^2$ is therefore $\hat{\mathcal{J}}_{2,\infty}$. It is interesting to examine this a little more closely. Similarly to the $\hat{x}$ coordinate in (10.12), the operator $\hat{p}_x^2$ can be written in the following way in terms of the $\hat{a}_x$ mode operators of the Penning trap (4.22):

$$\hat{p}_x^2 = \frac{\hbar m \omega_1}{4} \left(2\hat{n}_x + 1 - \left(\hat{a}_x^\dagger \hat{a}_x^\dagger + \hat{a}_x \hat{a}_x \right) \right). \tag{10.14}$$

Direct squeezing transformations upon these potential and kinetic "coordinates" by the operators defined in (5.35) are straightforward to calculate:

$$\begin{aligned}\hat{S}(\zeta_x)\hat{x}^2\hat{S}^\dagger(\zeta_x) &= \hat{x}^2\exp(2\zeta_x)\,,\\ \hat{S}(\zeta_x)\hat{p}_x^2\hat{S}^\dagger(\zeta_x) &= \hat{p}_x^2\exp(-2\zeta_x)\,,\end{aligned} \tag{10.15}$$

so that in the infinitely squeezed limit:

$$\hat{x}^2 \overset{\zeta_x\to\infty}{\longrightarrow} \infty, \qquad \hat{p}_x^2 \overset{\zeta_x\to\infty}{\longrightarrow} 0, \tag{10.16}$$

where results for the $\hat{z}$ and $\hat{p}_z$ operators follow analogously. This is in general agreement with the result of the quadrature squeezing achieved by these operators [112]. The relevant consequence of (10.16) is as follows. The zeroth, first and third component operators of any Schwinger boson set become, in the limit of (positively) infinite squeezing, operators comprised entirely of potential energy coordinates. Furthermore, if the squeeze parameters of the two modes are identical, then $\hat{\mathcal{J}}_2$ remains unchanged. In other words, a vector pointing along an axis with its perpendicular plane squeezed by the *same* amount in both directions will remain pointing along that axis. In contrast, the zeroth, first and third components contain only separate position and momentum operators, so that their coordinate representation changes dramatically upon squeezing of the axis, in accordance with (10.16).

The sets $\underline{\mathcal{J}}$, $\underline{\mathcal{J}}_\zeta$ and $\underline{\mathcal{J}}_\infty$

$\underline{\mathcal{J}}$: From (5.10), the definition of the set $\underline{\mathcal{J}}$ of Schwinger boson operators in the Penning trap in terms of position and momentum operators is straightforward to determine. In the Penning trap with circular symmetry, the x and y motions are bound in an isotropic potential of frequency $\omega_1/2$, so that $\hat{I}_2/2$ is the real canonical momentum along the z axis:

$$\begin{aligned}\hat{S}(\zeta_x)\hat{S}(\zeta_y)\,\{\underline{I}\}\,\hat{S}^\dagger(\zeta_x)\hat{S}^\dagger(\zeta_y) &= \{\underline{I}\}\\ &\Longrightarrow \underline{I}\equiv\underline{\mathcal{I}}.\end{aligned} \tag{10.17}$$

That is, the set of Schwinger boson operators corresponding to the motion in the xy plane of the Penning trap does not need to be squeezed to form an appropriately commuting set around $\hat{L}z/2$. From (5.55), it therefore follows:

$$\zeta_x = \zeta_y = 0, \tag{10.18}$$

and so only the z axis in the Penning trap must be squeezed in order that all three components $\hat{I}_2$, $\hat{J}_2$ and $\hat{K}_2$ describe the three components of spatial angular momentum

in the trap. From (5.48), it is clear that this squeezing parameter ζ_z is given entirely by the right hand side of (10.9). This enables straightforward calculation of the components $\underline{\mathcal{J}}$ in terms of quantum coordinates:

$$\begin{aligned}
\hat{\mathcal{J}}_0 &= \frac{1}{8}m\omega_1(\hat{z}^2+\hat{x}^2)+\frac{1}{2m\omega_1}(\hat{p}_z^2+\hat{p}_x^2)-\frac{\hbar}{2},\\
\hat{\mathcal{J}}_1 &= \frac{1}{4}m\omega_1\hat{z}\hat{x}+\frac{1}{m\omega_1}\hat{p}_z\hat{p}_x,\\
\hat{\mathcal{J}}_2 &= \frac{1}{2}\left(\hat{z}\hat{p}_x-\hat{x}\hat{p}_z\right),\\
\hat{\mathcal{J}}_3 &= \frac{1}{8}m\omega_1(\hat{z}^2-\hat{x}^2)+\frac{1}{2m\omega_1}(\hat{p}_z^2-\hat{p}_z^2).
\end{aligned} \tag{10.19}$$

$\underline{\mathcal{J}}_\zeta$ and $\underline{\mathcal{J}}_\infty$: Rather than squeezing the x and z modes separately, the operator

$$\hat{S}_{xz}(\zeta)=\exp\left\{-\frac{\zeta}{2}\left(\hat{a}_x^{\dagger 2}-\hat{a}_x^2+\hat{a}_z^{\dagger 2}-\hat{a}_z^2\right)\right\};\quad \zeta\in\Re \tag{10.20}$$

is defined, which has the effect of squeezing the modes by equal degrees:

$$\begin{aligned}
\hat{S}_{xz}(\zeta)\hat{a}_{x(z)}\hat{S}_{xz}^\dagger(\zeta) &= \hat{a}_{x(z)}\cosh(\zeta)+\hat{a}_{x(z)}^\dagger\sinh(\zeta),\\
\hat{S}_{xz}(\zeta)\hat{a}_{x(z)}^\dagger\hat{S}_{xz}^\dagger(\zeta) &= \hat{a}_{x(z)}^\dagger\cosh(\zeta)+\hat{a}_{x(z)}\sinh(\zeta).
\end{aligned} \tag{10.21}$$

In terms of position and momentum operators, the set $\underline{\mathcal{J}}$ are transformed upon its application:

$$\begin{aligned}
\hat{\mathcal{J}}_{0,\zeta} &= \hat{S}_{xz}(\zeta)\hat{\mathcal{J}}_0\hat{S}_{xz}^\dagger(\zeta)=R\frac{1}{8}m\omega_1\left(\hat{z}^2+\hat{x}^2\right)+\frac{1}{2mR\omega_1}(\hat{p}_z^2+\hat{p}_x^2)-\frac{\hbar}{2},\\
\hat{\mathcal{J}}_{1,\zeta} &= \hat{S}_{xz}(\zeta)\hat{\mathcal{J}}_1\hat{S}_{xz}^\dagger(\zeta)=R\frac{1}{4}m\omega_1\left(\hat{z}\hat{x}\right)+\frac{1}{mR\omega_1}\hat{p}_z\hat{p}_x,\\
\hat{\mathcal{J}}_{2,\zeta} &= \hat{S}_{xz}(\zeta)\hat{\mathcal{J}}_2\hat{S}_{xz}^\dagger(\zeta)=\frac{1}{2}\left(\hat{z}\hat{p}_x-\hat{x}\hat{p}_z\right),\\
\hat{\mathcal{J}}_{3,\zeta} &= \hat{S}_{xz}(\zeta)\hat{\mathcal{J}}_3\hat{S}_{xz}^\dagger(\zeta)=R\frac{1}{8}m\omega_1\left(\hat{z}^2-\hat{x}^2\right)+\frac{1}{2mR\omega_1}(\hat{p}_z^2-\hat{p}_x^2),
\end{aligned} \tag{10.22}$$

where

$$R=\exp(2\zeta). \tag{10.23}$$

Defining the squeezing operator in the limit of (countably[1]) infinite squeezing

$$\hat{S}_\infty(\zeta)=\zeta\overset{\lim}{\to}\infty\left[\hat{S}_{xz}(\zeta)\right], \tag{10.24}$$

and the transformed components

$$\hat{\mathcal{J}}_{0,\infty}=\hat{S}_\infty(\zeta)\hat{\mathcal{J}}_0\hat{S}_\infty^\dagger(\zeta),\quad \hat{\mathcal{J}}_{1,\infty}=\hat{S}_\infty(\zeta)\hat{\mathcal{J}}_1\hat{S}_\infty^\dagger(\zeta),\quad \hat{\mathcal{J}}_{3,\infty}=\hat{S}_\infty(\zeta)\hat{\mathcal{J}}_3\hat{S}_\infty^\dagger(\zeta), \tag{10.25}$$

it is clear that they become functions of position coordinates only, while $\hat{\mathcal{J}}_2$ remains unchanged.

[1] From (5.55), the limit is defined by $\tanh(\zeta)=1$. Since the tanh function tends to its limiting value of one very rapidly, it follows that the infinite limit of ζ is countable.

The potential energy quantum number

The unitary nature of the squeezing operator reveals

$$\begin{aligned}\hat{S}_{xz}(\zeta)\hat{J}_3\hat{S}_{xz}^{\dagger}(\zeta)\cdot\hat{S}_{xz}(\zeta)|n_x,n_z\rangle &= \hat{S}_{xz}(\zeta)\hat{J}_3|n_x,n_z\rangle \\ &= \hat{S}_{xz}(\zeta)\,\frac{\hbar}{2}l'|n_x,n_z\rangle \\ &= \frac{\hbar}{2}l'\left(\hat{S}_{xz}(\zeta)|n_x,n_z\rangle\right). \end{aligned} \tag{10.26}$$

Without loss of generality, the squeezed Fock states $\hat{S}_{xz}(\zeta)|n_x,n_z\rangle$ are the eigenstates of the squeezed angular momentum components with eigenvalues $\hbar/2\,l'$. Now, (10.25) shows how $\hat{\mathcal{J}}_3$ becomes a function of position operators as $\zeta\to\infty$. The eigenstates in this limit are given by

$$\hat{S}_{\infty}(\zeta)|n_x,n_z\rangle, \tag{10.27}$$

and it therefore follows

$$\hat{\mathcal{J}}_{3,\infty}\;\hat{S}_{\infty}(\zeta)|n_x,n_z\rangle = \Gamma\frac{1}{8}m\omega_1\left(\hat{z}^2-\hat{x}^2\right)\;\hat{S}_{\infty}(\zeta)|n_x,n_z\rangle, \tag{10.28}$$

where

$$\Gamma=\zeta\overset{\lim}{\to}\infty\,[\exp(\zeta)]\,. \tag{10.29}$$

Comparing this to (10.26), it appears that in the infinitely squeezed limit

$$\Gamma\frac{1}{8}m\omega_1\left(\hat{z}^2-\hat{x}^2\right)\;\hat{S}_{\infty}(\zeta)|n_x,n_z\rangle\to\frac{\hbar}{2}l'\,\hat{S}_{\infty}(\zeta)|n_x,n_z\rangle. \tag{10.30}$$

This suggests that the squeezed Fock states in this limit, $\hat{S}_{\infty}(\zeta)|n_x,n_z\rangle$, become eigenstates of the potential energy of the system only. It is evident, however, that these states are not identically $|x,z\rangle$. This can be seen by considering the following:

$$\begin{aligned}\langle n_x,n_z|\hat{J}_1|n_x,n_z\rangle &= 0 \\ \Longrightarrow\langle n_x,n_z|\hat{\mathcal{J}}_1|n_x,n_z\rangle &= 0 \\ \langle n_x,n_z|\,\hat{S}_{\infty}^{\dagger}(\zeta)\hat{S}_{\infty}(\zeta)\;\hat{\mathcal{J}}_1\;\hat{S}_{\infty}^{\dagger}(\zeta)\hat{S}_{\infty}(\zeta)\,|n_x,n_z\rangle &= 0 \\ \Longrightarrow\langle n_x,n_z|\,\hat{S}_{\infty}^{\dagger}(\zeta)\;\hat{\mathcal{J}}_{1,\infty}\;\hat{S}_{\infty}(\zeta)|n_x,n_z\rangle &= 0. \end{aligned} \tag{10.31}$$

That is, just as $\hat{J}_1$ is non-diagonal in the number state basis, $\hat{\mathcal{J}}_{1,\infty}$ is non-diagonal in the infinitely squeezed Fock basis. From (10.25):

$$\langle x,z|\hat{\mathcal{J}}_{1,\infty}|x,z\rangle=\Gamma\frac{1}{4}m\omega_1(xz). \tag{10.32}$$

Comparing this to (10.31), it therefore follows:

$$\hat{S}_{\infty}(\zeta)|n_x,n_z\rangle\neq|x,z\rangle. \tag{10.33}$$

10.1.4 The adiabatic basis

Consider again the creation of a double well through the RF-induced potentials in atom traps [62], as discussed in 2.4. In the calculation, the kinetic energy contribution of the dressed system is effectively thrown away [60], and in this way the remaining potential (2.47) in the Hamiltonian becomes the *adiabatic* potential of the system.

The consequence of seeking a variation in the *potential* energy of the Penning trap through some $\xi(\hat{x}, \hat{z})$, is that the resulting potential term is no longer adiabatic in the same sense. Thus the problem becomes one of finding a potential which can be *approximated* as adiabatic as closely as possible.

Plotting the resulting potential of some $f(\hat{x}, \hat{z})$ in a coupled Hamiltonian effectively measures this term in the basis $|x, z\rangle$:

$$\langle x, z|f(\hat{x}, \hat{z})|x, z\rangle = f(x, z); \tag{10.34}$$

f is an arbitrary function of the x and z coordinates. Yet 10.1.3 suggests that $\hat{S}_\infty|n_x, n_z\rangle$, and *not* $|x, z\rangle$, is the adiabatic basis of potential energy. A useful potential energy term resulting from some $\xi(\hat{x}, \hat{z})$ must therefore behave appropriately along the x and z axis, with a diagonal form in the potential energy basis.

10.2 Generating a sinusoidal potential (I)

10.2.1 The electric field and quantum potential

The following classical electric field component is defined:

$$E_{d,x} = [\epsilon_d \cos(\omega_d\, t) \cos\left(k\, z\right) z]\, \hat{e}_x, \tag{10.35}$$

so that the potential is given by

$$V_d = -\int E_{d,x}\, dx = -\epsilon_d \cos(\omega_d\, t) \cos(k\, z)\, z\, x. \tag{10.36}$$

In terms of quantum operators (1.37, 4.22, 4.23), this is written

$$\begin{aligned}\hat{V}_d &= -\epsilon_d \cos(\omega_d\, t) \cos(k\, \hat{z})\, \hat{z}\, \hat{x} \\ &= -\epsilon_d \cos(\omega_d\, t) \cos\left(k\sqrt{\frac{\hbar}{2m\omega_z}}(\hat{a}_z^\dagger + \hat{a}_z)\right) \times \\ &\quad \times \left(\frac{\hbar}{m}\sqrt{\frac{1}{2\omega_1\omega_z}}(\hat{a}_x^\dagger + \hat{a}_x)(\hat{a}_z^\dagger + \hat{a}_z)\right),\end{aligned} \tag{10.37}$$

which must first be transformed to the $\hat{I}_1$ frame (6.12) :

$$\begin{aligned}\hat{V}'_d &= \hat{U}_1\hat{V}_d\hat{U}_1^\dagger \\ &= -\epsilon_d\cos(\omega_d\,t)\cos\left(k\sqrt{\frac{\hbar}{2m\omega_z}}(\hat{a}_z^\dagger+\hat{a}_z)\right)\times \\ &\quad\times\frac{\hbar}{2m}\sqrt{\frac{1}{\omega_1\omega_z}}\left[\hat{a}_z^\dagger\hat{a}_x^\dagger+\hat{a}_z^\dagger\hat{a}_x+\hat{a}_x^\dagger\hat{a}_z+\hat{a}_z\hat{a}_x\right. \\ &\quad\left.-i\left(\hat{a}_z^\dagger\hat{a}_y^\dagger-\hat{a}_z^\dagger\hat{a}_y+\hat{a}_y^\dagger\hat{a}_z-\hat{a}_z\hat{a}_y\right)\right].\end{aligned} \tag{10.38}$$

The operator $\hat{U}_x(t)$ is defined

$$\hat{U}_x(t)=\exp\left\{i\omega_d t\left(\hat{n}_x+\frac{1}{2}\right)\right\}=\exp\left\{\frac{i}{\hbar}\omega_d\,t\left(\hat{J}_0-\hat{J}_3+\frac{1}{2}\right)\right\}, \tag{10.39}$$

so that, expanding out the $\cos(\omega_d t)$ term,

$$\begin{aligned}\hat{V}'_{dt} &= \hat{U}_x(t)\hat{V}'_d\hat{U}_x^\dagger(t) \\ &= -\frac{\epsilon_d}{2}\sqrt{\frac{\hbar}{2m\omega_1}}\cos(k\,\hat{z})\,\hat{z}\times \\ &\quad\times\left[\hat{a}_x^\dagger\left(e^{i(\omega_d+\omega_d)t}+\underbrace{e^{i(\omega_d-\omega_d)t}}_{RWA}\right)+\hat{a}_x\left(\underbrace{e^{i(-\omega_d+\omega_d)t}}_{RWA}+e^{i(-\omega_d-\omega_d)t}\right)\right. \\ &\quad\left.-i\hat{a}_y^\dagger\left(e^{i\omega_d t}+e^{-i\omega_d t}\right)+i\hat{a}_y\left(e^{i\omega_d t}+e^{-i\omega_- dt}\right)\right].\end{aligned} \tag{10.40}$$

Making a secular approximation,

$$\hat{V}'_{dt}=-\frac{\epsilon_d}{2\sqrt{2}}\cos(k\,\hat{z})\,\hat{z}\hat{x}. \tag{10.41}$$

10.2.2 The Hamiltonian

The static potential energy resulting from the potential in (10.41) is added to the Hamiltonian in the same frame of reference. From the Hamiltonian in the $\hat{I}_1$ frame (6.13), this must be further transformed by $\hat{U}_x(t)$. Since $\left[\hat{U}_x(t),\hat{\mathcal{H}}'\right]=0$, the only contribution is from the $i\hbar\dot{\hat{U}}_x(t)\hat{U}_x^\dagger(t)$ term:

$$\begin{aligned}&\hat{U}_x(t)\hat{\mathcal{H}}'\hat{U}_x^\dagger(t)+i\hbar\dot{\hat{U}}_x(t)\hat{U}_x^\dagger(t) \\ &=\hbar(\omega_+-\omega_d)\left(\hat{n}_x+\frac{1}{2}\right)-\hbar\omega_-\left(\hat{n}_y+\frac{1}{2}\right)+\hbar\omega_z\left(\hat{n}_z+\frac{1}{2}\right).\end{aligned} \tag{10.42}$$

Adding this to the potential energy from the coupling field, $q\hat{V}'_{dt}$:

$$\begin{aligned}\hat{\mathcal{H}}_{\cos} &\equiv \hat{U}_x(t)\hat{\mathcal{H}}'\hat{U}_x^\dagger(t)+i\hbar\dot{\hat{U}}_x(t)\hat{U}_x^\dagger(t)+q\hat{V}'_{dt} \\ &=\hbar(\omega_+-\omega_d)\left(\hat{n}_x+\frac{1}{2}\right)-\hbar\omega_-\left(\hat{n}_y+\frac{1}{2}\right)+\hbar\omega_z\left(\hat{n}_z+\frac{1}{2}\right)+\frac{e\epsilon_d}{2\sqrt{2}}\cos(k\,\hat{z})\hat{z}\hat{x} \\ &=(\omega_+-\omega_d+\omega_z)\hat{J}_0-(\omega_+-\omega_d-\omega_z)\hat{J}_3-\hbar\omega_-\left(\hat{n}_y+\frac{1}{2}\right)+\xi_d\cos(k\,\hat{z})\hat{z}\hat{x}+\hbar\frac{(\omega_+-\omega_d+\omega_z)}{2},\end{aligned} \tag{10.43}$$

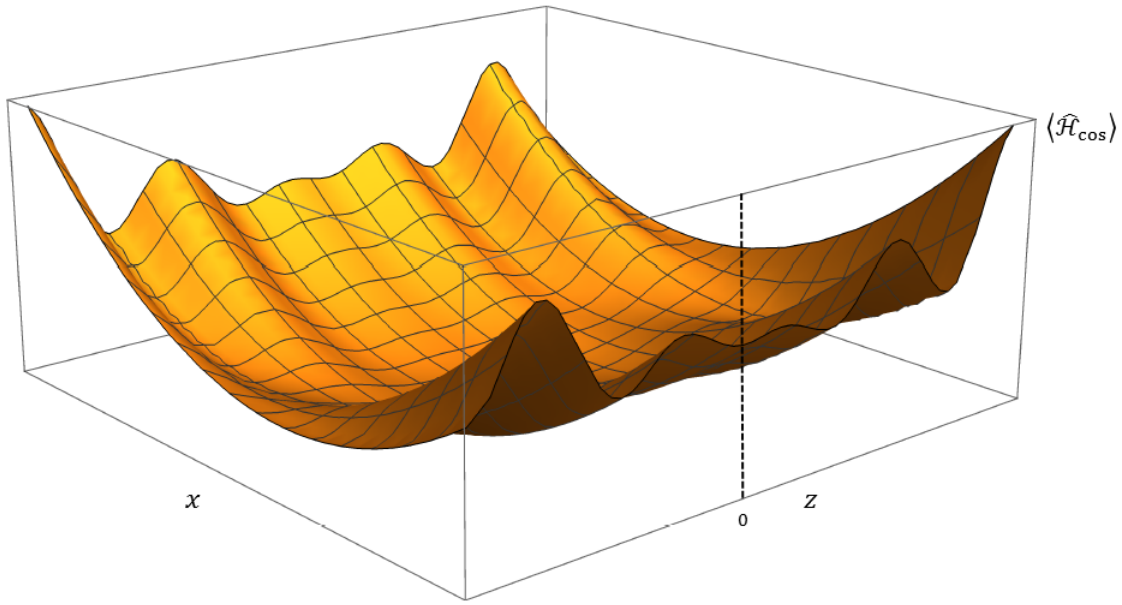

Figure 10.4: General form of $\langle x, z|\hat{\mathcal{H}}_{\cos}|x, z\rangle$ (10.43). In this frame of reference, the potential energy along the z axis is clearly modified by the cosine function of the coupling potential in (10.36).

where

$$\xi_d = \frac{e\,\epsilon_d}{2\sqrt{2}}. \tag{10.44}$$

The mixture of operator styles here looks a little cumbersome, but it is helpful in what follows.

10.2.3 Projection onto the real axes

The expectation value of the Hamiltonian (10.43) in the state $|x, z\rangle$ is found, and the result is a 3D plot of the potential energy along the x and z axes, as shown in Figure 10.4.
The potential energy terms in (10.43) are already diagonal $|x, z\rangle$. Seeking a solution to this Hamiltonian, consider the following. At this point in the calculation, a further $\pi/2$ rotation around the real y axis by $\hat{\mathcal{J}}_2$ would transform the $\hat{x}\hat{z}$ in the coupling term into a symmetric contribution of $\hat{x}^2$ and $\hat{z}^2$. Likewise, $\cos(k\,\hat{z}) \to \cos(k/\sqrt{2}\,(\hat{z} + \hat{x}))$ by such a transformation. However, any rotation by $\hat{\mathcal{J}}_2$ in an effort to diagonalise the coupling term will result in non-diagonal contributions in the $\underline{J}$ terms of (10.43).

Removing the non-diagonal contributions

Two modifications must be made in order that Hamiltonian (10.43) remains "diagonal" after transformation around the real y axis. Firstly, the system must be made isotropic: $\omega_z = \omega_1/2$ must be set.[2] Secondly, the $\hat{J}_3$ term must be effectively removed from Hamiltonian (10.43). For this purpose,

$$\begin{aligned} \omega_+ - \omega_d =& \omega_z \\ \Longrightarrow \omega_d =& \omega_+ - \omega_z \end{aligned} \tag{10.45}$$

is set. The new isotropy of the two modes then implies $\hat{\mathcal{J}}_2 \to \hat{J}_2$ so that transformation by this operator should not affect $\hat{J}_0$ in Hamiltonian (10.43). It is redefined

$$\hat{\mathcal{H}}_{\cos} \to \hat{\mathcal{H}}_c = 2\omega_z \hat{J}_0 - \hbar\omega_- \left(\hat{n}_y + \frac{1}{2}\right) + \xi_d \cos(k\,\hat{z})\hat{z}\hat{x} + \hbar\omega_z. \tag{10.46}$$

10.3 Generating a sinusoidal potential (II)

10.3.1 The redefined axial operators

The calculation will proceed in this section with the modifications described in 10.2.3. Setting $\omega_z = \omega_1/2$, means that the ω_z terms in the definition of the mode operators $\hat{a}_z$ and $\hat{a}_z^\dagger$ (1.37) should be replaced by $\omega_1/2$. The result of this is that the set of Schwinger Boson operators $\underline{J}$ in (5.10) is now expanded out as the previous definition of the set $\underline{\mathcal{J}}$ as given in (10.19). However, no squeezing operators have been applied in the calculation; as should be clear by now, the change of frequency is mathematically manifest as a squeezing transformation. In the following calculation, the use of the symbol ω_z will be continued only to distinguish contributions from the different modes, but the new definition of this frequency and the equivalence of $2\omega_z$ and ω_1 should be borne in mind throughout.

10.3.2 Rotation around the y axis

As discussed, a $-\pi/2$ transformation of Hamiltonian (10.46) around $\hat{J}_2$, now completely equivalent to a $-\pi/4$ rotation around the y axis, has the following effect upon Hamiltonian (10.46):

$$\begin{aligned} \hat{\mathcal{H}}_c'' &= \exp\left\{\frac{i}{\hbar}\left(-\frac{\pi}{2}\right)\hat{J}_2\right\}\left(\hat{\mathcal{H}}_c - \mathcal{H}_-\right)\exp\left\{\frac{i}{\hbar}\left(\frac{\pi}{2}\right)\hat{J}_2\right\} \\ &= 2\omega_z\left(\hat{J}_0 + \frac{\hbar}{2}\right) + \xi_d \cos\left(\frac{k}{\sqrt{2}}(\hat{z}+\hat{x})\right)\cdot\frac{1}{2}\left(\hat{x}^2 - \hat{z}^2\right) - \hbar\omega_-\left(\hat{n}_y + \frac{1}{2}\right), \end{aligned} \tag{10.47}$$

[2] This is within the allowed frequency range imposed by the condition in (1.32); it demands $\omega_+/\omega_z = 1 + \sqrt{3/2}$.

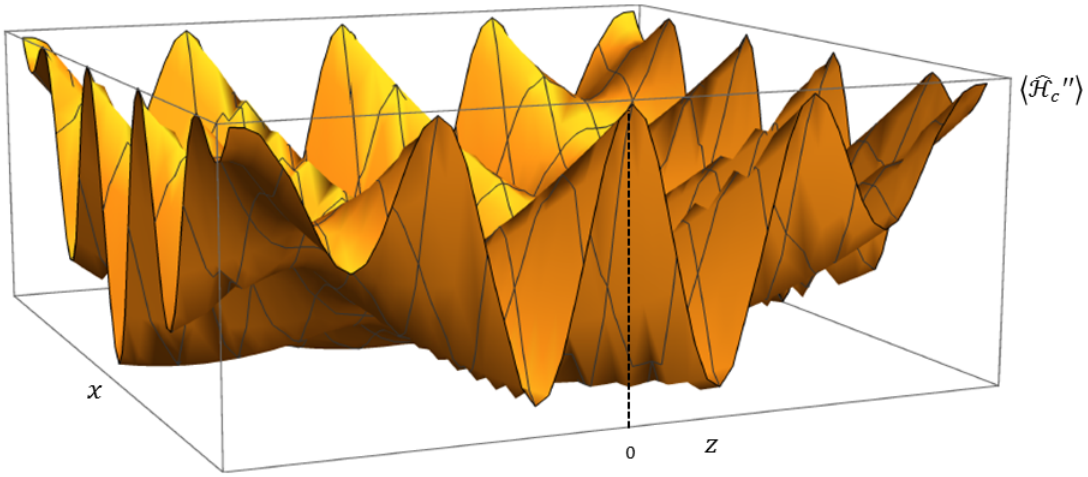

Figure 10.5: General form of $\langle x, z|\hat{\mathcal{H}}_c''|x, z\rangle$ (10.47). In this frame of reference, the potential energy along the z axis clearly forms a double well structure around the point $z = 0$.

where additionally the magnetron Hamiltonian (1.63) has been removed. The expectation value of this Hamiltonian in the $|x, z\rangle$ basis is plotted in Figure 10.5. Both plots 10.4 and 10.5 are drawn to the same scale, and it is clear that different frame transformations made and the setting of $\omega_z = \omega_1/2$ generates a hugely different static potential of $\hat{\mathcal{H}}_c''$ in Figure 10.5. In particular, along the z axis there is a clear double well structure at $z = 0$. In the following section, a solution to Hamiltonian (10.47) is sought.

10.4 Solutions of the sinusoidal potential

10.4.1 Approximate eigenstates of the coupled Hamiltonian

The above Hamiltonian (10.47) is expanded out into position and momentum coordinates as

$$\hat{\mathcal{H}}_c'' = \frac{1}{2m}(\hat{p}_z^2 + \hat{p}_x^2) + \frac{1}{2}m\left(\frac{\omega_1}{2}\right)^2(\hat{z}^2 + \hat{x}^2) + \xi_d \cos\left(\frac{k}{\sqrt{2}}(\hat{z} + \hat{x})\right) \cdot \frac{1}{2}\left(\hat{x}^2 - \hat{z}^2\right). \quad (10.48)$$

Now, the cosine function is approximated as

$$\cos\left(\frac{k}{\sqrt{2}}(\hat{z}-\hat{x})\right) \approx 1-\frac{1}{2!}\left(\frac{k}{\sqrt{2}}(\hat{z}-\hat{x})\right)^2, \tag{10.49}$$

so that the total coupling term around the origin in the xz plane becomes

$$\xi_d\left[\frac{1}{2}\left(\hat{x}^2-\hat{z}^2\right)+\frac{k^2}{8}\left(\hat{z}^2+\hat{x}^2+2\hat{z}\hat{x}\right)\left(\hat{z}^2-\hat{x}^2\right)\right]. \tag{10.50}$$

From (10.22):

$$\begin{aligned}&\hat{\mathcal{J}}_{0,\zeta}+\frac{\hbar}{2}+\hat{\mathcal{J}}_{1,\zeta}\\&\quad=R\frac{m\omega_1}{8}\left[\hat{z}^2+\hat{x}^2+2\hat{z}\hat{x}\right]+\frac{1}{2mR\omega_1}\left[\hat{p}_z^2+\hat{p}_x^2+2\hat{p}_z\hat{p}_x\right].\end{aligned} \tag{10.51}$$

Moreover, multiplying this by $k^2\,\hat{\mathcal{J}}_{3,\zeta}$ reveals:

$$\begin{aligned}&k^2\left(\hat{\mathcal{J}}_{0,\zeta}+\frac{\hbar}{2}+\hat{\mathcal{J}}_{1,\zeta}\right)\hat{\mathcal{J}}_{3,\zeta}\\&\quad=\left(\frac{kRm\omega_1}{8}\right)^2\left[\left(\hat{z}^2+\hat{x}^2+2\hat{z}\hat{x}\right)\left(\hat{z}^2-\hat{x}^2\right)\right]\\&\quad+\left(\frac{k}{2Rm\omega_1}\right)^2\left[\left(\hat{p}_z^2+\hat{p}_x^2+2\hat{p}_z\hat{p}_x\right)\left(\hat{p}_z^2-\hat{p}_x^2\right)\right]\\&\quad+\frac{k^2}{16}\left[(\hat{x}+\hat{z})^2\left(\hat{p}_z^2-\hat{p}_x^2\right)+(\hat{p}_z+\hat{p}_x)^2\left(\hat{x}^2-\hat{z}^2\right)\right],\end{aligned} \tag{10.52}$$

and it is straightforward to verify

$$\begin{aligned}&k^2\left(\hat{\mathcal{J}}_{0,\zeta}+\frac{\hbar}{2}+\hat{\mathcal{J}}_{1,\zeta}-\frac{Rm\omega_1}{4k^2}\right)\hat{\mathcal{J}}_{3,\zeta}\\&\quad=\frac{(kRm\omega_1)^2}{8}\left[\frac{1}{2k^2}\left(\hat{x}^2-\hat{z}^2\right)+\frac{1}{8}\left(\hat{z}^2+\hat{x}^2+2\hat{z}\hat{x}\right)\left(\hat{z}^2-\hat{x}^2\right)\right]\\&\quad+\left(\frac{k}{2Rm\omega_1}\right)^2\left[\left(\hat{p}_z^2+\hat{p}_x^2+2\hat{p}_z\hat{p}_x\right)\left(\hat{p}_z^2-\hat{p}_x^2\right)\right]\\&\quad+\frac{k^2}{16}\left[(\hat{x}+\hat{z})^2\left(\hat{p}_z^2-\hat{p}_x^2\right)+(\hat{p}_z+\hat{p}_x)^2\left(\hat{x}^2-\hat{z}^2\right)+\frac{2}{k^2}\left(\hat{p}_x^2-\hat{p}_z^2\right)\right].\end{aligned} \tag{10.53}$$

The coupling term at $(0,0)$ in (10.50) can therefore be written

$$\begin{aligned}&\xi_d\left[\frac{1}{2}\left(\hat{x}^2-\hat{z}^2\right)+\frac{k^2}{8}\left(\hat{z}^2+\hat{x}^2+2\hat{z}\hat{x}\right)\left(\hat{z}^2-\hat{x}^2\right)\right]\\&\quad=\frac{k^2 8\,\xi_d}{(Rm\omega_1)^2}\left\{\left(\hat{\mathcal{J}}_{0,\zeta}+\frac{\hbar}{2}+\hat{\mathcal{J}}_{1,\zeta}-\frac{Rm\omega_1}{4k^2}\right)\hat{\mathcal{J}}_{3,\zeta}\right.\\&\quad-\left(\frac{1}{2Rm\omega_1}\right)^2\left[\left(\hat{p}_z^2+\hat{p}_x^2+2\hat{p}_z\hat{p}_x\right)\left(\hat{p}_z^2-\hat{p}_x^2\right)\right]\\&\quad\left.-\frac{1}{16}\left[(\hat{x}+\hat{z})^2\left(\hat{p}_z^2-\hat{p}_x^2\right)+(\hat{p}_z+\hat{p}_x)^2\left(\hat{x}^2-\hat{z}^2\right)+\frac{2}{k^2}\left(\hat{p}_x^2-\hat{p}_z^2\right)\right]\right\}.\end{aligned} \tag{10.54}$$

Again using (10.22), the $\hat{J}_0$ term in Hamiltonian (10.47) is given by

$$\omega_1\left(\hat{J}_0+\frac{\hbar}{2}\right)=\frac{1}{R}\omega_1\left(\hat{\mathcal{J}}_{0,\zeta}+\frac{\hbar}{2}\right)+\frac{1}{2m}\left(\hat{p}_z^2+\hat{p}_x^2\right)\left(1-\frac{1}{R^2}\right). \tag{10.55}$$

Hamiltonian (10.47) is therefore approximated at the origin in terms of the set $\underline{\mathcal{J}}_\zeta$:

$$\begin{aligned}
&\text{(I)} \quad \hat{\mathcal{H}}_c''(0,0) = \frac{1}{2m}\left(\hat{p}_z^2 + \hat{p}_x^2\right) \\
&\text{(II)} \qquad + \frac{1}{R}\left[\omega_1\left(\hat{\mathcal{J}}_{0,\zeta} + \frac{\hbar}{2}\right) - \frac{2\xi_d}{m\omega_1}\hat{\mathcal{J}}_{3,\zeta}\right] \\
&\text{(III)} \qquad + \frac{k^2}{R^2}\left[\frac{8\xi_d}{(m\omega_1)^2}\left(\hat{\mathcal{J}}_{0,\zeta} + \frac{\hbar}{2} + \hat{\mathcal{J}}_{1,\zeta}\right)\hat{\mathcal{J}}_{3,\zeta}\right. \\
&\text{(IV)} \qquad \left. - \frac{2\xi_d}{(m\omega_1)^2}\left((\hat{x}+\hat{z})^2\left(\hat{p}_z^2 - \hat{p}_x^2\right) + (\hat{p}_z + \hat{p}_x)^2\left(\hat{x}^2 - \hat{z}^2\right) + \frac{2}{k^2}\left(\hat{p}_x^2 - \hat{p}_z^2\right)\right) - \frac{1}{2mk^2}\left(\hat{p}_z^2 + \hat{p}_x^2\right)\right] \\
&\text{(V)} \qquad - \frac{k^2}{R^4}\left[\frac{2\xi_d}{(m\omega_1)^4}(\hat{p}_z + \hat{p}_x)^2\left(\hat{p}_z^2 - \hat{p}_x^2\right)\right].
\end{aligned} \tag{10.56}$$

Since

$$\begin{aligned}
\langle n_x, n_z|\hat{S}_{xz}^\dagger(\zeta)\,\hat{\mathcal{J}}_{0,\zeta}\,\hat{S}_{xz}(\zeta)|n_x, n_z\rangle &= \langle n_x, n_z|\hat{J}_0|n_x, n_z\rangle = \frac{\hbar}{2}N', \\
\langle n_x, n_z|\hat{S}_{xz}^\dagger(\zeta)\,\hat{\mathcal{J}}_{3,\zeta}\,\hat{S}_{xz}(\zeta)|n_x, n_z\rangle &= \langle n_x, n_z|\hat{J}_3|n_x, n_z\rangle = \frac{\hbar}{2}l',
\end{aligned} \tag{10.57}$$

it follows that

$$\begin{aligned}
&\langle n_x, n_z|\hat{S}_{xz}^\dagger(\zeta)\;\hat{\mathcal{H}}_c''(0,0)\;\hat{S}_{xz}(\zeta)|n_x, n_z\rangle \\
&= \frac{1}{R}\left[\hbar\omega_1(N'+1) - \frac{2\xi_d}{m\omega_1}\frac{\hbar}{2}l'\right] \\
&\quad + \frac{k^2}{R^2}\left[\frac{8\xi_d}{(m\omega_1)^2}\left(\frac{\hbar}{2}\right)^2\left(N'+1\right)l'\right].
\end{aligned} \tag{10.58}$$

From (10.23), $R > 0$, and so the above formulation reveals the hierarchy of diagonal and non-diagonal contributions of Hamiltonian (10.56) in the state $\hat{S}_{xz}(\zeta)|n_x, n_z\rangle$. The size of R itself is determined by the approximate adiabatic states being considered.

10.4.2 Compensation fields and non-diagonal contributions

Of course, even retaining terms only up to $O\left(\frac{1}{R}\right)^2$ in $\hat{\mathcal{H}}_c''(0,0)$ means that significant contributions (line (IV), (10.56)) are neglected by assuming these states. It is proposed that additional electric fields can be added to act as compensation for the terms which are non-diagonal in the squeezed Fock state basis. For example, consider the following field:

$$E_{d,z} = [\epsilon_{d,z}\cos(\omega_d\, t)\cos(k\, y)\, x]\,\hat{e}_z, \tag{10.59}$$

which contributes the quantum potential

$$\hat{V}_{d,z} = -\epsilon_{d,z}\cos(\omega_d\, t)\cos(k\,\hat{y})\,\hat{x}\hat{z}. \tag{10.60}$$

In the $\hat{I}_1$ frame, the $\hat{y}$ coordinate becomes a combination of $\hat{y}$ and $\hat{p}_x$ (5.4), and rotating to a frame using $\hat{U}_x(t)$ in (10.39) retains only the $\hat{p}_x$ contribution. Once the potential has

been transformed through $-\pi/2\,\hat{J}_2$, the result is of the form

$$\cos\left(\frac{\sqrt{2}k}{m\omega_1}\left(\hat{p}_x-\hat{p}_z\right)\right)\frac{1}{2}\left(\hat{x}^2-\hat{z}^2\right)\approx\frac{1}{2}\left(\hat{x}^2-\hat{z}^2\right)+\frac{1}{2}\left(\frac{k}{m\omega_1}\right)^2\left(\hat{p}_x+\hat{p}_z\right)^2\left(\hat{z}^2-\hat{x}^2\right). \tag{10.61}$$

Comparing this to (10.56), it is clear that such additions to the coupling field in (10.35) could begin to remove some of the non-diagonal contributions.

Taking the approximate adiabatic states as $\hat{S}_{xz}(\zeta)|n_x,n_z\rangle$ furthermore neglects the $\hat{\mathcal{J}}_{1,\zeta}$ term line (III) of (10.56). Since this term is *attached* to $\hat{\mathcal{J}}_{3,\zeta}$, it is not possible to write these combined operators in a diagonal form of the states $\hat{S}_{xz}(\zeta)$. Compensating for this would require a potential of the form $\sim\cos(\hat{x}+\hat{z})\hat{x}\hat{z}$. This cannot be created by an oscillating field in a way which allows the time dependence of the resulting potential to be successfully removed. There are, however, many combinations of fields possible which may yet provide a useful potential that be more readily approximated as adiabatic.

Adiabatic driving to an approximate double well potential

In this way, it is proposed that expansion of the cosine function in (10.49) at different points along the axes of the trap could be used to generate an approximate solution of the coupling potential in (10.36).

Of course, it would be more straightforward to approximate the solutions of the trap directly as $|x,z\rangle$. In this way, only the $\hat{p}_z^2+\hat{p}_x^2$ term in Hamiltonian (10.48) need be neglected. This approach, however, does not readily allow a connection to the bare basis, $|n_x,n_z\rangle$ of the system. Since the aim is to create an adiabatic double well potential from a trap with no initial coupling field, any approximate solutions must be mapped from the original eigenstates $|n_x,n_z\rangle$ as the field coupling field is switched on. The solution $\hat{S}_{xz}(\zeta)|n_x,n_z\rangle$ is thus proposed so that the potential energy along the z axis can be mapped to an (approximate) adiabatic double well [26] .

Constructing an adiabatic double well

The above calculations illustrate how a desired adiabatic potential must be very carefully constructed. From [113], the potential of a double well along a general z axis is given by

$$V(z)=\frac{V_{max}}{b^4}\left(\left(z-\frac{a}{2}\right)^2-b^2\right)^2, \tag{10.62}$$

where the height of the potential barrier is V_{max}, and $a/2\pm b$ gives the position of the two minima. When expanded out fully, $V(z)$ contains z^4, z^3, z^2, z, as well as constant

contributions. Following from the above treatment, such an exact adiabatic potential is not possible in the Penning trap through mode coupling. In fact, only potentials of the form $V(z) = \sum_{n=0} C_n z^{2n}$ are possible. Although restricted, this may yet allow manipulation of the potential landscape in a useful way.

10.4.3 Further ideas and applications

A 2D lattice potential

Of course, a semi-classical calculation may reveal that the theory can be extended so that any shape of potential can be produce from the mode coupling technique. For example, one intriguing possibility is the production of a 2D lattice potential in the ultra-elliptical regime of the trap. If all contributions from a coupling potential of the form $xz(\cos(kx)+\cos(kz))$ could be retained after removal of the time dependence, then such a configuration is possible. In the case of the ultra-elliptical trap, this would produce an effective 2D Wigner crystal [114], expanding the capabilities of the Penning trap to include study of solid state systems.

Varying the magnetic field strength

Another possible means of manipulating the potential energy in the Penning trap is unique to the Geonium Chip. It relies on the unique planar design and magnetic field production, which enable the near field of $\vec{B}$ to be varied over small distances of microns [67], the lengthscale of the axial motion in the trap, (1.33). The idea itself is based on a "magnetic bottle", which provides a local inhomogeneity of the magnetic field of the particular form [14],

$$\Delta\vec{B}_{bottle} = B_2\left[\left(z^2 - \frac{r^2}{2}\right)\hat{e}_z - z\cdot r\hat{e}_r\right]. \tag{10.63}$$

where B_2 is the strength of the magnetic bottle. Such a configuration is illustrated in the upper part of Figure 10.6, where the regions of different magnetic field strength along the z axis are indicated above the field lines.

They are primarily used in Penning traps to determine the spin state of the particle [115], since as the axial frequency becomes spin dependent in this "analysis trap". If $\omega_{z,0}$ now represents the axial frequency outside the magnetic bottle (1.80), and μ_z is the component of the magnetic moment of the electron aligned along the z axis, the resulting shift is of the form [14]

$$\omega_z = \sqrt{2V_r\, c_{002}\frac{q}{m} - \frac{2\mu_z B_2}{m}} \simeq \omega_{z,0} - \frac{\mu_z B_2}{m\omega_{z,0}}. \tag{10.64}$$

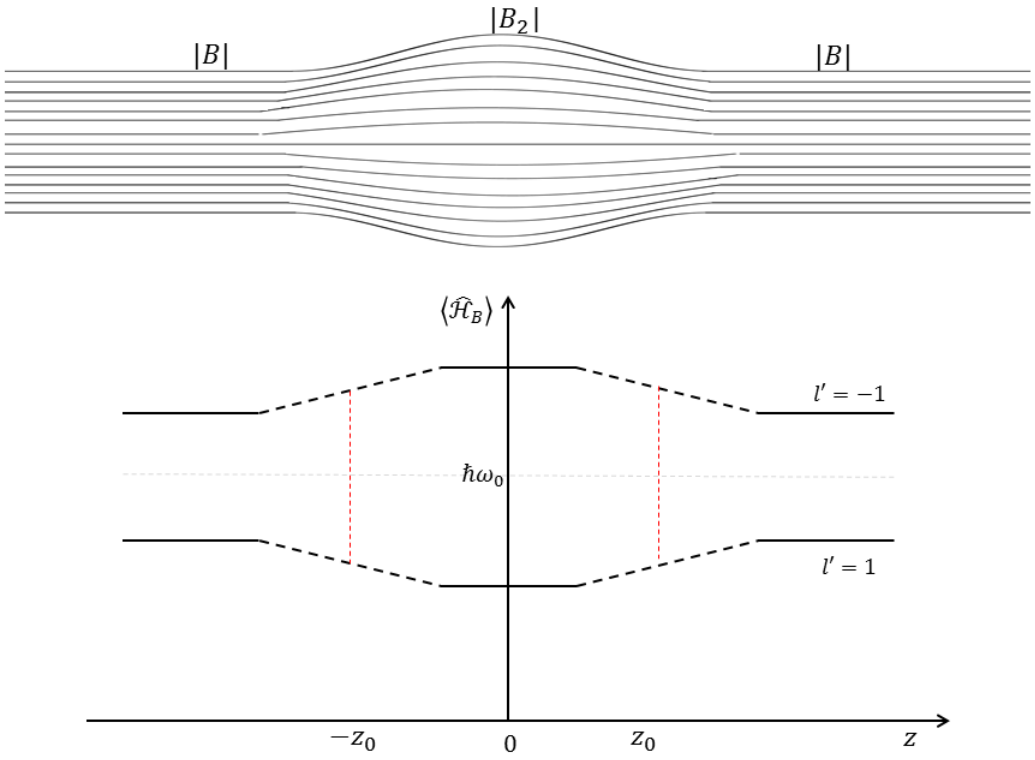

Figure 10.6: The upper plot illustrates a local magnetic bottle along the z axis (10.63). At the centre of this configuration, where the field lines are approximately flat, the strength is a constant value B_2. Towards the edges of the bottle, B_2 and therefore ω_z must vary in space (10.64). The lower plot indicates how the l' levels of the magnetic bottle Hamiltonian $\hat{\mathcal{H}}_B$ may vary along the z axis as a result. In this way, resonant coupling of the modes could be configured at precise locations along the axis, $\pm z_0$, and the avoided crossings at these positions could lead to the creation of a double well structure.

The axial frequency is thus a function of the field strength B_2. In the lower part of Figure 10.6, is sketched the variation of the expectation value of the l' levels of the magnetic bottle Hamiltonian $\langle\hat{\mathcal{H}}_B\rangle$. In Figure 2.2, the splitting between the bare and dressed levels varies with the detuning δ [3]. In this way, it is proposed that variation of B_2 can be configured so that the coupling of the modes is resonant ($\delta = 0$) at two precise locations $\pm z_0$ along the z axis. This would lead to a similar situation as facilitates the creation of a double well in the atom chip [70] (Figure 2.3).

The quantum theory of this technique has not yet been well established. The Hamiltonian of the electron in a magnetic bottle in the presence of an xz coupling field is non-trivial to solve, but some progress has so far been made using many of the techniques developed throughout this thesis.

This chapter has extensively discussed the manipulation of potential energy in the Penning trap through mode coupling. It has revealed that an analogy between RF-induced double wells in atom traps and the dressed-atom approach with $\xi(x, z)$ in the Penning trap is rather beguiling. The comparison has nonetheless lead to an approximate solution of the potential plotted in Figure 10.5 at the centre of the trap, a state which can be mapped adiabatically from the eigenstates of the uncoupled trap. It is therefore proposed that a tunable, approximately adiabatic double well potential is possible through the technique of sideband coupling in the Penning trap. The problem is a topic of ongoing investigation.

[3] This is a plot of the dressed levels in the lab frame, and as such shows the coupled l levels of the axial and cyclotron modes, rather than the l' levels of the axial and x modes. As discussed in 7.2.3, the two pictures are completely equivalent.

Chapter 11

Summary and Outlook

11.1 Summary

The main results of this thesis can be divided into four general categories.

The separate dynamics of the x and y motions

The quantum Hamiltonian of the Penning trap was reformed in the $\{x, y\}$ basis, and compared to the conventional formulation extensively. By this approach, the rotating frame of the Penning trap was shown to be inconsistent in identifying the individual dynamics of the x and y degrees of freedom. Through a fastidious discussion of interpretation of the quantum solution of the trap by rotation of the Hamiltonian, vs. effective dressing of modes, the root of this inconsistency was identified. This lead on to the analysis of the role played by a set of Schwinger boson operators in the trap. Moreover, the carefully distinct interpretations were shown later to be effective for different purposes in development of the theory.

Schwinger boson operators in the Penning trap

It was shown how a Hamiltonian comprising three independent harmonic oscillators can be separated into three, 2D systems in an effective way. Isolation of these subsystems allows each to be treated consistently in a dressed-atom formalism for coupled terms in the Hamiltonian. The development of the map of commutation relations serves several purposes. It enables straightforward calculation of unitary transformations involving these operators, and, once familiar with how to read it, serves to illustrate how each of these transformations affects the spatial coordinates in the trap. Moreover, the scrupulous calculation of each of the commutation relations between the three sets ensure that their

simultaneous use in the Penning trap is absolutely robust. This enables confidence in the use of these methods, and extension of the theory to the elliptical Penning trap.

The quantum elliptical trap

A quantum solution to the elliptical trap in both the $\{x, y\}$ and $\{+, -\}$ basis was found, reproducing well known classical results from the literature. Straightforward development of the theory to include the ultra-elliptical regime of the Geonium chip is discussed. Adiabatic driving to this regime is proposed, leading to calculation of the exact eigenstates, and a demonstration of the quantum control enabled by these methods. The formalism developed throughout the previous chapters was shown to provide a natural framework for these calculations. The unitary mapping between 2D and 3D systems by quantum transformation was shown to agree intuitively with the discussion of the analogous classical system.

The dressed-atom method in the Penning trap

The final two chapters of the thesis harness some of the ability lent by adopting the dressed-atom formalism in the Penning trap. A simple extension of cyclotron-axial mode coupling theory was shown to lead to a scheme for interferometry, through the well known method of an applied LZS driving field. Analysis of the spectrum of the coupled modes in this chapter provide an illuminating interpretation of how this driving field acts upon the infinite number of energy levels in the trap. Development of the statistical formalism throughout the thesis additionally leads to a proposed scheme for detection of results from an effective TLS of the coupled modes. Furthermore, the scheme allows the resulting interference between any of the coupled levels to be probed, enabling experimental study of this novel system.

Manipulation of the potential energy through sideband coupling is addressed in the final chapter. Although the formation of dressed levels in the trap is a very natural extension of the basic coupling calculation, the further development of dressed *potentials* is not equally forthcoming. The difficulties of this proposed scheme, and subsequent departure from established theory, are laid out at the beginning of the chapter. The formulation of squeezed sets of Schwinger boson operators is shown to lead to an approximate quantum solution of an applied sinusoidal coupling field at the centre of the trap. It is proposed that the potential energy along the z axis could be adiabatically driven to a double well by these methods. Furthermore, construction of other interesting potential landscapes in

the trap seem possible for a semi-classical treatment of the calculation.

11.2 Outlook

Following this research, there are a number of topics which seem worthy of further investigation.

In particular, the theory of the Chapters (9) and (10) must be further developed before any experimental investigation of them can be attempted. For LZS interferometry, the effects of decoherence and imperfections in the trap must be included to allow for a more complete analysis. It is possible that other methods of solving the problem allow a more natural inclusion of these effects. In addition, different regimes within the adiabatic-impulse model may be worthwhile to investigate.

The creation of tunable adiabatic potentials in the trap is also a promising topic for future study. The solution reached in this thesis is by no means complete, but serves as a useful starting point for this. From a theoretical point of view, future study of squeezed Fock states is intriguing, and how these solutions transform as the squeezing parameter is driven to an infinite limit.

A thorough semi-classical calculation of this landscape manipulation is necessary to expand the capabilities of the proposed technique. This must be additionally combined with the developed elliptical trap theory to study the generation of lattice potentials in the ultra-elliptical regime. The method of altering the potential energy with the use of a magnetic bottle in the trap must be extensively developed before application in the Geonium Chip.

The adopted formalism of dressed-atoms examined throughout this thesis extends the capabilities of the Penning trap. There may be many more techniques adaptable from atom traps which could lead to novel schemes in this trap.

The theory developed so far has promising potential for use in Penning trap experiments. Extensive quantum control of the electron is achievable in the Geonium chip from the analysis of the ultra-elliptical regime of the trap and the exact calculation of sideband coupling. Additionally, the research reveals a number of interesting theoretical ideas, and unique systems worthy of further study.

Appendix

A Transformations of $\hat{a}$ and $\hat{a}^\dagger$ continued

The Schwinger boson sets $\underline{J}$ and $\underline{K}$ (5.10) have the following effect upon their constituent operator pairs:

$\underline{J}$

$$\exp\left\{\frac{i}{\hbar}\phi\hat{J}_1\right\}\begin{pmatrix}\hat{a}_z^\dagger\\ \hat{a}_x^\dagger\end{pmatrix}\exp\left\{-\frac{i}{\hbar}\phi\hat{J}_1\right\}=\begin{pmatrix}\cos\frac{\phi}{2} & i\sin\frac{\phi}{2}\\ i\sin\frac{\phi}{2} & \cos\frac{\phi}{2}\end{pmatrix}\begin{pmatrix}\hat{a}_z^\dagger\\ \hat{a}_x^\dagger\end{pmatrix}, \tag{1}$$

$$\exp\left\{\frac{i}{\hbar}\gamma\hat{J}_2\right\}\begin{pmatrix}\hat{a}_z^\dagger\\ \hat{a}_x^\dagger\end{pmatrix}\exp\left\{-\frac{i}{\hbar}\gamma\hat{J}_2\right\}=\begin{pmatrix}\cos\frac{\gamma}{2} & -\sin\frac{\gamma}{2}\\ \sin\frac{\gamma}{2} & \cos\frac{\gamma}{2}\end{pmatrix}\begin{pmatrix}\hat{a}_z^\dagger\\ \hat{a}_x^\dagger\end{pmatrix}, \tag{2}$$

$$\exp\left\{\frac{i}{\hbar}\theta\hat{J}_3\right\}\begin{pmatrix}\hat{a}_z^\dagger\\ \hat{a}_x^\dagger\end{pmatrix}\exp\left\{-\frac{i}{\hbar}\theta\hat{J}_3\right\}=\begin{pmatrix}\exp\left(i\frac{\theta}{2}\right) & 0\\ 0 & \exp\left(-i\frac{\theta}{2}\right)\end{pmatrix}\begin{pmatrix}\hat{a}_z^\dagger\\ \hat{a}_x^\dagger\end{pmatrix}. \tag{3}$$

$\underline{K}$

$$\exp\left\{\frac{i}{\hbar}\phi\hat{K}_1\right\}\begin{pmatrix}\hat{a}_y^\dagger\\ \hat{a}_z^\dagger\end{pmatrix}\exp\left\{-\frac{i}{\hbar}\phi\hat{K}_1\right\}=\begin{pmatrix}\cos\frac{\phi}{2} & i\sin\frac{\phi}{2}\\ i\sin\frac{\phi}{2} & \cos\frac{\phi}{2}\end{pmatrix}\begin{pmatrix}\hat{a}_y^\dagger\\ \hat{a}_z^\dagger\end{pmatrix}, \tag{4}$$

$$\exp\left\{\frac{i}{\hbar}\gamma\hat{K}_2\right\}\begin{pmatrix}\hat{a}_y^\dagger\\ \hat{a}_z^\dagger\end{pmatrix}\exp\left\{-\frac{i}{\hbar}\gamma\hat{K}_2\right\}=\begin{pmatrix}\cos\frac{\gamma}{2} & -\sin\frac{\gamma}{2}\\ \sin\frac{\gamma}{2} & \cos\frac{\gamma}{2}\end{pmatrix}\begin{pmatrix}\hat{a}_y^\dagger\\ \hat{a}_z^\dagger\end{pmatrix}, \tag{5}$$

$$\exp\left\{\frac{i}{\hbar}\theta\hat{K}_3\right\}\begin{pmatrix}\hat{a}_y^\dagger\\ \hat{a}_z^\dagger\end{pmatrix}\exp\left\{-\frac{i}{\hbar}\theta\hat{K}_3\right\}=\begin{pmatrix}\exp\left(i\frac{\theta}{2}\right) & 0\\ 0 & \exp(-i\frac{\theta}{2})\end{pmatrix}\begin{pmatrix}\hat{a}_y^\dagger\\ \hat{a}_z^\dagger\end{pmatrix}. \tag{6}$$

B Resulting transformations from the non-cyclic commutation relations of the Schwinger boson operators

The non-cyclic commutation relations in the commutation map in Figure 5.2 result in the following associated transformations.

Transformations by $\hat{I}_1$

$$\begin{aligned}
\exp\left\{\frac{i}{\hbar}\phi\hat{I}_1\right\}\hat{J}_0\exp\left\{-\frac{i}{\hbar}\phi\hat{I}_1\right\} &= \hat{J}_0 + \frac{1}{2}\sin\phi\hat{I}_2 + \frac{1}{2}(\cos\phi - 1)\hat{I}_3,\\
\exp\left\{\frac{i}{\hbar}\phi\hat{I}_1\right\}\hat{J}_3\exp\left\{-\frac{i}{\hbar}\phi\hat{I}_1\right\} &= \hat{J}_3 - \frac{1}{2}\sin\phi\hat{I}_2 - \frac{1}{2}(\cos\phi - 1)\hat{I}_3,\\
\exp\left\{\frac{i}{\hbar}\phi\hat{I}_1\right\}\hat{K}_0\exp\left\{-\frac{i}{\hbar}\phi\hat{I}_1\right\} &= \hat{K}_0 - \frac{1}{2}\sin\phi\hat{I}_2 - \frac{1}{2}(\cos\phi - 1)\hat{I}_3,\\
\exp\left\{\frac{i}{\hbar}\phi\hat{I}_1\right\}\hat{K}_3\exp\left\{-\frac{i}{\hbar}\phi\hat{I}_1\right\} &= \hat{K}_3 - \frac{1}{2}\sin\phi\hat{I}_2 - \frac{1}{2}(\cos\phi - 1)\hat{I}_3.
\end{aligned} \tag{7}$$

Transformations by $\hat{I}_2$

$$\begin{aligned}
\exp\left\{\frac{i}{\hbar}\phi\hat{I}_2\right\}\hat{J}_0\exp\left\{-\frac{i}{\hbar}\phi\hat{I}_2\right\} &= \hat{J}_0 - \frac{1}{2}\sin\phi\hat{I}_1 + \frac{1}{2}(\cos\phi - 1)\hat{I}_3,\\
\exp\left\{\frac{i}{\hbar}\phi\hat{I}_2\right\}\hat{J}_3\exp\left\{-\frac{i}{\hbar}\phi\hat{I}_2\right\} &= \hat{J}_3 + \frac{1}{2}\sin\phi\hat{I}_1 - \frac{1}{2}(\cos\phi - 1)\hat{I}_3,\\
\exp\left\{\frac{i}{\hbar}\phi\hat{I}_2\right\}\hat{K}_0\exp\left\{-\frac{i}{\hbar}\phi\hat{I}_2\right\} &= \hat{K}_0 + \frac{1}{2}\sin\phi\hat{I}_1 - \frac{1}{2}(\cos\phi - 1)\hat{I}_3,\\
\exp\left\{\frac{i}{\hbar}\phi\hat{I}_2\right\}\hat{K}_3\exp\left\{-\frac{i}{\hbar}\phi\hat{I}_2\right\} &= \hat{K}_3 + \frac{1}{2}\sin\phi\hat{I}_1 - \frac{1}{2}(\cos\phi - 1)\hat{I}_3.
\end{aligned} \tag{8}$$

Transformations by $\hat{J}_1$

$$\begin{aligned}
\exp\left\{\frac{i}{\hbar}\phi\hat{J}_1\right\}\hat{I}_0\exp\left\{-\frac{i}{\hbar}\phi\hat{J}_1\right\} &= \hat{I}_0 - \frac{1}{2}\sin\phi\hat{J}_2 - \frac{1}{2}(\cos\phi - 1)\hat{J}_3,\\
\exp\left\{\frac{i}{\hbar}\phi\hat{J}_1\right\}\hat{I}_3\exp\left\{-\frac{i}{\hbar}\phi\hat{J}_1\right\} &= \hat{I}_3 - \frac{1}{2}\sin\phi\hat{J}_2 - \frac{1}{2}(\cos\phi - 1)\hat{J}_3,\\
\exp\left\{\frac{i}{\hbar}\phi\hat{J}_1\right\}\hat{K}_0\exp\left\{-\frac{i}{\hbar}\phi\hat{J}_1\right\} &= \hat{K}_0 + \frac{1}{2}\sin\phi\hat{J}_2 + \frac{1}{2}(\cos\phi - 1)\hat{J}_3,\\
\exp\left\{\frac{i}{\hbar}\phi\hat{J}_1\right\}\hat{K}_3\exp\left\{-\frac{i}{\hbar}\phi\hat{J}_1\right\} &= \hat{K}_3 - \frac{1}{2}\sin\phi\hat{J}_2 - \frac{1}{2}(\cos\phi - 1)\hat{J}_3.
\end{aligned} \tag{9}$$

Transformations by $\hat{J}_2$

$$\begin{aligned}
\exp\left\{\frac{i}{\hbar}\phi\hat{J}_2\right\}\hat{I}_0\exp\left\{-\frac{i}{\hbar}\phi\hat{J}_2\right\} &= \hat{I}_0+\frac{1}{2}\sin\phi\hat{J}_1-\frac{1}{2}(\cos\phi-1)\hat{J}_3,\\
\exp\left\{\frac{i}{\hbar}\phi\hat{J}_2\right\}\hat{I}_3\exp\left\{-\frac{i}{\hbar}\phi\hat{J}_2\right\} &= \hat{I}_3+\frac{1}{2}\sin\phi\hat{J}_1-\frac{1}{2}(\cos\phi-1)\hat{J}_3,\\
\exp\left\{\frac{i}{\hbar}\phi\hat{J}_2\right\}\hat{K}_0\exp\left\{-\frac{i}{\hbar}\phi\hat{J}_2\right\} &= \hat{K}_0-\frac{1}{2}\sin\phi\hat{J}_1+\frac{1}{2}(\cos\phi-1)\hat{J}_3,\\
\exp\left\{\frac{i}{\hbar}\phi\hat{J}_2\right\}\hat{K}_3\exp\left\{-\frac{i}{\hbar}\phi\hat{J}_2\right\} &= \hat{K}_3+\frac{1}{2}\sin\phi\hat{J}_1-\frac{1}{2}(\cos\phi-1)\hat{J}_3.
\end{aligned}\tag{10}$$

Transformations by $\hat{K}_1$

$$\begin{aligned}
\exp\left\{\frac{i}{\hbar}\phi\hat{K}_1\right\}\hat{I}_0\exp\{-\frac{i}{\hbar}\phi\hat{K}_1\} &= \hat{I}_0+\frac{1}{2}\sin\phi\hat{K}_2+\frac{1}{2}(\cos\phi-1)\hat{K}_3,\\
\exp\left\{\frac{i}{\hbar}\phi\hat{K}_1\right\}\hat{I}_3\exp\{-\frac{i}{\hbar}\phi\hat{K}_1\} &= \hat{I}_3-\frac{1}{2}\sin\phi\hat{K}_2-\frac{1}{2}(\cos\phi-1)\hat{K}_3,\\
\exp\left\{\frac{i}{\hbar}\phi\hat{K}_1\right\}\hat{J}_0\exp\{-\frac{i}{\hbar}\phi\hat{K}_1\} &= \hat{J}_0-\frac{1}{2}\sin\phi\hat{K}_2-\frac{1}{2}(\cos\phi-1)\hat{K}_3,\\
\exp\left\{\frac{i}{\hbar}\phi\hat{K}_1\right\}\hat{J}_3\exp\{-\frac{i}{\hbar}\phi\hat{K}_1\} &= \hat{J}_3-\frac{1}{2}\sin\phi\hat{K}_2-\frac{1}{2}(\cos\phi-1)\hat{K}_3.
\end{aligned}\tag{11}$$

Transformations by $\hat{K}_2$

$$\begin{aligned}
\exp\left\{\frac{i}{\hbar}\phi\hat{K}_2\right\}\hat{I}_0\exp\left\{-\frac{i}{\hbar}\phi\hat{K}_2\right\} &= \hat{I}_0-\frac{1}{2}\sin\phi\hat{K}_1+\frac{1}{2}(\cos\phi-1)\hat{K}_3,\\
\exp\left\{\frac{i}{\hbar}\phi\hat{K}_2\right\}\hat{I}_3\exp\left\{-\frac{i}{\hbar}\phi\hat{K}_2\right\} &= \hat{I}_3+\frac{1}{2}\sin\phi\hat{K}_1-\frac{1}{2}(\cos\phi-1)\hat{K}_3,\\
\exp\left\{\frac{i}{\hbar}\phi\hat{K}_2\right\}\hat{J}_0\exp\left\{-\frac{i}{\hbar}\phi\hat{K}_2\right\} &= \hat{J}_0+\frac{1}{2}\sin\phi\hat{K}_1-\frac{1}{2}(\cos\phi-1)\hat{K}_3,\\
\exp\left\{\frac{i}{\hbar}\phi\hat{K}_2\right\}\hat{J}_3\exp\left\{-\frac{i}{\hbar}\phi\hat{K}_2\right\} &= \hat{J}_3+\frac{1}{2}\sin\phi\hat{K}_1-\frac{1}{2}(\cos\phi-1)\hat{K}_3.
\end{aligned}\tag{12}$$

C The dressed states of the axial-magnetron coupled modes

The axial-magnetron mode coupled Hamiltonian can be interpreted in terms of dressed modes. Hamiltonian (8.74) is rewritten in terms of dressed mode operators $\hat{a}_\tau(\epsilon)$ and $\hat{a}_\mu(\epsilon)$:

$$\hat{\mathcal{H}}_{\zeta mt}(\epsilon)=\hbar\varepsilon_\tau(\epsilon)\left(\hat{n}_\tau(\epsilon)+\frac{1}{2}\right)+\hbar\varepsilon_\mu(\epsilon)\left(\hat{n}_\mu(\epsilon)+\frac{1}{2}\right)\hbar+\tilde{\omega}_+\left(\hat{n}_x+\frac{1}{2}\right);\tag{13}$$

$$\begin{aligned}
\varepsilon_\tau(\epsilon) &= \frac{1}{2}\left(\tilde{\omega}_{0,m}(\epsilon)+\sqrt{4\tilde{\xi}_m^2(\epsilon)+\delta^2}\right),\\
\varepsilon_\mu(\epsilon) &= \frac{1}{2}\left(\tilde{\omega}_{0,m}(\epsilon)-\sqrt{4\tilde{\xi}_m^2(\epsilon)+\delta^2}\right);
\end{aligned}\tag{14}$$

$$\hat{a}_\tau^\dagger(\epsilon) = \cos\frac{\tilde{\theta}_m(\epsilon)}{2}\hat{a}_y^\dagger - i\sin\frac{\tilde{\theta}_m(\epsilon)}{2}\hat{a}_z^\dagger, \qquad \hat{a}_\tau(\epsilon) = \cos\frac{\tilde{\theta}_m(\epsilon)}{2}\hat{a}_y + i\sin\frac{\tilde{\theta}_m(\epsilon)}{2}\hat{a}_z,$$
$$\hat{a}_\mu^\dagger(\epsilon) = \cos\frac{\tilde{\theta}_m(\epsilon)}{2}\hat{a}_z^\dagger - i\sin\frac{\tilde{\theta}_m(\epsilon)}{2}\hat{a}_y^\dagger, \qquad \hat{a}_\mu(\epsilon) = \cos\frac{\tilde{\theta}_m(\epsilon)}{2}\hat{a}_z + i\sin\frac{\tilde{\theta}_m(\epsilon)}{2}\hat{a}_y, \tag{15}$$

where $\tilde{\omega}_{0,m}(\epsilon)$ and $\tilde{\theta}_m$ are given in (8.75) and (8.78) respectively.

D Collective transformation of coordinates by $\hat{I}_1$, $\hat{J}_3$ and $\hat{J}_2$

From the lab frame to the dressed frame of Hamiltonian (10.2), there are three unitary transformations, by $\hat{U}_1$, $\hat{U}_p'(t)$ and $\hat{U}_2$, which rotate the coordinates. As a reminder:

$$\hat{U}_1 = \exp\left\{\frac{i}{\hbar}\left(-\frac{\pi}{2}\right)\hat{I}_1\right\}, \qquad \hat{U}_p'(t) = \exp\left\{\frac{i}{\hbar}(-\omega_p t)\hat{J}_3\right\}, \qquad \hat{U}_2 = \exp\left\{\frac{i}{\hbar}\theta\hat{J}_2\right\}. \tag{16}$$

The coordinates $\hat{x}$, $\hat{y}$, $\hat{z}$, $\hat{p}_x$, $\hat{p}_y$ and $\hat{p}_z$ transform to this frame in the following way:

$$\begin{aligned}
\hat{x} \xrightarrow{\hat{I}_1} & \frac{1}{\sqrt{2}}\left(\hat{x} - \frac{2}{m\omega_1}\hat{p}_y\right) \xrightarrow{\hat{J}_3} \frac{1}{\sqrt{2}}\left(\cos\frac{\omega_p t}{2}\hat{x} + \sin\frac{\omega_p t}{2}\frac{2}{m\omega_1}\hat{p}_x - \frac{2}{m\omega_1}\hat{p}_y\right) \\
\xrightarrow{\hat{J}_2} & \frac{1}{\sqrt{2}}\left(\cos\frac{\omega_p t}{2}\left(\cos\frac{\theta}{2}\hat{x} + \sin\frac{\theta}{2}\sqrt{\frac{\omega_z}{\omega_1}}\hat{z}\right) + \sin\frac{\omega_p t}{2}\frac{2}{m\omega_1}\left(\cos\frac{\theta}{2}\hat{p}_x + \sin\frac{\theta}{2}\sqrt{\frac{\omega_1}{2\omega_z}}\hat{p}_z\right) - \frac{2}{m\omega_1}\hat{p}_y\right)
\end{aligned} \tag{17}$$

$$\begin{aligned}
\hat{y} \xrightarrow{\hat{I}_1} & \frac{1}{\sqrt{2}}\left(\hat{y} - \frac{2}{m\omega_1}\hat{p}_x\right) \xrightarrow{\hat{J}_3} \frac{1}{\sqrt{2}}\left(y - \frac{2}{m\omega_1}\left(\cos\frac{\omega_p t}{2}\hat{p}_x - \frac{m\omega_1}{2}\sin\frac{\omega_p t}{2}\hat{x}\right)\right) \\
\xrightarrow{\hat{J}_2} & \frac{1}{\sqrt{2}}\left(\hat{y} - \cos\frac{\omega_p t}{2}\left(\frac{2}{m\omega_1}\cos\frac{\theta}{2}\hat{p}_x - \frac{1}{m}\sin\frac{\theta}{2}\sqrt{\frac{2}{\omega_1\omega_z}}\hat{p}_z\right)\right. \\
& \left. + \sin\frac{\omega_p t}{2}\left(\cos\frac{\theta}{2}\hat{x} + \sin\frac{\theta}{2}\sqrt{\frac{\omega_z}{\omega_1}}\hat{z} - \frac{2}{m\omega_1}\hat{p}_y\right)\right)
\end{aligned} \tag{18}$$

$$\begin{aligned}
\hat{z} \xrightarrow{\hat{I}_1} & \hat{z} \xrightarrow{\hat{J}_3} \cos\frac{\omega_p t}{2}\hat{z} - \sin\frac{\omega_p t}{2}\frac{1}{m\omega_z}\hat{p}_z \\
\xrightarrow{\hat{J}_2} & \cos\frac{\omega_p t}{2}\left(\cos\frac{\theta}{2}\hat{z} - \sin\frac{\theta}{2}\sqrt{\frac{\omega_1}{2\omega_z}}\hat{x}\right) - \sin\frac{\omega_p t}{2}\frac{1}{m\omega_z}\left(\cos\frac{\theta}{2}\hat{p}_z - \sqrt{\frac{2\omega_z}{\omega_1}}\sin\frac{\theta}{2}\hat{p}_x\right)
\end{aligned} \tag{19}$$

$$\begin{aligned}
\hat{p}_x \xrightarrow{\hat{I}_1} & \frac{1}{\sqrt{2}}\left(\hat{p}_x + \frac{1}{2}m\omega_1\hat{y}\right) \xrightarrow{\hat{J}_3} \frac{1}{\sqrt{2}}\left(\left(\cos\frac{\omega_p t}{2}\hat{p}_x - \frac{m\omega_1}{2}\sin\frac{\omega_p t}{2}\hat{x}\right) + \frac{1}{2}m\omega_1\hat{y}\right) \\
\xrightarrow{\hat{J}_2} & \frac{1}{\sqrt{2}}\left(\cos\frac{\omega_p t}{2}\left(\cos\frac{\theta}{2}\hat{p}_x + \sqrt{\frac{\omega_1}{2\omega_z}}\sin\frac{\theta}{2}\hat{p}_z\right) - \frac{m\omega_1}{2}\sin\frac{\omega_p t}{2}\left(\cos\frac{\theta}{2}\hat{x} + \sqrt{\frac{2\omega_z}{\omega_1}}\sin\frac{\theta}{2}\hat{z}\right)\right. \\
& \left. + \frac{1}{2}m\omega_1\hat{y}\right)
\end{aligned} \tag{20}$$

$$\begin{aligned}\hat{p}_y \xrightarrow{\hat{I}_1} & \frac{1}{\sqrt{2}}\left(\hat{p}_y + \frac{1}{2}m\omega_1\hat{x}\right) \xrightarrow{\hat{J}_3} \frac{1}{\sqrt{2}}\left(\hat{p}_y + \frac{1}{2}m\omega_1\left(\cos\frac{\omega_p t}{2}\hat{x} + \frac{2}{m\omega_1}\sin\frac{\omega_p t}{2}\hat{p}_x\right)\right) \\ \xrightarrow{\hat{J}_2} & \frac{1}{\sqrt{2}}\left(\hat{p}_y + \frac{1}{2}m\omega_1\left(\cos\frac{\omega_p t}{2}\left(\cos\frac{\theta}{2}\hat{x} + \sqrt{\frac{2\omega_z}{\omega_1}}\sin\frac{\theta}{2}\hat{z}\right)\right.\right. \\ & \left.\left. + \frac{2}{m\omega_1}\sin\frac{\omega_p t}{2}\left(\cos\frac{\theta}{2}\hat{p}_x + \sqrt{\frac{\omega_1}{2\omega_z}}\sin\frac{\theta}{2}\hat{p}_z\right)\right)\right)\end{aligned} \tag{21}$$

$$\begin{aligned}\hat{p}_z \xrightarrow{\hat{I}_1} & \hat{p}_z \xrightarrow{\hat{J}_3} \cos\frac{\omega_p t}{2}\hat{p}_z + \sin\frac{\omega_p t}{2}\hat{z} \\ \xrightarrow{\hat{J}_2} & \cos\frac{\omega_p t}{2}\left(\hat{p}_z\cos\frac{\theta}{2} - \sqrt{\frac{2\omega_z}{\omega_1}}\hat{p}_x\sin\frac{\theta}{2}\right) + \sin\frac{\omega_p t}{2}\left(\cos\frac{\theta}{2}\hat{z} - \sqrt{\frac{\omega_1}{2\omega_z}}\sin\frac{\theta}{2}\hat{x}\right)\end{aligned} \tag{22}$$

Bibliography

[1] Oscar Wilde. *The picture of Dorian Gray*. Oxford University Press, 1999. 1

[2] F. M. Penning. Verzögerungen Bei Der Zündung Von Gas Gefüllten Photozellen Im Dunkeln. *Physica*, III:563–568, 1936. 1

[3] Hans Dehmelt. Experiments with an Isolated Subatomic Particle at Rest. *44th Annual Symposium on Frequency Control*, pages 525–531, 1990. 1

[4] D. Wineland, P. Ekstrom, and H. Dehmelt. Monoelectron Oscillator. *Physical Review Letters*, 31:1279–1282, 1973. 1

[5] Klaus Blaum. High-accuracy mass spectrometry with stored ions. *Physics Reports*, 425:1–78, 2006. 1, 4

[6] S Sturm, F Köhler, J Zatorski, A Wagner, Z Harman, G Werth, W Quint, C H Keitel, and K Blaum. High-precision measurement of the atomic mass of the electron. *Nature*, 506:467–70, 2014. 1

[7] S Ulmer J L Verdú, S Kreim, J Alonso, K Blaum, S Djekić, W Quint, S Stahl, M Vogel, J Walz, and G Werth. Penning Trap Measurement of the Magnetic Moment of the Antiproton. *AIP Conference Proceedings, LEAP*, 796:260–265, 2005. 1

[8] G. Gabrielse, R. Kalra, W. S. Kolthammer, R. McConnell, P. Richerme, D. Grzonka, W. Oelert, T. Sefzick, M. Zielinski, D. W. Fitzakerley, M. C. George, E. A. Hessels, C. H. Storry, M. Weel, A. Müllers, J. Walz, and J. Walz. Trapped Antihydrogen in Its Ground State. *Physical Review Letters*, 108:113002–4, 2012. 1

[9] Yasunori Yamazaki. Antimatter Matters: Progress in Cold Antihydrogen Research. *Journal of Physics: Conference Series*, 388:012002, 2012. 1

[10] D. Hanneke, S. Fogwell, and G. Gabrielse. New measurement of the electron magnetic moment and the fine structure constant. *Physical Review Letters*, 100:120801–4, 2008. 1

[11] C C Rodegheri, K Blaum, H Kracke, S Kreim, A Mooser, W Quint, S Ulmer, and J Walz. An experiment for the direct determination of the g-factor of a single proton in a Penning trap. *New Journal of Physics*, 14:063011, 2012. 1

[12] A. Mooser, S. Ulmer, K. Blaum, K. Franke, H. Kracke, C. Leiteritz, W. Quint, C. C. Rodegheri, C. Smorra, and J. Walz. Direct high-precision measurement of the magnetic moment of the proton. *Nature*, 509:596–599, 2014. 1

[13] G. Ciaramicoli, I. Marzoli, and P. Tombesi. Trapped electrons in vacuum for a scalable quantum processor. *Physical Review A*, 70:032301–4, 2004. 1

[14] Lowell S. Brown and Gerald Gabrielse. Geonium theory: Physics of a single electron or ion in a Penning trap. *Reviews of Modern Physics*, 58:233–311, 1986. 1, 4, 6, 8, 9, 10, 12, 13, 14, 16, 17, 26, 28, 29, 38, 94, 174

[15] Martin Kretzschmar. Theory of the elliptical Penning trap. *International Journal of Mass Spectrometry*, 275:21–33, 2008. 1, 10, 23, 24, 25, 26, 87, 93, 94, 110, 111, 112, 115, 116, 126

[16] G. Ciaramicoli, I. Marzoli, and P. Tombesi. Quantum spin models with electrons in Penning traps. *Physical Review A*, pages 012338–9, 2008. 1

[17] Martin Kretzschmar. Theoretical investigations of different excitation modes for Penning trap mass spectrometry. *International Journal of Mass Spectrometry*, 349:227–239, 2013. 1

[18] D. Porras and J. I. Cirac. Quantum Manipulation of Trapped Ions in Two Dimensional Coulomb Crystals. *Physical Review Letters*, 96:250501–4, 2006. 1

[19] Michol Massini, Mauro Fortunato, Stefano Mancini, Paolo Tombesi, and David Vitali. Schrödinger-cat entangled state reconstruction in the Penning trap. *New Journal of Physics*, 2:20.1–20.14, 2000. 1

[20] I Marzoli, P Tombesi, G Ciaramicoli, G Werth, P Bushev, S Stahl, F Schmidt-Kaler, M Hellwig, C Henkel, G Marx, I Jex, E Stachowska, G Szawiola, and A Walaszyk. Experimental and theoretical challenges for the trapped electron quantum computer. *Journal of Physics B*, 42:154010–154020, 2009. 1

[21] G. Ciaramicoli, I. Marzoli, and P. Tombesi. Scalable Quantum Processor with Trapped Electrons. *Physical Review Letters*, 91:017901–4, 2003. 1

[22] L. H. Pedersen and C. Rangan. Controllability and Universal Three-qubit Quantum Computation with Trapped Electron States. *Quantum Information Processing*, 7:33–42, 2008. 1

[23] L. Lamata, D. Porras, J. I. Cirac, J. Goldman, and G. Gabrielse. Towards electron-electron entanglement in Penning traps. *Physical Review A*, 81:022301–5, 2010. 1

[24] G. Ciaramicoli, I. Marzoli, and P. Tombesi. Realization of a quantum algorithm using a trapped electron. *Physical Review A*, 63:052307–052315, 2001. 1

[25] S. Stahl, F. Galve, J. Alonso, S. Djekić, W. Quint, T. Valenzuela, J. Verdú, M. Vogel, and G. Werth. A planar Penning trap. *The European Physical Journal D*, 32:139–146, 2005. 1, 4, 19

[26] G. Ciaramicoli, I. Marzoli, and P. Tombesi. From a single- to a double-well Penning trap. *Physical Review A*, 82:044302–4, 2010. 2, 173

[27] Jonathan Pinder. *The Geonium Chip: engineering a scalable planar Penning trap*. PhD thesis, University of Sussex, 2016. 2, 4, 8, 18, 39

[28] Martin Kretzschmar. Octupolar excitation of ion motion in a Penning trap: A theoretical study. *International Journal of Mass Spectrometry*, 357:1–21, 2014. 2, 10, 11, 12, 28, 35

[29] J. Pinder and J. Verdú. A planar Penning trap with tunable dimensionality of the trapping potential. *International Journal of Mass Spectrometry*, 356:49–59, 2013. 3, 19, 21, 24, 25, 26, 27, 85, 106, 119, 121, 123, 125, 126

[30] R. S. Van Dyck, P. B. Schwinberg, and H. G. Dehmelt. Precise Measurements of Axial, Magnetron, Cyclotron, and Spin-Cyclotron-Beat Frequencies on an Isolated 1-meV Electron. *Physical Review Letters*, 38:310–314, 1977. 3

[31] Gerald Gabrielse and F. Colin Mackintosh. Cylindrical Penning traps with orthogonalized anharmonicity compensation. *International Journal of Mass Spectrometry and Ion Processes*, 57:1–17, 1984. 4

[32] J. R. Castrejón-Pita and R. C. Thompson. Proposal for a planar Penning ion trap. *Physical Review A*, 72:013405–7, 2005. 4, 19

[33] M Hellwig, A Bautista-Salvador, K Singer, G Werth, and F Schmidt-Kaler. Fabrication of a planar micro Penning trap and numerical investigations of versatile ion positioning protocols. *New Journal of Physics*, 12:065019, 2010. 4, 19

[34] J. Goldman and G. Gabrielse. Optimized planar Penning traps for quantum-information studies. *Physical Review A*, 81:052335–25, 2010. 4, 19

[35] P M Morse and H Feshbach. *Methods of Theoretical Physics McGraw-Hill, Pt. 1 Chapters 1 to 8*. McGraw-Hill, 1953. 5

[36] L. D. Landau and E. M. Lifshitz. *The classical theory of fields: Volume 2 (Course of Theoretical Physics)*. Pergamon Press, 1975. 5

[37] L D Landau and E M Lifshitz. *Mechanics: Volume 1 (Course of Theoretical Physics)*. Pergamon Press, 1976. 5, 6, 77

[38] John David Jackson. *Classical Electrodynamics*. Wiley, New York, 1962. 6, 160

[39] J. Verdú. Theory of the coplanar-waveguide Penning trap. *New Journal of Physics*, 13:113029–113046, 2011. 8, 19, 20, 22, 23, 26

[40] L. D. Landau and E. M. Lifshitz. *Quantum Mechanics: Non-Relativistic Theory: Volume 3 (Course of Theoretical Physics)*. Butterworth-Heinemann, 1965. 11, 12, 36, 39, 40, 47, 52, 136

[41] Stephen Barnett and Paul Radmore. *Methods in Theoretical Quantum Optics*. Oxford University Press, New York, 2002. 12, 14, 15, 30, 32, 39, 78, 81, 90, 113, 147, 154, 158

[42] Lowell S. Brown and Gerald Gabrielse. Precision spectroscopy of a charged particle in an imperfect Penning trap. *Physical Review A*, 25:2423–2425, 1982. 14

[43] L. D. Landau and Lifshitz E. M. *Statistical physics. Part 1: Volume 5 (Course of Theoretical Physics)*. Pergamon Press, 1980. 15, 16

[44] D. Wineland and H. Dehmelt. Line shifts and widths of axial, cyclotron and G-2 resonances in tailored, stored electron (ion) cloud. *International Journal of Mass Spectrometry and Ion Physics*, 16:338–342, 1975. 16, 17, 28

[45] S. Peil and G. Gabrielse. Observing the Quantum Limit of an Electron Cyclotron: QND Measurements of Quantum Jumps between Fock States. *Physical Review Letters*, 83:1287–1290, 1999. 18

[46] Joseph F Goodwin. *Sideband Cooling to the Quantum Ground State in a Penning Trap*. PhD thesis, Imperial College London, 2015. 18, 154

[47] A Mann and M Revzen. Thermal coherent states. *Physics Letters A*, 134:273–275, 1989. 18

[48] M. S. Kim, F. A M De Oliveira, and P. L. Knight. Properties of squeezed number states and squeezed thermal states. *Physical Review A*, 40:2494–2503, 1989. 18

[49] Li Yi-min, Xia Hui-rong, Wang Zu-geng, and Xu Zai-xin. Squeezed coherent thermal state and its photon number distribution. *Acta Physica Sinica (Overseas Edition)*, 6:681–689, 1997. 18

[50] J. Verdú. Patent, Ion Trap, WO 2013/041615 A2, 2013. 19

[51] J. Verdú. Patent, Ion Trap, US 8362423 B1, 2013. 19

[52] Alexandre Blais, Ren-Shou Huang, Andreas Wallraff, S. M. Girvin, and R. J. Schoelkopf. Cavity quantum electrodynamics for superconducting electrical circuits: An architecture for quantum computation. *Physical Review A*, 69:062320–14, 2004. 19

[53] A Wallraff, D I Schuster, A Blais, L Frunzio, R.-S Huang, J Majer, S Kumar, S M Girvin, and R J Schoelkopf. Strong coupling of a single photon to a superconducting qubit using circuit quantum electrodynamics. *Nature*, 431:162–167, 2004. 19

[54] A. Al-Rjoub and José L Verdú. Electronic detection of a single particle in a coplanar-waveguide Penning trap. *Applied Physics B*, 107:955–964, 2012. 19, 22, 26

[55] Robert S. Van Dyck, Paul B. Schwinberg, and Hans G. Dehmelt. New high-precision comparison of electron and positron g factors. *Physical Review Letters*, 59:26–29, 1987. 28

[56] Eric A Cornell, Robert M Weisskoff, Kevin R Boyce, and David E Pritchard. Mode Coupling in a Penning trap: π pulses and a classical avoided crossing. 41:312–315, 1990. 28, 29, 33, 38

[57] J. Dalibard and C. Cohen-Tannoudji. Dressed-atom approach to atomic motion in laser light: the dipole force revisited. *Journal of the Optical Society of America B*, 2:1707–1720, 1985. 29, 38, 39, 43, 98, 127, 156

[58] C Cohen-Tannoudji and S Reynaud. Dressed-atom description of resonance fluorescence and absorption spectra of a multi-level atom in an intense laser beam. *Journal of Physics B*, 10:345–363, 1977. 31, 99, 118, 122, 130

[59] C. J. Isham. *Lectures on quantum theory : mathematical and structural foundations*. Imperial College Press, 1997. 33, 87

[60] Barry M Garraway and Hélène Perrin. Recent developments in trapping and manipulation of atoms with adiabatic potentials. *Journal of Physics B*, 49:172001–1720021, 2016. 33, 39, 40, 41, 42, 131, 156, 166

[61] J. Schwinger. *On Angular Momentum*. Dover Publications, New York, 1965. 35, 53, 66, 68, 97

[62] T. Schumm, S. Hofferberth, L. M. Andersson, S. Wildermuth, S. Groth, I. Bar-Joseph, J. Schmiedmayer, and P. Krüger. Matter-wave interferometry in a double well on an atom chip. *Nature Physics*, 1:57–62, 2005. 39, 156, 166

[63] G. B. Jo, Y. Shin, S. Will, T. A. Pasquini, M. Saba, W. Ketterle, D. E. Pritchard, M. Vengalattore, and M. Prentiss. Long phase coherence time and number squeezing of two Bose-Einstein condensates on an atom chip. *Physical Review Letters*, 98:030407–4, 2007. 39

[64] J. J P Van Es, S. Whitlock, T. Fernholz, A. H. Van Amerongen, and N. J. Van Druten. Longitudinal character of atom-chip-based rf-dressed potentials. *Physical Review A - Atomic, Molecular, and Optical Physics*, 77:063623–9, 2008. 39

[65] G. B. Jo, J. H. Choi, C. A. Christensen, T. A. Pasquini, Y. R. Lee, W. Ketterle, and D. E. Pritchard. Phase-sensitive recombination of two Bose-Einstein condensates on an atom chip. *Physical Review Letters*, 98:180401–4, 2007. 39

[66] M. A. Cirone, A. Negretti, T. Calarco, P. Krüger, and J. Schmiedmayer. A simple quantum gate with atom chips. *European Physical Journal D*, 35:165–171, 2005. 39

[67] J. Verdú. Private communication. 2013. 39, 42, 174

[68] C. J. Foot. *Atomic physics*. Oxford University Press, 2005. 39, 40

[69] Claude Cohen-Tannoudji and David Guéry-Odelin. *Advances in Atomic Physics*. World Scientific, 2011. 40

[70] T. Schumm, P. Krüger, S. Hofferberth, I. Lesanovsky, S. Wildermuth, S. Groth, I. Bar-Joseph, L. M. Andersson, and J. Schmiedmayer. A double well interferometer on an atom chip. *Quantum Information Processing*, 5:537–558, 2006. 41, 176

[71] Claude Cohen-Tannoudji, Bernard Diu, and Franck Laloe. *Quantum mechanics*. Wiley, 2005. 44, 45, 46, 47, 52

[72] R. K. Bhaduri, Shuxi Li, K. Tanaka, and J. C. Waddington. Quantum gaps and classical orbits in a rotating two-dimensional harmonic oscillator. *Journal of Physics A: General Physics*, 27:553–558, 1994. 48, 50, 61, 62, 144

[73] Ivan Niven, Herbert S. Zuckerman, and Hugh L. Montgomery. *An introduction to the theory of numbers*. Wiley, 2008. 48

[74] Andrew M. Steane. arXiv:1312.3824v1, 2013. 53, 72, 89, 93

[75] M Kretzschmar. Particle motion in a Penning trap. *European Journal of Physics*, 12:240–246, 1991. 54, 55

[76] R C Thompson and D C Wilson. The motion of small numbers of ions in a Penning trap. *Zeitschrift für Physik D*, 42:271–277, 1997. 54

[77] Martina Knoop, Niels Madsen, and Richard C Thompson. *Physics with Trapped Charged Particles*. Imperial College Press, London, 2014. 54

[78] J. F. Cornwell. *Group theory in physics : an introduction*. Academic Press, 1997. 68

[79] Richard A. Campos, Bahaa E. A. Saleh, and Malvin C. Teich. Quantum-mechanical lossless beam splitter: SU(2) symmetry and photon statistics. *Physical Review A*, 40:1371–1384, 1989. 68, 88

[80] Michael Martin Nieto. Displaced and squeezed number states. *Physics Letters A*, 229:135–143, 1997. 113

[81] M. Born and V. Fock. Beweis des Adiabatensatzes. *Zeitschrift für Physik*, 51:165–180, 1928. 124

[82] Daniel Comparat. General conditions for quantum adiabatic evolution. *Physical Review A*, 80:012106–7, 2009. 124

[83] Zhaoyan Wu and Hui Yang. Validity of the quantum adiabatic theorem. *Physical Review A*, 72:012114–5, 2005. 124

[84] Jie Liu and Li Bin Fu. Singularities of Berry connections inhibit the accuracy of the adiabatic approximation. *Physics Letters, Section A: General, Atomic and Solid State Physics*, 370:17–21, 2007. 124

[85] L Landau. Theory of energy transfer. II. *Phys. Z. Sowjetunion*, 2:46–51, 1932. 124, 128, 134, 135, 137

[86] Clarence Zener. Non-Adiabatic Crossing of Energy Levels. *Proceedings of the Royal Society of London. Series A*, 137:696 – 702, 1932. 124, 128, 134, 135

[87] Jin-Dan Chen, Xue-Da Wen, Guo-Zhu Sun, and Yang Yu. Landau-Zener-Stückelberg interference in a multi-anticrossing system. *Chinese Physics B*, 20:088501–7, 2011. 128, 147, 153

[88] L Landau. The Theory of Energy Exchange in Collisions. *Physikalische Zeitschrift Der Sowjetunion*, 1:88–98, 1932. 128, 142

[89] E.C.G Stückelberg. Theory of Inelastic Collisions between Atoms. *Helv. Phys. Acta 5*, 5:369–423, 1932. 128, 137, 142

[90] S. N. Shevchenko, S. Ashhab, and Franco Nori. Landau-Zener-Stückelberg interferometry. *Physics Reports*, 492:1–30, 2010. 128, 131, 132, 133, 134, 135, 136, 137, 138, 139, 140, 141, 142, 143, 155

[91] D. T. Pegg and G. W. Series. On the Reduction of a Problem in Magnetic Resonance. *Proceedings of the Royal Society of London A*, 332:281–289, 1973. 133

[92] J.M. LopezCastillo, A. FilaliMouhim, and J.P. JayGerin. Periodic motion around the crossing point in a twolevel system. *The Journal of Chemical Physics*, 97:1905–1910, 1992. 133

[93] Yu-Xi Liu, C P Sun, and Franco Nori. Scalable superconducting qubit circuits using dressed states. *Physical Review A*, 74:052321–10, 2006. 133

[94] Ya. S. Greenberg. Low-frequency Rabi spectroscopy of dissipative two-level systems: Dressed-state approach. *Physical Review B*, 76:104520–13, 2007. 133

[95] Milena Grifoni and Peter Haggi. Driven quantum tunneling. *Physics Reports*, 304:229–354, 1998. 133, 143

[96] Bogdan Damski and Wojciech H. Zurek. Adiabatic-impulse approximation for avoided level crossings: From phase-transition dynamics to Landau-Zener evolutions and back again. *Physical Review A*, 73:063405–11, 2006. 133

[97] Bogdan Damski. The Simplest Quantum Model Supporting the Kibble-Zurek Mechanism of Topological Defect Production: Landau-Zener Transitions from a New Perspective. *Physical Review Letters*, 95:035701–4, 2005. 133

[98] W H Zurek. Cosmological experiments in condensed matter systems. *Physics Reports*, 276:177–221, 1996. 133

[99] B. M. Garraway and N. V. Vitanov. Population dynamics and phase effects in periodic level crossings. *Physical Review A*, 551:4418–4432, 1997. 133, 136, 139, 140

[100] V. P. Yakovlev and Krainov V. P. Quasienergy states of a two-level atom in a strong low-frequency electromagnetic field. *Sov. Phys. JETP*, 51:1104–1108, 1980. 136

[101] Mark S Child. Molecular Collision Theory. *Academic Press, London (1974)*, 1974. 136

[102] B M Garraway and S Stenholm. Interferometer within a molecule. *Physical Review A*, 46:1413–1421, 1992. 137

[103] E. E Drake, Gordon W. F., Nikitin. *Atomic, Molecular and Optical Physics Handbook*. AIP Press, 1996. 137

[104] A.M. Dykhne Yu.A. Bychkov. Breakdown in semiconductors in an alternating electric field. *Sov. Phys. JETP*, 58:928–932, 1970. 140

[105] A. V. Shytov, D. A. Ivanov, and M. V. Feigel'man. Landau-Zener interferometry for qubits. *European Physical Journal B*, 36:263–269, 2003. 142

[106] Sang-Kil Son. Floquet formulation for the investigation of multiphoton quantum interference in a superconducting qubit driven by a strong ac field. *Physical Review A*, 79:032301–11, 2009. 143

[107] Guozhu Sun, Xueda Wen, Yiwen Wang, Shanhua Cong, Jian Chen, Lin Kang, Weiwei Xu, Yang Yu, Siyuan Han, and Peiheng Wu. Population inversion induced by LandauZener transition in a strongly driven rf superconducting quantum interference device. *Applied Physics Letters*, 94:102502–3, 2009. 143

[108] S. Ashhab, J. R. Johansson, A. M. Zagoskin, and Franco Nori. Two-level systems driven by large-amplitude fields. *Physical Review A*, 75:063414–9, 2007. 143

[109] Guozhu Sun, Xueda Wen, Bo Mao, Jian Chen, Yang Yu, Peiheng Wu, and Siyuan Han. Tunable quantum beam splitters for coherent manipulation of a solid-state tripartite qubit system. *Nature Communications*, 1:1–7, 2010. 153

[110] B. M. Garraway and S. Stenholm. Population transfer at periodically repeated level crossings. *Physical Review A*, 45:364–374, 1992. 155

[111] Alexander Streltsov, Uttam Singh, Himadri Shekhar Dhar, Manabendra Nath Bera, and Gerardo Adesso. Measuring Quantum Coherence with Entanglement. *Physical Review Letters*, 115:020403–6, 2015. 155

[112] Ulf Leonhardt. *Essential quantum optics : from quantum measurements to black holes*. Cambridge University Press, 2010. 163

[113] V. Jelic and F. Marsiglio. The double-well potential in quantum mechanics: a simple, numerically exact formulation. *European Journal of Physics*, 33:1651–1666, 2012. 173

[114] E. Wigner. On the Interaction of Electrons in Metals. *Physical Review*, 46:1002–1011, 1934. 174

[115] K Blaum, Yu N Novikov, and G Werth. Penning traps as a versatile tool for precise experiments in fundamental physics. *Contemporary Physics*, 51:149–175, 2010. 174